The Synthesis and Testing of Fast Switching, Novel Conjugated Polymers for Electrochromic Applications

Submitted by

Sandeep Kaur Shahi

A thesis submitted in fulfilment of the requirements for the degree of Doctor of Philosophy in Department of Pure and Applied Chemistry, University of Strathclyde

2017

This thesis is the result of the author's original research. It has been composed by the author and has not been previously submitted for examination which has led to the award of a degree at University of Strathclyde in 2017.

Signed:

Date:

Acknowledgements

Firstly, I wish to thank Prof. Peter Skabara for the valuable Ph.D. opportunity he has given me whilst under his supervision. I appreciate his confidence, faith, encouragement and support he has shown me throughout the course of this project. The skills I have developed, knowledge gained, professional maturity and international networking exposure has greatly been endorsed by my respected Professor and his team.

I am grateful to DSTL, EPRSC and University of Strathclyde for funding my project and thankful to my CASE supervisor, Dr. Rory Berridge at DSTL, for his enthusiastic interest and informative suggestions in the development of the projects presented. I wish to sincerely thank him for his friendly nature and generous hospitality whilst I visited DSTL, Porton Down UK. I would also like to thank Dr. Debra Willison who has followed and supported my academic progression since I started my undergraduate degree at University of Strathclyde since 2003, thank you for your encouraging advice and guidance.

I would also like to acknowledge the people I collaborated with, and who helped in the realisation of the work presented in this thesis: Dr. Alexander Kanibolotsky and Dr. John Forgie for teaching the electrochemical analysis techniques and results interpretation, Dr. Neil Findlay for his support in the synthesis of polymer **PBDF** in Chapter 4, Dr. Fiona Coomer for measuring the powder X-ray diffraction of **PBDF**, Dr. Craig. Combe and Dr. L. Biniek for the GPC analysis of **PBDF** in Chapter 4 (Imperial College London), Dr. Simon Coles and Dr. Claire Wilson for their crystallography service of compound **3.6** in chapter 3 (University of Southampton). Mrs. Denise Gilmour for elemental analysis, Miss Pat Keating for mass spectrometry, Mr. Jim Morrow for TGA measurements, Mr. Craig Irving for taking care of the NMR facilities and not forgetting the friendly boys in stores and the glass blower Neil Hodgson who I had to visit often.

Special thanks goes to all past and present members of the Skabara group who have all contributed to make our lab a nice and stimulating workplace. Working within the Skabara group has been great fun and often more like family; to all past and

present members of the group I truly am grateful in sharing my postgraduate years with you all. However, I would like to dedicate a very sincere thank you to both Dr. Neil Findlay and Dr. Alexander Kanibolotsky for their tremendous amount of patience, guidance, knowledge, support, and the remarkable job in correcting and revising this thesis, which has finally seen me through to the end of my studies. Thank you for putting up with me *all* these years and having patience with me to do so; to you both, I am indebted.

For those who have walked through the journey of scientific research, you may agree that each project is never the same and can be a self realisation experience. A Ph.D. can take the form of your very own Mount Everest to survive and conquer. I extend my heartfelt thanks to my best friends Clara, Zuzka, and Sunna who have been my sanity, strength, happiness and backbone in getting me here and I adore you all dearly.

Finally and most importantly, thank you to my beloved family. It has been a journey for you all to be watching patiently as I finally come to completion. I must sincerely apologise to you all for the time it has taken for me to get here and the adjustments you all have had to make. It has been a testing period but I applaud you all for your abundant patience, unwavering support and understanding.

Johnny, words cannot describe how much I love, respect and appreciate you, you carried me when I could not walk. We can now un-pause our lives.

Abstract

Modern technology is an essential aspect of our everyday lifestyle being vitally important to lighting, mobile phones, laptops, toys etc. The majority of these gadgets concentrate on visual electronic displays as a key selling feature. Hence, industry is in constant competition to excel while delivering new consumer demands of higher colouration efficiency, faster response times, inexpensive yet robust hardware, flexible displays and with the possibility of incorporating electronics into textiles.

Traditionally, inorganic small molecules were extensively used for optical displays devices such as cathode ray tubes, liquid crystal displays, light emitting diiodes and plasma screens. However, in the past decade, significant progress in polymer electrochromism has shown many organic electroactive polymers to have the potential to satisfy the above consumer demands. Electrochromic materials (EC) have the ability to undergo a reversible colour transformation switch upon electrochemical doping, such as colour bleaching transformations.

Herein, this thesis discusses how organic chemistry facilitates the advantage of structurally modifying monomeric heterocyclics to fine tune materials with interesting optical and physical properties. The polymeric form of an teraryl monomer containing a 1,4-dithiin-furan illustrated superior switching performances and electrochromic properties when compared to its parent poly 3,4-ethylene dioxythiophene (PEDOT). Poly(dithienylfuran) films displayed fast switching and reversible colour transformation at high colour contrast (CE = 212 cm^2 C^{-1} cf. 183 cm^2 C^{-1} for PEDOT at 95% optical switch).

Formerly overlooked furan materials in organic electronics was revisted here, in which a polyfuran substituted at the 2,3-positions with an S-alkylated dithiin unit, was studied. The employment of the dithiin moiety provides intrinsic additional electroactivity, as well as a functional handle for substitution with alkyl groups, enhancing the processability of the polymer. The new polymer is compared with the closely related and well-established literature compounds PEDOT and PEDTT as well-studied, highly chalcogenated polythiophenes.

The electrochromism phenomenon is not only of importance for visual optical displays but also has the potential for extended application in telecommunications with electromagnetic responses into the near infra-red (NIR) region. Herein, describe a series of symmetric and asymmetric chalcogenated azomethine monomers, robustly exherting electrochemical activity within the NIR.

Abbreviations

2D	two dimensional
3D	three dimensional
A	Ampere / area
BLA	bond length alternation
CC	chronocoulometry
CE	colouration efficiency/ counter electrode
CIE	Commision Internationale de L'Eclairage
CP	conjugated polymers
CR	optical contrast
CV	cyclic voltammetry
CWE	carbon-working electrode
D-A	donor-acceptor
DFT	density functional theory
dm	decimeter
DPV	differential pulse voltammetry
DSC	differential scanning calorimetry
EA	elemental analyses
EC	electrochromic
ECD	electrochromic devices
ECPs	electrochromic polymers
EDOT	3,4-ethylenedioxythiophene
EDTT	3,4-ethylenedithiothiophene.
GPC	gel permeation chromatography
HOMO	highest occupied molecular orbital
HRMS	high resolution mass spectrum
IR	Infrared

ITO	indium tin oxide
IUPAC	International Union of Pure and Applied Chemistry
LCD	liquid crystal display
LSV	linear sweep voltammetry
LUMO	lowest unoccupied molecular orbital
mol	mole
Mpt	melting point
MS	mass spectroscopy
mv	millivolt
NBS	*N*-bromosuccinimide
NIR	near infrared
nm	nanometer
NMR	nuclear magnetic resonance
OD	optical density
OFETs	organic field effect transistors
OLEDs	organic light emitting diodes
OPVs	organic photovoltaics
PANI	polyaniline
PAT	poly(alkylthiophene)
PB	Prussian blue
PEB	poly(ethylenedioxythiophenedidodecyloxybenzene)
PEDOT	poly(3,4-ethylenedioxythiophene)
PEDTT	poly(3,4-ethylenedithiothiophene)
PET	Polyethylene tetraphthalte
PFu	polyfuran
PMMA	polymethyl methacrylate
PPI	poly (1,4-phenylene-methylidynenitrilo-1,4-phenylenenitrilomethylidyne
PPP	poly-para-phenylene

PProDOP	poly[3,4-(propylenedioxy)pyrrole]
PProDOT	poly(3,4-propylenedioxythiophene)
PPV	poly(p-phenylene-vinylene)
PPy	polypyrrole
PSD	pore size distribution
PSS	poly(styrenesulfonate)
PTh	polythiophene
PW	Prussian white
PXRD	powder X-ray diffraction
RE	reference electrode
R_f	Refractive Index
S	Seconds / Siemens
SCE	saturated calomel electrode
SHE	standard hydrogen electrode
SOMO	singly occupied molecular orbital
SWV	square wave voltammetry
TCNQ	tetracyano-p-quinodimethane
TGA	thermogravimetric analysis
TLC	thin layer chromatography
TTF	tetrathiafulvalene
UV	ultra-violet
Vis	visible
WE	working electrode
X	halide substituent
XRD	X-ray diffraction

Symbols & Greek

α	charge transfer coefficient/ ortho substitution position
A	absorbance/ electrode surface area
a	"red-green" co-ordinate
b	"blue-yellow" co-ordinate
C	electrical charge
c	chroma
D	diffusion coefficient
E^0	standard electrode potential
$E^{1/2}$	half-wave potential
E_a	anodic peak potential
E_{BLA}	energy of bond length alteration
E_c	cathodic peak potential
E_{eq}	energy of equilibrium potential
E_g	energy band gap
E_{Int}	energy of intermolecular interactions between monomers
E_{Res}	energy of aromatic resonance
E_{Sub}	energy of electron-donating or –withdrawing substituents
E_ϑ	deviations from planarity
F	Faraday's constant
Fc	ferrocene
Fc^+	ferrocenium
H	hue angle in radians
h	Planck constant
I	intensity of the transmitted light / current
L	lightness co-ordinate
L	luminance
M_n	molecular weight

n	non-bonding orbital / number of electrons
Q	inserted charge
Q_d	charge density
R	gas constant
x,y,z	chromaticity co-ordinates
X,Y,Z	tri-stimulus values
$^x I_\lambda, {}^y I_\lambda, {}^z I_\lambda$	illuminant weights
ΔG	Gibbs free energy change
$\Delta OD(\lambda)$	optical change
ΔT	optical contrast change
ε	molar extinction coefficient
η	colouration efficiency / overpotential
θ	angle of incidence
ϑ	mean dihedral angle
μ	mobility
μm	micrometer
π	pi-orbital
π^*	pi-orbital anti bonding
σ	conductivity/sigma bonding orbital

Table of Contents

1 Introduction

1.1 **Band Theory**

Band theory describes the electronic structure of materials and constitutes the solid-state analogue of molecular orbital (MO) theory. In a solid, the individual atomic orbitals of all atoms that make up the molecule combine and overlap, extending over the solid and forming defined bands of "allowed" electron locations that are separated by a "forbidden" band gap. This corresponds to the delocalisation of electrons throughout the material. Bands can be empty, filled or half-filled with electrons depending on the electron occupancy of the respective orbitals of the comprising atoms. The valence band is the energetically highest band that is filled with electrons and corresponds to the highest occupied molecular orbital (HOMO) in MO theory.   All bands that are energetically lower than the valence band are filled with electrons. The conduction band is the energetically lowest unfilled band and represents the solid state analogue of the lowest unoccupied molecular orbital (LUMO) in MO theory.[1, 2] The energy gap between the valence and the conduction band is called the band gap. The specific band structure of a compound determines various characteristics of the material such as its conductivity, reactivity, and optical properties. The conductivity of a material depends on the thermodynamic work that needs to be expended to introduce an electron to the material, which is reflected in the material's Fermi level. The Fermi level is a hypothetical energy level that marks the limit between occupied and unoccupied energy levels at a temperature of 0 K, see Figure 1.1. [1, 2,3]
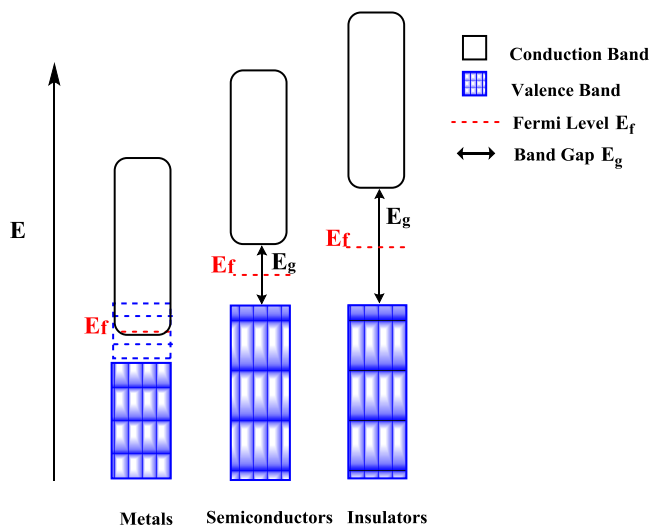

Figure 1.1: Band structure of metals, semiconductors, and insulators.

Materials can be classified as metals, semiconductors, or insulators.[3] They differ in the occupation of their energy bands as well as the size of their band gaps E_g, which significantly affects their conductive properties. Electrical conductivity results from the movement of charge carriers such as electrons or positively charged holes (i.e, a lack of an electron) along a sufficient number of thermodynamically accessible empty energy levels within the material.[1]

Metals are conductive as they either exhibit half-filled valence bands where electrons can move along the empty energy levels of the valence band, or they possess a filled valence band that overlaps with an empty conduction band wherein electron movement is enabled. The accessibility of empty energy levels is reflected by a Fermi level that is located within a band, thus E_g = 0 eV. However, metallic conductivity decreases upon temperature increases.[1, 2]

Insulators, in contrast, are characterised by a band structure with a large band gap (> 3 eV) between a filled valence band and the empty conduction band, and a Fermi level that is located within the forbidden band gap. The absence of empty states accessible for electron movement inhibits electrical conductivity for such solids. Hence, no charge carriers can be generated only upon thermal excitation and insulators do not conduct electricity.[1, 2]

Semiconductors are materials with conductivities between those of metals and insulators. The conductivity of semiconductors results from a structure with a band gap between the valence and the conduction band that is sufficiently small (E_g = 1.5-2.5 eV) to enable thermal promotion or photoexcitation of electrons from the filled valence band to the empty conduction band. The Fermi level of semiconductors is also located within the band gap, though closer to the conductive and valence bands than the Fermi level of insulators. Electron promotion to empty states renders semiconductors conductive based on the movement of electrons within the valence band due to newly-generated empty levels ("holes") as well as movement of the promoted electrons within the conduction band. The conductivity of *intrinsic* semiconductors increases exponentially with the temperature as the temperature increases the number of electrons promoted to the conduction band.[1, 2]

The conductivity of a pure, intrinsic semiconductor can be increased by replacing lattice atoms with atoms of a different number of valence electrons. This replacement is called doping and the resulting solid is called an extrinsic semiconductor. Doping with atoms that contain one electron more than the lattice atoms of the semiconductor (donor atoms) is called n-doping. This moves the Fermi level closer to the conduction band where additional electrons are propagated, which can move along the empty energy levels within this band. The corresponding doping with atoms that possess one valence electron less than the lattice atoms (acceptor atoms) is called p-doping, which moves the Fermi level closer to the valence band and generates empty energy levels ("electron holes"), which enables electron mobility in the valence band, see Figure 1.2.[1-4]
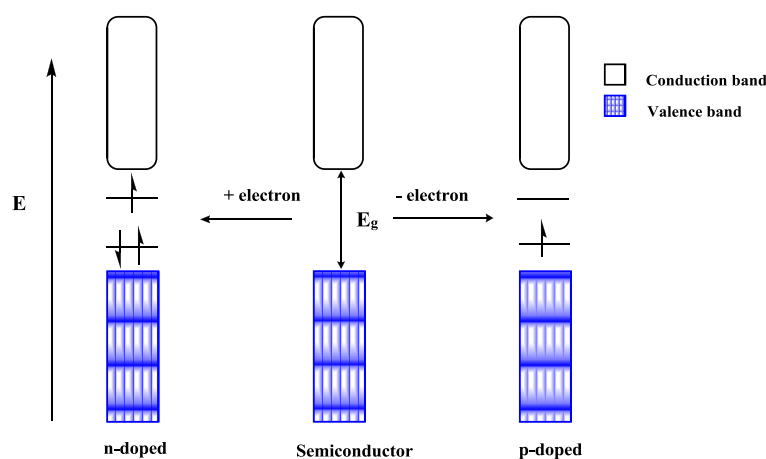
Figure 1.2: Band structures of intrinsic and extrinsic (p-doped and n-doped) semiconductors.

Organic semiconductors can be chemically doped, however they also can be electrochemically doped through either oxidation or reduction of the valence band. Doping using this method is achieved using an electrochemical cell; a working electrode (WE) coated in the material to be doped is held in an electrolyte solution (which the material is insoluble in) alongside counter and reference electrodes.[4-6]

An oxidation process involves the loss of an electron (p-doping) and the ability for the material to oxidise depends on its ionisation potential (HOMO level). Increasing the electrode charge to a higher positive potential, overcomes the material's ionisation energy and results in the material losing its electron to the electrode creating an anodic current, see Figure 1.3.[4-6]
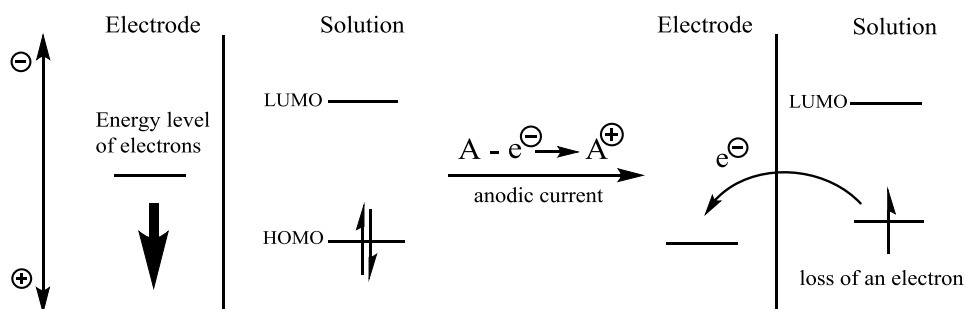
Figure 1.3: Illustration of an oxidation reaction in an electrochemical cell where A defines material solution.[4, 5]

Alternatively, the reduction process involves the gain of an electron.[6] The n-doping of the material depends on its electron affinity; the material's LUMO level should be lower than the increasing negative potential. Reduction reactions occur when the electrons from the electrode migrate into the material; creating a cathodic current, see Figure 1.4.[4, 7]
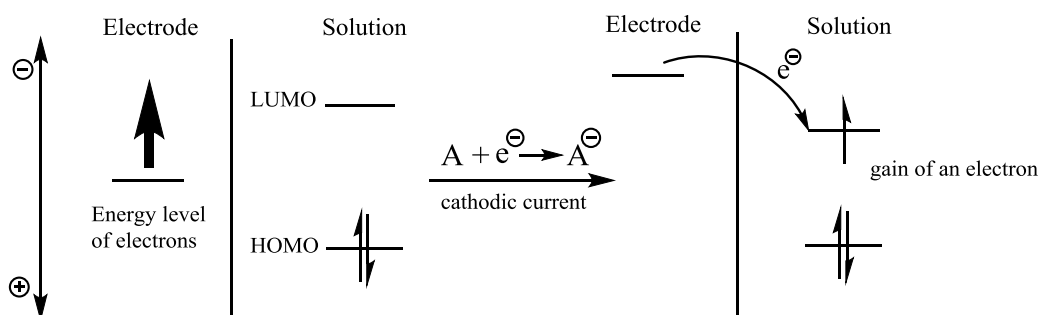
Figure 1.4: Illustration of a reduction reaction in an electrochemical cell where A defines material solution.[4, 5]

1.2 Organic Electronics

Organic electronics describes the field of materials and devices developed from semiconducting organic molecules. Historically, organic materials were regarded as insulators. However, in 1862 polyaniline was discovered as the first organic polymer with electrical conductivity.[8-11] Almost a century later, charge-transfer complexes of polycyclic aromatic compounds with conductive properties were reported.[12, 13] The discovery that doping of the insulating organic polymer poly(acetylene) induces a conductivity comparable to that of metals significantly promoted the research of organic conducting materials and led to a Nobel prize for Shirakawa, MacDiarmid and Heeger in 2000.[8-10]

Organic semiconductors bear various advantages over inorganic semiconductors such as lower material and production costs (especially for a large-scale production), the possibility for assembly on flexible substrates, and low energy consumption under operation.[14, 15] However, the major advantage lies in the possibility to tailor their electrical, mechanical and optical properties over a wide range to meet specific demands of various applications[16] This led to the development of different organic electronic devices such as organic light emitting diodes (OLEDs),[17] organic field effect transistors (OFETs),[18-20] organic memory devices,[21] organic photovoltaics (OPVs),[22-26] and organic electrochromic devices (ECDs).[27-29] Some of those devices have already found their way into everyday life and OLED displays, organic solar cells and organic transistors are already commercially available.[17, 30,31]

On the other hand, rapid technological progress in the electronics industry creates new demands for electronic devices regarding material properties, costs, and energy efficiency that often cannot be met by classical inorganic components and devices. For example, the cathode ray tube, long used for television and computer monitors, is being challenged by the increasing demand for displays to be brighter, lighter, more vibrant, larger, and energy efficient. The increasing use of displays in portable devices such as cameras, cell phones or latterly smartwatches furthermore requires displays to be thin, small and light.[7, 32, 33] Regarding these challenges, OLEDs promise to be one of the key technologies for the production of such displays.[35, 36]

Another display technology is organic electrochromic displays, which is based on the phenomenon of electrochromism, and is still in the very beginning of its development.[37] It promises to produce displays with high colouration efficiency, stability, fast response times, flexibility, a wide range of colours and colour changes with absorption characteristics from UV to near IR, compared to existing inorganic electrochromic materials.[33, 38-45]

1.2.1   *Organic conductivity characteristics*

The conductivity of organic semiconductors is determined by the nature of the C-C bond. The C-atoms in organic semiconductors are usually sp^2-hybridised, which enables two adjacent C-atoms to form a double bond consisting of one σ-bond and one π-bond. The σ-bond is more stable as it results from the very efficient 'head-on' overlap of two sp^2-orbitals. One bonding σ-orbital and one anti-bonding σ*-orbital are formed, which are separated by a large energy gap. The π-bond, in contrast, is less stable than the σ-bond since it is formed by the less efficient 'sideways' overlapping of the non-hybridised p_z-orbitals, which are oriented perpendicular to the sp^2-plane but aligned parallel to each other. The resulting bonding π- and π*-orbitals reveal a smaller energy gap and represent the HOMO and LUMO of the isolated molecular C-C unit, see Figure 1.5.[5]
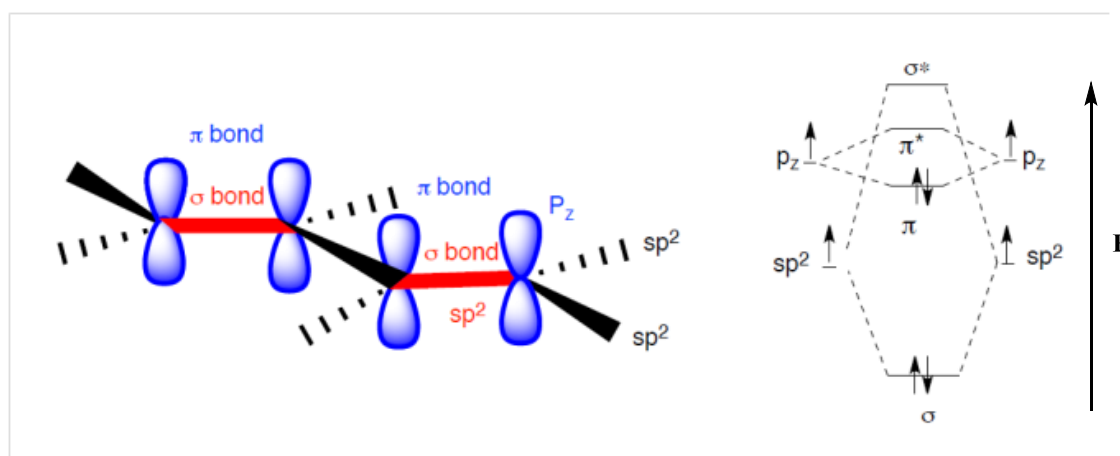
Figure 1.5: A) π-conjugation in chains of sp^2-hybridized c-atoms. B) MO-diagram of an isolated C-C double bond.

Within organic semiconductors, the overlap of a p_z-orbital with the p_z-orbitals of all neighbouring C-atoms leads to the formation of HOMO and LUMO bands of closely spaced energy levels, which are separated by a band gap (as discussed in Chapter 1.1).[46, 47] The electrons in such conjugated systems are delocalised, which is not only the prerequisite for conductivity but also improves the molecule's stability by decreasing its total energy. The HOMO and LUMO bands broaden with an increasing number of conjugated p_z-orbitals, whereas the band gap diminishes and leads to strong absorption in or near the visible spectra range.   Such conjugated systems are formed along the linear chains of conductive polymers, which comprise of alternating single and double bonds. Aromatic systems are closed, planar, cyclic rings that are stabilised by the

conjugation of the p_z-electrons over their ring atoms as long as a defined number of ring electrons are involved (4n+2). The possibility to contribute to a conjugated system is not limited to the p_z-orbitals of C-atoms; the lone pairs of heteroatoms can overlap with adjacent C p_z-orbitals, as in furan where an overlap of a lone pair of the oxygen atom renders this five-membered ring aromatic. [39, 48, 49]

1.3 **Conductive Polymers**

Conductive polymers are organic macromolecules and are composed of repeating units of small organic monomers. They can be synthesised by various synthetic approaches such as addition, condensation, oxidation, or neutralisation reactions.[29-31] Organic polymers generally possess a backbone of σ-bound C-atoms. The electrons of these single bonds are localised between two C-atoms and do not exhibit any mobility.
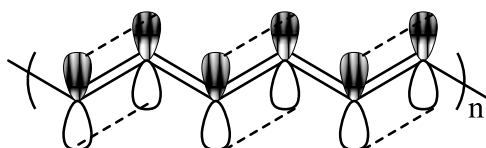
Figure 1.6: Overlapping of p-orbitals of adjacent atoms in polyacetylene.

Every sp^2- or sp-hybridised C-atom additionally possesses non-hybridized p-orbitals, which can overlap to form π-bonds between neighbouring C-atoms (Figure 1.6). As long as these π -bonds are not perfectly localised in systems of alternating single and double bonds, the π-electrons delocalise over the whole polymer and form pathways for the motion of charge carriers, which is the prerequisite for molecular conductivity.[48, 50, 51] Furthermore, these conjugated π-systems planarise and stabilise the polymer, which results in a lower total energy. The overlapping of various p-orbitals results in the formation of bands of closely spaced π- and π*-orbitals, which are separated by a band gap. In order to be conductive, a polymer needs to facilitate a certain amount of mobile charge carriers within its conjugated π-system. Equation (1.1) expresses how the conductivity depends on the number of electrons, the charge of an electron and the electron mobility within the polymer (σ = conductivity, n = number of electrons, μ = mobility, e = charge of an electron).[11, 16, 49, 52, 53]

$$\sigma = n\,\mu\,e \qquad\qquad (1.1)$$

Due to the relatively large band gap of conductive polymers in their neutral state, only a very small number of charge carriers are present at ambient temperature and thermal excitation is usually not sufficient to overcome the band gap. Therefore, mobile charge carriers need to be introduced by doping to render the polymers conductive (as described in Chapter 1.1). Doping either introduces electrons or hole charge carriers and generates negatively charged n-doped polymers or positively charged p-doped polymers, respectively.[39, 41, 48, 51]
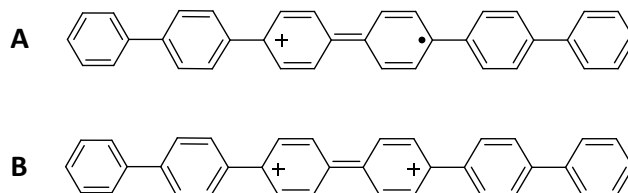
Figure 1.7: p-doping of poly(p-phenylene). A) Formation of a polaron in the polymer that is p-doped to a low degree. B) Formation of a bipolaron in the polymer that is p-doped to a high degree.

Figure 1.7 shows the p-doping of the polymer poly(p-phenylene). A low degree of p-doping (Figure 1.7A) initiates the production of a polaron – a radical cation with a spin and a charge that is delocalised over several monomer units, notice the mesomeric transformation from aromatic to low energy quinodial form.[42] Upon increasing the degree of doping the number of polarons increases as well as their likelihood of encountering each other. If two polarons are in close proximity, they can combine to form a bipolaron, which is a dication of lower energy than the comprising two polarons, see Figure 1.7B.[39, 48] Bipolarons are formed between two energetically degenerated moieties and can propagate along the polymer chain without affecting the energy of the polymer backbone. This energetically efficient mobility of bipolarons results in a very high polymer conductivity.[48, 50, 51] Doping can be generally performed during the polymer synthesis by chemical or electrochemical means or by photo excitation. Although the charge carrier pathway through the conjugated π-system significantly determines the conductivity of the conductive polymer, also other mechanisms such as electron hopping between polymer chains or the movement of counter ions within the polymer material significantly contribute to its conductivity.[49]
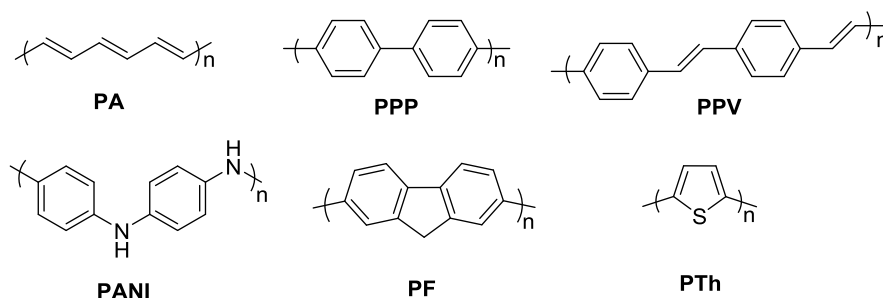
Figure 1.8: Common conjugated polymers.

The most commonly used conjugated polymers are illustrated in Figure 1.8. These include linear backbone polymers such as polyacetylene (PA), with the incorporation of phenyl units resulting in poly-*para*-phenylenes (PPP), poly-*para*-phenylene vinylenes (PPV), polyaniline (PANI) or polyfluorenes. Typical examples for polymers derived from heterocyclic monomers are polypyrrole (PPy) or polythiophenes (PT), which exhibit high conductivities.[12, 54, 55]

1.4 Band-Gap Engineering

As previously mentioned, the electronic properties of an organic semiconductor are determined by its band structure which is largely governed by the molecular structure of the semiconductor monomers. Specific structural parameters of the monomer building blocks exert an individual energetic influence on the size of the band gap, and the band gap can be fine-tuned towards the targeted electronic properties for the desired application by carefully designing the monomer building blocks.[46, 47]

According to eq. 1.2, the band gap energy E_g equals the sum of the energetic impact resulting from alternations in the bond length (E_{BLA}), the degree of aromatic resonance (E_{Res}), deviations from planarity (E_θ), the contribution from the introduction of electron-donating or –withdrawing substituents (E_{Sub}) and interchain or intermolecular coupling in the solid state (E_{Int}).[46]

$$E_g = E_{BLA} + E_{Res} + E_{Sub} + E_\theta + E_{Int} \qquad (1.2)$$

The electronic conductivity of organic semiconductors mainly results from the formation of an extended π-system. Structural parameters that disrupt the π-delocalisation increase the band gap, and are accounted for in the three energy terms

E_{BLA}, E_{Res}, and E_ϑ in eq.(1.2).[46] The energy term E_{BLA} (BLA: bond length alternation) reflects the π-delocalisation along the C-C bonds in the polymer chain, which has the largest impact on to the band gap.[46] Small alterations in the bond lengths vary the effectiveness of π-delocalisation along the polymer chain.[42, 43, 51, 56-58]
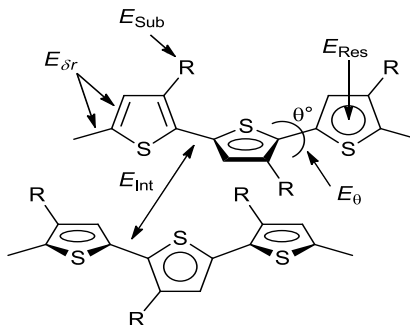
Figure 1.9: Schematic representation of the factors that affect the bandgap of linear π-oligothiophenes.

The term E_{Res} (Res: resonance) is derived from the difference in energy between the aromatic and quinodial mesomeric forms of aromatic rings. The resonance of aromatic systems tend to be confined to the π-delocalisation within the ring atoms, with additional contributions over additional molecular parts, before extending the π-delocalisation along the polymer in order to contribute to the decrease of the band gap. This results in an increase in the conductivity of the polymer. The quinoidal form of the aromatic ring increases the conjugation of aromatic π-electrons along a polymer chain. Therefore, increasing the quinoidal character of the polymer leads to a smaller band gap and a larger conductivity.[46] This can be realised by fusing aromatic rings with different resonance energies, such as benzene and thiophene, resulting in poly(isothianaphtene), PITN.[4] This provokes the dearomatisation of the thiophene ring since localising the aromaticity on the thiophene ring with the larger E_{Res} (here: benzene) leads to a lower total energy of the polymer.[46]

E_{Res} is not independent from E_{BLA} as, for example, changes in the π-delocalisation that alter the resonance energy often also cause changes in the bond lengths and thus affect the term E_{BLA}.[46] The fourth term E_θ accounts for the impact of the orientation of neighbouring aromatic rings on the size of the band gap. The orientation is measured by the mean dihedral angle θ between adjacent aromatic rings. A tilt between those rings

impedes the π-conjugation between their aromatic systems, which decreases the π-conjugation along the polymer and increases the band gap.

Electron-donating and -withdrawing substituents have an additional impact on the band gap of organic semiconductors, which is accounted for in the term E_{sub}. Both types of substituents decrease the band gap E_g. For electron-donating substituents this results from an increase of the HOMO energy level, while for electron-withdrawing substituents the effect is from a stabilization of the LUMO band.[46] The general impact of substituents onto the band gap is, however, rather small.[36, 37]   The four energy terms E_{BLA}, E_{Res}, E_{Sub}, and E_{Θ} explain the band gap of isolated conjugated systems. However, the interaction between individual polymer chains which is influenced by the polymers' packing efficiency in the final semiconducting material also affects the band gap, and is considered as the final term, E_{Int}.[44, 49-51]

1.5   Polymer Preparation

Polyarene systems are often synthesised *via* an iterative approach, using a wide variety of transition metal catalysed coupling procedures including by direct arylation, Kumada, Stille, Suzuki, Negishi or Yamamoto protocols. However, if the monomer forms a stable radical cation at the aryl peripheral edge upon oxidation, then oxidative coupling becomes an option as a polymerisation procedure. Various well-established synthetic procedures for the synthesis of polymers have been reported. Two of these methods that are relevant for this work will be described in detail below.

1.5.1   Oxidative Polymerisation

Oxidative polymerisations can proceed according to different mechanistic routes, which are initiated either by radicals or cations. Figure 1.10 illustrates the mechanism of the oxidative polymerisation of thiophene.[59-63]
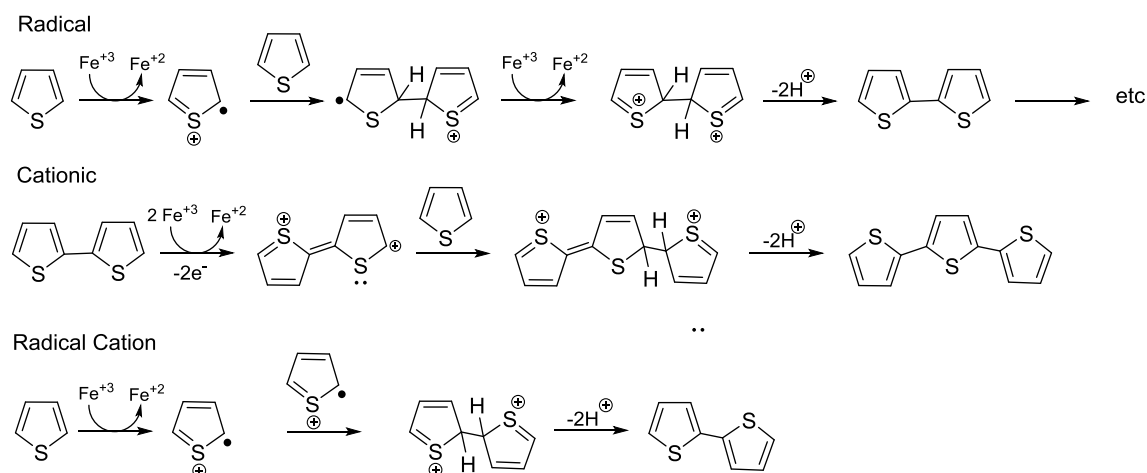
Radical

Cationic

Radical Cation

Figure 1.10: Possible mechanisms of the oxidative polymerisation of thiophene.

Transition metal halides, such as ferric chloride, are the most common reagents used for the oxidative polymerisation of thiophene.[59, 64, 65] However, these reagents lead to purification difficulties after polymerisation. Iron salt impurities can complex as Fe(III) and coordinate to the π-system of the polymer backbone or bond between the S-atoms of the thiophene rings.[64] Such impurities are detrimental for device performances.[64] Alternatively, the use of nitrosonium salts as the oxidant simplifies purification as the NO by-product evolves as a gas.[66, 67] Subsequently, the resultant positively charged polymer is required to be dedoped to neutrality by treatment with hydrazine.[68]

1.5.2 Yamamoto Coupling

The preferred method for the preparation of polythiophenes is typically the Yamamoto coupling approach, as it exclusively yields linear polymers (only two peaks are observed in ^{13}C-NMR) by polymerisation through the 2- and 5-positions.[69] The Yamamoto coupling is the Ni(0)-catalysed cross-coupling of two organohalide derivatives, which was established in the group of T. Yamamoto in 1994.[70] Disubstituted organohalides (e.g., thiophene and benzene derivatives) can undergo dehalogenation polycondensation reactions to yield π-conjugated polymers of high molecular weights.[71] Good yields can be easily obtained even with dichlorinated derivatives, although Cl exhibits the lowest reactivity amongst the halogens (I>Br>Cl). The yield can be further improved by using Ni(cod)$_2$ (cod=cyclooctadiene) instead of Ni(PPh$_3$)$_4$.[72] The relatively

low reactivity of the Ni(0) species allows the preparation of carbonyl and cyano functionalised conjugated polymers.[72]
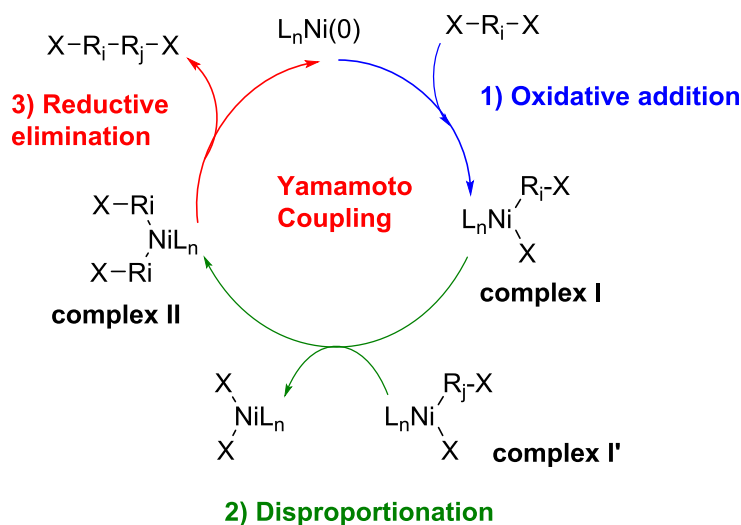
Figure 1.11: Mechanism of the Yamamoto coupling.

The mechanism of the Yamamoto coupling is depicted in Figure 1.11. The first step consists of the oxidative addition of the Ni(0) catalyst species. The resultant **complex I** further undergoes a disproportionation, which is favoured in polar solvents (usually DMF), followed by reductive elimination to give a longer, conjugated polymer end-capped with a halide. Although various types of copolymers can be achieved *via* Yamamoto polymerisation, this reaction is not suited to obtain 'regio-regular' alternating copolymers.[69]

1.5.3 Electropolymerisation

This method requires just a minute amount of monomeric material (a few micrograms) and forms a polymeric film on a conducting substrate. As such, this technique provides a facile strategy of evaluating the electronic and electrochemical properties of a freshly-made polymer film. Polymer films can be easily prepared electrochemically on the surface of a working electrode (anode) by the use of repetitive oxidative cycling of the monomer solution in a supporting electrolyte. Although the polymer cannot be prepared in bulk, in comparison with other chemical oxidative polymerisations the morphology of the electropolymerised film can be easily controlled

by the electro-deposition conditions. In addition it represents a fast, clean and cost effective method with high levels of reproducibility.[73] The film thickness can be adjusted by controlling the number of redox cycles, monomer concentration and scan rate of the experiment.[73-75] Conventional chemical polymerisation techniques require complex procedures with is both costly and time consuming.[76] On the other hand electropolymerisation can produce the polymers in a one-step process.

Electrochemical polymerisation can be performed using galvanostatic, potentiostatic or potentiodynamic techniques.[74] In galvanostatic electropolymerisation, a constant current is applied to the solution, whereas in the potentiostatic technique the potential is maintained constant. The main potentiodynamic technique is cyclic voltammetry, where the potential is cycled in succession between two fixed potential values. Even though, the polymerisation can start at the voltage of the onset of the ionisation potential peak (it is usually the peak at the lowest voltage), the higher potential is usually fixed several hundreds of millivolts higher than the ionisation potential. This method allows the polymer growth to be followed as the polymeric chains show a new developing peak at lower voltage, as a result of the increasing conjugation.[77,78] The formation of a polymer chain is achieved through the combination of cation radicals created during the process of oxidation.[79]

The synthesis of the polymer consists of two steps; initial oligomerisation in solution followed by nucleation at the surface of electrode. Daiz *et al.* has proposed an electropolymerisation mechanism that involves the formation of a radical cation from the monomer molecules followed by their dimerisation to produce oligomers.[80, 81]

X = S, O, NH etc
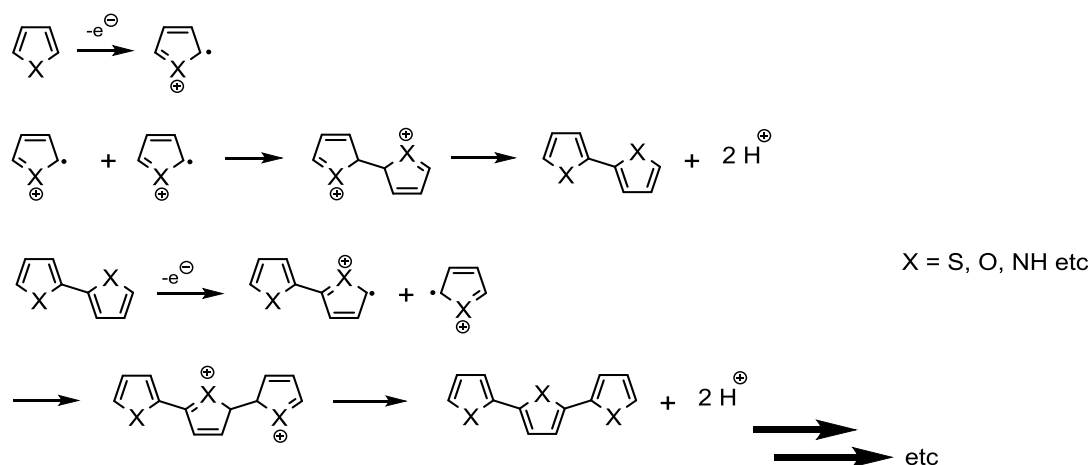
Figure 1.12: Electropolymerisation mechanism of a typical 5-membered aromatic heterocyclic.

The mechanism of electro-deposition of a typical aromatic heterocyclic is depicted in Figure 1.12. The first step describes the oxidation of the monomer solution to form radical cations.[82, 83] The high concentration of radical cations at the electrode surface results in the radical cations dimerising, forming a dication dimer. This electron transfer reaction is generally faster than the diffusion of the radical cation in solution. The dication species then undergoes deprotonation and re-aromatization to produce a neutral dimer molecule. The dimer, due to extended conjugation, is more readily oxidised so oxidises to a radical cation to combine with another radical cation, which again expels two protons to produce a conjugated trimer species. Rearomatisation and subsequent oxidations lead to the formation of the polymer which deposits onto the working electrode surface.[82]

The ionisation potential of the growing polymer is lower than the monomer molecules therefore the electrochemically obtained polymer is always doped. The oxidative electropolymerisation requires stoichiometric values of 2.07-2.5 Faradays/mol. Two electrons are consumed in the oxidation of monomer molecule and the excess of charge is attributed to the doping process.[78]

Figure 1.13: De-doping in polythiophene.

The doped form of a polymer exists with positive charges which are trapped throughout the polymer chain and balanced with a counter anion from the electrolyte. The prepared thin film is then immersed into a monomer free solution and subjected to cycling in a potential region (low V) where the polymer shows no electroactivity. This is termed the de-doping process and is shown in Figure 1.13. [84]
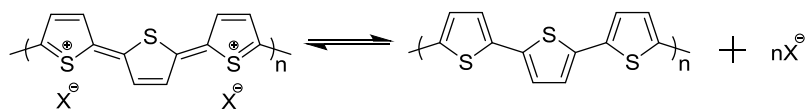
There are several problems which can hinder the growth of polymer during electropolymerisation. Firstly the stability of the radical cation can cause it to diffuse back into the bulk solution. Another problem can arise if the radical cation does not sit at the 2,5-positions of thiophene and thus a typical polymer growth is not achieved. In this regard molecular modelling of the singly un-occupied molecular orbitals (SUMO) of the polymer can be completed to determine the position of the radical. [85]

In addition to the above issues, the α,β-coupling of monomers instead of α,α-coupling can also affect polymer growth. In the former case, a non-conjugated bond is formed between two molecules such that α- or β-position of one thiophene is connected to the either of the β-positions of the other (see Figure 1.14). This can be prevented by blocking the β- positions of the heterocylic unit, thus resulting in only α,α-coupling.
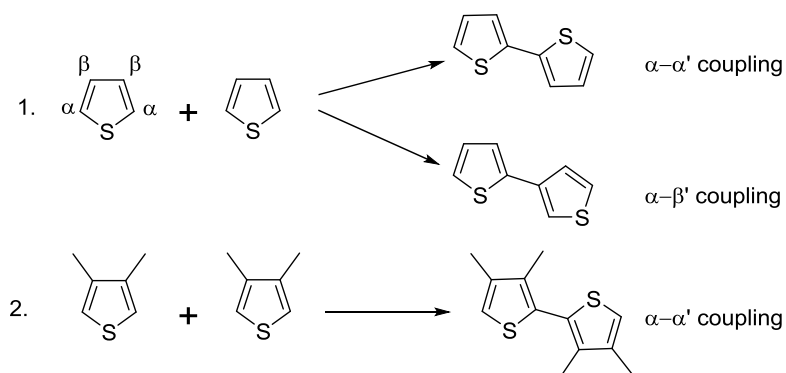
Figure 1.14: Representation of 1) α-β' and α-α' coupling 2) Blocking of β- position to produce α-α' coupling only.

The electro-deposition procedure is highly dependent on the process conditions including the nature of solvent, monomer concentration, temperature of the system and the type of electrodes used in the electrochemical setup. In addition it is also influenced by the nature of the substituents on the monomer molecules. The presence of water molecules in the solvent can cause the formation of carbonyl groups along the polymer backbone. Similarly the electrolyte in the system also plays a key role. During oxidation

the counter anion is bound to the polymer chain for electrical neutrality so the counter anion can also effect and modify the behaviour of the polymer.[86]

1.6 **Analytical Characterisation**

1.6.1 *UV-Vis Spectroscopy*

UV-Vis spectroscopy is a form of absorption spectroscopy where organic molecules absorb radiation of equal or larger energy than their HOMO-LUMO gap resulting in promotion of electrons (excitation) from a lower energy level to a higher energy level. The transition occurs from a filled bonding or non-bonding orbital to a formerly empty anti-bonding orbital. The energy gap is proportional to the frequency of absorption, and so UV-Vis spectroscopy is a source of bonding information. UV-Vis spectroscopy is most important in the structural analysis of compounds containing π-bonds, in particular conjugated systems. [87, 88]

The relation between the wavelength of light and its energy is expressed by the following equation, which indicates that radiation of larger wavelengths is of lower energy (*h*: Planck constant (6.63 x 10^{-34} J s), *v*: frequency of light (in Hz), *c*: speed of light (3 x 10^{8} m s^{-1}), *λ*: wavelength of light (in m)), see equation (1.3). It is worth noting, as the wavelength (λ) increases the energy needed to promote an electron decreases.[87, 88]

$$\Delta E = hv = \frac{hc}{\lambda} \qquad\qquad (1.3)$$

In UV-Vis absorption spectroscopy, a dilute sample solution in a non absorbing glass or quartz cuvette (path length = 1 cm), is exposed to separate beams of UV or visible light of the electromagnetic spectrum. UV or visible light is passed through the sample and the intensity of the transmitted beam (I) is recorded across the wavelength range of the instrument. Firstly, the intensity of the light is recorded against a reference blank cuvette with pure solvent (I$_0$, henceforth determines the intensity of incedent light); the absorbance due to the sample can then be computed as A =log$_{10}$ (I$_0$/I). Upon irradiation with light of the correct energy, absorbance by organic molecules causes electrons to be excited into higher electronic energy levels; hence why the intensity of light passing through sample is reduced. The spectra obtained generally show a broad

and smooth absorbance maxima (λ_{max}) peak without any fine structure. The broadening peak effect is attributed to the presence of discrete vibrational and rotational excitations and also interactions with the solvent molecules that suppress any fine structure of the UV-Vis absorbance. [87, 88]

The feature of a molecule that absorbs the incident light and is responsible for colour formation is called the chromophore. Both the chromophore and the transitions they undergo are classified according to the molecular orbitals involved such as n (non-bonding orbitals containing heteroatom lone pairs), σ (saturated bonds, e.g., C-H), or π (unsaturated π-bonds). Anti-bonding orbitals are denoted by superscript asterisks. [46, 87, 88] The typical forms of ground state orbitals in organic materials that can undergo electronic transitions upon UV-Vis excitation are illustrated in Figure 1.15.
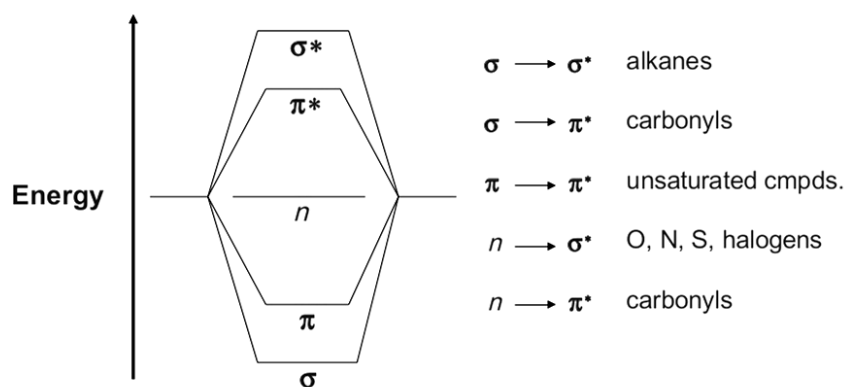
Figure 1.15: Molecular orbital diagram showing possible allowed electronic transitions.

Transitions observed in non-conjugated chromophores (e.g. σ→σ*, n→σ*/π*) are observed at higher energy (low λ_{max}) and are not usually observed in standard UV-Vis spectra.   Though isolated carbon-carbon π-bonds also have a low λ_{max} (~180 nm), conjugated multiple bonds systems, such as conjugated polymers described previously, give rise to a significant bathochromic shift to longer λ_{max} of the π→π* transitions to within the visible region of the UV-Vis spectrum. [46, 87, 88] Moreover, for a comprehensive understanding, one can refer to the Jablonski diagram which illustrates the electronic states of a molecule and all the possible transitions between them.[89]

Increasing the HOMO-LUMO gap of a molecule generally provokes a hypsochromic shift of λ_{max} to shorter wavelengths (higher energy - blue shift), whereas

decreasing the HOMO-LUMO gap causes a bathochromic shift to longer wavelengths (lower energy - red shift). Accordingly, the HOMO-LUMO gap of an organic molecule can be estimated from its UV-Vis absorbance. The HOMO-LUMO gap corresponds to the electron transition at the longest absorbed wavelength, which can be determined from the onset of the absorbance peak at higher wavelengths. The band gap energy E_g can be calculated in electron volts (elementary charge of electron e =1.602 x 10^{-19} C) from the wavelength onset according to the following simplified equation (1.4) given h, c and e are constants (Plank's constant h and speed of light c defined on page 18):

$$E_g = \frac{1240.68}{\lambda} \qquad (1.4)$$

While the absorbed wavelengths are related to the color of an organic molecule, the intensity of the absorbance is related to the concentration of the molecule. Beer's law indicates that the intensity of the absorption is proportional to the number of absorbing organic molecules.[88] This combines with Lambert's law, which states that the amount of absorbed light is independent of the intensity of the light source, to the Beer-Lambert law (A: absorbance, I_0: intensity of the incident light, I: intensity of the transmitted light, ε: molar extinction coefficient (in 1000 mol^{-1}cm^{-1}), c: concentration of the organic molecule (in mol dm^{-3}), l: path length of the sample of absorbing organic molecules (in cm)). [87, 88]

$$A = log_{10}\frac{I_0}{I} = \varepsilon \, l \, c \qquad (1.5)$$

This relation can be employed to calculate the concentration of organic molecules in the respective sample. While the concentration and the path length only depend upon the respective measurement setup, the molar extinction coefficient is a quantitative characteristic of the absorbance properties of the organic molecule at a defined wavelength. These are determined by the nature of the respective electron transitions, as allowed transitions cause intense absorptions and therefore higher values ε than the intensity of forbidden transitions. [87, 88]

1.6.2 Electrochemistry

Electrochemistry deals with electron transfer reactions where electrons are either released (oxidation) or accepted (reduction), where n is the number of electrons lost or gained:

$$\text{Oxidation:} \quad R \rightarrow O + n e\text{-} \quad\quad (1.6)$$

$$\text{Reduction:} \quad O + n e\text{-} \rightarrow R \quad\quad (1.7)$$

Oxidation and reduction are the two half-reactions of a redox reaction, which proceed simultaneously to obey the principle of electroneutrality, but can be carried out at spatially separated electrode/electrolyte interfaces. This generates a current flow between the reactive species, which is guided through the conductive wires that connect the electrodes. The electrical circuit is closed by a conductive electrolyte, which facilitates the movement of charge carriers. An integrated potentiostat allows the application of a specific potential difference to the electrodes and the detection of the current flow between the electrodes. An electrochemical cell can be driven in two oppositional operation modes; in a galvanic cell, electrical energy is generated from spontaneous redox reactions, whereas electrolytic cells are used to trigger non-spontaneous redox reactions upon application of the electrode potential E.[90-92]

The free energy ΔG (kJ mol^{-1}), is related to the concentrations of the oxidised species [O] (mol l^{-1}) and the reduced species [R] (mol l^{-1}) by:

$$\Delta G = \Delta G° + RT \ln \frac{[O]}{[R]} \quad\quad (1.8)$$

Where R is the gas constant (8.314 J mol^{-1} K^{-1}) and T is the temperature (K). The Gibbs free energy and the electrode potential, E (V), of the redox couple are related by:

$$\Delta G = -nFE \qu\quad (1.9)$$

Where n is the number of electrons and F is Faraday's constant (= 96485 C mol^{-1}). The standard electrode potential E^0 is the electrode potential measured against the standard hydrogen electrode (SHE) as the counter electrode. The SHE is a platinized platinum electrode in an acidic solution, which is saturated with hydrogen gas. It establishes the potential of the hydrogen redox couple under defined standard conditions:

$$2H^+ (aq) + 2e^- \rightarrow H_2 (g) \qquad\qquad (1.10)$$
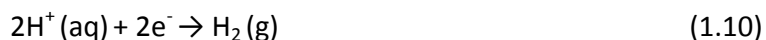
The potential of the SHE is set to zero to define the origin of the electrochemical potential series, which ranks the standard potentials of various redox couples of metals and other electroactive species. The standard potential E^0 of a redox couple is a characteristic value and reflects the ability of an electroactive species to accept or release electrons. Therefore, the electrochemical potential series presents the basis to predict the reactivity between different redox couples.

Electrolytic cells are employed for analytical or synthetic purposes, or for the separation of compounds. Industrially, electrolysis is applied for electrosynthesis, in electrorefining processes, or the chlor-alkali electrolysis. In an electrolysis experiment, typically only one redox couple is studied at the working electrode (WE), whereas any redox reaction of electrolyte molecules proceeds at the counter electrode (CE). WE and CE electrode materials are required to be highly conductive but electrochemically inert in the studied potential window. Typical WE materials are Au, glassy carbon or Pt, whereas Pt wire is often used as CE. The WE interface should be defined and well characterised for obtaining precise analytical information and it can be coated or modified to study the redox activity of solid species, (bio-)macromolecules, or polymers. An additional reference electrode (RE) is usually employed to establish a stable reference potential. An electrolyte is used to allow conduction through the solution in the electrochemical cell, where the electrochemical behaviour of the material depends on the kinetics of the anions and cations produced in the oxidation and reduction processes.[78,93,94] In the cyclic voltammetry system, the potential is applied between the working electrode and reference electrode and the current response is measured between the working

electrode and counter electrode.[94] The data obtained in CV analyses are measured with internal resistance (iR) compensation to avoid any potential drop between working and reference electrodes that can yield an experimental error. [90-92,95]

Non-aqueous electrolytes require the use of quasi-RE's, which employ metal wires, such as Pt or Ag wires. These provide non-defined electrode potentials, which can be calibrated by a dissolved redox couple as an internal standard. To allow a realiable comparison, the electrochemical results are referenced against a stable ferrocene/ferrocenium (Fc/Fc$^+$) redox couple as recommended by IUPAC (Figure 1.16), as it matches almost all of the required criteria:[96, 97]

- the molecule is spherical and has a large radius (not fulfilled in the case of (Fc/Fc$^+$));
- the charge carried by the ions is low;
- the equilibrium between the two redox states is reversible and fast;
- both the oxidised and reduced forms are soluble;
- there is no geometry change of the molecule or ligands in the two redox forms;
- the redox potential is accessible in a wide range of solvents;
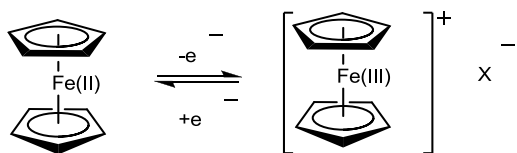- both redox forms are stable.

Figure 1.16: Ferrocene / ferrocenium redox couple (X is the counter-anion).

The Nernst equation describes the impact of the concentration ratios of oxidised and reduced species of a redox couple onto its equilibrium potential E_{eq}, also called Nernst potential, as:

$$E_{eq} = E^0 + \frac{RT}{nF} ln \frac{[O]}{[R]} \qquad (1.11)$$

Where E^0 is the standard electrode potential, which is equal to the individual electrode potential in the standard state. R is the universal gas constant (8.134 Pa m^3 mol^{-1} K^{-1}), T *is* the temperature, *F* is the Faraday constant (96485 C/mol), *n* is the number of moles of electrons transferred in the cell reactions and the concentration of oxidised/reduced species is represented by [*O*] and [*R*].

Voltammetry techniques apply a certain potential function to the WE and measure the generated electrical current *i*. Voltammetric methods differ in the applied potential program and the provided analytical information. They comprise of potential sweep methods, which apply a linear potential/time function, as well as potential-step methods, which apply a series of potential steps to the WE.

Cyclic voltammetry (CV) is the most widely used potential sweep voltammetry technique. It is highly informative with the ability to probe the electronic characteristics of a material at relatively low sensitivity. In a typical CV potential program, the WE potential *E* is linearly changed with a constant scan rate (*v = dE/dt*) according to a triangular-shaped potential/time course.
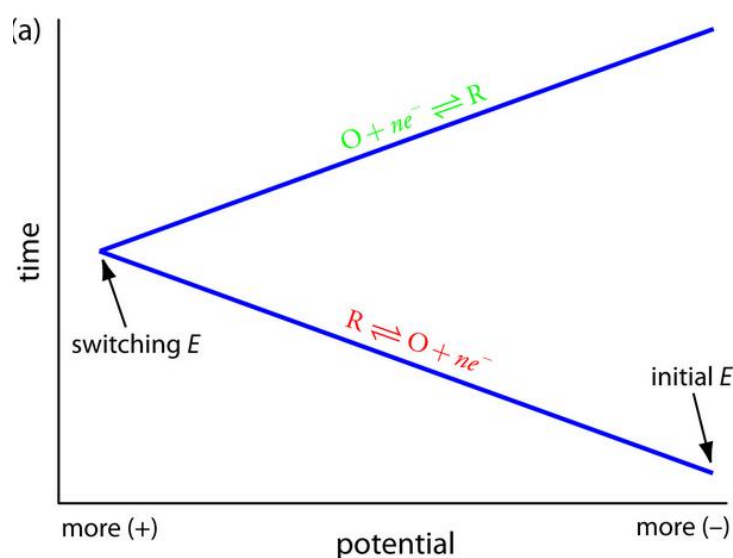

Figure 1.17: Potential sweep form used in CV experiments.

The potential is increased from the initial potential $E_{initial}$ to the switching potential ($E_{switching}$) in the anodic scan with $v = dE/dt$ and then again linearly decreased to return with $v = -dE/dt$ in the cathodic scan to the final value E_{end}. The anodic scan induces the oxidation of any electroactive species with ($E_{eq} + \eta$, *vide* defined) between $E_{initial}$ and $E_{switching}$, whereas the cathodic scan induces the corresponding reduction.

In a cyclic voltammogram, the generated current *i* is plotted against the applied potential *E*. Linear sweep voltammetry (LSV) comprises only the anodic or cathodic potential scan and allows for specifically studying only the oxidation or reduction of an electroactive species. In CV the potential is increased to a certain voltage and subsequently reversed back to the initial value whilst the current response is recorded. This results in a typical CV graph in which the output is in the form of a smooth wave of a current vs. potential plot, Figure 1.18.
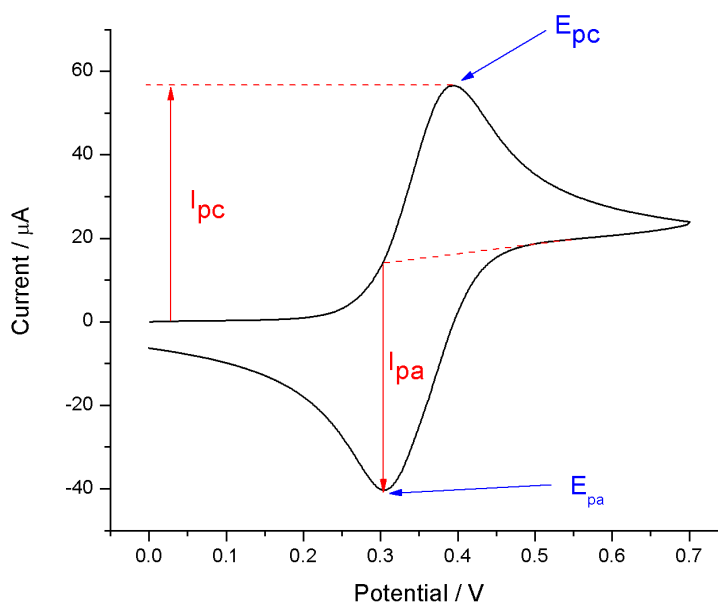

Figure 1.18: Typical cyclic voltammogram graph of current vs. potential.

A cyclic voltammogram provides the oxidation and reduction potentials E_{pa} and E_{pc}, the equilibrium potential E_{eq} (= ($E_{pa} + E_{pc}$)/2), the overpotential η (= E_{pa} - E_{eq}), the current ratio i_{pa}/i_{pc}, and the transferred electrical charge *C* as primary information about

the studied electroactive species. The simplest case of a fully-reversible, one-electron transition of a diffusing redox couple is, for example, characterised by a current ratio of i_{pa}/i_{pc} = 1 and a peak-to-peak separation of 2η = 57 mV. [90, 91, 98]

CV also provides information about energy levels of the frontier orbitals of an electroactive species. The electrochemical band gap is the difference of the onset of oxidation and reduction peaks in the CV. Substraction of the onset of oxidation and reduction from the HOMO of ferrocene (-4.8 eV) gives the HOMO and LUMO levels of the material, respectively. [96, 99, 100]

1.6.3   Spectroelectrochemistry

Spectroelectrochemistry combines both spectroscopic and a linear sweep voltammetric technique to elucidate the changes in electronic transitions during redox switching of a material. It also reveals the specific properties of the conducting polymer like the band gap and the intermediate states that appear during doping and de-doping in conjugated polymers. Although various spectroscopic techniques can be included in spectroelectrochemistry, the most commonly employed is UV-Visible spectroscopy. This technique involves the electrolysis of the materials with simultaneous or subsequent *in situ* spectroscopic investigations. The electrochemical cell is a three electrode assembly as in the cyclic voltammetry experiment, however the cell is fitted into the cuvette holder of the UV-visible spectrophotometer.[90, 92, 101] Chapter 6.3.1 describes experimental setup of both solid and solution state spectroelectrochemistry.

The experimental results are shown on a 2D graph where the individual scans at different voltages are plotted along with absorbance vs. wavelength plots. They can also be shown on a 3D plot with wavelength, absorbance and potential plotted on x, y and z axis respectively.

1.7 **Chromism**

Chromism is the reversible change of a substance's colour induced by an external stimulus – a phenomenon that is expressed by several inorganic and organic compounds. The applied stimulus alters the electron density of the material by disrupting its π- or d-electron state, which changes the interaction with light/electromagnetic radiation and causes the observed changes in the material's absorption characteristics.[14, 37, 102]

The main chromogenic technologies that exert a reversible colour change are classified according to the applied stimulus, as summarised in Table 1.1.

Table 1.1: Overview of chromogenic technologies.[14, 37]

Chromogenic Phenomena	Stimulation	Example materials	Application
Thermochromic	Heat induced	Transition metal oxides, e.g., VO_2, organic thermochromic inks	Aerospace surfaces, heat change indicators
Photochromic	Electromagnetic radiation	Metal oxides, titans, minerals, disulfoxides, camphor, pyrroles, etc.	Photography, displays OLEDs, chemical switch for computers
Electrochromic	Electrically induced redox reactions	Prussian Blue, transition metals WO_3, viologens, poly-pyrrole, PEDOT, etc.	Displays, smart windows, optical filters, computer data storage
Solvatochromic	Solvent polarity gradient	Metal complexes, poly(3-alkylthiophene)	Study of crystallinity in polymers
Halosolvatochromic	pH environment	Phenolphthalein titanium dioxide	End-point indicator in acid-base titrations
Ionochromism	Ions induced	M=H, phenols, aromatic amines	Non-destructive readout (write and erase)
Piezochromism	Mechanical pressure	Diphenylfulvene	Chemical plants safety

1.7.1   *Electrochromism*

Electrochromism is the colour change (evocation/bleaching) of a material as a result of an electron transfer reaction (reduction/oxidation). In practical applications of an electrochromic material, its optical properties are changed reversibly by increasing or decreasing an applied small voltage.[92, 103, 104]   Most electrochromic devices display a colour change from a single transparent state to a dark-coloured state or vice versa, although an initially coloured state could also transform into another coloured state due to a redox transition. If an electrochromic material exhibits more than two redox states, allowing for optical transformations between multiple colours, the related phenomenon is referred to as polyelectrochromism.[105]

The interest in electrochromic materials is promoted by their vast applications in smart mirrors, windows, and displays.[103] Desirable electrochromic properties for these applications are a high colour contrast between two optical states, a high response time and stability over repeated redox cycles. The first application of electrochromic materials was in display screens, such as clocks and calculators. However, with the advent of liquid crystal displays, their applications in this area became limited. In contrast, the future of electrochromic devices is still prominent in other applications such as airplane windows where manually operated windows are replaced by electrochromic ones allowing the passenger to block the sunlight just by pushing a button.[34]

Pioneering electrochromic materials include transition metal oxides, such as WO_3,[37] which find applications as smart windows for substituting curtains and blinds in corporate buildings.[34]   Common organic electrochromic compounds, such as thiazines and viologens, are employed in rear view mirrors of vehicles to attenuate headlight flashes of cars following behind.[37, 106]   Other important electrochromic materials are inorganic complexes, such as Prussian blue,[107] as well as conjugated polymers. Depending on their molecular design, conjugated polymers can act as cathodically or anodically colouring materials. A cathodically colouring polymer exhibits a colour change upon the insertion of ions, while an anodically colouring polymer exhibits a colour change upon the abstraction of ions.[108, 109]

1.7.2   Organic electrochromic Materials

Many organic compounds possess different oxidation states, characterised by their distinct electronic absorption spectra, and can thus also be denoted as electrochromic. Organic compounds have an edge over other electrochromic materials due to following attributes:

- An extended colour palette[110]
- The colour of different redox states can be tuned by structural modification[111]
- They can be easily processed to form thin films[112]
- Cost effective[113]

Due to these reasons, organic compounds are widely investigated for application in electrochromic devices. Organic compounds can mainly be classified as type I or type II electrochromic materials depending on whether one or both redox states are soluble in the electrolyte.[114] Electrochromic materials of type I are solution electrochromes in which the coloured species is dissolved in the electrolyte. Electrochromic materials of type II are solution-solid electrochromes, i.e., the colourless reactants are dissolved but form a coloured solid on the electrode surface during the electron transfer reaction.[92] Many organic electrochromic materials belong to type I or type II, e.g., viologen, quinone's, etc.[92, 115]   A third class, type III electrochromic materials, comprise electrochromes that are solid in all redox states.[92, 115] These solid state materials are considered to be the most interesting class of electrochromic materials, since they can be employed as solid-state electrochromic devices using a polymeric electrolyte. They demonstrate high memory effects and cycle lives.[115]   Typical examples of type III materials include conjugated polymers and metallated phthalocyanines.[92, 115]

1.7.2.1 Viologens

Viologens are 1,1-disubstituted-4,4-bipyridinium salts, which can be obtained by the quaternisation of 4,4-bipyridyl.[116] The redox states of viologens are shown in Figure 1.19. Among these three states, the colourless dication is the most stable one. The reduction of viologen dications produces coloured radical cations whose stability depends on the delocalisation of the radical electron in the bipyridyl π framework and the partial localisation of charge on the substituents.[116]
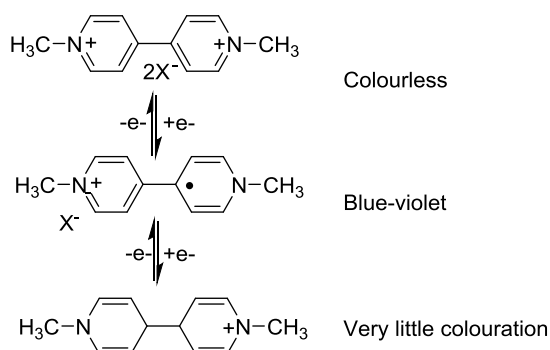
Figure 1.19: The interconversion of three redox states of viologen.

The substitution of the nitrogen atoms by various alkyl or aryl groups allows the colour modulation of radical cations to some extent.[116] It is to be noted that the colour intensity of fully reduced viologens is low owing to the absence of optical charge transfer or internal transitions in the visible range.[116]

The system explained above is employed in commercial *Gentex corporation mirrors* where a substituted viologen functions as a cathodically colouring material, while phenylene diamine acts as an anodically colouring material.[114] The colour switching of such a mirror results from the voltage-induced migration of charged species to the oppositely charged electrodes. After the initiation of this dual-electrochromic colouration process, the formed product diffuses away from the electrodes into the intervening solution and restores the original un-coloured species by a mutual reaction. Thus, a small voltage application is necessary in order to retain a constant colour of the electrochromic device.[114]

A recent study reported three new viologen compounds containing 1,1-di-*n*-heptyl-4,4'-bipyridinium dibromide, 1-heptyl-4-(4-pyridyl)pyridinium bromide, and 1,1'dis-(p-cyanophenyl)-4,4'-bipyridinium chloride for a colour electronic display application.[117] The addition of ferrocene to the electrolyte solution was shown to enhance the repetitive stability of all three electrochromic cells. A reversible colour change was observed from clear to red, green, and blue due to the electrochemical reduction of the three compounds in indium tin oxide sandwich-type cells. The mixture of three viologens was employed to build a multiviologen cell, and a multicolour change was observed under different applied voltages.[117]

1.7.2.2 Conjugated polymers

Another class of electrochromic materials are conjugated polymers. Common electrochromic polymers include polythiophene,[118, 119] polypyrrole,[120] and polyaniline.[121] They are well known for their rapid response time and high optical contrast.[110, 111, 122-126] These conducting polymers are a fascinating examples of electrochromism, as their optical properties can be tuned for absorbing in the UV-visible, IR, or NIR by modification of their chemical structure.[126] They are mostly used in the form of thin films that change their colour and absorption in the aforementioned spectral regions. Doping of neutral conducting polymers with counter anions leads to the formation of polarons/bipolarons and ultimately results in structural transformation to a delocalised, quinodial state.[127] The main absorption band of neutral conjugated polymers lies in the UV-visible region originating from $\pi \rightarrow \pi^*$ transitions. On the other hand, the low–energy, bipolaronic transitions are associated with absorption peaks at higher wavelengths.[127]

Thin films of the pristine polymers with band gaps greater than 3 eV are colourless, whereas their doped forms are coloured due to absorptions in the visible region of the spectrum. This is contrary to the lower-band-gap polymers (E_g = 1.5 eV) possessing a coloured neutral state and a colourless or faintly coloured doped state due to the shift of the absorption bands to the NIR region.[127] A fundamental advantage of conducting polymers is that their spectral properties can be easily modified by subtle structural modifications of the monomer, allowing a facile colour tuning of the material.[17, 128] This can be achieved in various ways such as modifying the HOMO/LUMO energy levels of the polymer building blocks, modulating the backbone planarity using sterically hindering substituents, varying the conjugation length of the system, and incorporating donor-acceptor systems in the repeat units. A detailed review on the colour tuning of conjugated polymers using different approaches has been published by Reynolds *et al.*[129] Therefore, the forthcoming sections will cover only the most representative examples.

1.7.2.2.1 Polyacetylene

The simplest conductive polymer is polyacetylene, which comprises only a chain of C-atoms with alternating single and double bonds. It was synthesised by Natta *et al.* in 1958 as a black powder and exhibited semi-conductor properties and an electric conductivity depending on the method of processing and structural manipulation.[1,12,13] In 1970, Shirakawa accidently synthesised a silvery film of free-standing polyacetylene with semiconductor-like properties. The low conductivity of undoped polyacetylene could be impressively enhanced by oxidative doping with iodine.[1,12,13] However, incorporation into device applications were limited due to a poor solubility, intractability and air sensitivity.[130,11]

1.7.2.2.2 Polyaniline (PANI)

Another early conjugated polymer is polyaniline, also known as aniline black.[131] An important benefit of polyaniline is that it's electrical and electrochromic properties can be controlled by not only the oxidation states, but also the protonation state of the material. This enables the use of both electrochemical and chemical routes for the preparation of the desired compounds.[132] Thin films of polyaniline exhibit polyelectrochromism, changing their colour from the transparent, insulating leucoemeraldine form to the yellow-green, conducting emeraldine state and then to the blue-black pernigraniline form, as illustrated in Figure 1.20.[132]
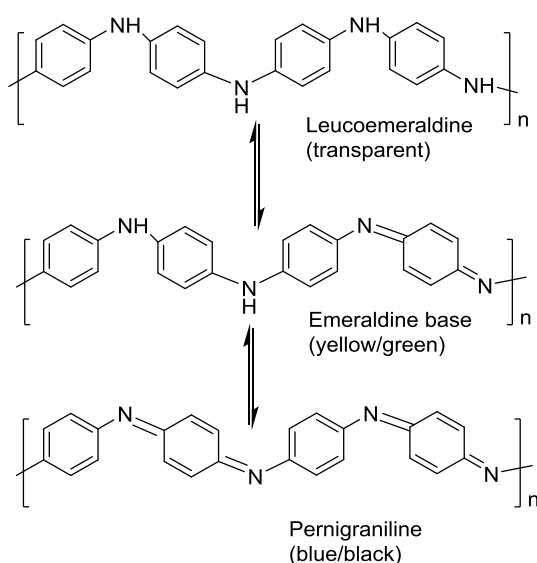

Figure 1.20: Transition between different redox states of aniline.[132]

Electropolymerisation is an adequate procedure for the production of thin films with a small surface area, while other methods have to be considered for the generation of large surface areas.[112] In this regard, efforts are devoted to the synthesis of soluble conducting polymers, e.g., poly(o-methoxyaniline), which can be deposited as thin film by casting from solution.[112] A large surface area coating has been obtained using a novel approach in which polyaniline was incorporated into a polyacrylate silica hybrid sol-gel network and then spray-brushed on the ITO substrates. Polyacrylate possesses silane groups, which improve the surface adhesion and thus the mechanical properties of the coatings.[112]

Various substituted polyaniline (PANI) derivatives are also studied as electrochromic materials. For example, polymers obtained by the polymerisation of *o*- and *m*-toluidine were found to exhibit an increased stability compared to polyaniline. The functionalisation of polyaniline with methoxy, methyl, and hydroxymethyl groups has been studied by D'Aprano *et. al.*[133] They observed that both *o*-methyl- and *o*-methoxy-functionalised monomers undergo electrochemical polymerisation at lower potentials than aniline. In addition, these monomers exhibit a red shift in their absorption maxima caused by the electron-donating effect of the methoxy group. A reduction of the band gap is reported for 2,5-dimethoxyaniline, which has a λ_{max} at 350 nm. Furthermore, the aqueous electropolymerisation of poly(*p*-styrene sulfonate) (PSS) along with ammonium persulfate yielded water dispersible PANI-PSS nanoparticles with an average diameter of 25-30 nm.[134, 135]

Polyaniline is employed in various electrochromic devices in combination with Prussian blue and WO_3. Electrochromic smart windows are a well-known application of such hybrid materials. The use of two electrochromes in one device results in better cyclic stability, retaining 90% of the initial performance even over 3700 cycles.[136]

1.7.2.2.3 Polycarbazoles

A thin film of an unsubstituted polycarbazole can be prepared by anodic polymerisation, which characteristically produces reversible yellow to green optical transitions upon p-doping at low potentials.[137] Polycarbazoles that are functionalised at the N-position exhibit hypsochromic shifts in the absorption spectrum of their parent structure. Chevrot *et al.*[138, 139] have reported colourless to green-blue transitions for both

N-butyl- and N-dodecyl substituted derivatives. Furthermore, N-oligoether-functionalised polycarbazoles demonstrated impressive cyclic stability, retaining 90% of their initial charge density even over 7000 cycles in acidic aqueous medium.[139]

Bezgin *et. al.* recently investigated the carbazole analogue fluorene.[140] Thin films of poly(9-fluorenecarboxylic acid) prepared electrochemically in $BF_3 \cdot Et_2O$ displayed a high colouration efficiency of 232 cm^2/C and a wide band gap of 3.1 eV. The polymer exhibited a colourless to orange-brown transition upon p-doping. It was then employed in a dual electrochromic device in combination with PEDOT having a dark-blue to colourless transition.[140]

1.7.2.2.4 **Polythiophenes**

Polythiophene was first synthesised in 1980 using electrochemical or chemical polymerisation.[69, 141] The red-coloured, neutral polythiophene film shows a transition to dark blue in the oxidised form, which is accompanied by a bathochromic shift of λ_{max} from 430 to 730 nm. The interconversion of redox states is displayed in Figure 1.21.
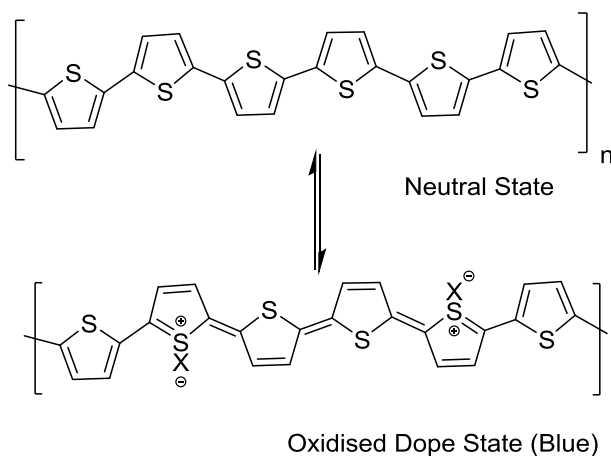
Figure 1.21: Interconversion of the electrochromic states of polythiophene.

Despite of the attractive colour changes, the stability of the material poses a problem as it starts to degrade at the potential required for polymer formation. This results in the formation of over-oxidised, non-electroactive material.[142] The stability of polythiophene is improved in various substituted polythiophene derivatives and further produces easily processable materials. Alkyl, alkoxy, or aromatic chains can be employed

to substitute thiophene in 3,4 position, producing highly soluble polymers with variable optical and electrical properties (see Figure 1.22 and Table 1.2).[74]

Figure 1.22: Chemical structure of 3,4-substituted thiophene.[74]
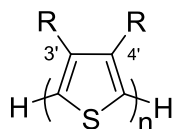
The incorporation of various substituents alters the electron density of thiophene, which affects the reactivity. The oxidation potentials of substituted thiophene derivatives are linked to the Hammet substituent constants. Thiophene monomers substituted with strong electron-withdrawing groups, such as carboxylates, aldehydes, cyano, and nitro functionalities, tend to have higher oxidation potentials (+0.5-0.7 eV) than thiophene. It is worth noting that thiophene derivatives with high oxidation potentials are unlikely to undergo anodic electropolymerisation.[31, 44, 143] Halogen-substituted monomers are also difficult to electropolymerise and yield very poor electron conductive polymers. Electron-donating groups, such as halogens, are known to lower the oxidation potential by stabilising the corresponding radicals.[29, 144] The generated radicals can further diffuse away from the electrode surface to form soluble oligomers in solution. Early attempts to electropolymerise 3-(methylthio) thiophene, 3-(ethylthio) thiophene, and 3,4-bis(ethylthio) thiophene were unsuccessful, as they led to the formation of soluble oligomers.[82]

PMT
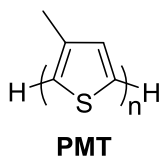
Figure 1.23. Poly(3-methylthiophene).

A derivative of polythiophene is poly(3-methylthiophene) (PMT), which is purple in its neutral form with an absorbance maximum of 530 nm.[145] Introducing an electron-donating methyl group at the 3-position of thiophene lowers its oxidation potential compared to the parent polythiophene.[82] The presence of methyl groups on the thiophene ring decreases the number of non-conjugated α-β' couplings, increases the conjugation length of the polymer chain, and improves the polymer's electronic

conductivity (PMT energy gap: 1.9 eV).[92] The oxidation of PMT shifts the absorbance maximum to induce an optical transition from red/yellow in its reduced from to pale-blue in its oxidised form.[146] This can be explained by the alteration of the polymer's effective conjugation length due to occupation of various backbone positions by methyl. This tunability of optical absorbance by functionalising the 3,4-position of polythiophene is an important aspect of conjugated polymers. Although a slight increase of the chain length at the 3-position does not cause a significant change in the electrochromic properties, it is beneficial for improving the solution processability of the material.[147] However, chemically synthesised PMT was found to be insoluble. This led to the investigation of poly(3-alkylthiophenes) (PAT) derivatives, substituted with longer alky chains, which exhibit an improved solubility.[74, 92, 148]

Elsenbaumer *et al.* first reported the chemical and electrochemical preparation of PATs. They reported that polymers with alkyl chains longer than butyl could readily melt or be solution-processed into thin films. These materials demonstrated high electrical conductivity in their oxidised forms.[56]

Arbizzani *et al.* investigated the effect of regioselectivity on the electrochromic properties of polythiophenes.[149] They synthesised poly(3-hexylthiophene)s, having a pale–green colour in the reduced form, by the electropolymerisation of 3,3'- and 4,4'-dihexyl-2,2'-bithiophenes. The replacement of organic solvents by Lewis acids assists in improving the film quality. Recent studies have shown that poly(3-hexylthiophene) is superconducting below 2.4 K due to its ability to self-organise polymer chains into closely packed structures.[56] However, steric problems are encountered when two adjacent units are in a 'head-to-head' conformation. The hexyl groups force the thiophene units out of co-planarity, which results in a reduction of the effective π-orbital overlap and the level of conjugation in the polymer chain.[150, 151]

Steric hindrance in a polymer affects the system's electronic properties. It was initially thought that disubstitution at the β-β' position would retain a stereo-regular conformation, since only α-α' positions were available for coupling.[149] However, polythiophene experiences chain distortion and disruption in conjugation due to the presence of two bulky substituents. These polymers have higher oxidation potentials

(and lower conductivities) than the mono-substituted polythiophenes and are also more difficult to polymerise.[152, 153]
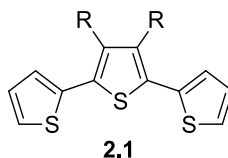

2.1

Figure 1.24: Terthiophene monomer with a 3,4-disubsituted thiophene unit.

Another approach to reduce steric hindrance is to incorporate a 3,4-disubsituted thiophene unit into a terthiophene unit (structure **2.1**; Figure 1.24). This conformation dilutes the steric effect of substituent groups in the resulting polymer, since the side chain fragments will be adjacent to non-substituted thiophene rings.

EDOT   **EDTT**
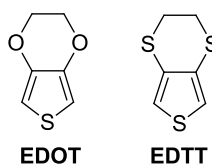
Figure 1.25: Chemical structures of 3,4-ethylenedioxythiophene (EDOT) and 3,4-ethylenedithiothiophene (EDTT).

Alternatively, to overcome the above disubstituted problems, various electron-donating substituents (thiol, alkoxy, and alkyl groups) can be introduced into the thiophene backbone in order to manipulate the band gap and the electrochemical and conductive properties of the material.[150, 152, 153] Alkoxy– and alkylthio-substituted thiophenes experience a large electron-donating effect due to a π-resonance contribution of the heteroatoms, which lowers the material's oxidation potential raising its HOMO and LUMO levels. Steric problems can be reduced by connecting the side groups on the thiophene backbone by cyclisation, as in the case of 3,4-ethylene dioxythiophene (EDOT) or 3,4-ethylene dithiothiophene (EDTT), see Figure 1.25.[150, 154, 155]

PEDOT

Figure 1.26: Structure of poly(3,4-ethylenedioxythiophene) (PEDOT).

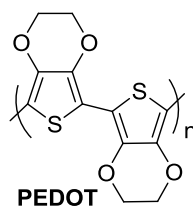PEDOT was first synthesised in the late 1980s by Bayer AG research laboratories in Germany by polymerising EDOT (see Figure 1.26). It has a low optical band gap of 1.6 eV and shows an optical transition from deep blue to light blue upon oxidation.[156] The reduced electrochemical band gap is attributed to the non-covalent, S-O chalcogen interactions, which force the polymer into a planar configuration and, in consequence, increase its effective conjugation length.

PEDOT absorbs in the red region (578 nm) due to the presence of two electron donating ethylene dioxy groups pushing electron density onto the frontier orbitals of the thiophene's π-system. The significance of this compound is related to its high conductivity in the oxidised form (*ca.* 300-550 S cm^{-1}),[157-159] its stability at high temperature and humidity, and processability even in water. The high conductivity of thin films of tosylate-doped PEDOT can be explained by its paracrystalline structure; given hardly any amorphous scattering was observed x-ray diffraction studies. Amorphous regions create insulating barriers and limit the conductivity of conductive polymers.[160]

PEDOT bears the drawback of being a relatively insoluble material, but it possesses very interesting optoelectronic properties; it is blue in the neutral state, whereas it bleaches to a colourless state upon oxidation, absorbing in the NIR.[114,148] A breakthrough regarding PEDOT's processability was the development of a PEDOT:PSS complex, which is a water dispersion of PEDOT stabilised by poly(styrene sulfonic acid). However, in electrochromic devices, PEDOT is preferred over PEDOT:PSS due to easy de-doping of the former. The synthesis of soluble, long-chain PEDOT (-C$_8$H$_{17}$, -C$_{14}$H$_{19}$) was followed by a large number of PEDOT derivatives with attached solubilising chains.[161-165] The appended chains were also proved to greatly enhance the cyclic stability of the materials. For example, PEDOT-C$_{14}$ was able to withstand 16000 cycles while retaining 60% electroactivity as compared to 65% of pristine PEDOT upon 6000 cycles.[164]

The attractive properties of PEDOT led to a wide range of applications, e.g., as antistatic and electrostatic coatings for metallisation of insulators and electrodes for capacitors or photodiodes.[30, 38, 49, 56] An enhancement of the durability of the capacitors using PEDOT would increase the range of applications about, e.g., electronic circuits for

cars and man-made satellites. The ability of PEDOT to easily switch between an absorptive and a transmissive state at low oxidation potentials makes it a useful material for electrochromic applications, optical displays, OLEDs, photovoltaic cells, and sensors.[44, 45, 153, 166, 167]

In developing a structure relative to EDOT, Kanatzidis[168] and co-workers first reported the synthesis of EDTT from thieno[3,4-*d*]-1,3-dithiole-2-thione **2.5A** (see Figure 1.27). EDTT is the sulfur analogue of EDOT where the oxygen atoms in the ethylene bridge are replaced by sulfur atoms.

2.5A   EDTT
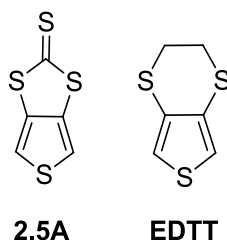
Figure 1.27: Structure of 3,4-ethylenedithiothiophene (EDTT).

Poly(3,4-ethylenedithiothiophene) (PEDTT) can be synthesised from its monomer EDTT (see Figure 1.27) by chemical polymerisation in the absence of solvent under ambient conditions.[169] Although the structures of PEDOT and PEDTT only differ by the chalcogen atoms residing in the ethylene bridge (see Figure 1.28), they exhibit a large difference in their optical and electronic bandgaps (E_g = 2.2 eV for PEDTT *c.f.* 1.6 eV of PEDOT).[168, 170] PEDOT is believed to be planar, but its analogue, PEDTT, is assumed to be twisted (see Figure 1.28).[171, 172]

PEDOT   PEDTT

Figure 1.28: Polymers of EDOT and EDTT (anti conformation).

PEDOT self-assembles in an anti-conformation through intra-molecular S—O chalcogen interactions, which enhances the effective conjugation length of the polymer chain.[169] In contrast, S—S interactions between the sulfur atoms of thiophene and the ethylene bridge of PEDTT do not 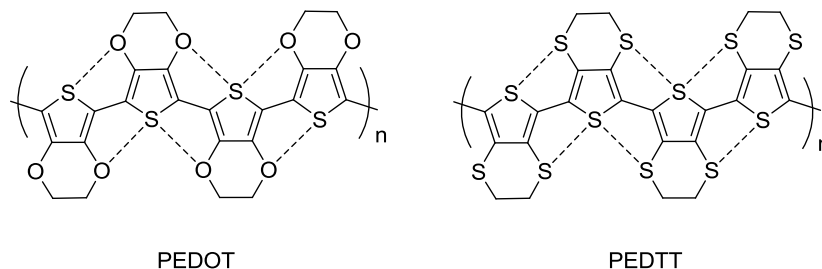support coplanarity between repeat units, which limits the effective conjugation length. Steric hindrance in PEDTT distorts the units with respect to each other. This causes a twist in the chain conformation, hindering electron delocalisation and increasing the band gap and the material's oxidation potential.[173]

The large difference between the optical and redox properties of the two polymers is a consequence of their conformations rather than the inductive resonance effects of the chalcogen substituents. Cyclic voltammetry of the solution state reveals a 20 mV lower oxidation potential for EDTT than for EDOT, which can only be explained by the larger and stronger electron-donating sulfur atoms. However, in their polymeric forms, PEDTT has a 780 mV higher oxidation peak than PEDOT.[172]

In summary, the extensive S—O interactions between repeat units in PEDOT rigidify the polymer, induce a pseudo-ribbon type structure, enforce planarity, and reduce the band gap. The present oxygen atoms impart inductive properties to PEDOT, which stabilise the generated radical cations and cause a much lower oxidation potential compared to the sulfur-analogue PEDTT.[172] Hence, in the solid state, the absorption maximum of PEDOT is bathochromically shifted by 137 nm with respect to that of PEDTT. The oxygen atoms of the dioxy-bridge exerts an electron-donating effect and lowers the reduction potential of PEDOT.[168, 170, 172, 174] Furthermore, the spectroelectrochemical properties, especially the transparency in the doped state, render PEDOT an attractive material for electrochromic applications,[175] whilst PEDTT absorbs in the visible region despite the application of a continuous oxidation potential.[169]

1.7.3 Coploymers

Copolymerisation of monomers is an important strategy for improving the electrochemical, optical, and electrochromic properties of the parent homopolymers.[168, 176-179] Furthermore, the challenges of reducing the band gap (E_g), shortening the switching time, boosting the electrical capacity, increasing the stability, and improving

the solubility are addressed by using substituents and co-repeat units to adjust the HOMO and LUMO energy levels of the π system.[174-177]

Within the Skabara group, copolymers of EDOT and EDTT have been investigated, which retain the absorption characteristics of PEDOT, as long as the EDTT:EDOT ratio does not exceed 1:2. Beyond this ratio, the continuous S—O chalcogen interactions lead to a mimicking of PEDTT characteristics (i.e., EDTT-EDOT-EDTT (SOS) analogues). One such copolymer is POSO, which is based on a terthiophene unit composed of the motif EDOT-EDTT-EDOT (OSO) and can be easily synthesised by a Negishi cross-coupling (see Figure 1.29).[172]
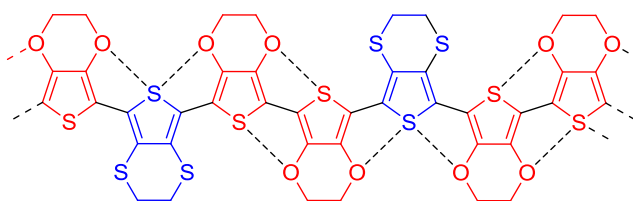

Figure 1.29: POSO copolymer of EDOT and EDTT with a 2:1 ratio.[169]

Despite the fact that the POSO copolymer has fewer O—S interactions than PEDOT, it still retains a planar configuration. Spectroscopically, POSO shows a small (25 nm) hyposochromic shift in the absorption maximum in comparison with PEDOT. The minor band gap difference between PEDOT and POSO (E_g = 1.35 eV *c.f.* 1.47 eV, respectively) is due to the influence of sterically demanding S—S interactions in POSO, inflicting a slight disparity in planarity and therefore restricting its effective conjugation length.[172] This shows how the planarity of PEDOT can be maintained by only a small dilution with EDOT units. The assembly of EDOT units within PEDOT works only if long-range coplanarity is retained with effective S—O interactions (1:2 ratio). POSO permits this and results in only subtle changes in its HOMO-LUMO levels with respect to PEDOT.[169]

Furthermore, 3,4-(ethylenedioxy)selenophene (EDOS) is a selenium analogue of EDOT. PEDOS, the polymer of EDOS, was electrochemically synthesised by Bendikov *et al*. EDOS is more electron rich and has a lower oxidation potential than EDOT. As a consequence, PEDOS possesses a lower band gap than PEDOT. In addition, PEDOS and its derivatives are known to exhibit interesting electrochromic properties. For example,

PEDOS-C$_6$ has a high contrast ratio, cycling stability, and a large colouration efficiency compared to PEDOT derivatives.[180-182]

Table 1.2 enlists the band gaps and colours of poly(thiophenes) and its derivatives in different redox states.

Table 1.2: Band gaps and coloured states of polythiophene and its important derivatives.

Polymers	Neutral state	Oxidised/Reduced	Band gap (eV)
Poly(thiophene)[183, 184]	**Red**	**Blue** (reduced)	2.20
Poly(3-methylthiophene)[145]	**Purple**	**Pale blue** (oxidised)	2.34
Poly(3,4-ethylenedioxythiophene) (PEDOT)[185]	**Blue**	**Colourless** (oxidised)	1.6-1.7
Poly(3,4-ethylenedithiothiophene) (PEDTT)[86]	**Golden yellow**	**Pomegranate** (oxidised)	2.2
Poly(3,4-(ethylenedioxy)selenophene) (PEDOS)[180]	**Deep blue**	**Transmissive grey** (oxidised)	1.4

PEDOT derivatives with expanded alkylene bridges have been evaluated for their electrochromic properties. They are either cathodically and/or anodically electrochromic materials and hence allow the construction of dual polymer ECDs. Examples of two such derivatives are displayed in Figure 1.30.
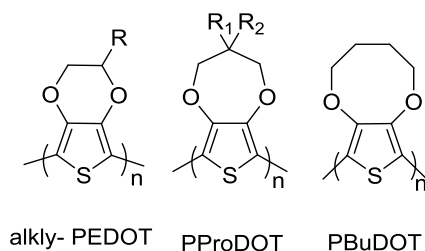

Figure 1.30: Examples of PEDOT derivatives with expanded alkylene bridges.

An extended investigation of the influence of the bridge size was carried out by Reynold *et al.* who electrochemically observed an enhancement of the redox properties upon replacing the ethylenedioxy bridge with propylenedioxy (PProDOT) or butylenedioxy (PBuDOT).[186] In addition, these derivatives exhibit higher contrasts and shorter switching times, which is attributed to the facile diffusion of counter ions due to the open morphology of larger bridges.[128] The stability of the compound is also affected by incorporating methylene bridges into EDOT. This is due to the disruption of the co-planarity of the ring system compared to the aromatic centre, which alters its electron donating effect. In this way, a greater stability is induced owing to the lowering of the HOMO relative to the air-oxidation threshold. Fascinated by their properties, a large number of PProDOT derivatives has been synthesised by Reynold *et al.*, and their electrochromic films were deposited by spray casting. It was also observed that the electrochromic contrast could be improved by increasing the length of alkyl substituents. For example, dibutyl-substituted PProDOT-Bu$_2$ exhibits a contrast of 51%, which increased to 79% for bis(2-ethylhexyl)-substituted PProDOT-EtHex$_2$.[187]

1.7.4   *Hybrid Polymers*

The electron donor ability of polyheterocyclic systems incorporating fused 1,4-dithiin units has been studied within the Skabara group. Two such interesting examples include thieno[3',4':5,6][1,4]dithiino[2,3-b]quinoxaline **9**[188] and the polymer of its terthiophene analogue 1,3-di-2-thienylthieno[39,49:5,6][1,4]dithiino[2,3-b]quinoxaline **Poly1**, see Figure 1.31.[189] An appealing feature of these materials, centres on the non-planar contribution of the 1,4-dithiin species.[188-190]
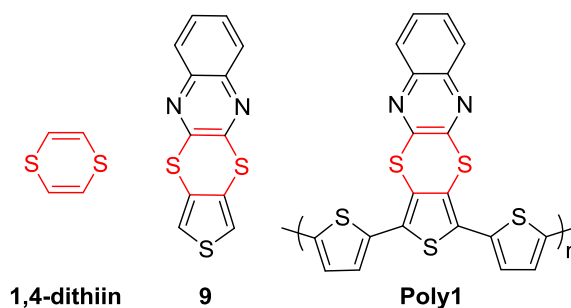

1,4-dithiin   9   Poly1

Figure 1.31: Structures of 1,4-dithiin ring, thieno[3',4':5,6][1,4]dithiino[2,3-b]quinoxaline **9**[189] and terthiophene polymer Poly1.[190]

43

The 1,4-dithiin ring is an eight π-electron heterocycle that usually adopts a boat conformation with folding along the S--S vector. The molecular structure of compounds containing 1,4 dithiin moieties, undergoes a significant change from a boat conformer to a planar system upon oxidation, yielding a fully aromatic dication species (six π-electrons) see Figure 1.32.[188, 189]
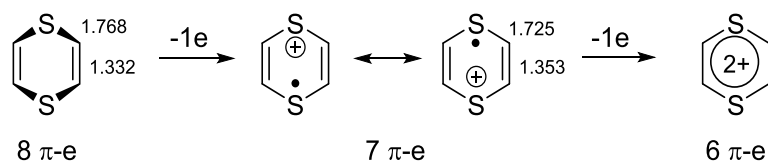

Figure 1.32: Evolution upon oxidation of the molecular structure of 1,4-dithiin calculated at the B3P86/6-31G* level. Bond lengths are in Å.[188]

The monomer **9** in the presence of a strong oxidant (e.g., tetracyano-*p*-quinodimethane (TCNQ)) adopts a planar conformation of the molecular structure due to the aromatisation of the dithiin moiety.[189] Organic electron donor systems incorporating moieties such as redox active, 1,4-dithiin unit, that can behave as oscillating folded donor (D) molecules to planar oxidised donor (D_z) species, become interesting candidates as components in potentially superconducting charge transfer materials.[188]

The qunioxaline moiety in compound **9** possesses two sp_2 nitrogen atoms which are known to coordinate to metal cations.[188] Experimental and theoretical studies performed by the Skabara group revealed the polymeric form of compound **9** displayed an increase in redox potential when coordinating with silver and mercury cations (Ag^+ and Hg^{2+} metal cations) in both aqueous and non aqueous mediums.[189] Theoretical studies performed on the trimer of compound **9**, calculated both silver cation and the mercury dications to interact at the dithiin sulphurs as the favoured chelating atoms in an apical coordination. These results indicate a new type of conjugated polymer system with sensing ability of transition metal ion in solution.[189]

The ability of the 1,4-dithiin heterocycle to undergo dramatic conformational conversion in response to a redox reaction can be further exploited in altering the

physical properties of conductive polymers.   Incorporation of 1,4 dithiin based on altering the extent of conjugation, chelating environment, or interchain packing.[189, 190]
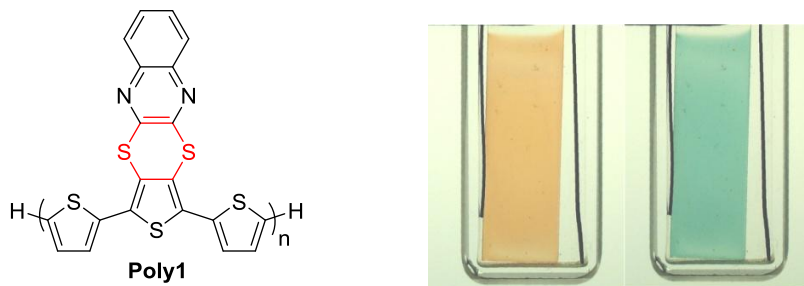

Figure 1.33A: Poly(terthiophene) analogue Poly1 with one dithiinoquinoxaline per repeat unit showing an orange colour in the neutral form and a blue colour in the oxidised state.[191]

Polymer **Poly1** bears one dithiinoquinoxaline per terthiophene repeat unit and exhibited an electrochromic performance superior to that of PEDOT, see Figure 1.33A.[190] The polymer showed two optical transformations from orange in the neutral state and blue in the oxidised state upon electrochemical redox reactions.   The switching characteristics at 650 nm revealed a change in transmittance of 44% with a 1 s switching rate (*cf*. PEDOT, 44% at 2.2 s).[190]   This fast switching performance is presumed to be assisted to the bent conformation of the 1,4-dithiin ring, which inhibits strong π-interactions between polymer chains, facilitating the ingression and egression of anions throughout the loosely packed polymer film upon redox switching (See Figure 1.33B).[190] The kinetics of electrochromicity is slower in well ordered, close packed structures such as PEDOT compared to amorphous and less dense polymers.[191]
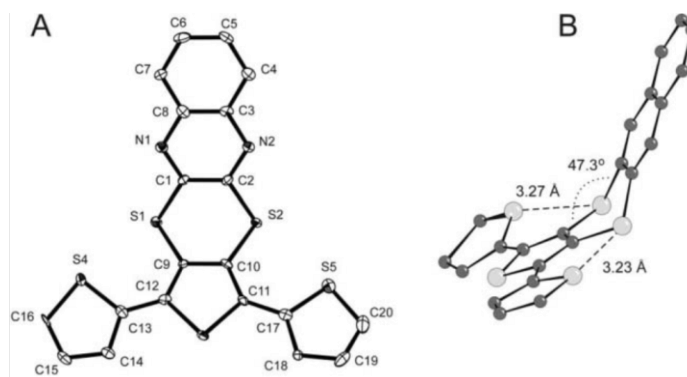

Figure 1.33B: A) The molecular structure of terthiophene monomer of **Poly1** unit in the crystalline state, B) a side-on view of close intramolecular S-S contacts and non-planarity in the dithiin ring [folding along the S(1)...S(2) vector is 47.3(2)°.[190]

Moreover, the introduction of a tetrathianaphthalene TTN unit, consisting of two fused 1,4-dithiin rings onto the backbone of polythiophene was studied. Three systems consisting of saturated (**P1**), open cyclic (**P2**), and TTN-fused (**P3**) side groups bound onto PTh backbone have been investigated within the Skabara group as electrochromic materials (Figure 1.34).[148] All three polymers (**P1-3**) exhibit similar oxidation and reduction potentials, and hence band gaps. Any slight variation was attributed to the difference in the side groups and difference in interchain interactions.[148]
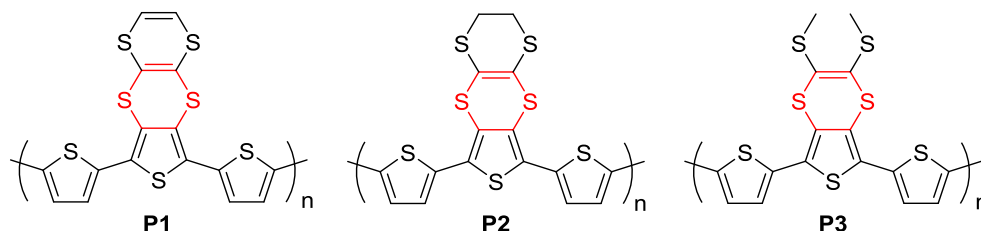

Figure 1.34: Polymers featuring the redox active unit tetrathianaphthalene.**[148]**

The calculated HOMO and HOMO-1 plots of the monomeric forms of the three polymers (**P1-3**), shows the removal of the first electron from each molecule originates from different sites.[148] In the monomer form of **P1**, the TTN unit is a better electron donor than the terthiophene fragment. In the monomer form of **P2**, the outer vinylene unit is reduced to a saturated bridge between the corresponding sulfur atoms, resulting the electron donating property of dihydro-TTN to be reduced and now sees the HOMO spread over both dithiin and thiophene. However, the monomer of **P3**, the dithiin ring holds little electron density and HOMO is dominant over the terthiophene chain.[148]

Further crystallographic studies of monomer form of **P1** revealed no evidence of molecules π-π stacking but weak intermolecular contacts between the sulfur of one peripheral thiophene with one sulfur atom of the neighbouring molecule's TTN core, giving rise to a remarkable packing motif of six molecules in an almost spherical arrangement.[148]

All three polymers displayed electrochromic behaviour with rapid optical transformations from red to yellow.[148] **P3** exhibited the greatest colour contrast out the three polymers in Figure 1.34 (ΔT% = 51.6 and 39.3 at 2.5 s and 1.25 s, respectively); the

more open polymer morphology assists in faster switching times with greater percentage absorbance change at various switching speeds.[148]

The above examples suggest that these loosely packed polymers allow efficient accessibility of ions to the electro-active sites. Other contributing factors, such as the ionic conductivity of the electrolyte, ion diffusion in thin films, magnitude of the applied potential, polymer film thickness, and morphology of the thin film can also influence a material's performance.[166] Presently, electrochromic (EC) performances show switching responses in the order of magnitude of milliseconds, which are easily achieved by using polymers and composites containing small organic electrochromes.[179]

1.7.5   Heterocyclic Furan
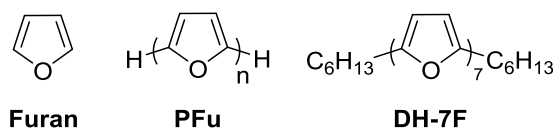

Furan   **PFu**   **DH-7F**

Figure 1.35: Structures of furan, polyfuran (PFu) and oligiofuran (DH-7F).[192]

The electrochemical and physical properties of conjugated polymers can be greatly affected by the electronegativity of their heteroatom.[193] Furan, a five membered heterocycle with oxygen as the heteroatom can be easily obtained from biorenewable resources and its materials are considered biodegradable thus making them attractive candidates for 'green' organic electronics (Figure 1.35).[194-196] Unfortunately, furan systems have been overlooked in research as organic electronic materials despite offering similar or even superior properties to their thiophene counterpart,[193, 197-200] such as an enhanced fluorescence, a higher HOMO, proficient packing, greater rigidity, and efficient processability, as demonstrated for oligofurans (nine units) by Bendikov *et al*.[192, 201-203] These oligofurans displayed comparable field effect mobilities to their thiophene analogues, proving their suitability as p-type semiconductors in OFETs.[201, 203] Furthermore, oligofurans have been reported to be thermally stable up to 300°C, which contributes to their remarkable device stability, as has been demonstrated by the comprehensive stress cycling of OFETs based on films of oligomer DH-7F (see Figure 1.35).[192]

It is known that the high oxidation potentials of furan monomers (*ca.* 2 V) render their handling more difficult than that of other five-membered rings and make their polymerisation susceptible to side reactions and resulting in irreversible oxidation of the polymer.[204-208]   Attempts to chemically prepare polyfuran (PFu) did not appear conjugated as a significant degree of ring opening occurring due the harsh chemical conditions employed. Given the great difficulty encountered in its synthesis, PFu is rarely characterised.[25] Li *et al* were first to successfully prepared PFu in a binary solvent system containing boron trifluoride-ethyl ether (BEFEE) and additional ethyl ether (EE).[208, 209]

Furthermore in attempt to lower the oxidation potential of furan to prevent over-oxidation, the preparation of monomeric bi-terfuran monomers or copolymerisation of furan with alternative monomer units, e.g., thiophene, was considered.[210,211] In addition hybrid-conjugated monomers, are now becoming of synthetic importance.[212, 213]

PDPP2FT: X= S, η = 5 %
PDPP3F: X= O, η = 4.1%
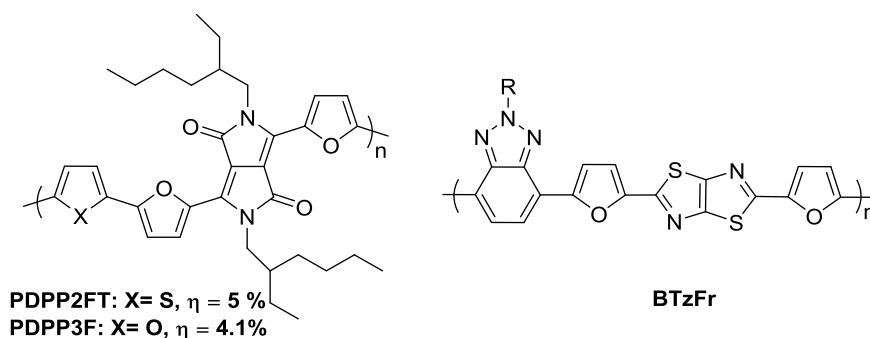
BTzFr

Figure 1.36: Published furan-containing copolymers PDPP2FT, PDPP3F and BTzFr.[194,214]

Frechét *et al.* have been pursuing this idea and demonstrated recently a bulk heterojunction solar cell fabricated from furan-containing polymers (**PDPP2FT** and **PDPP3F**) and PC$_{71}$BM with power conversion efficiencies of 4.1-5.0%.[194] The inclusion of furan units within the conjugated backbone allowed for shorter solubilising groups to be used, compared to those required to solubilise their all-thiophene analogues.[215] This furthermore highlights the beneficial morphological changes due to the presence of the smaller, more electronegative oxygen atoms in place of the larger sulfur atoms.[194, 197, 198] At last, furans are beginning to be recognised as EC materials with the recent benzotriazole-furan-thiazolothiazole-furan polymer (**BTzFr**) displaying an optical bandgap of 1.9 eV and fast switching speeds with a high optical contrast (0.5 s, ΔT% = 35, at 700 nm and ΔT% =25 at 1280 nm) see Figure 1.36.[214]

1.7.6   *Azomethine-based electrochromic materials*

Azomethine linkages (-N=CH-) can be conveniently adopted as an alternative to the vinylene linkage commonly used in conductive polymers as aryl connection. The azomethine linkage is isoelectronic to its carbon counterpart and exhibits similar opto-electronic properties.[216-218]

Azomethines are attractive conjugated materials possessing several advantages compared with their carbon analogues, such as the mild synthetic procedures, minimal purification steps, and increased product yields.[216, 217, 219-224] Conjugated azomethines can be synthesised by a simple condensation reaction between aryl amines and complementary aryl aldehydes, resulting in the robust covalent azomethine linkages, which exhibit a good hydrolytic and reductive resistance.[219, 221-223, 225-233] Extreme reaction conditions need to be employed for hydrolysis of the azomethine linkage, e.g., concentrated acid in wet organic solvents, whilst standard reductants (e.g., refluxing in presence of DIBAL) fail to reduce the linkage.[234-236] The carbon-heteroatom bond facilitates polymer oxidation and reduction and confers p- and n- type properties to the polymers. In contrast, their vinylene analogues are predominantly p-type materials.[217, 222, 225, 229]

The first reported polyazomethines (PAM) contained nitrogen atoms in their polymer backbone and were prepared by Adams and co-workers in 1923.[237] PPI (poly (1,4-phenylene-methylidynenitrilo-1,4-phenylenenitrilomethylidyne)[238]) is the simplest representative of aromatic conjugated PAMs. It is isoelectronic with poly(p-phenylene-vinylene) PPV and easily prepared from terephthaladehyde and 1,4-diaminobenzene (Figure 1.37).
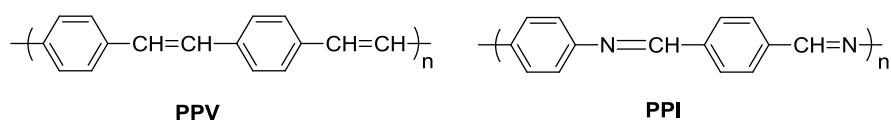

PPV   **PPI**

Figure 1.37: PPV and PPI structure.[237]

In contrast to its carbon analogue PPV, the azomethine polymer PPI exhibits beneficial chemical properties such as an increased solubility in concentrated sulfuric acid, chemical flexibility, and a site for complexation with Lewis acids, which result from

the presence of the imine nitrogen in its backbone.[238-246] PAM systems are known to be thermally stable,[247] coordinate to metals,[248] exhibit good electrical conductivity,[249, 250] and possess nonlinear optical properties.[251, 252]

Unfortunately, PAM systems are insoluble in common organic solvents, limiting polymer development and characterisation. Several structural modifications towards an improved processability of conjugated PAMs have been reported, such as unsymmetrical[243] or symmetrical[244] substitution of the main chain, incorporation of solubilising groups, such as alkyl or alkoxy side groups. Such modifications have resulted in promising PAMs with interesting optical band gaps in the range of 2.03-2.83 eV.[253]

Despite the synthetic advantages of azomethine-based materials, previous conjugated azomethines have not satisfied the device performance requirements for commercialisation.[239, 254] Structural enhancements of benzene azomethines have resulted in polymers with optoelectronic properties inferior to their vinylene analogues.[31, 56] This is a result of the inherent twist around the aryl-azomethine bonds, which restricts their degree of conjugation, leads to undesired oxidative decomposition and irreversible radical cation formation.[216, 241, 244, 253, 255, 256]

However, azomethine systems with optoelectronic properties comparable to those of their vinylene analogues could be obtained by the incorporation of thiophene derivatives.[221-223, 225] Thiophene units result in azomethine systems with a higher degree of conjugation than their benzene analogues due to the delocalisation of the heterocyclic π-electron system across the entire conjugated framework.[223]

Studies of Destri and co-workers showed that the band gap of conjugated PAMs was notably reduced by the incorporation of alternating sequences of thienylene and phenylene segments.[256-259] In addition, Kanatzidis *et al.*[253] presented the novel alternating PAM poly(3',4'-dibutyl-alpha-terthiophene-azomethine-1,4-phenylene-azomethine) (**PBTPV**), which possesses an optical band gap of 2.06 eV and an electrical conductivity in the order of 10^{-7}-10^{-8} S/cm (see Figure 1.38).[253]
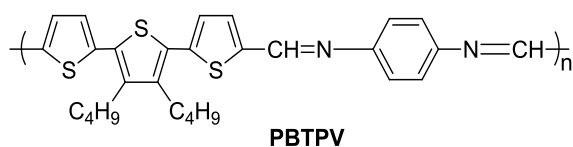
PBTPV

Figure 1.38: Structure of poly (3',4'-dibutyl-2,2':5',2''-terthiophene-1,2-ethylene-1,4-phenylene-1,2-ethenylene), PBTPV.[253]

Theoretical studies performed by Jenekhe *et al.*,[255] complimented by experimental studies of new thiophene-based conjugated PAMs, revealed that the thiophene-based systems have reduced band gaps in comparison with their parent PPI. Theoretical calculations indicated that the substitution of electron-donating or -withdrawing side groups on the aryl backbone significantly affects the backbone planarity and thus results in a variation of the electronic properties, ionisation potential, electronic affinity, and band gaps.[255]

Deducing from the instability of benzene azomethines that they are poorly suitable as functional materials for devices impeded their consideration for further research.[223] Yet device property enhancements are achievable with PAMs prepared exclusively from heterocycles such as thiophene.[223] Professor Will Skene from the University of Montreal has extensively researched on thiophene-based PAM systems over the past decade. Skene's group has prepared an efficient synthetic methodology that is capable to tailor spectroscopic properties and observe notable reversible oxidations, which is desirable for device functionality.[222, 228, 232, 233, 260-262]

Thiopheno-azomethines are conveniently prepared by Schiff base condensation reactions of aminothiophene precursors with functionalised thiophene derivatives.[263] Schiff base reactions are highly favourable due to their ease of purification, high yields, and lack of toxic metal catalysts.[222, 225, 263] Non-substituted, simple aminothiophenes are unstable and undergo spontaneous decomposition in ambient conditions. The stability of aminothiophene precursors was improved by the incorporation of electron-withdrawing groups such as esters and cyano groups.[219, 264-266]

The initial study dealt with azomethines consisting entirely of thiophenes that were prepared from stable diaminothiophene **5.1** and found to undergo controlled

anodic polymerisation *via* the desired α-α homo-coupling, affording thin film of highly conjugated polymers, see Figure 1.39.[217, 222, 223, 267, 268]

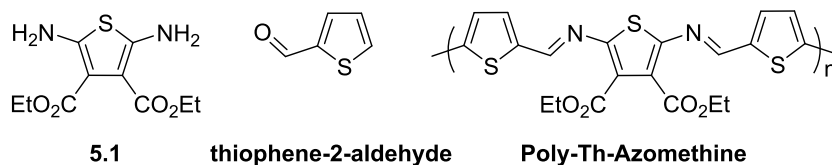**5.1**   **thiophene-2-aldehyde**   **Poly-Th-Azomethine**

Figure 1.39: Thiopheno azomethine polymer prepared from stable diaminothiophene **5.1** and thiophene monoaldehyde.

When increasing in the number of azomethine bonds, the degree of conjugation is increased with notable bathochromic shifts in both emission and absorption profiles. The intrinsic electron-withdrawing nature of azomethines led to colourful materials that absorbed strongly across the entire visible spectrum, particularly when coupled with electron-rich moieties.   Furthermore, the presence of additional terminal electron-withdrawing groups evoked multiple stable, reversible redox states with promising optical properties, which render thiophene-based azomethines ideal for use in electrochromic applications. [13, 25, 27, 60, 67]

New conjugated azomethine materials with analogous or enhanced properties compared with current materials can be easily prepared.   Extension of the donor-acceptor relationships in azomethine systems encouraged Skene's group to study the implementation of electron-rich EDOT moieties (see Figure 1.40).[225]   Polymers derived from EDOT are widely exploited in organic electronics due to the ability of the corresponding monomers to be electropolymerised producing the polymer which have low oxidation potential and stable p-doped state with good hole-injection properties and conductivities.[219, 225, 249, 269-271]

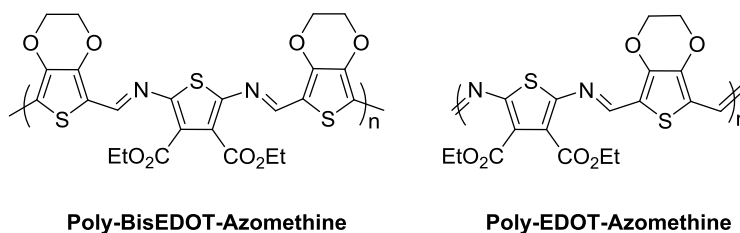**Poly-BisEDOT-Azomethine**   **Poly-EDOT-Azomethine**

Figure 1.40: EDOT-based polyazomethines.

Tailoring of spectroscopic properties was accomplished *via* the strong electron-donating EDOT moiety, which evokes a *ca.* 30 nm bathochromic shift in absorbance relative to its thiophene counterpart.[219] Furthermore, EDOT azomethines exhibited various oxidation potentials in the range of 0.75 to 1.3 V. The chemical structure of azomethine strongly influenced the reversibility of the observed oxidation processes.[219, 225] Excitingly, a wide palette of colours for both the neutral and doped states with high contrast ratios was achievable with the electron-rich conjugated azomethines.[217, 219, 222, 223, 225]

Skene's group has developed an extensive library of azomethine donor-acceptor (D-A) systems, which highlights the importance and suitability of azomethines as functional materials and suggests a spectroelectrochemical behaviour similar to that of their carbon analogues. Sequential, clean, and effective synthetic procedures have been optimised, encouraging many options for other heterocyclic systems to be incorporated into azomethine systems in either a symmetrical or an unsymmetrical fashion. [11-13, 25, 27]

1.7.7　Multi-colour complex electrochromic materials

A new strategy to achieve materials with multi-colour properties from single small molecules was reported by Zhang *et al.*[272] This multi-colour device was realised using a simple flying-fish shaped methyl ketone TM1 (see Figure 1.41). Colour-tuning was achieved by modulating the ratio of two plasticisers, namely propylene carbonate and diglycol, in a polymethyl methacrylate (PMMA) matrix.[272] This device was found to be durable exhibiting the colours green, blue, and magenta and a colouration efficiency of 350 cm^2/C. A fast switching time of 50 ms and good reversibility proves it to be a high-quality, multi-colour switching device that is based on a simple molecule.[272]
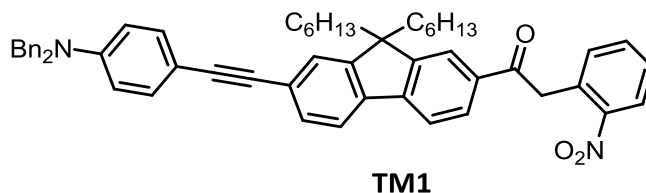

TM1

Figure 1.41: Flying-fish shaped methyl ketone **TM1:** 1-(7-((4-(dibenzylamino)phenyl)ethynyl)-9,9-dihexyl-9H-fluoren-2-yl)-2-(2-nitrophenyl)ethanone. [272]
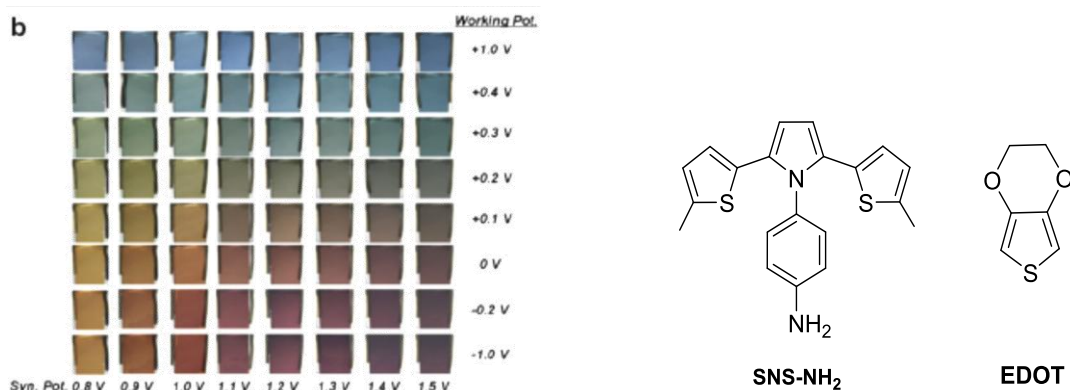
Figure 1.42: A) Representations of the colour space of copolymer synthesised at various potentials, B) Monomers EDOT and SNS-NH$_2$.[273, 274]

EDOT-based copolymers can be prepared pursuing both chemical and electrochemical polymerisation routes. Many copolymers of EDOT exhibit multichromic properties with different colours at various applied potentials. A soluble conducting copolymer of 4-(2,5-di(thiophen-2-yl)-1H-pyrrol-1-yl) benzenamine (SNS-NH$_2$) and EDOT has been reported (see Figure 1.42). Electrochromic switching studies demonstrated an optical switch contrast transmission of 11% at 491 nm at a switching rate of 0.8 s.[273]
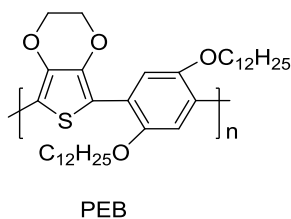
Figure 1.43: Chemical structure of multi coloured electrochromic material poly(3, 4-ethylenedioxythiophene-didodecyloxybenzene) (PEB).[274]

Derivatives of conjugated polymers, such as polythiophenes, polypyrroles, and polymers having alternative chromophore groups, for example, poly(ethylenedioxythiophenedidodecyloxybenzene) (PEB), are being investigated as multi-coloured electrochromic materials (see Figure 1.43). A colouration efficiency greater than 1200 cm^2/C has been reported for PEB.[274] In addition, PEB and other high-colouration-efficiency polymers can be combined with tungsten oxide to form charge-balanced, variable transmission electrochromic windows. Stacking electrochromic window devices provides two-dimensional surfaces in the colour space. A two- or three-layer system can provide a fully colour-tunable pixel element.[274]

1.8   Electrochromic performance characterisation

In order to establish whether an EC material or ECD is a suitable candidate for a commercial or research application, its operating performances are measured against specific properties or parameters. Such measurable parameters enable the direct comparison between various devices and materials. A variety of such categories exists in the literature, whereof the most important ones in characterising EC's are presented in the following in detail. Device performance parameters measured would be next step to elucidate the validity of such potential EC material. Testing parameters of all of the aforementioned techniques as well as memory effect, write erase and cycle life has been intensely reviewed by Mortimer[114] and will not detailed within this chapter.

1.8.1   Optical Contrast

Optical contrast (ΔT) is the difference in transmittance between the two redox states of an EC/ECD. These states are most commonly the bleached and the coloured ones. Optical contrast is a measure of how efficiently an EC/ECD is powered on and off. Different methodologies have been employed to report the optical contrast.   Among them, the following methodologies have been the most popular:[104, 113, 114]

- Measurement at absorbance maximum and comparison to applied potential
- Photopic contrast
- Colour contrast [ΔE^*]
- Relative luminance

Optical contrast is commonly calculated using equation (1.12) where CR is the optical contrast (or contrast ratio), R_x is the intensity of light that is reflected by diffusion through the coloured state of an EC/ECD, and R_0 is the intensity of the same light being reflected by diffusion by a white, non-shiny card.[7] Measurements are performed at the absorbance maximum. Contrast ratios of 10:1 up to 60:1 have been reported for the WO_3/electrolyte/NiO cell and heptyl viologen radical cation-based devices, respectively.[92, 275]

$$CR \; = \; \frac{R_o}{R_x} \hspace{3cm} (1.12)$$

In the latter case, the lightness variation (ΔL^*) is commonly used, which depends only on chromaticity coordinates in the CIE 1976 $L^* \alpha^* b^*$ colour space.

Optical contrast measurement and reporting is not an unambiguous proof of electrochromic activity. The optical contrast is only determined by alterations of the absorbance maximum; however, this may be also locally influenced by additional interactions resulting from redox reactions. It has been reported that the contrast of such interactions is desired for most commercial and research applications.

The transmission of electrochromic devices is greatly affected by the components of the device. Therefore, it is imperative to acknowledge the measurement settings for electrochromic devices (ECDs) and electrochromic polymers (ECPs).[34] For ECPs, the measurements are performed using a reference cuvette consisting of blank substrate, which allows for the evaluation of the maximum obtainable contrast of the polymer. However, a complete electrochromic device consists of other components such as electrolyte, electrode substrate, and charge-balancing electroactive polymer, which also influence the optical contrast. In this regard, glass is considered the least disruptive substrate, and a 1 mm thick glass slide (without electrode) reduces the transmittance to about 10 owing to the challenges associated with flexible substrates, as demonstrated by several research groups for ECD window materials.[276-278]

1.8.2   Response time

Response time or switching speed correlates to the time required to evoke a transmittance change (at λ_{max}) upon the application of a certain potential. Response time requirements vary greatly among different commercial and research applications; energy-saving applications, such as 'smart' windows, require smooth and long transitions between redox states in order not to disturb inhabitants of spaces due to abrupt modifications of light intensities, whereas applications such as screens require sub-second responses. Response times of 60 s and 180 s have been previously reported for WO_3 and NiO ECDs, respectively.[279] On the other hand, response times of 0.8-2.2 s and 250 ms have been reported for two different fast-switching ECDs.[165]

A common issue with reporting and comparing response times are the different formats used by various groups to include different data such as redox states, colour transition ratios, applied voltages, etc. The response time can be compared with the optical contrast. A smaller transmittance change is correlated with a faster electrochromic performance.[280] Therefore, transmission changes must be taken into consideration for comparing response times, which should be only compared for the same contrast ratios. However, for thoroughly comparing response times, they have to be reported on different levels of optical contrast, as the majority of redox reactions take place in the beginning of the switch. For instance, 90% of the switch may occur in 2 s, and the remaining 10% may take 5 s.[34] This is due to the fact that reaction rates decay exponentially; they are extremely high in the beginning of the reaction, they are smoothened as the reaction proceeds, and slowed down towards completion of the reaction. The redox kinetics can be investigated based on the reaction order of each transition. This mechanism, which depends on the ion concentrations in the parts of ECDs, reveals that the actual transition times (response times) should be taken around 90% instead of 100% completion of the transition. Response times are valuable in the kinetic controlled rather than the thermodynamically controlled region.

1.8.3   CIE Colorimetry

The colour of the material is the result of interaction of light with the object through absorption, transmission and reflection. An estimate shows that a human eye can perceive about 10 million colours. Colour of the electrochromic device is of great concern and it can be quantified within the visible wavelength range of 380 to 780 nm.[281]

The description of colour constitutes three attributes. Firstly, the wavelength at which maximum colour contrast occurs in the spectrum is determined and is commonly denoted as its *hue*, *dominated wavelength* or *chromatic colour*. This feature is commonly incorrectly identified to as colour. The second feature is the relative levels of white and/ or black within the colour, referred to as *saturation*, *chroma*, *tone*, *intensity* or *purity*. The third quality defining colour is its brightness, referred to as *value*, *lightness* or *luminance.* Luminance details the perceived transparency of a sample over the entire visible spectrum.[114, 282]

Realisation of these three attributes; hue, saturation and luminance, any colour can be described and further quantified numerically in a given colour system. The most recognized colour system is devised by the Commission Internationale de l'Eclairage, commonly known as the CIE colorimetric system.[92] The CIE was first formulate in 1931 and calibrated against a '2° Standard Observer' which is based on characteristic results of people visually matching three colours within a 2° field of vision. [114, 282]

This system has been employed in a large number of studies to quantify the colours of electrochromic devices.[283] In this system a colour specification is provided for normal vision in the form of tristimuli values. The mathematical quantification of these colour tristimuli is given by the CIE standards which form a colour space for visible region. These mathematical relationships are employed in measurement devices such as the Minolta CR-5 bench top colorimeter, to provide tristimuli values and details regarding the colour of the material. However the ordinary spectroscopic data obtained from a spectrophotometer scan can be utilised to extract required colorimetric data using relevant equations. For example, translating spectral data into an equivalent colour using a well-known CIE standard CIE 1931 2° mathematical calculations are done to obtain tristimuli values for a material representing the spectral response of human eye. These functions vary for emissive and transmissive / reflective cases. This is because the transmissive and reflective samples need an illuminant to be viewed and / or measured. The equations used for electrochromic devices are as follows:

$$X = \frac{1}{N} \int_{\lambda min}^{\lambda max} X(\lambda)T(\lambda)I(\lambda)d\lambda \qquad (1.13)$$

$$Y = \frac{1}{N} \int_{\lambda min}^{\lambda max} y(\lambda)T(\lambda)I(\lambda)d\lambda \qquad (1.14)$$

$$Z = \frac{1}{N} \int_{\lambda min}^{\lambda max} Z(\lambda)T(\lambda)I(\lambda)d\lambda \qquad (1.15)$$

Where N is equal to:

$$N = \int_{\lambda min}^{\lambda max} Y(\lambda)I(\lambda)d\lambda \qquad (1.16)$$

Here X, Y and Z denotes CIE 1931 2° standard observes colour matching functions whereas λ and T corresponds to the wavelength and transmittance. N is the normalization factor which is used to normalize the reference light source. It produces the values of light colours under a particular light source.

The numerical integration is required on the measured transmittance data by the following equations:

$$X = I/N \sum x_\lambda T_\lambda I_\lambda \tag{1.17}$$

$$Y = I/N \sum y_\lambda T_\lambda I_\lambda \tag{1.18}$$

$$Z = I/N \sum z_\lambda T_\lambda I_\lambda \tag{1.19}$$

Where $N = \sum y_\lambda I_\lambda$ and λ is the wavelength range. In order to obtain the x-y coordinates of CIE diagram the following calculations are employed;

$$x = X / (X+Y+Z) \tag{1.20}$$

And

$$y = Y / (X+Y+Z) \tag{1.21}$$

Here x and y are the colour coordinates determining the hue and Y is the luminescence whose value is 1 for a perfect transmitter. Any necessary colour calculations can be done following these equations using the calculated tristimuli values of X, Y and Z.

For any commercial electrochromic material, the specific and reproducible colour states and contrast ratios are required. Therefore, *in situ* colorimetric analysis is used as a means of precisely defining colour coordinates in electrochromic polymers. CIE colour depictions are actually 3D diagrams (contrours). However, they can be separated between brightness and chromaticity to reduce required plotting dimensions. The plot used to exhibit all chromaticities visible to human eye is termed a 'chromaticity diagram' and is depicted in Figure 1.44.
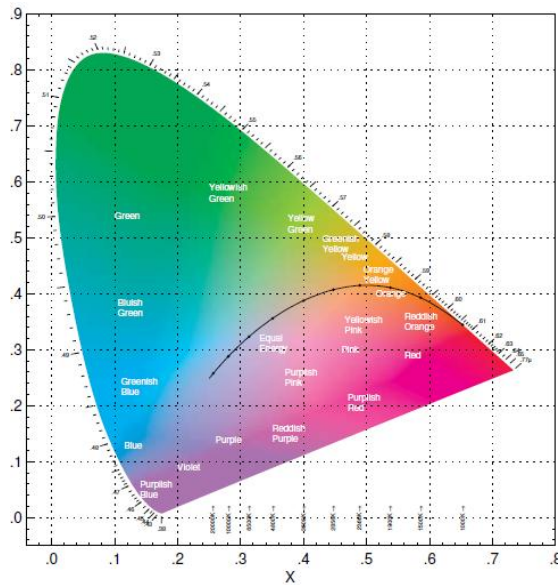
Figure 1.44: CIE 1931 chromaticity diagram.[114]

Various shortcomings of this approach have led to the development of the CIELAB and CIELUV colour spaces. CIELAB introduced the use of L^*, α^* and b^* that were functions of the tristimuli values of the test object's colour stimulus and of a specified white object's stimulus. CIELUV system included the saturation, chroma and hue angle as describing variables.

Of the above systems, CIE 1931 and CIELAB have been widely adopted for reporting optical performance measurements of ECs and ECDs. In these measurements, *Y* is defined as the luminance of the CIE XYZ *tristimuli* values, based on the three-component theory of colour vision using three primary colours; red, green and blue curves respectively.[284] The *L** measures the lightness of the material ranging from 0-100, whilst *a** and *b** represent the hue and saturation of the chroma (as do the *xy* coordinates). Within the *L* a* b** chromaticity diagram the +*a** value relates to the red direction, -*a** is the green direction, +*b** is the yellow direction and -*b** is the blue direction.[179]

In order to take into account human eye's sensitivity, colourimetric testing and measurements are commonly conducted in commercial colourimeters rather than measuring absorption bands in spectrum measurements.[102, 284]

One such important parameter is colour differences that can be defined as the numerical comparison of a sample's colour to the standard. It indicates the difference between two colours to identify inconsistencies and helps the user control the colour of their products more effectively or monitor device or display degredation.[102, 179 284]

Deltas for *L** (*ΔL**), *a** (*Δa**) and *b** (*Δb**) may be positive (+) or negative (-). The total difference, Delta E (*ΔE**), however, is always positive.

- ΔL* (*L** sample minus *L** standard) = difference in lightness and darkness
  - (ΔL*+ = **lighter**, ΔL*- = **darker**)
- Δa* (*a** sample minus *a** standard) = difference in red and green
  - (Δa*+ = **redder**, Δa*- = **greener**)
- Δb* (*b** sample minus *b** standard) = difference in yellow and blue
  - (Δb*+ = **yellower**, Δb* - = **bluer**)

To determine the total color difference between all three coordinates (*ΔE**), the following formula is used:

$$\Delta E^* = [(\Delta L^*)^2 + (\Delta a^*)^2 + (\Delta b^*)^2]^{1/2}$$

<div align="right">eq. (1.22)</div>

The smallest colour change that a human eye can perceive is of *ΔE** values of 1.0, below 1.0 is imperceptible and greater *ΔE** values (>1.0) are noticeable changes. Estabilishing the *ΔE** value of a material is crucial in commercial industries to determine whether a device has drifted, effectiveness of particular profile printing/proofing colouration efficiencies for optical displays, developed from colour tunable materials.[102, 179 284]

1.8.4   Colouration Efficiency

The composite colouration efficiency (CE) is a general method developed in order to characterise the efficiency of electrochromic materials. CE is a measure of the change in optical density of a material at λ_{max} relative to the total amount of injected/ejected charge. CE is thus a measure of how much charge is required to affect bleaching or colouration in an EC material and is often expressed as:[285]

$$\Delta OD = \log [\%T_b (\lambda_{max})/ \%T_c (\lambda_{max})]$$

<div align="right">(1.23)</div>

$$\eta = \Delta OD(\lambda_{max})/ Q_d \qquad\qquad (1.24)$$

The optical density at a specific wavelength (λ_{max}) is determined by using *%T* values of the electrochemically oxidised (*%T*$_b$) and reduced films (*%T*$_c$) as expressed in equation (eq. 1.22). The colouration efficiency (*η*) of the material can then be calculated by using equation (eq. 1.23), where $\Delta OD(\lambda)$ is the change in optical absorbance, and Q_d is the charge density which causes $\Delta OD(\lambda)$.[285]

CE is also a measure of the ratio of colour changing centres in relation to overall centres in an EC. Differentiation is made among EC and ECD colouration efficiency. ECD CE is most commonly represented by calculating the EC CE with a correction factor. This factor accounts for all the effects on CE that specific structures of the ECD exhibit. Those factors include:

- Electrode material effects
- Electrolyte matrix effects
- Side interactions (Faradaic nature) within the device/ apparatus

Reporting and measuring ECD colouration efficiencies instead of EC material CEs allows for direct comparisons of ECDs based on the same or different components, structure and manufacturing pathways. CEs must always be provided at specific wavelengths. If a CE is positive, it is due to cathodic processes, and the opposite is true for negative values. CEs reported in the literature for various films are presented in Table 1.3.

Table 1.3: Colouration efficiencies n of various electrochromes.[114]

Electrochrome	λmax /nm	n (cm^2 C^{-1})
Methyl Viologen	604	176
Indigo Blue	608	-158
Safranin O	530	-274
Poly (3,4 - ethylenedioxithiophene	585	183

1.9   **Design & construction of electrochromic devices**

The design of electrochromic displays depend on the mode of operation of the device. For reflective electrochromic devices the material is either coated onto a reflective electrode or has a reflective counter electrode.   A thin film of primary electrochrome on ITO coated glass placed on a reflective counter electrode is the most common design. A secondary electrochromic layer is also coated with an electrolytic gel in it. The construction of such a device is shown in Figure 1.45.
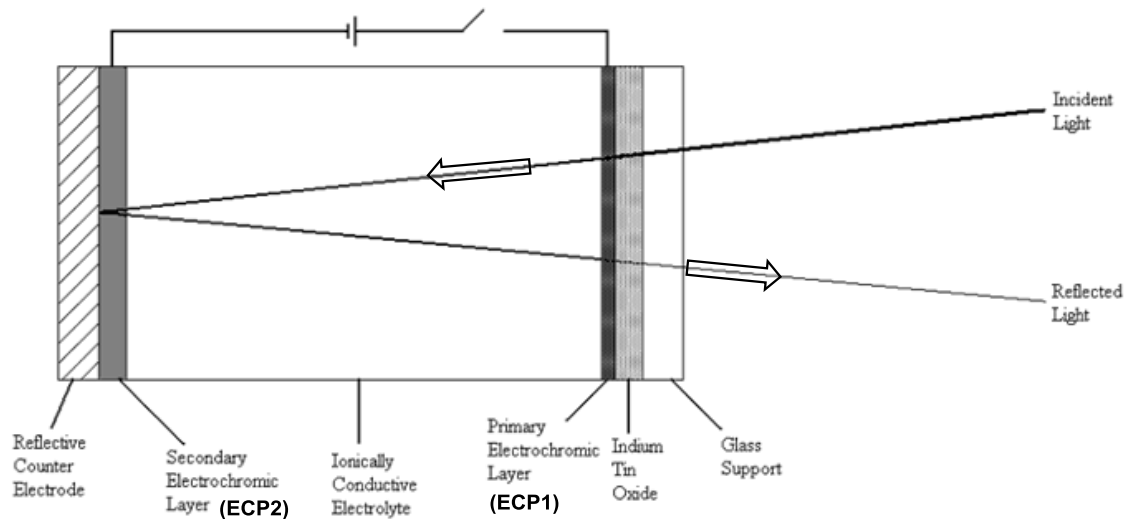

Figure 1.45: Design of a reflective electrochromic device.

The device operates by the absorption of light which is reflected by platinum or rhodium alloy.[286]   The advantage of reflective electrochromic device over transmissive electrochromic device is that the light passes through the device twice therefore the thickness of electrochromic material is reduced to half in the former. Thus a faster electrochromic system is obtained.

In constructing a transmissive electrochromic device a mirror is substituted for another glass substrate. The light passes straight through to the effect. These devices are operated with a back light. The schematic diagram for transmissive electrochromic device is shown in Figure 1.46.
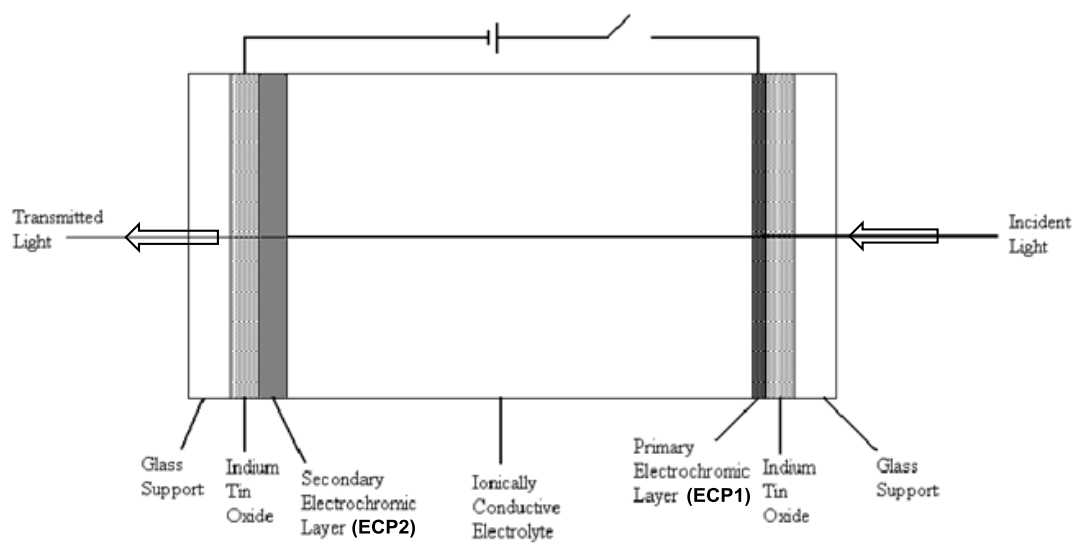
Figure 1.46: Schematic diagram of transmissive electrochromic device.

Many electrochromic devices such as windows, shutters, goggles, and spectacles are based on absorptive or transmissive devices. These devices are composed of two electrochromic polymers namely ECP1 and ECP2 with an electrolyte layer sandwiched in between them. These polymers are deposited on transparent substrates ITO electrodes that allows the viewer to see through it under transmissive condition.[34] The majority of colour change is due to ECP1 while ECP2 is a charge balancing polymer. Many other materials are also explored to function as electro-active counter material in hybrid devices.[287, 288]

A dual type device function is based on a complementary approach where ECP1 switches complementary to ECP2. Thus ECP1 is cathodically colouring while ECP2 is anodically colouring resulting in the simultaneous colouring / bleaching of both the electrochromic polymers.[289] As a consequence the optical density is enhanced in the coloured state however the overall optical contrast is reduced.[289] Another complexity in this approach is the difficulty of finding polymers with exactly complementary colours.[17, 122, 162]

A symmetrical device approach is the one in which both the polymers are identical.[34] The optical contrast is obtained due to the difference of low and high transmittance state. In the former state one side of the device is fully reduced while the other is fully oxidised. In high transmittance state both polymer films are in the

intermediate transmittance state. This approach limits the optical contrast due to the fact that both polymers are never simultaneously coloured or bleached. The benefit of this approach us that it enable the device construction with interpenetrable network of electrochromic polymers and electrolyte layer.[289]

A third approach is a minimal colour approach where ECP2 maintains a colourless state during redox process. A little research is done using this approach. Sotzing *et al*. has reported poly(thieno[3,4-b]thiophene) with a limited absorbance in the visible region in both redox states. A thin layer was found sufficient for charge balance due to high doping level.[290, 291] A donor-acceptor polymer consisting of a similar heterocycle is reported by Toppare *et. al*. The compound namely thieno[3,2-b]-thiophene was also highly doped.[292] An N-alkyl substituted Polypyrrole synthesised by Reynold is more solution processable in addition to being colourless.[292]

1.10 **Aim and chapter summaries**

Advancements made in polymer electrochromism show the closeness in realisation of a full-colour electrochromic device.[115] The synthetic ease of monomer design emphasises the possibilities of generating new molecular structures that can be utilised as electrochromic materials with promising optical results.[143]

This thesis presents the synthesis of several novel organic polymers that project interesting optical and physical properties. These polymers have undergone several studies to quantify their electrochromic performances. Key studies investigated are the potential redox range, spectroelectrochemical response, switching rates, chronocoulometry colouration efficiency, C.I.E colour coordinates and polymer stability.

- Chapter 1 covers the general theory required to understand electrical capacity of materials, with the evolution of organic electronics and its technological applications. The phenomenon of chromism and its advantage in organic polymeric form for optical usage is described. The importance of monomer design is reviewed followed by a description of material characterisation, performance testing and device structure principles.

- Chapter 2 reports the proposed synthesis of a new fast-switching electrochromic material. Focusing on a PEDOT-core structure, the favourable switching characteristics of PEDOT should be improved by replacing every third repeat unit with a dithiin-modified PEDOT monomer. Unfortunately, the attempted synthesis of the target monomer was challenging as the regioselectivity of the PEDOT-precursor only allowed for the synthesis of a bi-functionalised precursor. Although different challenges were successfully met, a successful synthesis of the desired target monomer was finally impeded.

- Furans have not been intensively investigated as an electrochromic material, despite possessing many similar characteristics to thiophene.[199, 293, 294] Furans are naturally occurring materials, biodegradable[295, 296] and relatively soluble in many organic solvents. In Chapter 3, furans are targeted as a general synthetic route to the preparation of three furan-containing monomers is presented.   A dithienylfuran monomer was successfully electropolymerised and demonstrated superior electrochromic performances in comparison to its all-thiophene analogue. This indicates that the incorporation of a furan unit is a successful approach for improving electrochromic properties with respect to the all-thiophene analogue, which furthermore renders the synthesised polymer a promising candidate for future organic electronic applications.

- In Chapter 4, the chemical synthesis of a novel polyfuran, poly(2,3-bis(hexylthio)-[1,4]dithiino[2,3-c]furan) (**PBDF**), substituted at the 3,4-positions with an S-alkylated dithiin unit, is reported. **PBDF** polymer was analysed by electrochemistry, UV-Vis spectroscopy, and spectroelectrochemistry, which

revealed a relatively low band gap of 2.0 eV. Its molecular structure was analysed by X-ray diffraction (PXRD) and predicted by molecular modeling, which revealed that **PBDF** mimics the "inverse" pseudo-ribbon morphology of **PEDOT** with a planar *anti*-conformation in its molecular structure, for which an extensive network of sulfur/oxygen interactions is made responsible. Furthermore, its thermal stability was studied by thermogravimetry and differential scanning calorimetry, which revealed a promising thermal stability until 150°C. The favourable thermal stability, the solution processability, and the independent electroactivity of the dithiin moiety render **PBDF** a promising candidate for a novel organic sensor.

- In Chapter 5 two new azomethine-containing electrochromic materials were synthesised. Azomethines are p/n-type materials with stable covalent linkages, which can be obtained in a facile and non-toxic synthesis. However, optimisation towards an improved performance and solubility for device fabrication is required. Four EDOT/EDTT azomethine monomers were synthesised and characterised by standard organic analytics, and their electrochemical and physical properties were studied by electrochemistry (CV) and UV-Vis spectroscopy. The superior performance of the asymmetric EDOT/EDTT azomethine polymer in comparison to bis-EDOT azomethine polymer, which displayed great optical transmittance changes in the NIR range upon oxidation render this azomethine polymer as an interesting candidate for NIR EC materials.

- Chapter 6 details the experimental and general procedures used in Chapters 2-5.

- Chapter 7 provides Appendix- supplementary information.

2   Towards the Synthesis of Fast Switching Electrochromic Conjugated Monomers

2.1 **Aim**

Towards the goal of synthesising fast-switching electrochromic polymers based on terthiophene monomers, herein the focus is on synthesising monomers retaining the PEDOT core structure, as PEDOT remains a favourable material to use due to its large colour contrast.[148] Based on the studies of the conjugated systems described in Chapter 1.7.4, it is understood that switching performance and optical properties can be optimised through structural manipulation, such as introducing various substituents at the polymer backbone and altering monomer repeat units. Additionally, the switching speeds of PEDOT can be improved substantially by adopting the POSO configuration and incorporating the dithiin ring to provide structural diversity in Chapter 1.7.4.[148, 190]

As a monomer target structure, the monomer **2.1**, dimercapto-dithiinothiophene-bis(ethylenedioxythiophene (EDOT-DMDTT-EDOT), was chosen, which is depicted in Figure 2.1. Polymers synthesised from this monomer could contain various alkyl groups, which would allow for studying the effect of alkyl chain length (C_4-C_{14}) and alkyl branching effects on the polymer properties.
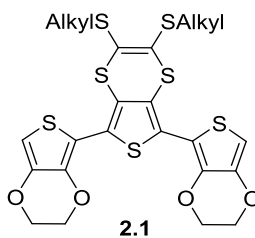

Figure 2.1: Target structure of the EDOT-DMDTT-EDOT monomer **2.1**.

2.2 Synthesis Plan

The proposed strategy for the synthesis of the target EDOT-DMDTT-EDOT terthiophene system is depicted in Scheme 2.1. This multistep synthesis involves the bromination of compound **2.2** to give the bromoacetyl derivative **2.3**. This is converted into the aminoacetyl derivative **2.4**, which undergoes a nucleophilic substitution with **2.3** to form the quaternary salt **2.5**. Steven's rearrangement of **2.5** results in the formation of butene-1,4 dione **2.6**, and the cycloaddition of the latter with oligomer **2.7** is expected to give the thione compound **2.8**. Concluding steps involve the transchalcogenation of **2.8** to its carbonyl derivative **2.9**, followed by cyclisation to **2.10**, which is finally alkylated to give the target monomer **2.1**.
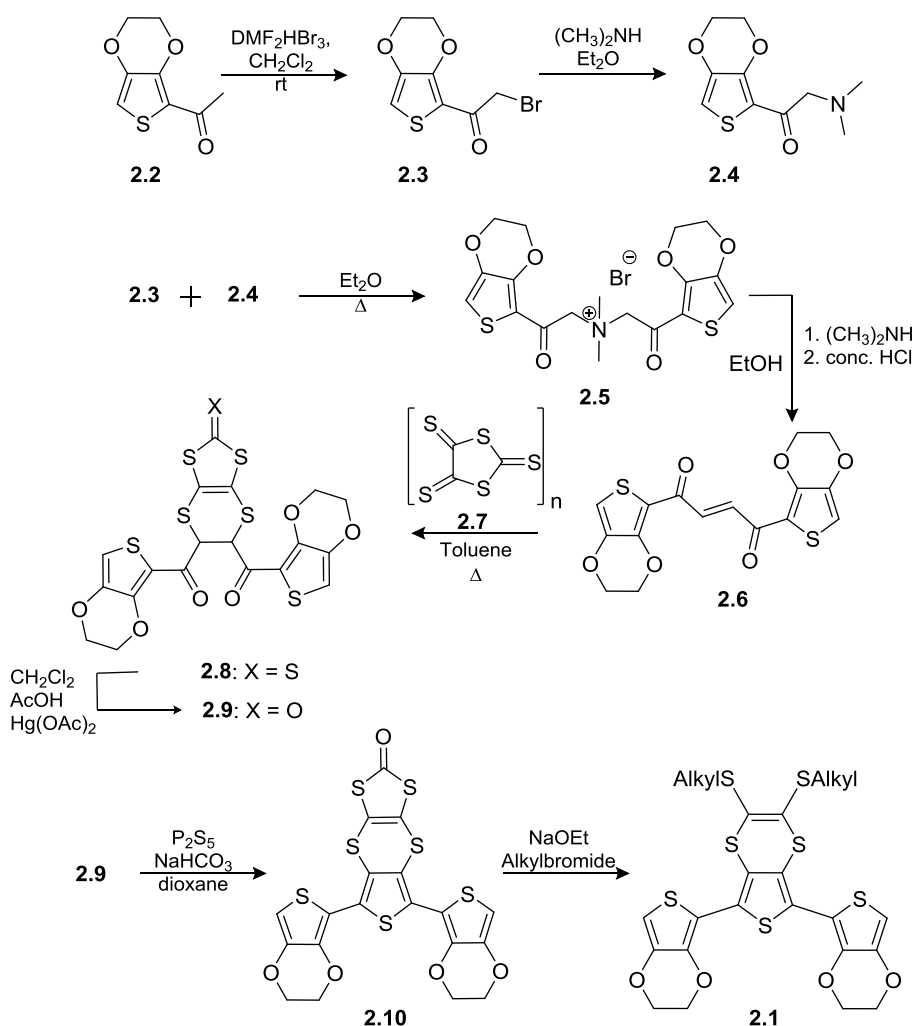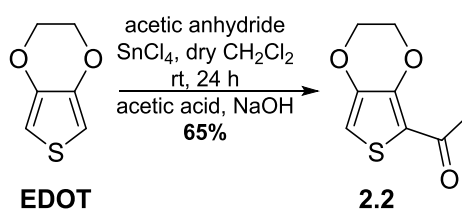

Scheme 2.1: Proposed reagents and conditions for the synthesis of terthiophene monomer **2.1**.

2.3   Results and Discussion

2.3.1   Synthesis according to Scheme 2.1: Proposed reagents and conditions for the synthesis of terthiophene monomer 2.1.

Mono 2-acetyl-3,4-ethylenedioxythiophene (2.2)

2-Acetyl-3,4-ethylenedioxythiophene **2.2**, the starting material of the synthetic route depicted in Scheme 2.1, was successfully synthesised according to Scheme 2.2 by the acetylation of commercially available 3,4-ethylenedioxythiophene (EDOT) with acetic anhydride in a 65% yield.

Scheme 2.2: Reagents and conditions for the preparation of 2-acetyl-3,4-ethylenedioxythiophene **2.2**.

However, using slightly more than two equivalents of acetic anhydride and tin(IV) chloride under reflux conditions promoted the formation of diketones in 70% yield, whereas the desired ketone was only obtained in 13% yield. This can be explained by the electron-donating capacity of the ethylenedioxy bridge functionality of EDOT, which predominates over the deactivating nature of the intially formed ketone at the 2-position to yield diketones.[297] This diketone formation could be completely suppressed by using less than two equivalents of acetic anhydride and tin (IV) chloride.

2-bromo-1-(2,3-dihydrothieno[3,4-b][1,4]dioxin-5-yl) ethanone (2.3)
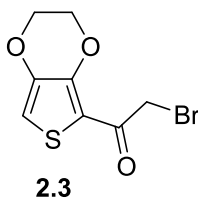

Figure 2.2: Chemical structure of target molecule **2.3**.

The first step of the synthetic route shown in Scheme 2.1 comprises the bromination of 2-acetyl-3,4-ethylenedioxythiophene **2.2** to form the bromomethylene derivative **2.3**. Unfortunately, the desired compound **2.3** was not obtained despite using different mild brominating agents, such as bis(dimethylformamide) hydrogentribromide (DMF$_2$HBr$_3$) or bis(dimethylacetamide) hydrogentribromide (DMA$_2$HBr$_3$). The electron-donating effect of the ethylenedioxy substituent made the thiophene ring susceptible to electrophilic substitution despite of the presence of acetyl functionality and led to monobromination at this site, forming 5-bromo-(2-acetyl)-3,4-ethylenedioxythiophene **2.11** in 50% yield. A significant fraction (40%) of unreacted compound **2.2** was recovered, see Scheme 2.3.
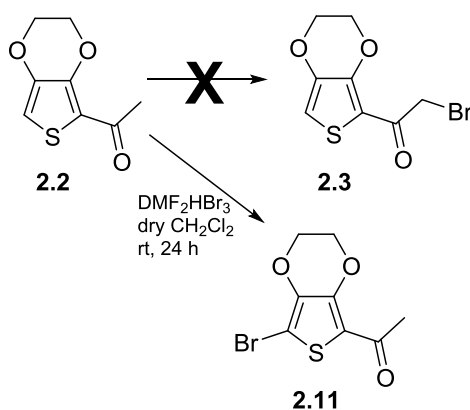
Scheme 2.3: Reagents and conditions for the preparation of mono and dibromo acetyl derivative, **2.11**.

Since the target compound **2.3** could not be obtained under the described bromination conditions, the compound **2.12** was chosen as the intermediate product in this project. Taking into account that the brominations by complexes DMF$_2$HBr$_3$ and DMA$_2$HBr$_3$ is not regioselective and leads to both aromatic substitution and formation of bromoketone **2.12**, N-bromosuccinimide (NBS) was studied as an alternative, mild brominating agent to fully and regioselectively brominate the aromatic position of **2.2** (see Scheme 2.4).
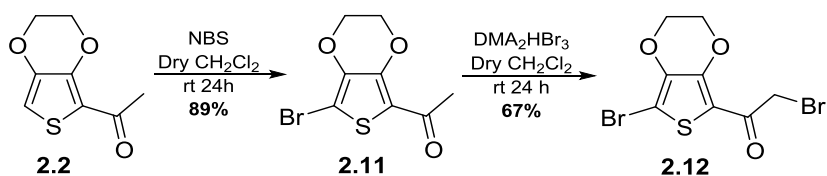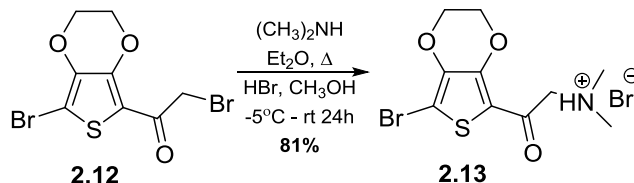
Scheme 2.4: Reagents and conditions for the synthesis of brominated derivatives **2.11** and **2.12**.

Treatment of **2.2** with NBS brominated the 5-position of the thiophene ring to give the monobromo derivative **2.11** in a high yield of 89% without any bromination of the acetyl group due to the absence of acidic catalysis. This was easily recrystallised and further brominated by DMA_2HBr_3 to give the bromoacetyl derivative **2.12** in a 67% yield, whereas 14% of unreacted **2.11** could be recovered.

Synthetic attempts were performed in order to cleave the bromide at the 5-position of compound **2.12** by using zinc powder and acetic acid in mild reduction conditions. Unfortunately, this was not successful and resulted in the complete reduction of **2.11** to the starting material **2.2**, which was recovered in an 85% yield, *vida infra* (see Scheme 2.9).

Concluding, no attempts to synthesise the target compound **2.3** were successful. However, its dibromo derivative **2.12**, which is monobrominated at the desired alpha position of its acetyl group but carries a second bromo substituent at the 5-position of its thiophene ring, was synthesised in good yield and promises to be an adequate replacement for **2.3** in the proposed synthesis depicted in Scheme 2.1 Therefore, Scheme 2.1 was modified using **2.12** instead of **2.3** as starting material, with all following products now carrying an additional bromo substituent at the thiophene's 5-position.

5-Bromo-2-(N,N-dimethylamino)acetyl-3,4-ethylenedioxythiophene (2.13)

Scheme 2.5: Reagents and conditions for preparation of amino acetyl derivative **2.13**.

The dibromo derivative **2.12** of compound **2.3** shown in Scheme 2.1 was converted into its amino acetyl derivative **2.13** (HBr salt of the bromo analogue of **2.4**) *via* a nucleophilic substitution of the bromide at the alpha-position of the acetyl group of **2.12** by dimethylamine. Hydrogen bromide was added to obtain **2.13** as the amino ketone salt, which is more stable than the respective free amine (Scheme 2.5). Compound **2.13** precipitated from a cold concentrated solution of **2.13** in methanol and obtained as bright yellow crystals with a high yield of 81%.

Bis-N,N-5-bromo3,4-ethylenedioxythiophene-(2-oxoethyl-1)-N,N-dimethyl ammonium bromide (2.14)
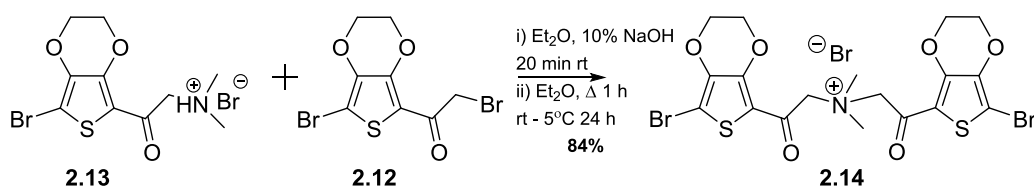
Scheme 2.6: Reagents and conditions for preparation of quaternary amino salt **2.14**.

In the next step, the synthesised aminoacetyl derivative **2.13** reacted with the bromoacetyl derivative **2.12** to form the quaternary amino salt **2.14**, the dibromo analogue of compound **2.5** shown in Scheme 2.1. Thereby, the free amine of **2.13** performed a nucleophilic substitution of the bromide in the alpha-position of the acetyl function of **2.12** (Scheme 2.6). The reaction was straightforward and produced the desired derivative **2.14** in a high yield of 84%.

(E)-1,4-Bis(7-bromo-2,3-dihydrothieno[3,4-b][1,4]dioxin-5-yl)but-2-ene-1,4-dione (2.15)

The next synthesis step of Scheme 2.1 constitutes the rearrangement of the quaternary salt **2.14** to the butene-1,4-dione derivative **2.15**, the dibromo analogue of **2.6** of Scheme 2.1.
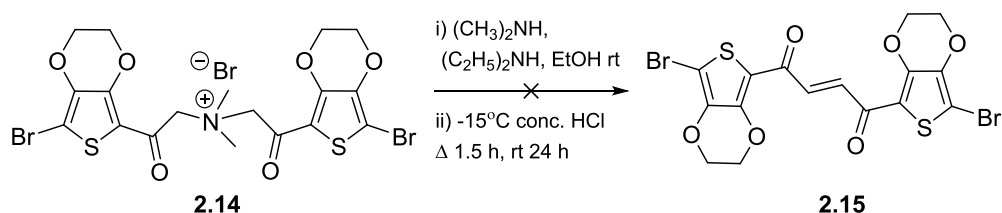
Scheme 2.7: Synthetic attempt in preparing the butene-1-4 dione derivative **2.15** using DMA and DEA in ethanol.

Initial attempts to synthesise **2.15** involved the modified procedure of Stevens rearrangement[298], which was proved to be successful in the synthesis of 1,4-di(thien-1-yl)substituted but-2-en-1,4-dione[299] and comprised the treatment of compound **2.14** with dimethylamine (DMA) and diethylamine (DEA) in ethanol, followed by acidification with conc. hydrochloric acid (HCl; see Scheme 2.7). Unfortunately, compound **2.15** could not be obtained under these conditions. Instead, 75% of starting material **2.14** could be recovered and the effort was put into finding an improved procedure for the synthesis of **2.15**.

A major challenge was the solubility of the quaternary salt **2.14**, which was not sufficiently soluble in either ethanol or diethyl ether. Solubility studies showed that compound **2.14** was only soluble in hot dimethylsulfoxide (DMSO). Thus, the initial reaction conditions were modified by using hot DMSO (80°C), which led to a colour change from yellow to deep brown/red upon HCl treatment and the formation of an insoluble material. NMR and MS analysis revealed that this material, unfortunately, did not contain the desired compound **2.15**. Therefore, this synthetic approach was discarded for synthesis of **2.15**.
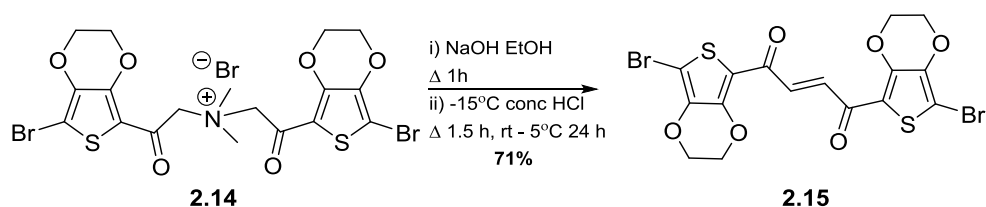

Scheme 2.8: Reagents and conditions for preparation of butene-1,4 dione derivative **2.15**.

As an alternative, a conventional procedure of Stevens rearrangement was attempted for the synthesis of **2.15** using sodium hydroxide (NaOH) as the base.[300] According to the reported procedure, the above recycled material of **2.14** was treated

with 10% NaOH in ethanol, which induced the expected elimination of the dimethylammonium chloride followed by the isolation of the desired butene-1,4-dione derivative **2.15**. This reduction of the quaternary salt could be monitored based on a colour change from yellow to pink, whereas the following acidification regenerated the initial yellow colour, mixture was cooled for 24 hr. This simplified route afforded compound **2.15** in a reasonable 71% yield (see Scheme 2.8) and thus proved to be an adapted procedure for the synthesis of **2.15**. However, the formation of the butene-1,4 dione **2.15** was only possible when using the recycled material **2.14** from Scheme 2.7 and any direct attempts to synthesis **2.15** according to Scheme 2.8 were unsuccessful. Furthermore, any attempts to replicate the '*recycled*' compound **2.14** from Scheme 2.7 again and perform the Stevens rearrangement were also unsuccessful. There is a possibility of anion exchange upon HCl treatment, which could have assisted the material reactivity in Scheme 2.8.

The proposed synthetic route presented in Scheme 2.1 comprises the incorporation of oligomer **2.7** into the core of compound **2.6** via a Diels-Alder-type cycloaddition to form compound **2.13**. Unfortunately, a limited solubility of butene-1,4 dione **2.15** (dibromo derivative of **2.6**) in common organic solvents, such as ethanol, chloroform, carbon disulfide or propyl benzene, impeded progression according to the synthetic Scheme 2.1 Solubility limitations may result from the presence of the extra bromine atoms at the α-positions of the thiophene units of **2.15**. Therefore, efforts were made to remove the bromine atoms of the amino ketone salt **2.13** – one of the precursors of **2.15** – by reducing them with zinc powder in acetic acid.
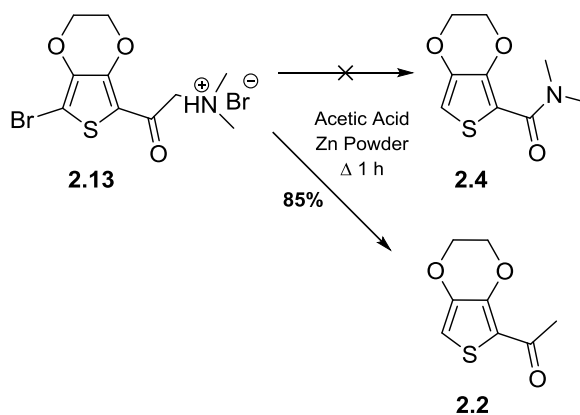
Scheme 2.9: The reduction of amino ketone salt **2.13** yielded the monoacetyl EDOT precursor **2.2** instead of the desired compound **2.4**.

Amino ketone salt **2.13** is relatively insoluble in acetic acid, thus it was treated with excess zinc powder and refluxed. Unfortunately, the desired reduction of **2.15** was not successful and compound **2.4** did not form under these conditions; instead, compound **2.13** was completely reduced to the monoacetyl EDOT precursor **2.2**, as illustrated in Scheme 2.9.

However, the solubility problems of compound **2.15** could easily be solved by the addition of long alkyl chains. The bromide substitutents at the α-positions of the thiophene rings present optimal coupling sites for further functionalisation. In order to obtain efficient electrochromic monomers, any functionalisation should retain conjugation and a planar conformation. Therefore, incorporation of hexylthiophene derivative **2.16** (see Scheme 2.10) was attempted, which promises to solve the solubility issues whilst retaining structural conjugation.
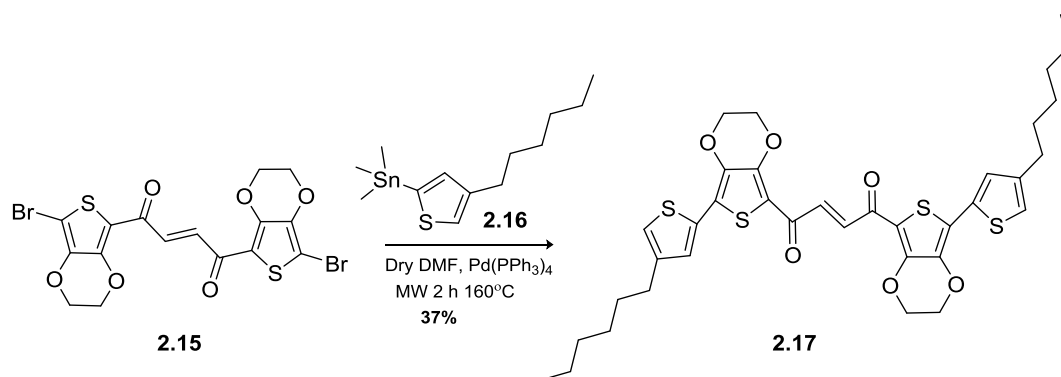
Scheme 2.10: Reagents and conditions for preparing bishexyl butene-1-4, dione derivative **2.17**.

Dibromo butene-1-4 dione **2.15** was functionalised with (3-hexylthiophen-5-yl)trimethylstannane **2.16** in a Stille cross-coupling initiated by microwave irradiation in the presence of a palladium catalyst, which resulted in the formation of the bishexylthiophen-2-yl butene-1-4-dione derivative **2.17** in a 37% yield (see Scheme 2.10). The small yield of **2.17** was linked to an extremely challenging purification. This, in combination with poor synthesis reproducibility, limited the total yield of **2.17**. Unfortunately, the low quantity obtained of **2.17** (50 mg) renders a further progression of Scheme 2.1 challenging, and was discontinued at this point. Reproduction of this reaction was also attempted, but the yield was considerably lower and also resulted in an impurity with the same R_f as the product. This complex mixture could not be

successfully separated either *via* recrystallisation or by column chromatography using various solvent mixtures.

2.3.2 Alternative to Synthetic Scheme 2.1: Proposed reagents and conditions for the synthesis of terthiophene monomer 2.1.

In order to synthesise the desired S-alkylated EDOT-DMDTT-EDOT monomer **2.1**, an alternative synthetic methodology can be investigated, which could provide access to the terthiophene **2.10**.
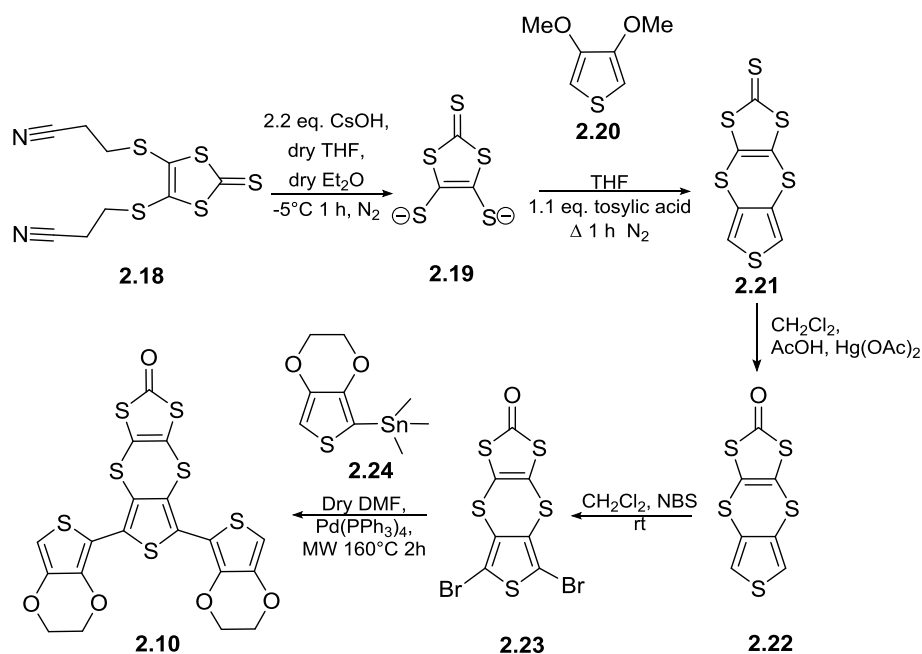
Scheme 2.11: Reagents and conditions proposed in synthesizing terthiophene precursor **2.10**.

The first step of the synthetic route shown in Scheme 2.11 constitutes the intermediary formation of the nucleophile **2.19** from compound **2.18**. Subsequently, **2.19** undergoes a nucleophilic substitution on dimethoxythiophene **2.20** (routinely prepared according to a reported procedure[301, 302]) by substituting the two OMe substituents of **2.20** with the nucleophilic sulfide groups of **2.19** in the presence of a catalyst, leading to the addition of a thiophene derivative to compound **2.18** and the formation of [1,3]dithiolo[4,5-b]thieno[3,4-e][1,4]dithiine-2-thione **2.21**. Subsequently, the transchalcogenation of **2.21** to its carbonyl derivative **2.22** would be followed by bromination of the thiophene's 2,5-positions in preparation of precursor **2.23** for the Stille cross coupling with stannylated EDOT **2.24** to yield compound **2.10**. Concluding

steps would involve de-protection of dinucleophilic functionality in **2.10** and alkylation of corresponding dianion to afford terthiophene EDOT-DMDTT-EDOT monomer **2.1**.

2.4　**Summary and Future Work**

The initial aim of this project was to synthesise a polymer with alternating bis(EDOT) and dithiinothiophene units in a 2:1 ratio by means of polymerisation of the corresponding monomer **2.1**, which would exhibit structural diversity but retain the desirable characteristics of PEDOT.[148, 190] Upon the successful synthesis of monomer **2.1**, the synthesis of additional precursors with alkyl chains of varying lengths from C_4-C_{14} was planned to facilitate the study of both linear and branched chain effects to understand their electrochemical properties and electrochromic performances.

The synthesis of the EDOT-DMDTT-EDOT monomer **2.1** was attempted according to the synthesis route shown in Scheme 2.1. Unfortunately, this synthesis exhibited major challenges. The first challenge was the synthesis of compound **2.3**, which did not succeed as the bromination of the thiophene's 5-position was preferred over the desired bromination at the α-position of the carbonyl function of **2.2**, which was required for further functionalisation according to Scheme 2.1. However, this issue was solved by the successful synthesis of compound **2.12**, which contained bromide substituents at both described positions and allowed the synthesis to continue according to a modified version of Scheme 2.1. A second major challenge was the poor solubility of compound **2.15**, which was successfully faced by introducing long hexylthiophene substituents to obtain compound **2.17**. This issue presumably arose due to the presence of the additional bromide atoms at the 5-positions of the thiophene. Therefore, and since it cannot be excluded that also the originally envisioned compound **2.3** would have caused similar solubility issues, the use of **2.12** instead of **2.3** cannot be regarded as a disadvantage at this stage of the synthesis. However, the resulting hexylthiophene derivative **2.17** exhibited purification difficulties and limitations due to reproducibility issues of precursor **2.15**, which finally hindered a progression of the synthetic route shown in Scheme 2.1. In conclusion, the successful solutions that were discovered to overcome the inherent challenges faced in the synthetic route shown in Scheme2.1 unfortunately led to unpredictable issues for later

stages of the synthesis. As an alternative to this route, an alternative approach to synthesise a derivative of monomer **2.1** according to the synthetic route shown in Scheme 2.11 has been provided.

Further work is required to resolve the synthetic reproducibility of the two precursors **2.15** and **2.17** in order to continue the synthesis towards a quinquithiophene analogue **2.25** of monomer **2.1** according to Scheme 2.1 (see Figure 2.3).
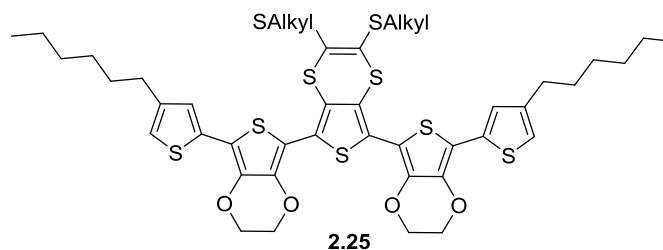

Figure 2.3: Proposed S-alkylated pentathiophene monomer **2.25**.

In parallel, this quinquithiophene **2.25** with fused dialkylthiodithiin unit can facilitate an interesting study of the steric effects of different alkyl chain lengths and the impact of substituting various positions on EC performance, e.g. by replacing (4-hexylthiophen-5-yl)trimethylstannane in the reaction shown in Scheme 2.10 by its isomer (3-hexylthiophen-5-yl)trimethylstannane. However, the quinquithiophene monomer **2.25** draws away from the initial aim of preparing a polymer retaining a PEDOT-like configuration characterised by a 2:1 (EDOT:DMDTT) ratio, since now a spacer hexyl-thiophene moiety would be incorporated. In order to avoid the loss of the desirable intrachain S-O chalcogen interactions, as seen in PEDOT and POSO, the incorporation of an alkylated EDOT (ProDOT) derivative would be favourable. This could be realised using the two bromide substituents of derivative **2.15** as linkage sites for ProDOT derivatives. Nishinaga *et al.* studied ProDOT and EDOT oligomers that had a similar effective conjugation length, a ProDOT-Hex dimer diiodide crystal was studied and reported the two thiophene rings of dimer adopt a coplanar conformation in the crystal, with a C=C—C=C dihedral angle of 180°.[303]

It is well-known that the basic problem affecting conjugated polymers in general, and polythiophenes in particular, is the significant twist that is caused even by

small substituents on the conjugated backbone, leading to reduced conjugation and a significant higher band gap.[158] A computational study reported by Bendikov's group has shown oligoselenophenes to be more difficult to twist than oligothiophenes, suggesting that larger substituents can be introduced onto their backbones without distorting conjugation.[304] Oligoselenophenes are more difficult to twist due to the inter-ring C-C bonds have more double character than in oligothiophenes.[171] Polyselenophenes have been proven to be superior to polythiophenes for some applications since they maintain planarity over a wider range of substituents, have strong quinodial character and lower band gaps.[171] Poly(3,4-ethylenedioxyselenophene) (PEDST) has been shown to exhibit well-defined spectroelectrochemistry with a band gap of 1.4 eV, which is slightly lower than that of PEDOT 1.6 eV.[157, 171]
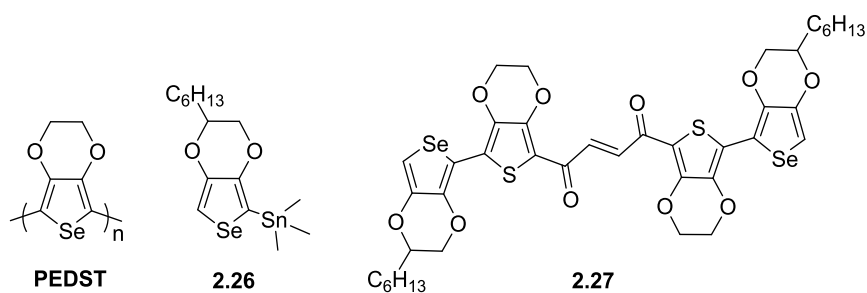
Figure 2.4: **PEDST**: poly(3,4-ethylenedioxyselenophene, **2.26**: (2-hexyl-2,3-dihydroselenopheno[3,4-b][1,4]dioxin-5-yl)trimethylstannane (hexylEDST-SnMe$_3$), **2.27**: corresponding hexylEDST-capped bisEDOT-butene-1,4-dione derivative.

Replacing the hexylthiophene derivative **2.16** by the selenophene derivative **2.26** in the synthetic route shown in Scheme 2.1 would be highly interesting, as the hexyl chain would solve the solubility problems of compound **2.15**, whilst the selenophene derivative would maintain conjugation and a planar structure (see Figure 2.4). In this chapter, two monomers have been presented that can be further functionalised and used to study the impact of PEDOT-like chalcogen intrachain interactions on optical transitions or the impact of varying alkyl lengths, substituent positions, and branching effects on the EC performances, such as optical transition switching studies etc. Such subtle structural modifications and their effects on EC performances provide greater understanding and the possibility to fine tune material characteristics and further tailor designer monomers to suit the requirements of future applications.

3   Electrochromic Properties of a Poly(dithienylfuran) Derivative Featuring a Redox-Active Dithiin Unit

3.1　**Aim**

　　Today there is a conscious effort for leading scientific research to progress towards green chemistry and renewable energy.　One aspect of this focus has led to studying the potential of furan chemistry.　Sections 1.7.4 and 1.7.5 summarises the recent advancement made with furan in organic electronics.　Within this chapter a furan-containing polymer that exhibits improved chemical and physical properties in comparison to the all-thiophene analogue **PEDOT, Poly1** and **P3**, see Figure 3.1, was targeted.
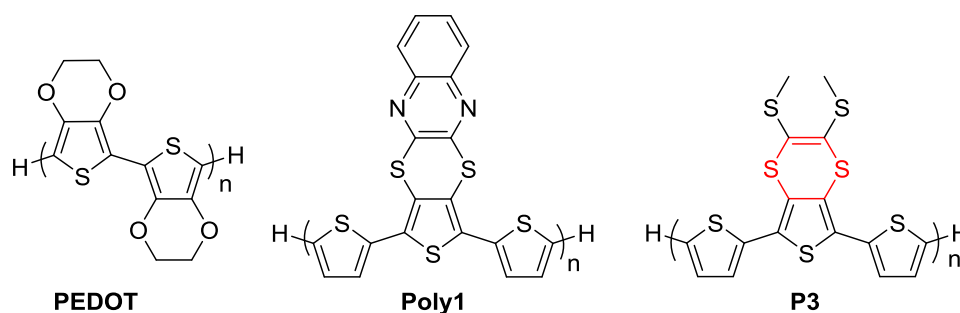
Figure 3.1: Polymer structures of **PEDOT**, **Poly1** featuring the redox active unit tetrathianaphthalene and **P3** bearing a fused dithiin ring.[148, 190]

　　It is anticipated that a promising target polymer might result from a hybrid-conjugated monomer of a dithiin and a furan unit.[305]　This chapter describes a general synthetic route to three novel hybrid furan monomer units, **3.1**, **3.2**, and **3.3**, as well as the successful electropolymerisation of dithienylfuran monomer **3.3** to the polymer **Poly3.3**, see Figure 3.2. The electrochromic properties of **Poly3.3** were investigated further for a possible application as an electrochromic material.[305]

Figure 3.2: Conjugated furan dithiin hybrid monomers **3.1**-**3.3** and poly(dithienylfuran) **Poly3.3**.[305]

3.2   Results and Discussion

Some results described herein have already been published as:

'*Electrochromic properties of a poly(dithienylfuran) derivative featuring a redox-active dithiin unit*' S. Kaur, N. J. Findlay, A. L. Kanibolotsky, S. E. T. Elmasly, P. J. Skabara, R. Berridge , C. Wilson and S. J. Coles. *Polymer Chemistry*, 2012, **3**, 2277.

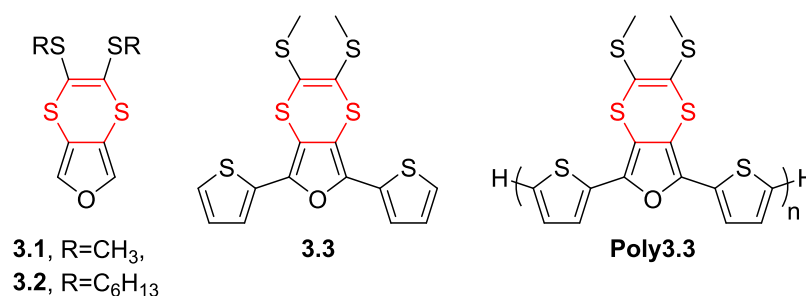X-ray crystallographic studies were performed and solved by C. Wilson at National Crystallography Service, Diamond Light Source Ltd, Oxfordshire, UK (see Appendix 1). Computational modelling calculations were prepared by P. J. Skabara at the University of Strathclyde, Glasgow, UK.

3.2.1   Synthesis

Two synthetic pathways can be adopted for the synthesis of target monomer **3.6**. The Skabara group used a pathway for the synthesis of the monomer **3.7** of polymer **P3**, which yields **3.7** in five steps from bis-thienyl diketone derivative **3.4**.[148] Target polymer **Poly3.3** differs from **P3** by one furan ring, which substitutes the central thiophene ring of **P3**. Therefore, one approach would involve the acid-catalysed cyclisation of diketone **3.6** to afford a bis(thienyl)furan precursor which would be alkylated to yield the monomer **3.3** of **Poly3.3**, see Figure 3.3.[148, 306]
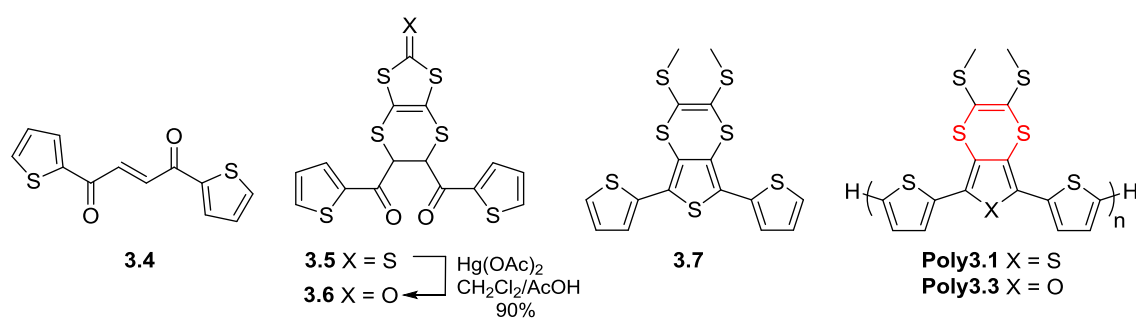
Figure 3.3: Structural intermediates of the synthesis of the terthiophene monomer **3.7** of the polythiophene **P3**.

However, an alternative synthetic route was attempted, as depicted in Scheme 3.1. In comparison to the first synthetic route, this route forms the fused central core **3.12**[307] instead of the bis-thienyl diketone derivative **3.4**.[306] This is advantageous as **3.12** can be functionalised for further aryl coupling to alternative aryl units.
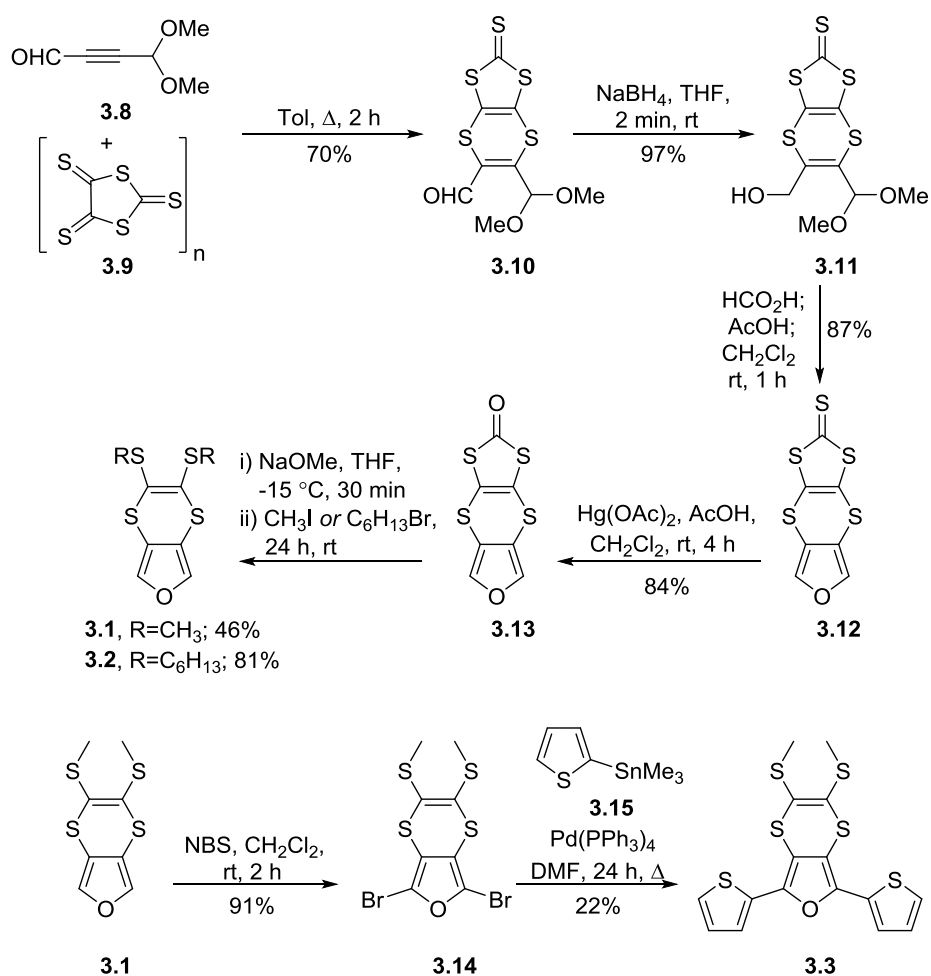
Scheme 3.1: Synthetic route to furan-containing monomers **3.1**, **3.2** and **3.3**.

According to Scheme 3.1, the synthesis of **3.12** starts from the precursors DMIT **3.9**[308] and the dimethylacetal of acetylene dicarboxaldehyde **3.8**.[309] Compound **3.8** had been chosen as a less reactive alternative to its diethylacetal derivative, which had been used in literature, but suffers from safety issues during synthesis (*e.g.*, the acetylene gas precursor), requires expensive starting materials, and generates intermediate precipitates that hinder the overall product yield (~24%).[309, 310]

Synthesis of dimethylacetal of acetylene dicarboxyaldehye 3.8

The precursor **3.8** can be synthesised according to the synthesis shown in Scheme 3.2, which allows for a large scale synthesis without major safety issues.[309]
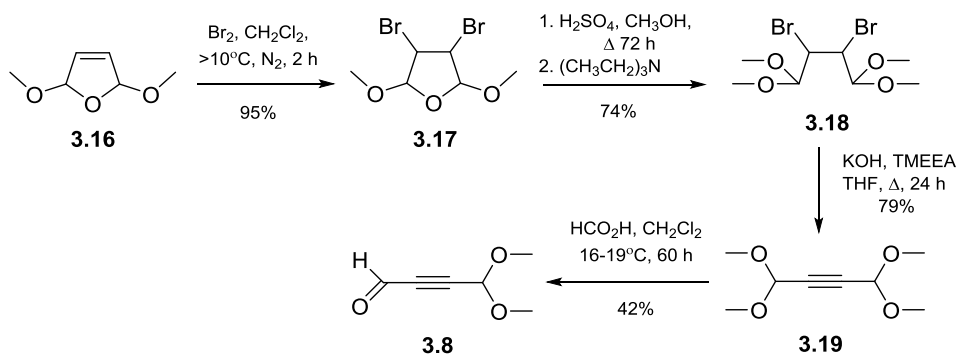
Scheme 3.2: Synthetic preparation of 4,4-dimethoxybut-2-ynal **3.8**.[309]

Commercially available 2,5-dimethoxy-2,5-dihydrofuran **3.16** was treated with stoichiometric amounts of bromine at low temperature, which afforded the light-coloured semi-solid material **3.17** in a crude 95% yield. The temperature was maintained below 20°C during reaction work-up to avoid product decomposition. The acid-catalysed ring-opening reaction of **3.17** was achieved by refluxing with conc. sulfuric acid for 72 h, affording **3.18** as a crude yellow oil in 74% yield. The formation of the alkyne **3.19** (79% yield) was successfully accomplished *via* the solid-liquid, phase-transfer catalysed dehydrohalogenation of **3.18** using potassium hydroxide (85%, pellets) and tris[2-(2-methoxyethoxy)ethyl]amine (TMEEA). The dehydrobromination step can also be performed with potassium *tert*-butoxide in DMSO (2 h, 20°C, smaller scale). However, this procedure was not chosen as the synthesis was reported to be less efficient on a larger scale and to yield a lower product purity.[309] Lastly, the acid-catalysed diacetal hydrolysis of 4,4-dimethoxybut-2-ynal **3.19** yielded a yellowish-coloured oil of **3.8**.[309]

Synthesis of oligo(1,3-dithiole-2,4,5-trithione) DMIT 3.9

Several synthetic methods are reported for the preparation of oligo(1,3-dithiole-2,4,5-trithione) **3.9**, which start with the synthesis of 1,3-dithiole-2-thione-4,5-dithiolate (DMIT) **3.20** in the first step. This intermediate can be isolated as the zinc chelate **3.22** as formulated by Hoyer laboratories (see Scheme 3.3).[308]
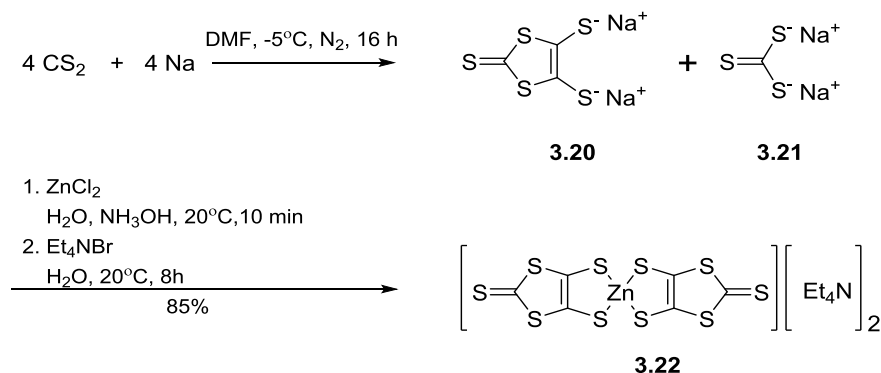
Scheme 3.3: Synthetic preparation of zincate salt **3.22**.[308]

The formed zincate salt **3.22** is far more stable than the lithium, sodium, or potassium salts of DMIT, and can be easily stored under ambient conditions for several months without decomposition.[308]
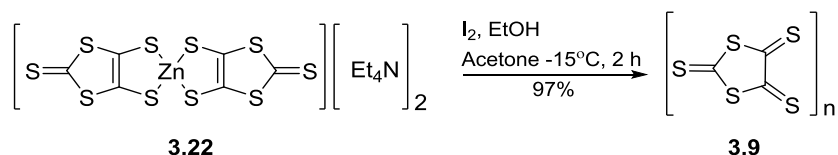
Scheme 3.4: Synthetic preparation of oligo(1,3-dithiole-2,4,5-trithione) **3.9**.[308]

Subsequently, a solution of zincate salt **3.22** in acetone (0.2 mol/L) was oxidised with two equivalents of iodine in ethanol, forming the stable oligo(1,3-dithiole-2,4,5-trithione) **3.9** in 97% yield (see Scheme 3.4).[308]

Synthetic methodology in preparing novel hybrid furan-containing monomers
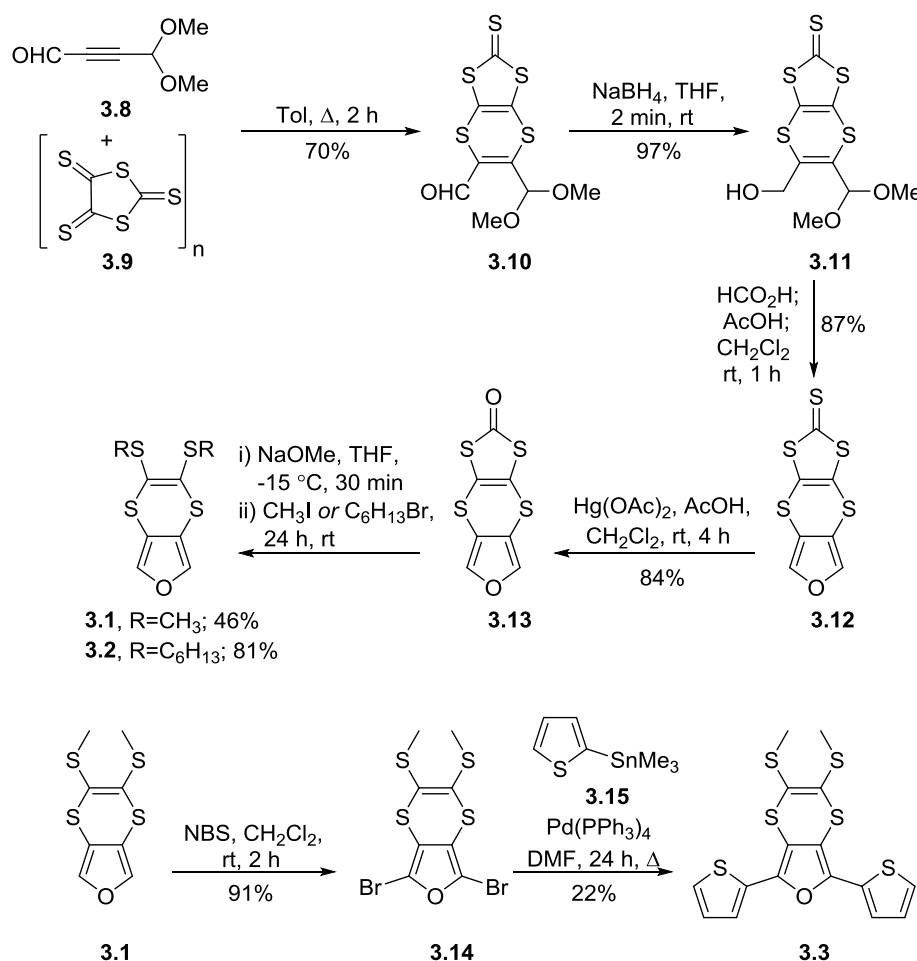
Scheme 3.5: Synthetic route to furan-containing monomers **3.1**, **3.2**, and **3.3**.

Three novel fused furan monomers **3.1**-**3.3** were synthesised from precursors **3.8** and **3.9** according to the synthetic route depicted in Scheme 3.5. Upon completion of the Diels-Alder cycloaddition of alkyne **3.8**[309] and oligomer **3.9**,[308] the resultant aldehyde **3.10** was reduced to give alcohol **3.11** in 97% yield. The subsequent acid-catalysed cyclisation of alcohol **3.11** afforded the furan derivative **3.12** in an 87% yield, which was then transchalcogenated into the corresponding carbonyl derivative, **3.13**. This compound was subsequently converted into its dithiolate and then alkylated to give bis(methylthio)dithiinofuran **3.1** or bis(hexylthio)dithiinofuran **3.2** in 46% and 81% yields, respectively. Compound **3.1** was further brominated with NBS and then converted by a Stille cross-coupling with stannylated thiophene **3.15** to monomer **3.3**.[305] This synthetic procedure provides an efficient route in preparing furan-fused cores, which can be further modified by various moieties.

3.2.2 Absorption spectroscopy and electrochemistry of fused-furan monomers 3.1-3.3

Monomers **3.1**-**3.3** were investigated by UV-Vis absorption spectroscopy and electrochemistry applying the general strategies described in Chapters 6.1.11, 6.1.12, 0 and 6.1.12. The colour code defined in Figure 3.4 is respected in all graphs in this chapter.
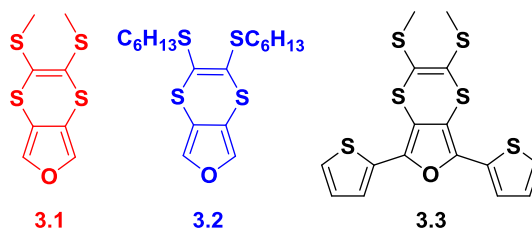
Figure 3.4: Structures of three novel fused furan monomers **3.1**-**3.3**.

UV-Vis spectroscopy reveals that both monomers **3.1** and **3.2** exhibit a similar absorption maximum (see Figure 3.5), which can be explained by their near identical structures. They strongly absorb in the shortwave UV region (268 and 267 nm, respectively), potentially due to the n-σ* transition of the sulfur lone pairs. They furthermore exhibit a π-π^* transition at 323 nm and 325 nm, respectively, resulting from an influence of the dithiinofuran heterocycle. As anticipated, the increase in conjugation length from monomer **3.1** to **3.3** induces a bathochromic shift in the absorption maxima – the absorption in the shortwave UV region is diminished compared with **3.1**, whereas a strong π-π^* transition developed at 342 nm. The HOMO-LUMO optical gap was determined from the onset of the longest wavelength absorption edge, and monomers **3.1**-**3.3** exhibited values of 3.39, 3.41, and 3.07 eV, respectively (see Table 3.1).
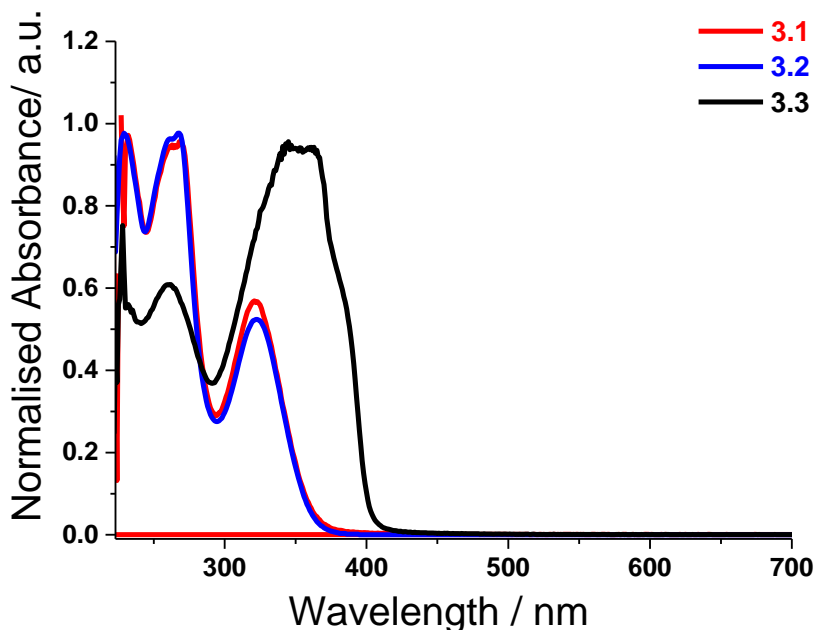
Figure 3.5: Absorption profiles of furan monomers **3.1**-**3.3** recorded from the respective solutions (10^{-4} M) in CH_2Cl_2.

The structurally related monomers **3.1** and **3.2** also displayed similar behaviours in cyclic voltammetry (CV) measurements by exhibiting one quasi-reversible oxidation peak at +0.55 and +0.65 V, respectively, and a second irreversible oxidation peak at +0.91 and +0.98 V, respectively. The difference between monomers **3.1** and **3.2** oxidation potentials suggests there is an effect of the alkyl chain on these energies (see Figure 3.6 and Table 3.1). The di(thienyl)furan monomer **3.3** revealed similarly a quasi-reversible oxidation process at +0.76 and an irreversible oxidation peak at +1.11 V, which were both shifted to positive potentials with respect to the oxidation processes of monomers **3.1** and **3.2**. The shift to positive potentials for monomer **3.3** is unexpected given increased conjugation, this disparity may indicate the lower oxidation potentials for monomers may **3.1** and **3.2** not arise from aromatic furan core. An irreversible reduction of the monomers occured at -2.07, -2.08, and -2.36 V for **3.1**, **3.2**, and **3.3**, respectively see Figure 3.6.
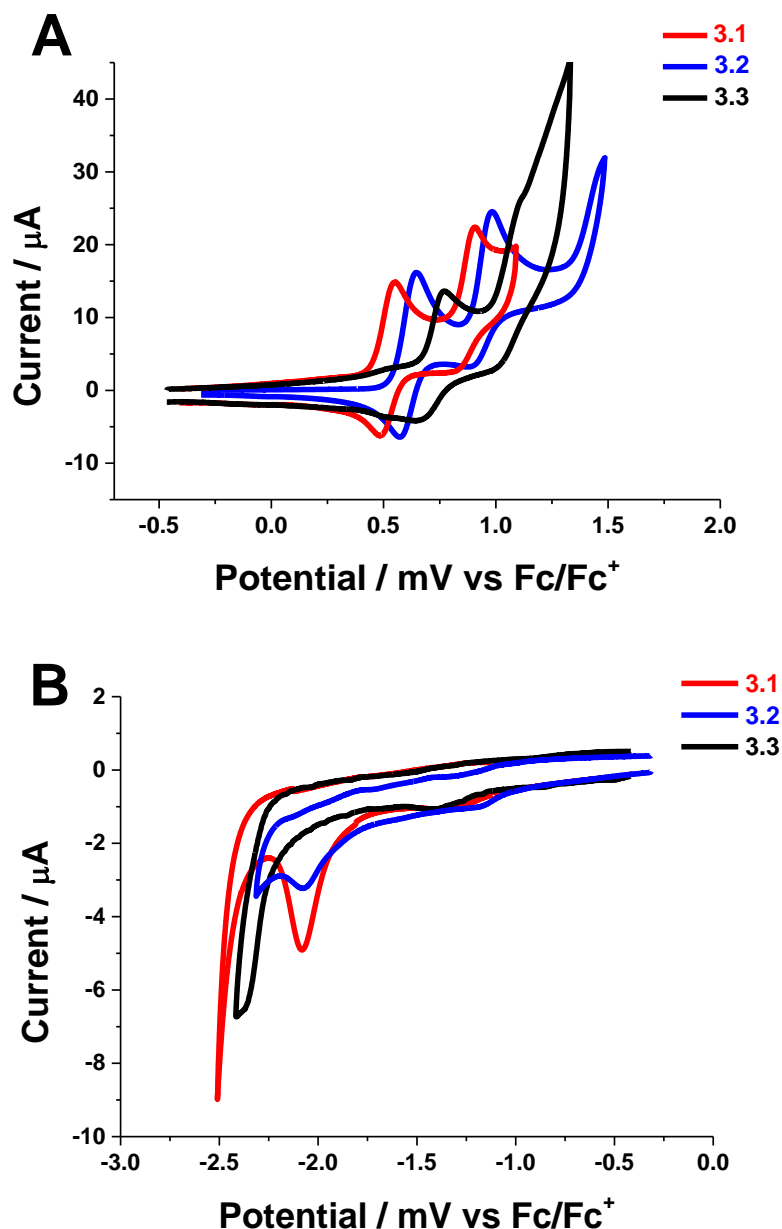
Figure 3.6: Cyclic voltammograms. A) oxidation processes and B) reduction processes of monomers **3.1**, **3.2** and **3.3** in CH_2Cl_2. The potentials were referenced to the Fc/Fc$^+$ redox couple.

Electrochemical HOMO-LUMO gaps of the monomers **3.1**-**3.3** were calculated from the difference in the onset potentials of their first oxidation and reduction peaks. Using data referenced to the Fc/Fc$^+$ redox couple, HOMO and LUMO energies were determined by subtracting the onset potentials from the HOMO of ferrocene, which has a reported value of -4.8 eV.[96, 99, 100] A summary of the data is shown in Table 3.1. It is known that with increased conjugation length the HOMO-LUMO gap will contract. However, the electrochemical HOMO-LUMO gap of monomer **3.3** of 2.98 eV is significantly larger than those of monomers **3.1** and **3.2** (2.42 eV and 2.37 eV, respectively). This unexpectedly large value can be explained by a shift of the LUMO

level of monomer **3.3** towards vacuum, while its HOMO level remains at a similar level to those of monomers **3.1** and **3.2**. This elevated LUMO of monomer **3.3** can be justified by the π-donating effect of the thiophene ring pushing electron density towards the central furan core, which renders monomer **3.3** a poor electron acceptor. The optical and electrochemical HOMO-LUMO gaps of all three monomers show significant differences, suggesting that the 1,4-dithiin ring side groups exert a significant impact on the redox properties independent from the dithiino furan core unit.[190,148]

Table 3.1: Electrochemical and absorption spectroscopy analysis of monomers **3.1**-**3.3**.

Monomer	E_{ox1}^{A}/E_{ox1}^{C} (V)	E_{ox2} (V)	E_{red} (V)	HOMO* (eV)	LUMO* (eV)	HOMO-LUMO (eV)	UV-Vis λ_{max} nm)	ε (mol^{-1}cm^{-1})	Optical Gap (eV)
3.1	0.55^a/0.48	0.91^b	-2.07	-5.34	-2.90	2.42	268	9460	3.39
3.2	0.65^a/0.57	0.98	-2.08	-5.28	2.91	2.37	267	9779	3.41
3.3	0.76^a/0.67	1.11^b	-2.36	-5.43	-2.45	2.98	342	9604	3.07

^{A} Anodic peak, ^{C} Cathodic peak, ^{a} Quasi-reversible peak, ^{b} Irreversible peak; * HOMO and LUMO values were calculated from the onset of the first peak of the corresponding redox wave and referenced to ferrocene (HOMO: -4.8 eV). ε molar absorptivity (mol^{-1} cm^{-1}).

3.2.3 Electropolymerisation

The three furan monomers **3.1**-**3.3** were further subjected to electrochemical oxidative polymerisation in CH$_2$Cl$_2$ (*ca.* 10 mM) as per the general setup detailed in Chapter 6.2. Unfortunately, the polymerisation of monomers **3.1** and **3.2** failed despite continuous anodic cycling over the first oxidation peaks (+0.55 and +0.65 V vs. Fc/Fc$^+$, respectively) and then both oxidation peaks (in addition +0.91 and +0.98 V vs. Fc/Fc$^+$, respectively; see below). Nonetheless, monomer **3.3** successfully polymerised on a carbon-working electrode during repetitive cycling over the first oxidation peak at +0.76 V vs. Fc/Fc$^+$. The polymer growth trace of monomer **3.3** is displayed in Figure 3.7.
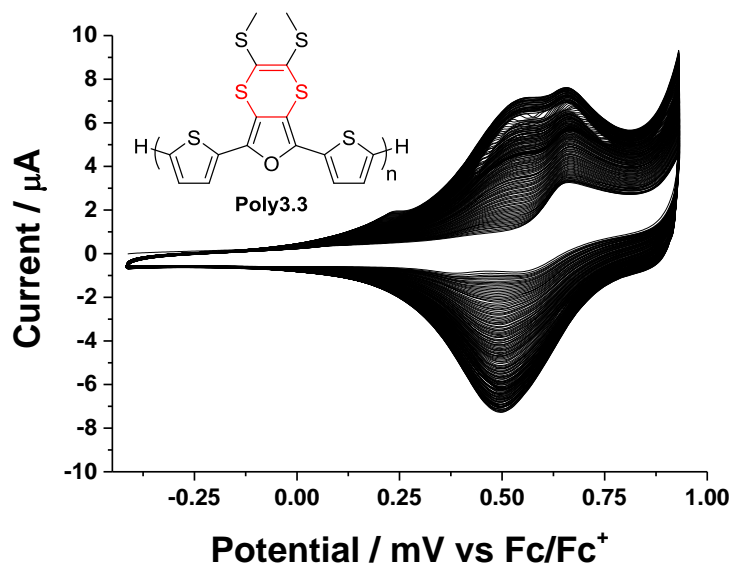
Figure 3.7: Electrochemical growth of monomer **3.3** using a carbon working electrode (substrate concentration 10^{-4} M, oxidative voltage sweep from 0 to 1 V over 150 cycles).

In order to understand why both monomers **3.1** and **3.2** were unsuccessful for electropolymerisation, molecular modelling calculations were studied. Computational calculations were performed on monomer **3.1** using density functional theory (DFT) at the B3LYP/6-31G* level (Spartan '10).

HOMO   LUMO   SOMO
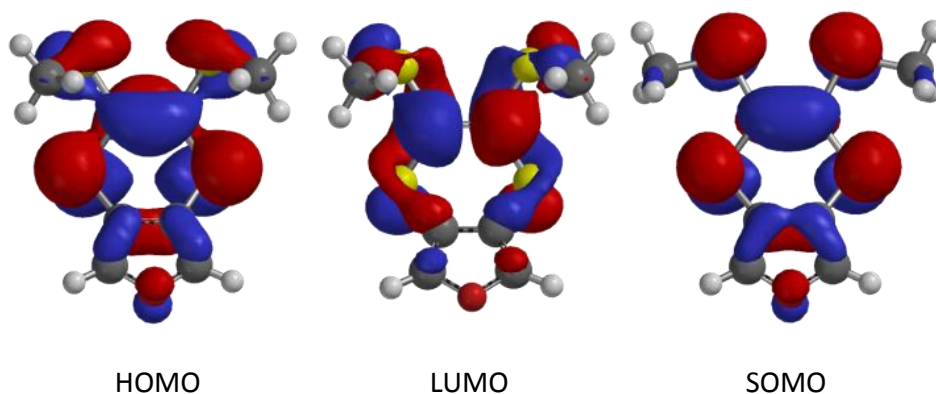
Figure 3.8: Isosurface plots of the HOMO (left), LUMO (middle), and SOMO (right) of monomer **3.1**.

The modelling calculations revealed that the HOMO of monomer **3.1** resides predominantly on the dithiin ring exerting only a subtle influence on the furan ring (see Figure 3.8). As the electron-donating properties of the 1,4-dithiin ring exceed those of the furan moiety, it is most likely that the first electron is being removed from the 1,4-dithiin ring upon oxidation. The LUMO extends over the four sulfur atoms and the two sp^2–hybridised carbon atoms between them. Examination of the singly occupied

molecular orbital (SOMO; the radical cation of monomer **3.1**) reveals that electron spin density is localised within the dithiin ring. In order to initiate a successful radical polymerisation of monomer **3.1**, electron spin density needs to reside either on the 2- or 5-position of the furan ring, which is not the case for monomer **3.1** as the calculations indicated.[54, 311] This shows that the molecular prerequisites for a successful electrochemical polymerisation of monomer **3.1** are not present. Therefore, further attempts to electrochemically polymerise monomer **3.1** were discarded at this point.

In contrast to monomers **3.1** and **3.2**, monomer **3.3** contains an extended π-conjugated system due to the two peripheral thiophenes and an enhanced electron density within the molecule. The electrochemical behaviour of monomer **3.3** mimics that of its terthiophene analogue **3.7** (see Figure 3.3) displaying one quasi reversible and one irreversible wave. Monomer **3.7** was successfully electropolymerised by anodic cycling over its first redox wave.[148] In an analogous manner, a solution of monomer **3.3** in CH_2Cl_2 was repetitive oxidatively cycled over the first redox wave and successfully induced the formation of polymer **Poly3.3** on the surface of the CWE. As **Poly3.3** was deposited in the doped state, it required to be dedoped to a neutral state by repetitive cycling in a potential region where **Poly3.3** exhibits no electroactivity (-0.4 to +0.1 V). The electrochemical behaviour of **Poly3.3** was studied in a monomer-free acetonitrile solution containing supporting electrolyte (n-TBAPF$_6$ (0.1 M); see Figure 3.9 A). Polymerisation extends the effective conjugation length, invoking a new lower oxidation wave, as seen in Figure 3.9 A. The oxidation of **Poly3.3** exhibits a large broad reversible wave at +0.63 V. In contrast, its all-thiophene analogues **Poly1**[190] and **P3**[148] exhibit reversible waves at +0.40 V and +0.60 V, respectively. The broad redox wave of **Poly3.3** could be due to the simultaneous oxidation of the 1,4-dithiin and bithiophene units, which are both electroactive.[148]

Furthermore, recent literature reported modelling calculations that furan-containing copolymers display lower overall oxidation potentials and a more destabilised HOMO level in comparison to thiophene-containing analogues due to the more electron-rich, oxygen-containing furan rings.[102]

A

B
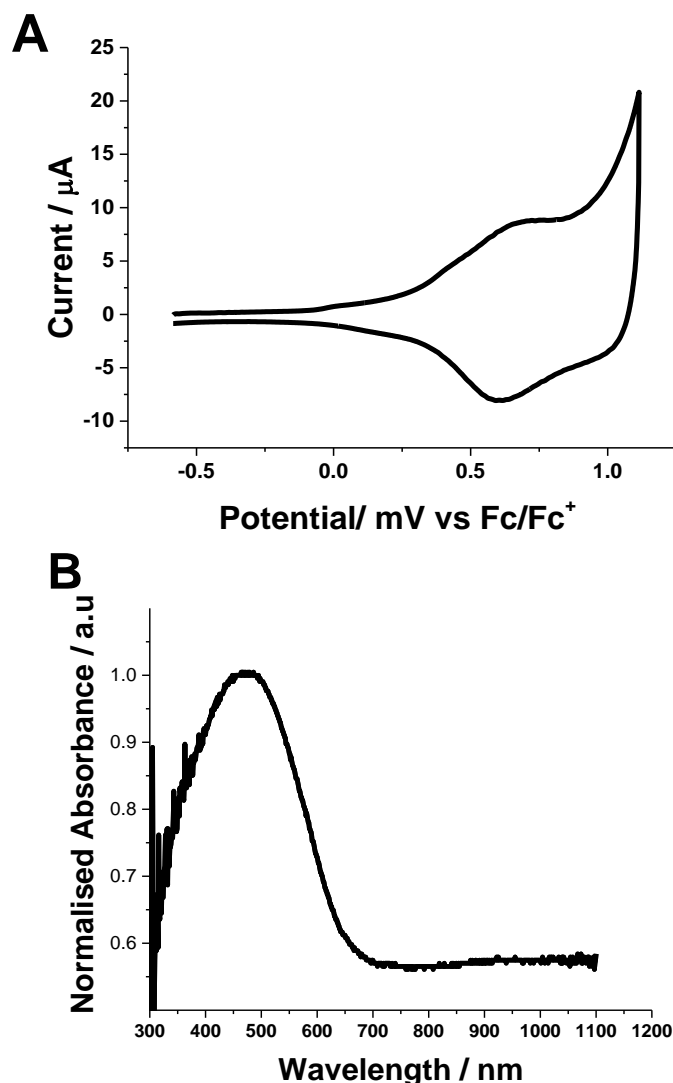
Figure 3.9: A) Oxidation of a **Poly3.3** film after dedoping in MeCN solution. The data is referenced to the Fc/Fc$^+$ redox couple. B) Electronic absorption spectrum of **Poly3.3** deposited as a thin film on ITO glass.

In order to determine the absorption characteristics of **Poly3.3**, the polymer was electrochemically polymerised on a transparent and conductive ITO glass substrate from a solution of monomer **3.3** in CH$_2$Cl$_2$ (10^{-3} M), containing n-TBAPF$_6$ (0.1 M) as supporting electrolyte. The newly-formed polymer was air-dried and then rinsed with CH$_2$Cl$_2$ in order to remove excess monomer or any small oligomeric species before the polymer film was dedoped back to neutrality.

The UV-Vis absorption of the neutral **Poly3.3** film (Figure 3.9 B) revealed a significant bathochromic shift (132 nm) compared to its monomer **3.3** (474 nm for **Poly3.3** *c.f.* 342 nm for monomer **3.3**, see Figure 3.9), a result of the increased effective conjugation length. The onset of the absorption edge of the longest wavelength band

is at 650 nm, giving an optical band gap of 1.90 eV. This value corresponds closely to the electrochemical band gap of **Poly3.3** obtained by cyclic voltammetry (1.97 eV, see Table 3.2).
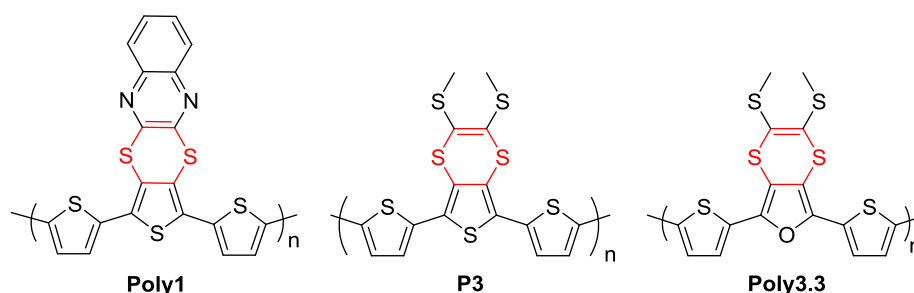
Figure 3.10: Polymers featuring the redox active dithiin unit.

Table 3.2: Electrochemical and absorption spectroscopy data of a **Poly3.3** thin film compared to the analogous polymers **Poly1** and **P3**.

Polymer	E_{ox1} (V)	E_{ox2} (V)	E_{red} (V)	HOMO (eV)	LUMO (eV)	E_g (eV)	UV-Vis λ_{max} (nm)	Optical Gap (eV)
Poly1[46]	0.40	1.20	-1.87	-	-	1.85	467	1.90
P3[47]	0.60	0.83	-1.93	-5.30	-3.19	2.11	450	2.00
Poly3.3	0.63^a/0.22^b	-	-2.14	-5.02	-3.05	1.97	474	1.90

^{a} Broad quasi-reversible anodic peak, ^{b} Onset peak potential.

Previously, Önal *et al.*[312] successfully polymerised 2,5-di-(2-theinyl)-furan (SOS) in ethanol and reported its co-polymer film (**PSOS)** to possess a bandgap of 2.2 eV, which lies within the bandgap range of the corresponding homopolymers (polythiophene Eg = 2.0 eV and polyfuran Eg = 2.35 eV).[312] However, it is encouraging that the furan-containing polymer **Poly3.3** displayed both a lower electrochemical and optical band gap in comparison to its thiophene analogue **P3** (see Figure 3.10 and Table 3.2). The narrower bandgap of **Poly3.3** can be attributed to the difference in electronegativity and the weaker aromatic character of the furan ring in comparison to the thiophene ring, thus making it more susceptible to oxidation. In addition, Bunz *et al.* recently reported a torsion twist of 22.6° between the bithiophene rings, whilst bifuran monomers are relatively planar.[197] The twist in the bithiophene units is caused by the steric hindrance between the larger sulfur atom and the 3'-hydrogen of the adjacent thiophene ring. However, this was not observed in bifuran units, presumably due to the presence of smaller oxygen atoms, which allow efficient orbital overlap with their neighbouring carbon atoms.[197]

3.2.4   X-ray Crystallography
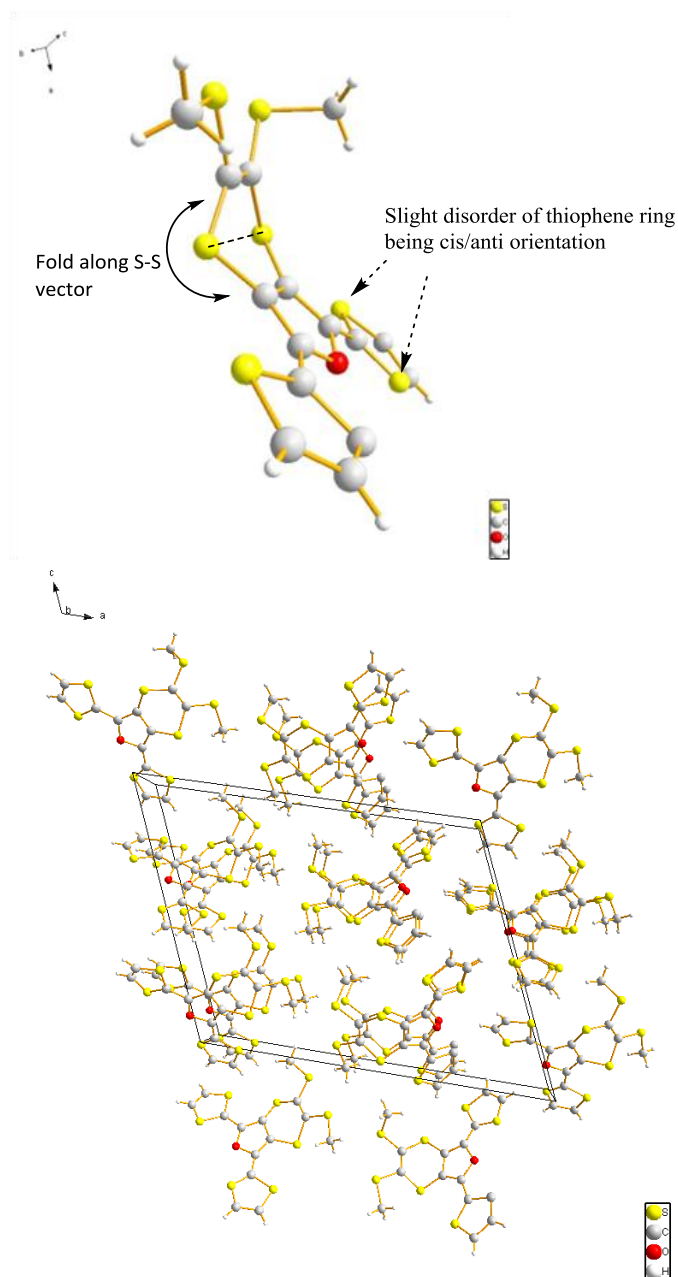
Figure 3.11: Top: X-ray crystal structure of monomer **3.3** viewed along the a-axis. The peripheral thiophenes are present in form of two different conformers: in one conformer, both sulfur atoms are oriented *anti* to furan, whereas in the other conformer, one sulfur atom is oriented *anti*, while the other one adopts either *cis* or *anti* conformation with respect to the central furan ring. Bottom:X-ray packing diagram of monomer **3.3** viewed along the b axis.

The structure of monomer **3.3** was determined by single crystal X-ray diffraction studies using synchrotron radiation (see Appendix 1). Crystals of monomer **3.3** were obtained by recrystallisation from hot acetonitrile. It is well known that 1,4-dithiin rings adopt a boat conformation in the crystalline state, with the degree of bending in the

ring expressed as a folding along the S---S vector (see Figure 3.11). Monomer **3.3** retains a high degree of planarity between the adjacent thiophene units bound to the furan core. Two molecular conformers are present within the unit cell. In one conformer, both peripheral thiophene units are in *anti*-conformation to the furan (torsion angles O1-C1-C9-S2 169(2)° and O1-C4-C5-S1 176(2)°) forming close S---S intramolecular contacts with the 1,4-dithiin ring on the furan (S2¨S4 3.43 Å and S1¨S3 3.33 Å). In the other conformer of the unit cell, one peripheral thiophene ring is in *anti*-conformation with respect to the furan (O1a-C4a-C5a-S11a = -176(2)°, S11a¨S3a =3.39 Å), and the other thiophene unit is either in *anti-* or *cis*-conformation to the furan in a ratio of 1:1 (O1a-C1a-C9a-S2a = 173(2)° and O1a-C1a-C9a-S2a = -7(3)° as well as S2a¨S4a =3.35 Å for the *anti*-conformation).

3.2.5   *Spectroelectrochemistry*

Spectroelectrochemistry combines electrochemical and spectroscopic monitoring and is a comprehensive technique for the analysis of transient chemical species formed *in situ* during redox reactions occurring at the electrode surface.[313, 314] The UV-Vis spectroelectrochemical analysis of a **Poly3.3** film prepared on ITO glass substrate was studied in monomer-free acetonitrile solution, using the same electrolyte concentration as previously (*n*-TBAPF$_6$ (0.1 M); see Figure 3.12, ref. Chapter 6.3.1).

Figure 3.12: 3D Absorption spectroelectrochemical plot for the oxidation of **Poly3.3** on ITO glass substrate (in acetonitrile).

The polymer film **Poly3.3** was subjected to a constant potential until the complete UV-Vis profile was recorded. The film was oxidised by increasing the potential from 0 to 2 V in 100 mV increments. The spectroelectrochemical plot of **Poly3.3** (see Figure 3.12) shows the simultaneous formation of a new absorption wave in the wavelength region of 600-1000 nm, and the concomitant decrease of absorption intensity of the π-π* band at a wavelength of 474 nm when subjected to a potential of +0.9 V. This new optical transition observed at a wavelength of ~600 nm indicates the formation of delocalised polaron species within the polymer chain and, upon increasing oxidation, yields a broader absorption wave in the NIR region (900-1100 nm) representing the propagation of doubly-charged bipolaron species.[313] These spinless bipolaron species are thermodynamically stable when the polymer chain tautomerises from its aromatic form into the quinoidal polymer structure.[313, 315] In its quinoidal form, the polymer adopts double bond character between neighbouring heterocycles, supporting effective orbital overlap and charge delocalisation.[313, 314] In addition, comparison of the CVs of monomers **3.1**-**3.3** as well as polymer **Poly3.3** indicates that the 1,4-dithiin pendant groups oxidise at lower oxidation potentials (see Figure 3.6 and Figure 3.9 A). Herein, no significant spectral transformations are observed upon increasing the potential until 0.8 V, suggesting that the oxidised 1,4-dithiin rings are not spectroscopically detected due to their weak sulfur n-π* transitions.
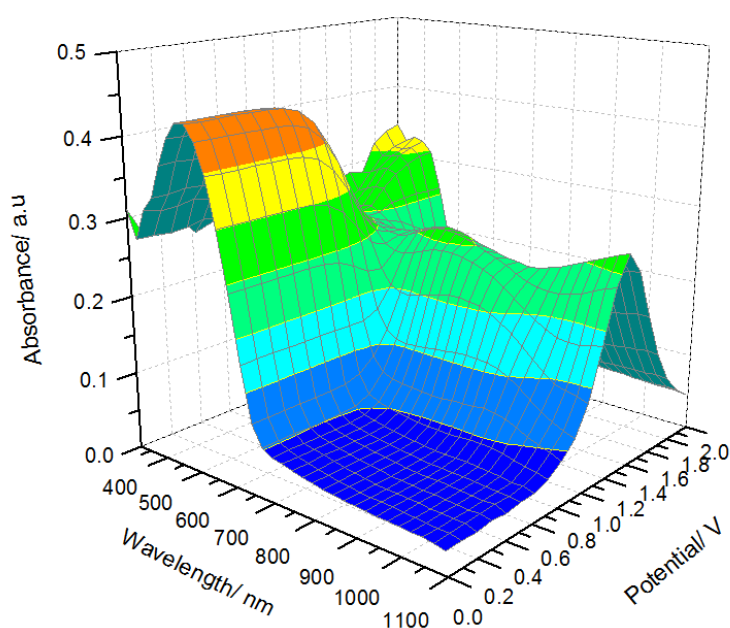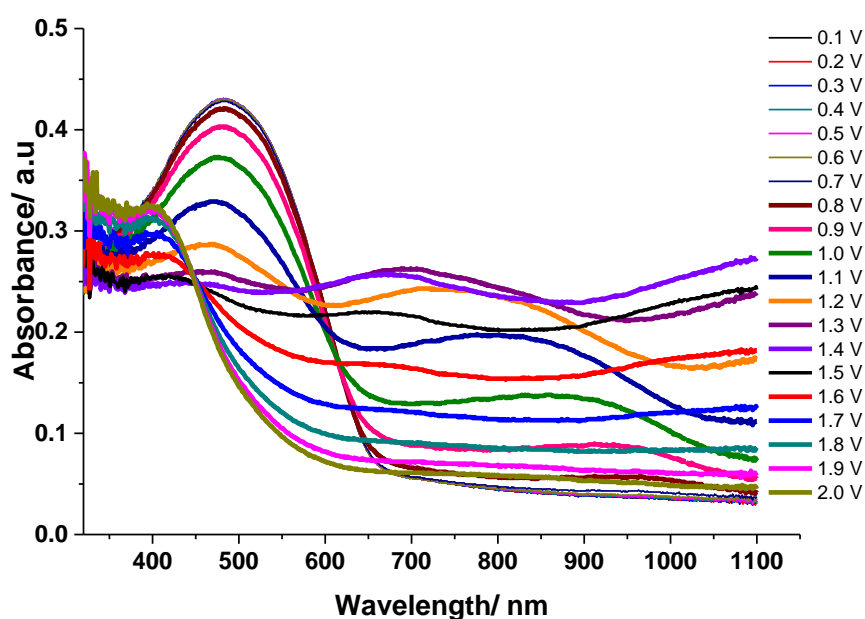

Figure 3.13: 2D absorption spectroelectrochemical plot of the oxidation of **Poly3.3** prepared on ITO glass substrate (in acetonitrile).

Figure 3.13 shows an overlay of the UV-Vis spectra of **Poly3.3** recorded at different potentials between 0 and 2 V, which clearly demonstrates the generation of polarons and bipolarons with an increasing potential. Interestingly, a new absorption wave develops at a wavelength of *ca.* 400 nm upon application of higher oxidation potentials (>1.4 V). This peak formation at high energies implies that the polymer morphology has altered, probably due to the excess generation of bipolaron species, which increases the polymer's electrophilicity and affinity for attack by nucleophiles such as water molecules/OH$^-$ ions or other nucleophilic impurities that may be present in solution.[315, 316] These nucleophilic processes non-reversibly break the polymer into smaller segments, which shortens the average conjugation length. In order to prevent this, EC polymer films can be encapsulated into devices or supported within a gel electrolyte coating.[314, 317] Spectroelectrochemical studies have clearly illustrated that **Poly3.3** exhibits various optical transitions within the visible to NIR region in response to different redox processes that are induced by an increasing redox potential.

3.2.6 Switching Studies

For an application as electrochromic material, current scientific interest does not only focus on the potential-induced molecular transformations and the related change in the UV-Vis absorbance of **Poly3.3** films, but furthermore on the kinetics of these reversible transformations. This switching rate of the **Poly3.3** film can be determined by monitoring the change in absorbance at maximum λ_{max} of the neutral polymer as a function of time, whilst the polymer is repeatedly switched between two different potentials (ref. Chapter 6.3.2). These parameters can be deduced from the spectroelectrochemical plots of **Poly3.3** depicted in Figure 3.12 and Figure 3.13. Ideally, the polymer film is subjected to a potential step by applying an initial potential where the polymer is fully neutral and a final potential where the polymer is fully doped. Monitoring the rate of change in absorbance upon redox reactions provides a direct indication of the material's switching capability, which is an imperative property for the display industry.

Switching the potential between 0 to +1.3 V evokes in **Poly3.3** the greatest absorbance change at a wavelength of 705 nm, causing the polymer to change from neutral to p-doped. As mentioned previously, **Poly3.3** was electrochemically prepared on ITO glass, dedoped to neutrality, and studied in acetonitrile solution. The

absorbance of the **Poly3.3** film at 705 nm was monitored while the potential was switched from 0 to +1.3 V (vs. Ag wire) at various potential switching rates (10, 5, 2.5, 1.25, 0.5, and 0.25 s) using square wave potentiometry, as shown in Figure 3.14.
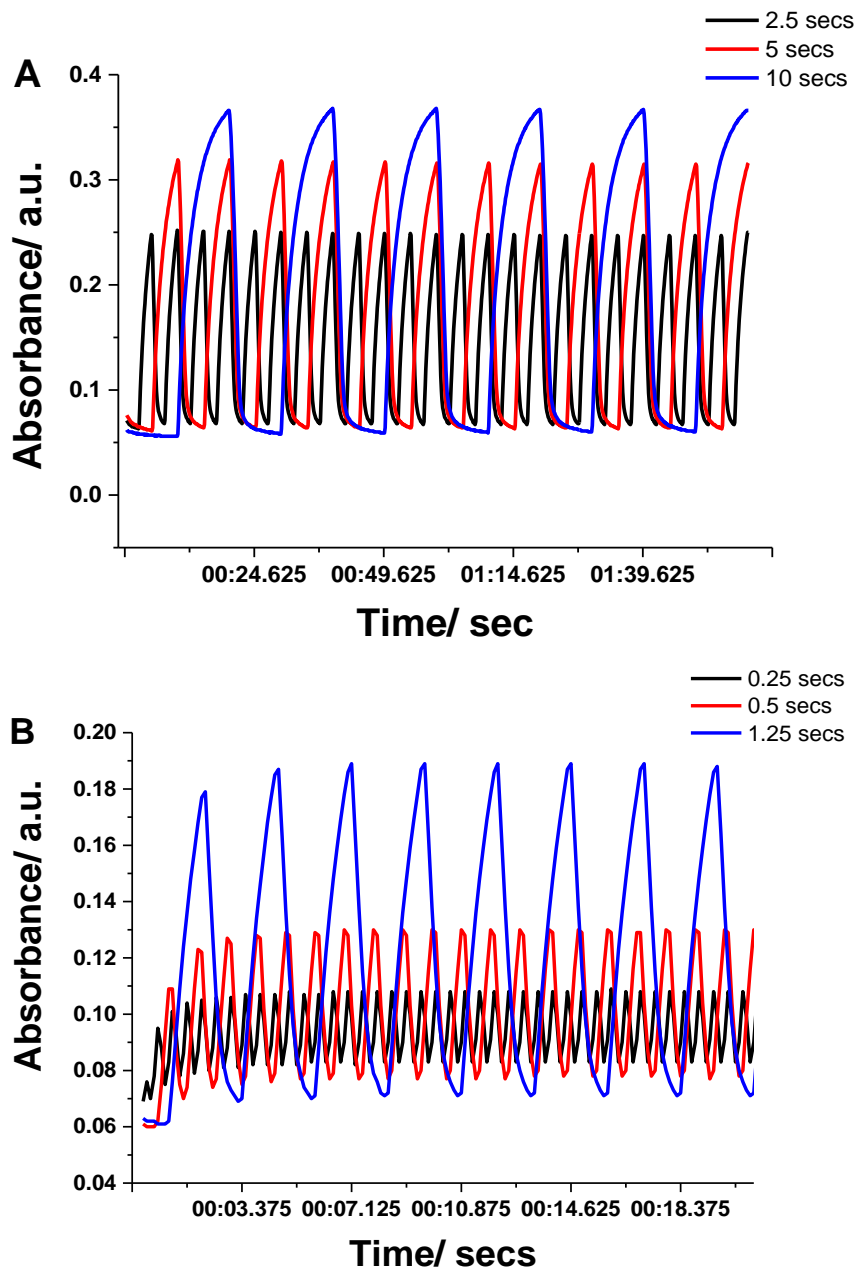

Figure 3.14: Both graphs A and B show a change in absorbance upon p-doping at various switching rates for **Poly3.3** (in acetonitrile). The absorbance was monitored at 705 nm while switching the potential between 0 and +1.3 V.

The switching characteristics of **Poly3.3** were reported as the change in absorbance and documented in Table 3.3.

Table 3.3: Switching times and percentage change in absorbance **Poly3.3** film compared with a film of **P3**.

	Time (s)					
	10	**5**	**2.5**	**1.25**	**0.5**	**0.25**
ΔT% **Poly3.3**	83.9	79.8	72.9	62.4	39.8	23.8
ΔT% **P3**[a]	79.8	66.2	51.6	39.3	19.0	9.3

[a]Absorbance was measured at 755 nm between potentials of -0.4 and 1.5 V of **P3** in acetonitrile solution.[148]

Table 3.3 clearly details the fast switching properties of both terthiophene and furan-containing polymers **P3** and **Poly3.3** when subjected to an electrochemical stimulus. These fast switching performances can be justified by the presence of the bent 1,4-dithiin ring conformation, a feature present in both polymers, which disrupts any π-π stacking, creates an open morphology, and thus allows the efficient flow of counter-ions into and out of the polymer film.[148, 190]

Polymer structures that favour a more open morphology are known to yield higher contrast ratios and faster switching speeds.[17, 179] Novel EC materials with switching speeds in the magnitude of milliseconds have recently been reported. These polymer systems use pendant groups such as triphenylamine, fluorides, or alkoxy side chains (in propylene dioxythiophene systems), which may also contribute in creating an amorphous polymer morphology.[166, 179, 318]

3.2.7   Chromaticity Analysis

Any electrochromic material is characterised by its specific and reproducible colour states as well as its contrast ratios, which need to be reported for the commercialisation of an electrochromic material. The colour coordinates of any electrochromic polymer can be precisely determined by *in situ* chromaticity analysis as per Chapter 6.3.3 methodology. The optical colour conversions of a **Poly3.3** film can be defined based on its colour space coordinates using the 1931 (XYZ) CIE and 1964 (*L* a* b**) CIE representation of colour as developed by the "Commision Internationale de L'Eclairage'' (CIE).[282] **Poly3.3** was grown on an ITO glass substrate and measured in monomer-free acetonitrile solution containing n-TBAPF$_6$ (0.1 M) as electrolyte. The measurements were recorded with a 10° standard observer and source C illuminant (overcast daylight, CIE 1964, 6770 K).[282]

A potential of 0 V followed by +1.3 V was applied to the **Poly3.3** film (each potential held constant for 90 s) to convert the polymer into its neutral or doped state, respectively. The potential-induced colour transformation was quantified by measuring the colour coordinates; see Table 3.4 and Figure 3.15.

Table 3.4: CIE XYZ 1931 and $L*a*b*$ 1964 colour space for neutral and doped **Poly3.3**.

Poly3.3	Neutral	Doped	Δ	Colour Change from Neutral
X	55.45	50.56	-4.89	
Y	55.78	57.50	+1.72	
Z	45.48	54.84	+9.36	
x	0.3660	0.331	-0.035	
y	0.3338	0.3420	+0.0082	
z	0.3002	0.3262	+0.026	
L	76.41	80.46	+4.05	Lighter
a*	16.21	-0.42	-16.63	Greener
b*	13.01	10.57	-2.44	Bluer
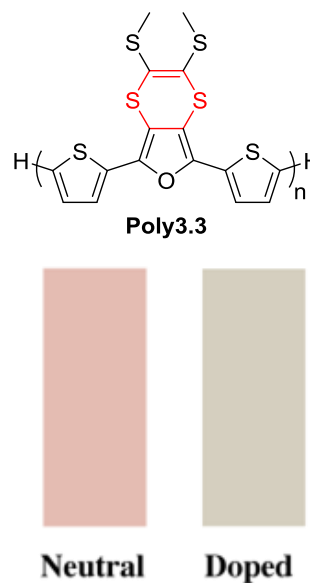
Figure 3.15: **Poly3.3** colour graphic representation converted from CIE*Lab* to CIE XYZ coordinates.

The chromaticity analysis of **Poly3.3** was measured in the UV-Vis range where the formation of polarons and bipolarons was observed (see Figure 3.12 and Figure 3.13). Thus, the optical transformation of **Poly3.3** can be directly detected visually showing a reversible colour change from salmon-red to a beige tan colour upon application of the indicated potential (see Figure 3.15). Table 3.4 clearly indicates the decrease of $a*$ from a positive value of 16.2, corresponding to a red hue, to a negative value of -0.42, corresponding to green, causing the red salmon colour to change upon oxidation. Furthermore, the value $b*$ indicates a subtle drop in yellow direction. The combination of the slight green and yellow hues with the increase in luminance $L*$ explains the observed tan beige colour in the oxidised state, as shown in Figure 3.15. In comparison to **Poly3.3**, the closely-related terthiophene polymer **P3** shows a different optical change from red to yellow and the total difference between the two coloured states is calculated to be ΔE = 17.29, which is visually obvious to the human eye.[148]

3.2.8 Colouration Efficiency (Chronocoulometry)

This study is based on the tandem chronocoulometry (CC) method in which the transmittance at λ_{max} is monitored along with the charge passed as the polymer film is switched between two redox states.[319, 320] CC studies were performed on neutral **Poly3.3**, which had been electrochemically prepared on ITO glass and studied in monomer-free acetonitrile solution containing n-TBAPF$_6$ as the electrolyte (0.1 M), as in the experimental strategy detailed in Chapters 6.1.11 & 6.2.

3.2.8.1 Colour forming efficiency of Poly3.3 film

Figure 3.16 shows an overlay of the percentage change in transmittance and the charge flow of the oxidised **Poly3.3** film during a complete dedoping process. The absorbance of the film was monitored at λ_{max} = 705 nm while 10 s square-wave potential pulses were applied to switch the film between its neutral (0 V) and doped (1.3 V) state (See Figure 3.16).
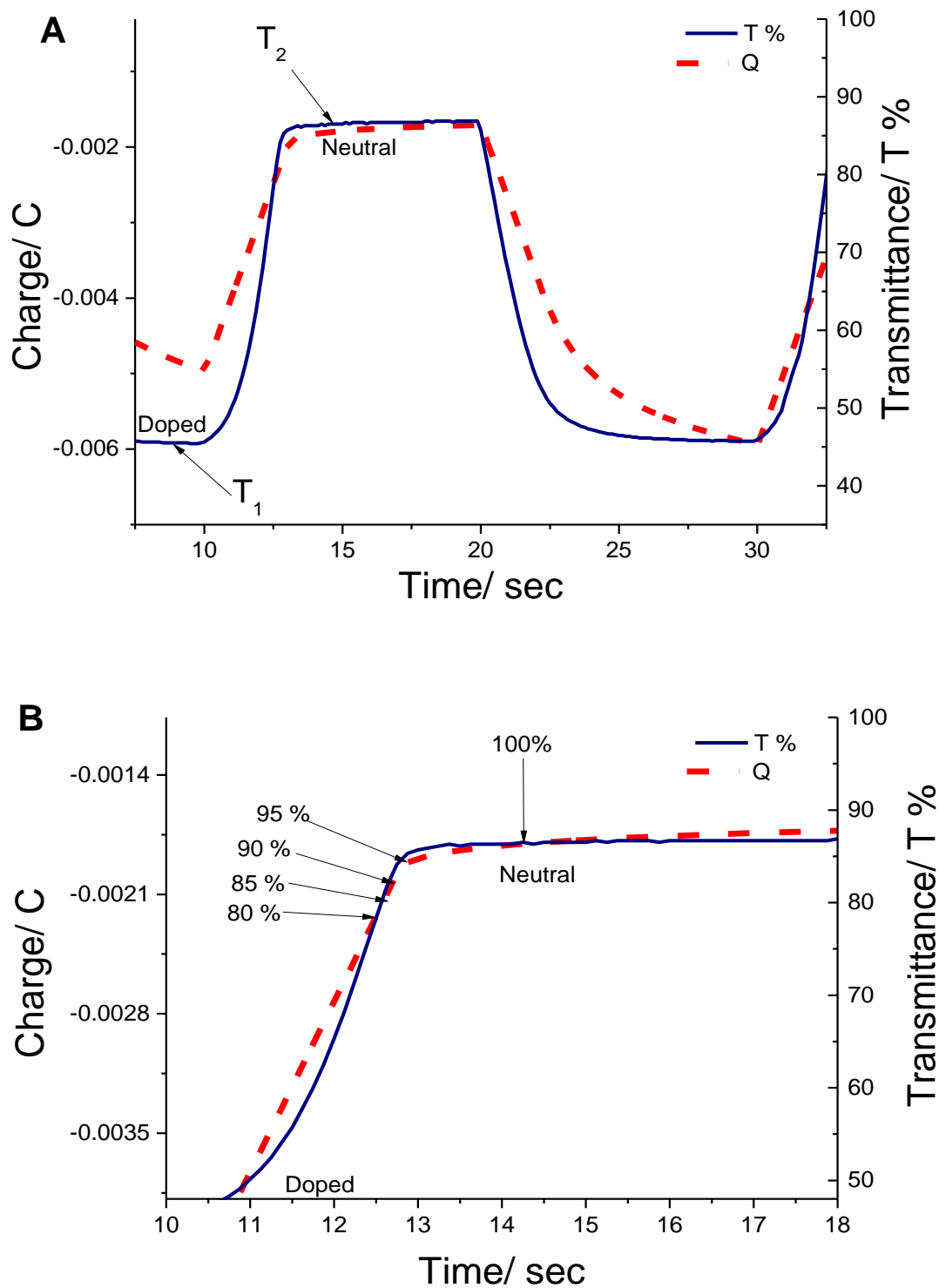
Figure 3.16: A: Colouration efficiencies (Chronocoulometry) experiments of **Poly3.3** film on ITO, switched from fully oxidised state (+1.3 V) to neutral state (0 V) and back to oxidised state, 3 steps for 10 s pulse and transmittance measured at λ_{max} = 705 nm. B: graph shows various % optical changes from which to calculate CEs for the dedoping process.

Table 3.5 summarises the colouration efficiencies of the reduction process at various

%T. All chronocoulometric data in

Table 3.5 were baseline corrected.

Table 3.5: Colouration efficiencies of **Poly3.3** at various percentages of an optical switch from tan beige to salmon-red, dedoping process. Data has been baseline corrected.

$\Delta T^{a,b}$ (%)	% change	T_b^a(%)	T_c^a(%)	τ (s)	Q (C)	Q_d^c	Δ_{OD}^d	η^e (cm^{2}C^{-1})
40.91	100	45.51	86.42	5.36	0.003021	1.34×10^{-3}	0.279	207
38.86	95	45.51	84.37	3.86	0.002840	1.26×10^{-3}	0.268	212
36.82	90	45.51	82.33	3.76	0.002740	1.12×10^{-3}	0.257	211
34.77	85	45.51	80.28	3.68	0.002660	1.18×10^{-3}	0.247	209
32.73	80	45.51	78.24	3.61	0.002600	1.16×10^{-3}	0.235	204

[a] transmittance measured at λ_{max} = 705 nm; [b] $\Delta T\% = T_c\% - T_b\%$; [c] $Q_d = Q/A$, where A (electrode area) = 2.25 cm^2; [d] $\Delta_{OD} = \log[\%T_b / \%T_c]$; [e] $\eta = \Delta OD(\lambda)/ Q_d$.

In a standard experiment, the CE is calculated at 95% of the maximum optical contrast. At this point of time, only a minimal additional colour change is visually perceivable, which avoids complications due to increasing background charges. The CE of the reduction process of the **Poly3.3** film, going from oxidised to neutral state, was calculated to be 212 cm^2 C^{-1} at 95% of the full switch (λ_{max} = 705 nm).

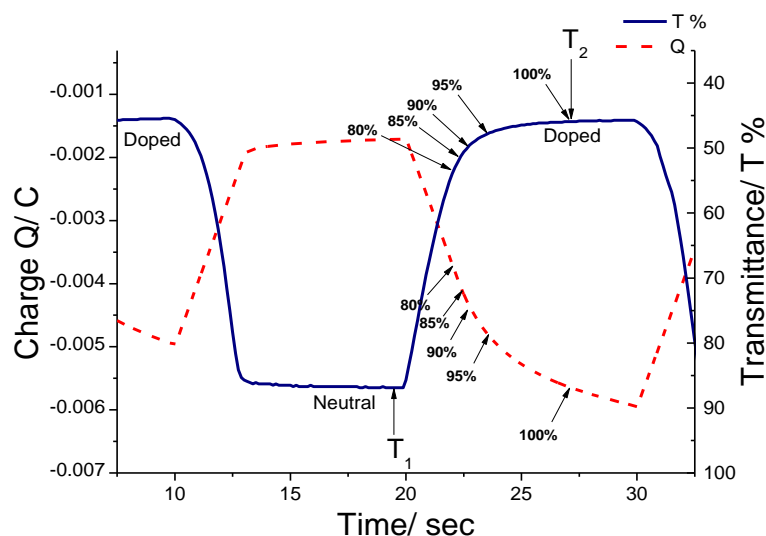### 3.2.8.2   Colour bleaching efficiency of Poly3.3 film

Figure 3.17: Chronocoulometrically measured colouration efficiencies of the **Poly3.3** film on ITO, switched from neutral state (0 V) to oxidised state (+1.3 V) and back to neutral state (three steps for a 10 s pulse; transmittance measured at λ_{max} = 705 nm). The graph shows the optical changes at various percentages based on which the CEs were calculated for the doping process.

Table 3.6: Colouration efficiencies of **Poly3.3** at various percentages of a complete optical switch from salmon-red to tan-beige. Data has been baseline corrected.

$\Delta T^{a,b}$ (%)	% change	T_1^a(%)	T_2^a(%)	τ (s)	Q (C)	$Q_d^{\ c}$	$\Delta_{OD}^{\ d}$	$\eta^{\ e}$ (cm^{2}C^{-1})
41.16	100	86.88	45.72	7.60	-0.00392	-1.74 x 10^{-3}	-0.279	-160
39.10	95	86.88	47.78	4.06	-0.00304	-1.35 x 10^{-3}	-0.260	-192
37.04	90	86.88	49.84	3.17	-0.00259	-1.15 x 10^{-3}	-0.241	-210
34.98	85	86.88	51.89	2.82	-0.00234	-1.04 x 10^{-3}	-0.224	-215
32.93	80	86.88	53.96	2.51	-0.00202	8.98 x 10^{-4}	-0.207	-230

[a] transmittance measured at λ_{max} = 705 nm; [b] $\Delta T\% = T_2\% - T_1\%$; [c] $Q_d = Q/A$, where A (electrode area) = 2.25 cm^2; [d] $\Delta_{OD} = \log [\%T_2 / \%T_1]$; [e] $\eta = \Delta OD(\lambda)/ Q_d$.

The CE of the doping process of **Poly3.3** at 95% of a full optical switch (λ_{max} = 705 nm) was calculated to be -192 cm^{-2} C^{-1}, which is slightly higher than that of a closely packed PEDOT film[321] (183 cm^{-2} C^{-1} for a film with a thickness of 150 nm), but lower than that of PProDOT (285 cm^2 C^{-1}),[321] see Figure 3.1 and Table 3.6. In comparison, **Poly1** (possessing large pendant quinoxaline groups) shows a superior CE of 381 cm^2 C^{-1} measured at 650 nm for 95% of a full switch.[190]

The doping process of **Poly3.3** results in a lower CE value as opposed to its dedoping process (-192 cm^{-2} C^{-1} *vs.* +212 cm^2 C^{-1} respectively), which highlights the importance of measuring the charge passed at a very specific transmittance value and not simply dividing the total absorbance change by the maximum charge passed. The overall CEs are affected by the rate of uptake or loss of counter ions, which must accompany the colour-transforming electron transfer to preserve the electroneutrality of the solid electrochrome. These colouration efficiency studies highlight how structural modification in organic polymers can influence a material's electrochromic performance.[166, 179, 321] Therefore, the advantage of the boat conformation of the dithiin ring in addition to a beneficial electronic properties of furan containing polymer assists in creating an open morphology and resulted in improved switching speeds and moderate CE's.[148]

3.3 **Conclusion**

The synthesis of three novel furan-based monomers has been described, and all three have been characterised by absorption spectroscopy and cyclic voltammetry.
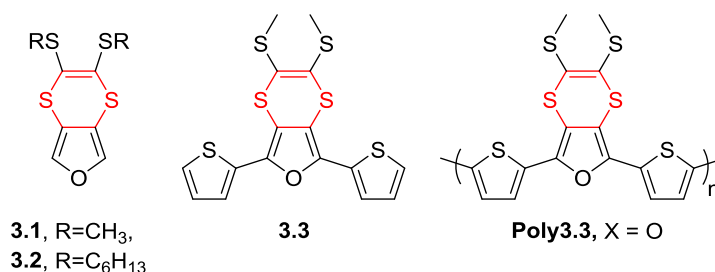

Figure 3.18: Structure of conjugated furan dithiin hybrid monomers **3.1**-**3.3** and Poly(dithienylfuran).

The dithienylfuran monomer **3.3** successfully underwent an electrochemical polymerisation to form **Poly3.3**, which was investigated by CV, UV-Vis spectroelectrochemistry, and electrochromic switching studies. It exhibited a lower electrochemical band gap and superior switching speeds compared to the corresponding terthiophene analogue **P3** (e.g., 1.97 eV, *cf.* 2.11 eV).[148] The narrower band gap of **Poly3.3** can be explained not only by the presence of the smaller oxygen atom in furan (*c.f.* sulfur of thiophene ring), allowing more efficient orbital overlap across the polymer backbone, but also due to the lower aromaticity of furan in comparison to thiophene.[197, 322] The furan-based polymer **Poly3.3** displayed reversible optical transformations from red salmon colour to beige tan upon switching from neutral to oxidised state. Impressively, **Poly3.3** displayed higher colouration efficiencies of +212 cm^2 C^{-1} for colour bleaching and -192 cm^2 C^{-1} for colour forming processes compared with PEDOT at 183 cm^2 C^{-1} at 95% of a full optical switch.[148] In conclusion, the incorporation of a furan unit has improved the electrochromic properties compared with its all-thiophene analogue[148], proving polymer **Poly3.3** to be a promising candidate for future organic electronic applications.

4 Synthesis, Electrochemistry, and Optoelectronic Properties of an all Furan-Containing Polymer

4.1 **Aim**

Organic CPs commonly exhibit poor solubility, which limits their processability for applications in organic electronic devices. Conventionally, this challenge was circumvented by either the addition of solubilising alkyl chains or copolymerisation with soluble co-monomers, yielding processable polymers suitable for optoelectronic applications.[82]

Benedikov *et al.* reported oligofurans with improved solubility compared to their all-thiophene analogues. These "naked" oligofurans were constructed iteratively with up to nine units, providing a means for monodisperse comparison with polymeric furan derivatives.[192, 201, 202] They displayed a blue fluorescence and a sufficient stability over several weeks in the absence of light and oxygen. Furthermore, furan and its precursors are renewable natural products ensuring easy and cost-efficient access to oligofuran precursors (ref. Chapter 1.7.5).[192] Motivated by these favourable and promising properties of oligofurans, a novel all-furan polymer with improved solubility and optical characteristics was targeted.
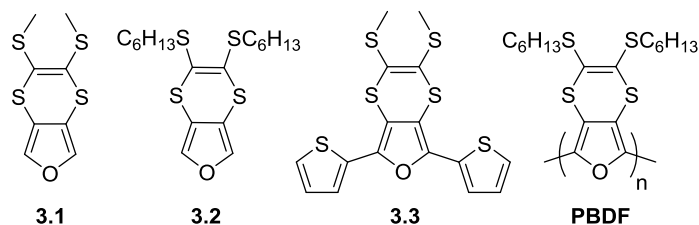
Figure 4.1: Structure of three novel fused furan monomers **3.1**-**3.3** and polymer **PBDF**.[323]

In Chapter 3, the synthesis of three novel furan intermediates (**3.1**-**3.3**) was described. Of these, the bis(hexylthio)dithiino furan monomer **3.2** was proposed as the basis for the synthesis of the corresponding furan homopolymer poly(2,3-bis(hexylthio)-[1,4]dithiino[2,3-c]furan) (**PBDF**; Figure 4.1), which promises to exhibit good solubility and interesting optoelectronic properties. This polymer differs from the dithienylfuran polymer **Poly3.3** reported in Chapter 3 since **PBDF** possesses an all-furan backbone, while the **Poly3.3** backbone contains only one furan unit per two thiophene units. A special characteristic of **PBDF** is that it can be considered as the inverted analogue of **PEDOT** (albeit with a vinylene bridge instead of an ethylene unit) with an

oxygen atom in the aromatic ring and two sulfur atoms in the fused heterocycle (see Figure 4.2).
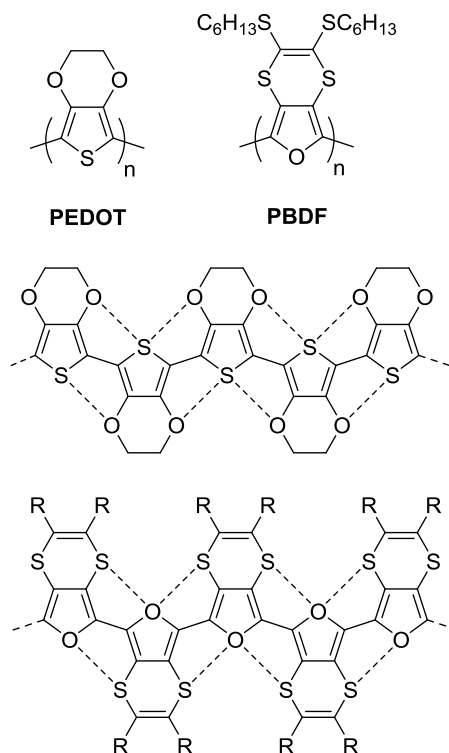
Figure 4.2: The structures of the chalcogenated polymers **PBDF** and **PEDOT** demonstrating the corresponding intramolecular interactions along the polymer chain of **PEDOT** and **PBDF**.

In theory, the molecular structure of **PBDF** is expected to mimic the substitution pattern of **PEDOT** – an extensive network of intrachain S--O interactions that promote a highly ordered conjugated chain (see Figure 4.2). The validity of such self-assembling planar conjugated materials through chalcogen-chalcogen interactions has been the subject of intense studies by the Skabara group[169, 324-327] and others.[328, 329]

Herein, the synthesis and study of the physical, electrochemical and thermal properties of the polymer **PBDF** will be reported and compared to well-known heterocyclic polymers such as **PEDOT** and **PEDTT**.[169]

4.2   Results and Discussion

The results described herein have already been published as:

'Poly([1,4]Dithiino[2,3-*c*]Furan): The Synthesis, Electrochemistry, and Optoelectronic Properties of a Furan-Containing Polymer' S. Kaur, N. J. Findlay, Fiona C. Coomer, R. Berridge , P. J. Skabara*. *Macromolecular Rapid Communication*, 2013, **34**, 1330-1334.

As discussed in Chapter 3, the molecular modelling of furan monomer **3.1**[305] revealed a lack of electron spin density residing at the 2- and 5-positions of the furan ring, which is vital for a successful electropolymerisation. Therefore, the synthesis of **PBDF** was performed by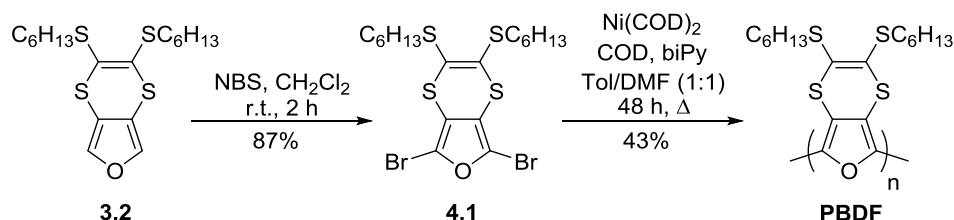 Yamamoto polymerisation, which is a metal mediated, reductive polymerisation technique, refer Chapter 1.5.2. Polymer electrochemical and spectroscopical analysis were completed according to the experimental setup detailed in Chapters 6.1.11, 6.1.12 and 6.2.

4.2.1 Synthesis

PBDF was synthesised according to the synthetic strategy depicted in Scheme 4.1.

Scheme 4.1: Synthetic preparation of **PBDF** from monomer **3.2** *via* the monomer intermediate **4.1**. The synthesis of monomer **3.2** has been reported in Chapter 3.[305]

According to Scheme 4.1, **PBDF** was obtained *via* a Yamamoto polymerisation from monomer **4.1**; a brominated derivative of monomer **3.2**. For the synthesis of monomer **4.1**, furan monomer **3.2**[305] was brominated with 2.1 equivalents of *N*-bromosuccinimide, yielding bisalkyl-dithiin furan **4.1** (**BDF**) as the functionalised precursor of target polymer **PBDF** in 87% yield. Subsequently, this monomer **4.1** was subjected to a Yamamoto homo-polymerisation, which is advantageous as only one type of functionality is required for the C-C coupling of the aryl halide monomer precursor. This reaction was mediated by using excess bis(1,5-cyclooctadiene)nickel(0) (Ni(COD)$_2$), 2,2'-bipyridine, and 1,8-cyclooctadiene in dry toluene/DMF (1:1) and refluxed for 48 h. The obtained crude mixture was poured into cold methanol and the

resultant precipitate was subjected to a Soxhlet extraction with methanol and acetone, removing any unreacted monomeric residues and impurities. A second Soxhlet extraction with dichloromethane gave 214 mg (43%) of the target polymer **PBDF** as a shiny dark brown powder. The obtained product was analysed by gel permeation chromatography, which revealed an average molecular weight (M_n) of 3800 g mol^{-1}, with a moderate polydispersity of 1.63.

4.2.2   *Thermal Analysis*

The thermal stability of a polymer is an important physical characteristic to be considered for the application of a polymer in device fabrication and other industrial processes where elevated temperatures are applied, as these can provoke undesired structural or morphological changes of thermally instable materials.

TGA analysis revealed that **PBDF** was relatively stable whilst being heat-treated from 40-250**°C** at a 5**°C**/min heating rate, as **PBDF** was completely stable until 170°C and only showed a mass loss of 11% at higher temperatures (see Figure 4.3). A subsequent heating run (See Figure 4.3: run 2 derivative) up to 550°C (10**°C**/min heating rate) displayed polymer degradation with a 60% mass loss upon reaching a temperature of 295°C.   In comparison, a thermal degradation temperature of 95°C has been reported for doped polyfuran.[330]
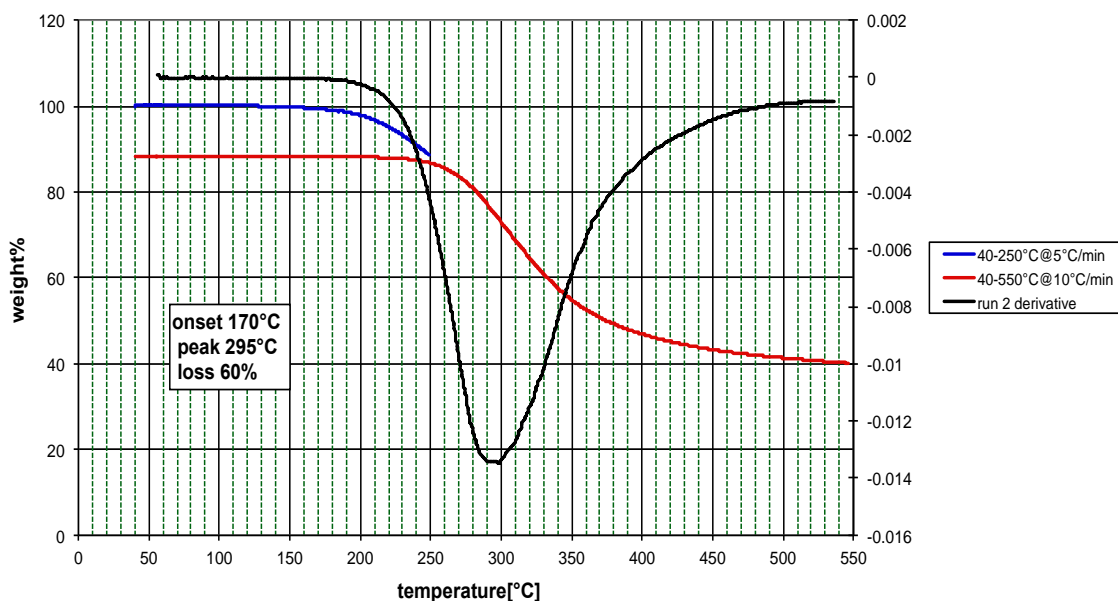
Figure 4.3: Thermogravimetric analysis (TGA) of **PBDF**.

The thermal transitions of PBDF were further investigated with differential scanning calorimetry (DSC). The heat-cool-reheat procedure revealed that **PBDF** possesses a glass transition temperature of T_g = 88 °C and a crystallisation temperature of 69 °C (upon cooling). The DSC showed that the polymer started to degrade at about 150°C and decomposed completely after reaching a temperature of 270°C (See Figure 4.4).
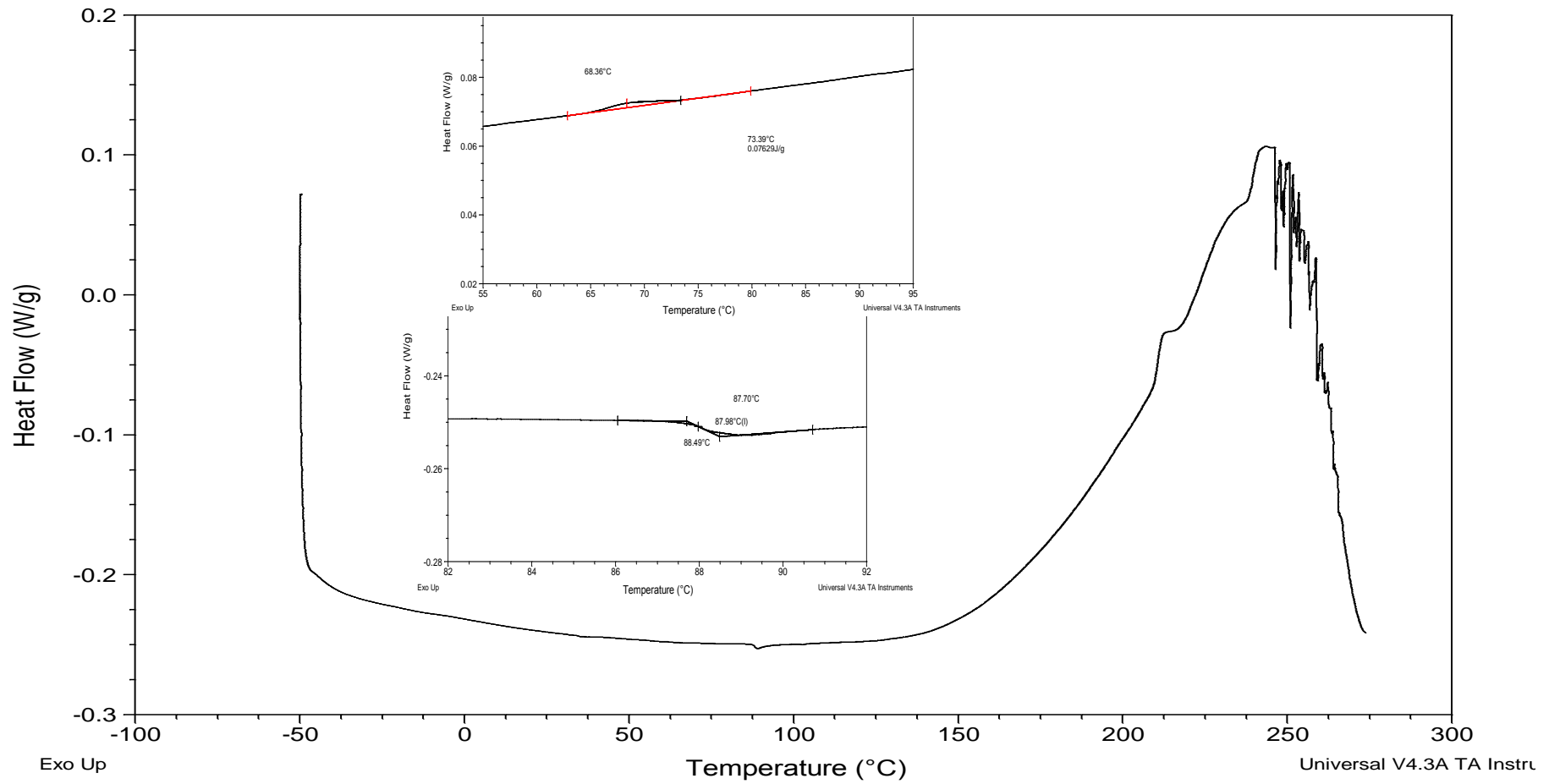
Figure 4.4: Differential scanning calorimetry (DSC) of **PBDF**.

4.2.3   UV-Vis Spectroscopy

UV-Vis absorption measurements of **PBDF** (See Figure 4.5) were recorded both in solution (33.6 µg/mL in CH_2Cl_2) and on a solid-state film (deposited on a quartz cuvette (1 mg/mL in CH_2Cl_2)) which revealed nearly identical absorption profiles. Comparison of the obtained UV-Vis spectra with the UV-Vis analysis of **PBDF**'s non-brominated monomer **3.2** (in CH_2Cl_2 solution, 10^{-4} M; see Figure 4.5) revealed a broadening and bathochromic shift of the absorption band at 320 nm, resulting from the π-π* transition of monomer **3.2**, to the corresponding absorption of the **PBDF** polymer at a wavelength of 469 nm. This indicates clearly an increase in the effective conjugation length proving the transition from monomeric to polymeric form and thus supporting the successful formation of polymer **PBDF**.
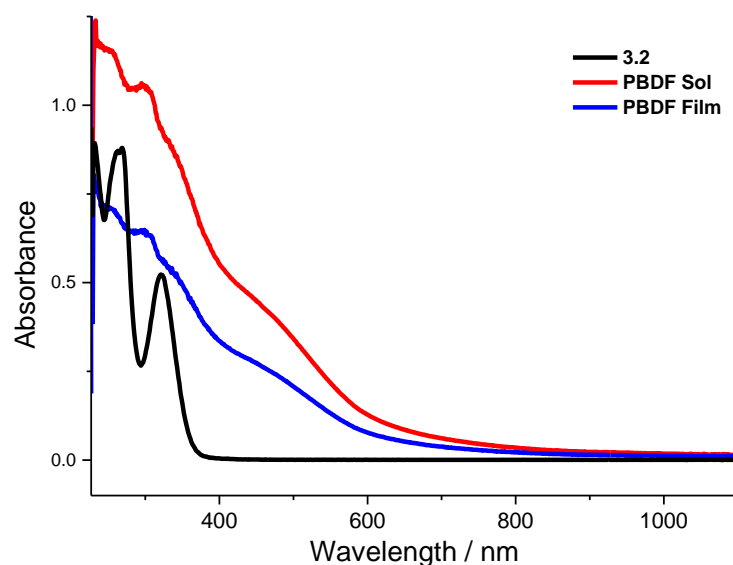
Figure 4.5: UV-Vis absorption spectra of **PBDF** (in CH_2Cl_2 solution and solid state) and of monomer **3.2** (CH_2Cl_2 solution).

The optical band gap (E_g) of **PBDF** was calculated from the onset of the longest wavelength absorption band at 469 nm, yielding $E_g \approx 2.0$ eV (see Table 4.1).

Table 4.1: Optical properties of monomer **3.2** (in solution) and **PBDF** (in solution and as solid-state film).[305, 323]

	$\lambda_{max}/$ nm	ε (mol^{-1} cm^{-1})	HOMO-LUMO/ eV	$E_g/$ eV
3.2^{Sol}	320	8836	3.34	-
PBDF^{Sol}	469	13435	-	2.04
PBDF^{Film}	474	-	-	1.97

4.2.4   Cyclic Voltammetry

The redox behaviour of **PBDF** was determined by cyclic voltammetry (CV) with an electrochemical cell consisting of a glassy carbon working electrode, a platinum counter electrode, and an Ag/AgCl pseudoreference electrode, using $(TBA)_4PF_6$ as the supporting electrolyte (0.1 M in the indicated solvent) and applying a scan rate of 100 mV s^{-1} (ref. Chapter 6.1.11). All voltamograms of **PBDF** were recorded in CH_2Cl_2 solution (4.2 mM) as well as in the solid state, using a glassy carbon working electrode upon which a thin film of **PDBF** had been drop casted, then studied in acetonitrile solution after dedoping (ref. Chapter 6.2.2). Both CVs were compared to those recorded of a solution of monomer **3.2** (10^{-4} M in CH_2Cl_2; Figure 4.6 and Table 4.2).
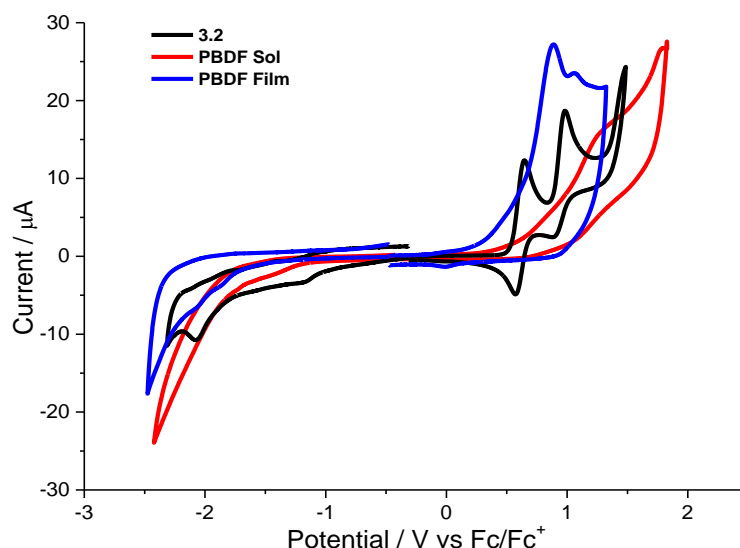
Figure 4.6: Cyclic voltammetry of **PBDF** (solution and thin film) and compound **3.2.**

Cyclic voltammetry of monomer **3.2** displayed one quasi-reversible and one irreversible oxidation peak at +0.55 V and +0.91 V, respectively. The first peak may be attributed to the oxidation of the monomer's dithiin ring rather than its furan ring, as the dithiin ring presents the electron-richest and thus strongest electron-donating substructure.[148, 305] Before analysing **PBDF** (in solution or solid state) with CV, the polymer was first dedoped to neutrality by oxidative cycling from -0.1 to +0.1 V (200 cycles). **PBDF** displayed one single broad irreversible oxidation wave (+1.22 V) when studied in solution state, which is characteristic for polymeric species.[33, 331] In contrast, the CV of solid-state **PBDF** exhibited two irreversible oxidation peaks at +0.92 V and +1.06 V. These potentials are lower than the potential measured for **PBDF** in solution

(+1.22 V), suggesting that **PBDF** adopts an aggregated morphology in the solid state, which promote its oxidation (see Figure 4.6 and Table 4.2).

Table 4.2: Summary of UV-Vis absorption spectroscopic and electrochemical data of **PBDF** and monomer **3.2**.

	λ_{max} (nm)	Optical E_g (eV)	E_{ox1} (V)	E_{ox2} (V)	E_{red1}/E_{red2} (V)	HOMO (eV)	LUMO (eV)	CV E_g (eV)
3.2	265, 322	3.34^a	$+0.55^b$	$+0.91^c$	-2.08^c	-5.22	-3.01	2.21^a
PBDF (sol)	257, 299, 349, 480	2.04	$+1.22^c$	-	-2.20^c	-5.26	-3.24	2.02
PBDF (film)	256, 299, 359, 483	1.97	$+0.92^c$	$+1.06^c$	$-1.85^c/$ -2.06^c	-5.18	-3.12	2.06

HOMO and LUMO values were calculated from the onset of the first peak of the corresponding redox wave and referenced to ferrocence (HOMO: -4.8 eV); [a] HOMO-LUMO gap of monomer **3.2**; [b] quasi-reversible redox process; [c] irreversible redox process.

The electrochemical HOMO-LUMO gaps (E_g) of monomer **3.2** and polymer **PBDF** were determined from the onset of the first oxidation and reduction waves, whilst their optical HOMO-LUMO gaps were determined from the onset of the longest wavelength absorption edge. The electrochemical band gaps of **PBDF** were calculated to be 2.02 eV and 2.06 eV for **PBDF** in solution and as thin film, respectively. Both values were in good agreement with their optical band gaps. However, monomer **3.2** showed a significant discrepancy between its electrochemical (2.12 eV) and optical HOMO-LUMO gap (3.34 eV). This is characteristic for molecules with independent electroactive moieties, such as the 1,4-dithiin substructure in monomer **3.2** (see Chapter 3 and Table 4.2).[305] The strong electron-donating ability of the dithiin ring determines the redox properties of monomer **3.2**, whereas its impact onto the monomers' UV-Vis absorbance (π-π^* transition) is negligible (see Figure 4.5 and Figure 4.6).

4.2.5 Spectroelectrochemistry

PBDF was investigated spectroscopically by recording its absorbance over a wavelength range of 300 – 1100 nm, whilst simultaneously being electrochemically stimulated with an increasing applied potential of 0 to +2 V (see Figure 4.7 and ref. Chapter 6.3.1). The **PBDF** polymer was drop-cast onto an ITO glass slide and air-dried to obtain a polymer film, which was subjected to dedoping before performing the

spectroelectrochemical analysis in acetonitrile containing (TBA)PF$_6$ (0.1 M) as the electrolyte.
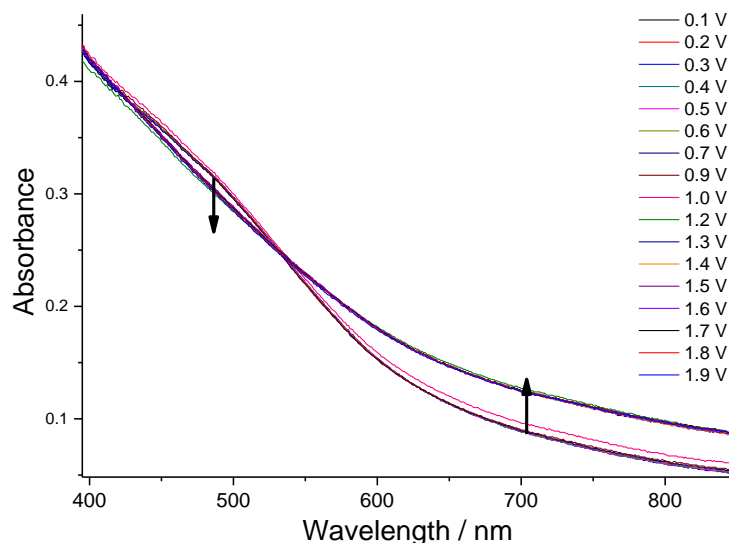
Figure 4.7: 2D-spectroelectrochemical plots of a thin **PBDF** film drop-cast onto an ITO slide, spectra prolific range displayed of (400-900 nm).

In theory, the generation of polarons and bipolarons along the conjugated polymer backbone in response to redox reactions is expected to be accompanied by the appearance of new spectral bands at higher wavelengths in the Vis-NIR region. However, no comparable distinct optical response was observed when the potential was increased to +2.0 V. Once the potential had reached +1.0 V, the absorbance of the polymer's π-π* transition at a wavelength 486 nm decreased only slightly while the absorbance over 500-800 nm slightly increased with an isobestic point of 537 nm (see Figure 4.7). Surprisingly, these findings do not correlate to the broad redox peaks observed in both solution and solid state CVs of **PBDF**, which prompts the question of what is responsible for the redox behaviour of **PBDF** (see Figure 4.6).

A rational conclusion may be drawn from compound **3.2**, whose redox behaviour is governed by its dithiin ring. It is likely that the redox behaviour of **PBDF** is dominated by its dithiin rings and not the conjugated polymer backbone. In order to verify this hypothesis, monomer **3.2**, containing only the dithiin ring but lacking the extended π-system, was also examined spectroelectrochemically (See Figure 4.7).
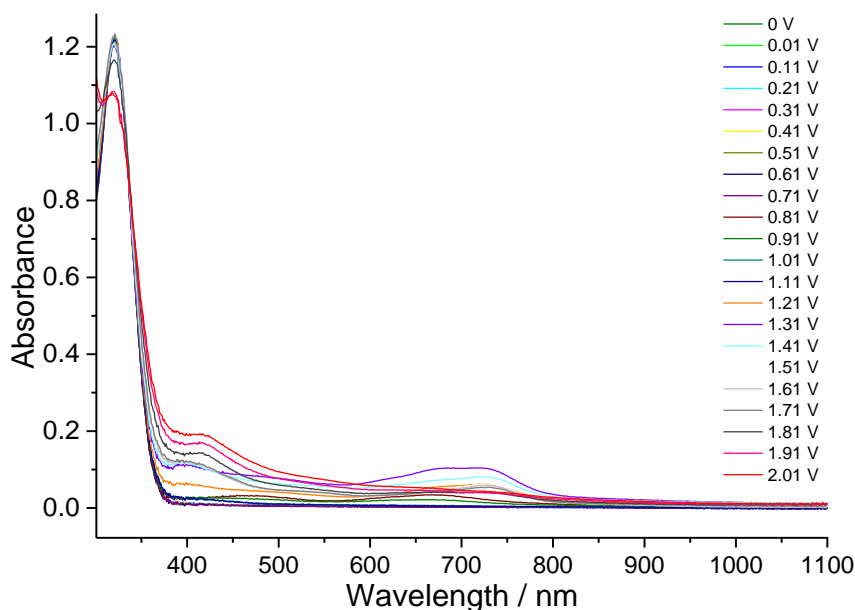
Figure 4.8: 2D spectroelectrochemical plot of a solution of monomer **3.2** in CH_2Cl_2 (1 mg/10 mL).

Therefore, a solution of monomer **3.2** in CH_2Cl_2 (1 mg/10 mL), containing $(TBA)PF_6$ (10^{-4} M) as electrolyte, was studied potentiostatically with an electrochemical cell (made from a 1 cm quartz cuvette) comprising of a platinum gauze working electrode, a silver wire pseudoreference electrode, and a platinum gauze counter electrode. Monomer **3.2** displayed the growth of two optical transitions with increasing electrical charge. In a potential range of 0.61 V to 0.81 V, a broad absorption between 430-750 nm increases, while two more defined optical transitions develop simultaneously at 0.81 V – one distinct transition at 410 nm and a broad band at 710 nm, which suggest the formation of a radical cation and a dicationic species, respectively. Both bands increase with an increasing electrical potential. However, the application of higher potentials (above +1.3 V) induced over-oxidation, as indicated by the bathochromic shift of the π-π* transition at 410 nm and the disappearance of the optical transition at 710 nm (see Figure 4.8).

Comparing the spectroelectrochemical plot of **PBDF** (See, Figure 4.6) with that of monomer **3.2** (See, Figure 4.7) reveals that **PBDF** does not display the distinct changes in its absorption spectrum as that of monomer **3.2** upon increasing the applied potential, but instead exhibits an overall broadening across the visible range. This suggests the redox behaviour observed may result from the presence of oxidised dithiin rings in **PBDF** as opposed to the conjugated backbone. In conclusion, comparing the

spectroelectrochemical analysis of **PBDF** to that of monomer **3.2** revealed that the pendant 1,4-dithiin rings may be responsible for the redox behaviour of both polymer **PBDF** and monomer **3.2**.[323]

4.2.6   Polymer Conformations

The molecular structure of **PBDF** is closely related to that of **PEDOT** and can be considered as an '*inverted*' analogue where the positions of the thiophene's sulfur atom and the 1,4-dioxane's oxygen atoms of **PEDOT** are interchanged. In addition, **PBDF** can also be referred to as a furan-analogue of **PEDTT** where the thiophene's sulfur atom has been replaced by an oxygen atom (see Figure 4.9). However, **PBDF** is not a perfect analogue of **PEDOT** or **PEDTT**, as **PBDF** contains a substituted 1,4-dithiine ring, whereas **PEDOT** and **PEDTT** contain both unmodified 1,4-dioxane or 1,4-dithiane rings, respectively. **PEDOT** retains an all-planar *anti*-conformation, enforced by strong chalcogen-chalcogen, non-covalent interactions between the thiophene's sulfur atom and the oxygen atoms of the neighbouring monomer. In contrast, the repulsive S-S interactions in **PEDTT** result in a non-planar, twisted conformation.[332]
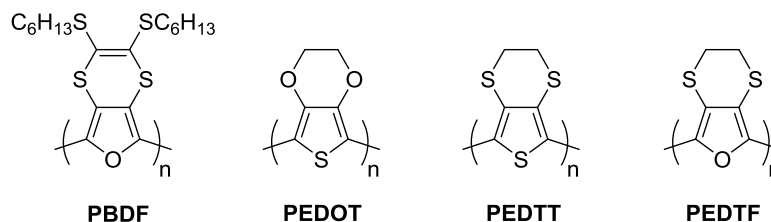
Figure 4.9: Molecular structures of **PBDF**, **PEDOT**, **PEDTT**, and **PEDTF**.

Poly(ethylenedithiafuran) (**PEDTF**) presents the ideal, theoretical inverse analogue of **PEDOT**, in which the thiophene ring of **PEDOT** has been replaced by a furan unit and the 1,4-dioxane ring by an unmodified 1,4-dithiane ring (see Figure 4.9). Molecular modelling was performed on 3,4-ethylenedithiafurane (**EDTF**) oligomers, which clearly exhibited that an increased conjugation length is linearly correlated with a decreased degree of planarity due to the development of disruptive S-S contacts between every second repeat unit along the polymer chain.[333, 334] However, the experimental studies of **PBDF** conflict this theory, as explained in the following.

The structural morphology of polymers has a great influence on their optical and physical properties. For example, the planar polythiophene **PEDOT** has an optical band gap of E_g = 1.63 eV, whereas its non-planar analogue **PEDTT** has a larger optical band gap of E_g = 2.15 eV.[169]

Table 4.3: Optical properties and comparison of known polymers.

Polymer	Optical E_g (eV)
PTh[335]	2.00
PEDOT[169]	1.63
PEDTT[169]	2.15
PFu[204]	2.35
PBDF	1.97

Comparing the band gap of **PEDOT** with that of its non-planar parent polythiophene **PTh** ($E_g \approx$ 2.0 eV) reveals that the rigidification of **PEDOT** due to S-O interactions narrows the band gap of **PTh** by about $\approx$ 0.37 eV (see Table 4.3).[335] Analogously, the band gap of the synthesised polymer **PBDF** (1.97 eV in the solid state) is 0.38 eV smaller than that of its unsubstituted parent polyfuran **PFu** (2.35 eV).[204] The lowering of the band gap from **PFu** to **PBDF** is of similar magnitude to that observed between **PTh** and **PEDOT**, which strongly supports the assumption of extensive S-O interactions within **PBDF**, giving rise to a rigidified polymer backbone.

4.2.7   X-Ray Diffraction Analysis

Given that polymer properties heavily depend on the adopted morphology, it is important to characterise polymers on a structural level. Polymer chains can move and fold, and chain folding is one means by which crystalline regions form *via* either hydrogen bonding or other intermolecular interactions. Polymeric structures may comprise in varying amounts of random crystalline domains called crystallite lamella.[336-338] In order to elucidate its polymeric structure, **PBDF** was studied by powder X-ray diffraction measurements (PXRD) using Cu Kα radiation. Figure 4.10 shows the PXRD spectrum of **PBDF**, which is compared with the spectrum of the Al plate sample holder as baseline.
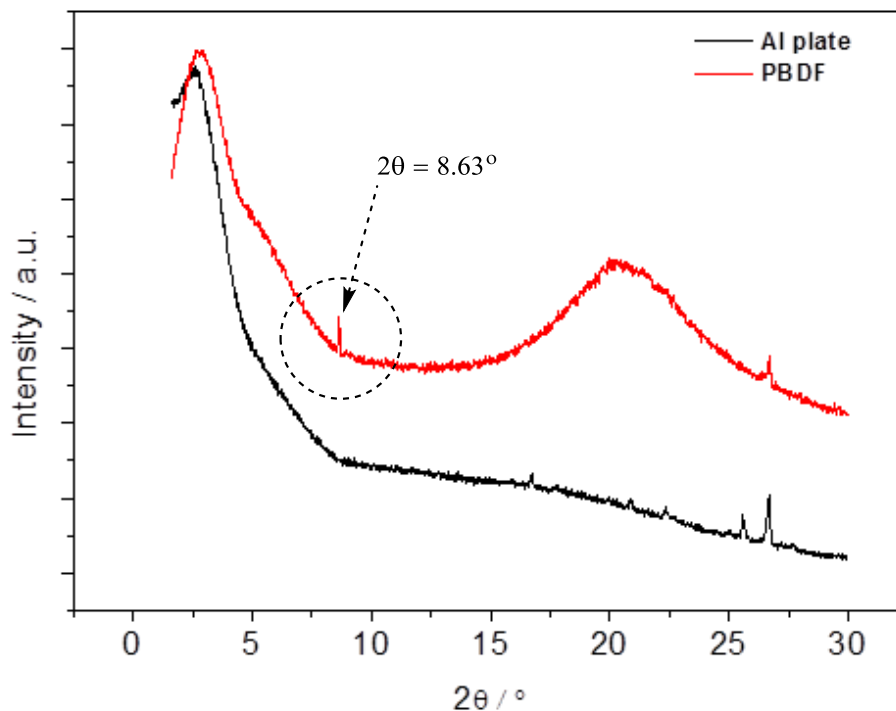
Figure 4.10: PXRD spectrum for **PBDF**; the Al plate sample holder is shown for comparison.

The sample of **PBDF** exhibited a sharp low angle peak at 2Θ = 8.63° (see Figure 4.10), which validates that the **PBDF** polymer possesses a crystalline character with an inter-planar d-spacing of 10.2 Å, which is shorter than that reported for **PEDOT** (a value of 13.0 Å).[339] The improved crystallinity in the **PBDF** polymer is attributed to both the strong intermolecular chalcogen-chalcogen interactions, which enforce more ordered, tightly packed chains, as well as the presence of the smaller oxygen atom in furan as opposed to the larger sulfur atom in thiophene. These results indicate that **PBDF**'s crystalline nature should mimic the 'inverse' pseudo-ribbon morphology of **PEDOT**.[143, 339]

4.2.8   Molecular Modelling Calculations

DFT calculations (B3LYP/6-31G*level (Spartan 10) in the gas phase) were performed on a trimer of bisalkyl-dithiin furan (**BDF**), as a representative section of the **PBDF** polymer, in order to consolidate the PXRD measurements (Chapter 4.2.7) and elucidate the structure of **PBDF**. Furthermore, DFT calculations were performed on optimized structures of trimers of the **PEDOT**-like analogue vinylene dioxythiophene (**VDOT**) and the all-sulfur analogue vinylene dithiathiophene (**VDTT**), which allows for a comparison of the importance of intermolecular chalcogen-chalcogen interactions for

polymer planarity as well as comparing **BDF/PBDF** to literature-known polymers for a structure-based classification of **PBDF**.
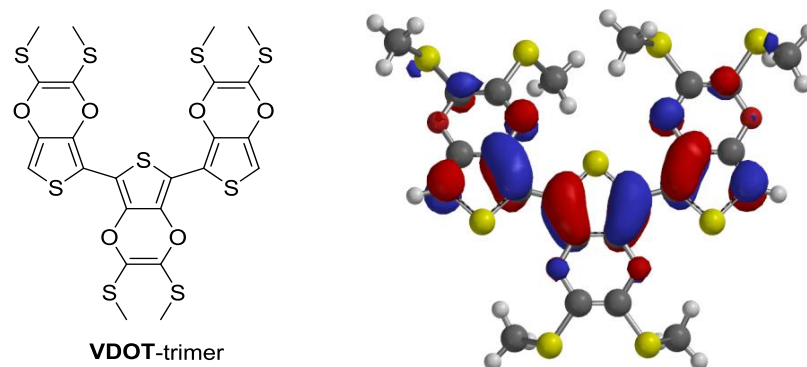
Figure 4.11: Optimised molecular structure of the vinylene dioxythiophene (**VDOT**) trimer.

The **VDOT**-trimer (Figure 4.11) exhibits an almost completely planar conformation, with torsion angles of 172.19° and 178.78° between neighbouring rings. These result from the planarising S-O contacts between the central and peripheral units.[169]
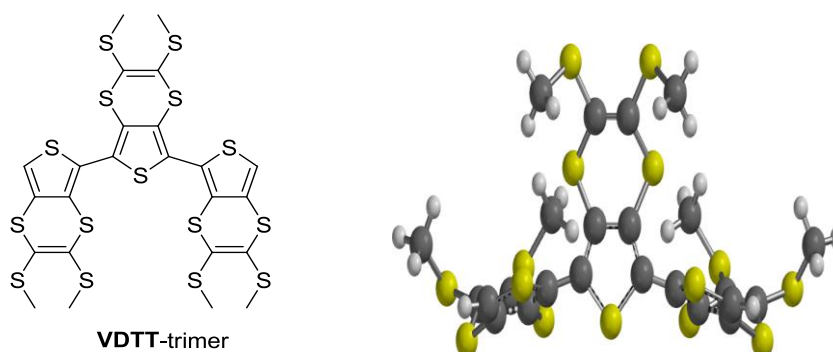
Figure 4.12: Optimised molecular structure of the vinylene dithiathiophene (**VDTT**) trimer.

In contrast, the all-sulfur analogue **VDTT** adopts an orthogonal conformation between its peripheral thiophene units with a calculated torsion angle of 87.83° (see Figure 4.12), which is most probably caused by disruptive S-S interactions. Both examples highlight the two structural extremes of conjugated oligomers and polymers.
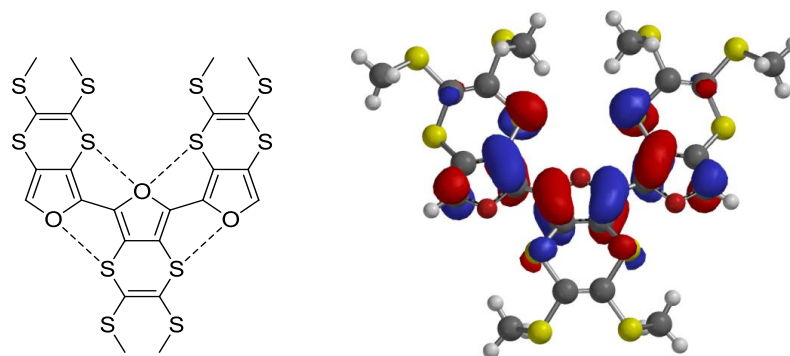
Figure 4.13: Optimised molecular structure of the bisalkyl-dithiin furan (**BDF**) trimer.

As anticipated, the all furan-based **BDF** trimer appears to adopt a near-planar conformation with a torsion angle of 171.22°, which is nearly identical to the value computed for the **VDOT** trimer (Figure 4.12 and Figure 4.13). The structure of **PBDF** can in one way be described as the '*inverted*' analogue of **PEDOT**, suggesting planar *anti*-conformation given the presence of a crystalline peak from PXRD results (see Figure 4.10). As with **PEDOT**, **PBDF** should assume an overall ribbon-like structure, enforced by the extensive network of S-O interactions. It is worth mentioning the central vinylene bridge of **BDF** shows little contribution towards the electronic properties of the conjugated backbone.

4.3 **Conclusion**

The chemical synthesis of the novel, solution-processable polyfuran poly(2,3-bis(hexylthio)-[1,4]dithiino[2,3-c]furan) (**PBDF**) has been described. DFT calculations confirmed that the molecular structure of **PBDF** corresponds to an '*inverted*' **PEDOT** structure with interchanged oxygen- and sulfur positions, carrying additional S-alkylated dithiin substituents at the 3,4-positions. This new polymer has been characterised regarding its electronic absorption as well as its electrochemical and thermal properties. **PBDF** displayed a comparatively low band gap of ~2.0 eV and a promising thermal stability.   It possesses the capability to form extensive S-O interactions between neighbouring monomers, similar to that of the analogous polymer **PEDOT**. These chalcogen-chalcogen interactions encourage a planar, pseudo-ribbon polymer conformation due to the promoting array of non-covalent S-O contacts. The incorporation of the dithiin moiety affords intrinsic supplementary electroactivity as well as a functional handle for alkylation, which enhances the processability of the polymer. The novel polymer **PBDF** has been extensively compared to its well-known and widely used polymer analogues **PEDOT** and **PEDTT**, which have been largely studied as chalcogenated polythiophenes.

In addition, **PBDF** closely resembles previously studied thieno[3',4':5,6][1,4]dithiino[2,3-b]quinoxaline **9** (see section 1.7.3) that has been calculated to show both silver cations and mercury dications to interact at the dithiin sulphurs in an apical coordination, evoking a conformational change and resulting in altered physical and optical properties.[189]   In parallel, the impressive '*independent*' electroactivity of the dithiin moiety can potentially see this **PBDF** polymer also being used as a novel organic sensor, i.e. sensing. transition metal ions in solution.

5 Synthesis and Electrochromic Studies of Heterocyclic Polyazomethines

5.1 **Aim**

Structural manipulation of organic materials has allowed '*tailor-made*' organic electronic materials to be realised for commercialisation over the past three decades.[340-342] Examples of fundamental molecular characteristics required for organic electronic applications include planarity, ease of processability, improved solubility and oxidative and reductive stability.[343 82, 344]

In the summary of Chapter 1.7.5, vinylene linkages (~HC=CH~) were introduced to improve conjugation and to avoid aryl-aryl bond rotation thus consequently increase planarity.[222, 229-231, 233] However, vinylene linkages are known to have extensive synthetic drawbacks in comparison to their isoelectronic azomethine linkages (~N=CH~), which are deemed a favourable alternative due to their easier synthesis *via* dehydration, lack of toxic reagents, water as a by-product and their robust covalent linkages that exhibit good hydrolytic and reductive resistance.[216-218] The presence of the azomethine linkage endows the initially p-type material (PTh) with n-type activity.[222, 226, 229, 230, 233, 345] Furthermore, conjugated polyazomethines are known to be poorly soluble in common device preparation solvents, which is a desired trait for resisting delamination from the electrode.[217, 267]

On the other hand, previously benzene azomethines showed inferior performance compared to their vinylene analogues due to twisting around the aryl-azomethine bonds.[252, 346, 347] However the influence of thiophene in azomethine systems led to higher degrees of conjugation compared with benzene analogues due to the delocalisation of the heterocyclic π-system across entire conjugated framework.[219, 255] Currently Skene *et al.* have developed an extensive library of thiopheno-azomethine D-A systems, highlighting their importance and suitability as functional organic electronic materials.[217, 219, 221-226, 228-233, 260-262, 267, 268, 345, 348, 349]
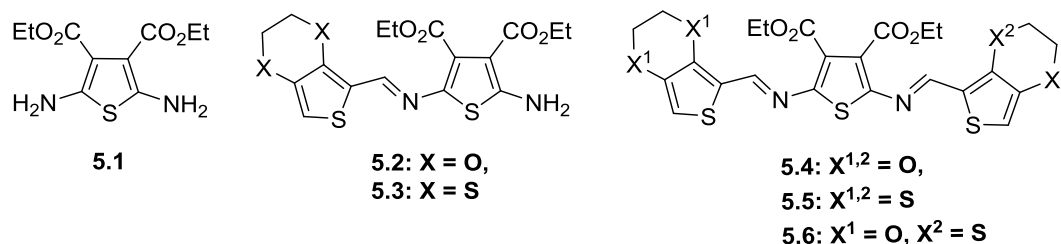
Figure 5.1: Structure of diamine **5.1** used in the preparation of mono-EDOT/EDTT azomethines **5.2** and **5.3** as well as their symmetric and asymmetric triad derivatives **5.4**-**5.6**.

The main objective of this project is to expand the library of thiopheno-azomethine derivatives and investigate the chalcogen effects within these systems. Will Skene and his group have published extensively in this field and have established routine synthetic procedures that have been utilised here in preparing EDOT azomethines (**5.2**, **5.4** and **Poly5.4**), see Figure 5.1 and Figure 5.2.[217, 219, 225] These oxygen-based analogues have been compared to sulfur-rich EDTT azomethines derivatives (see Figure 5.1).
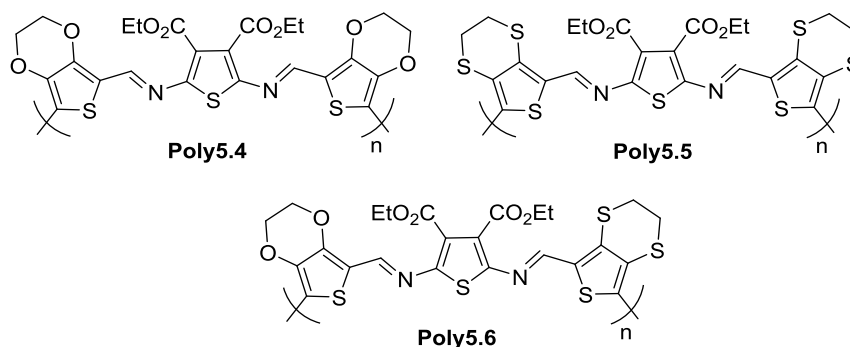
Figure 5.2: Polymeric forms of symmetric EDOT and EDTT azomethines **Poly5.4**[219] and **Poly 5.5**, respectively, and asymmetric EDOT/EDTT azomethine **Poly5.6**.

The polymerisations of this triad of azomethine monomers **5.4**-**5.6** are described in detail and the photophysical and electrochemical properties of the resulting polymers have been studied (see Figure 5.2). Although EDOT-containing polyazomethine **Poly5.4** was formerly reported by Skene *et al.*[219], it is yet to be investigated for its electrochromic performance. In this chapter, the electropolymerised azomethine polymers (**Poly5.4**-**5.6**) were investigated by reversible optical switching studies, chronocoulometry, and CIE coordinate determination.

2.1. Results and Discussion

5.1.1 Azomethine Monomers 5.2-5.6

5.1.1.1 Synthesis

The preparation of mono-condensed azomethines **5.2** and **5.3** and symmetric and asymmetric azomethines **5.4**-**5.6** is depicted in Scheme 5.1.
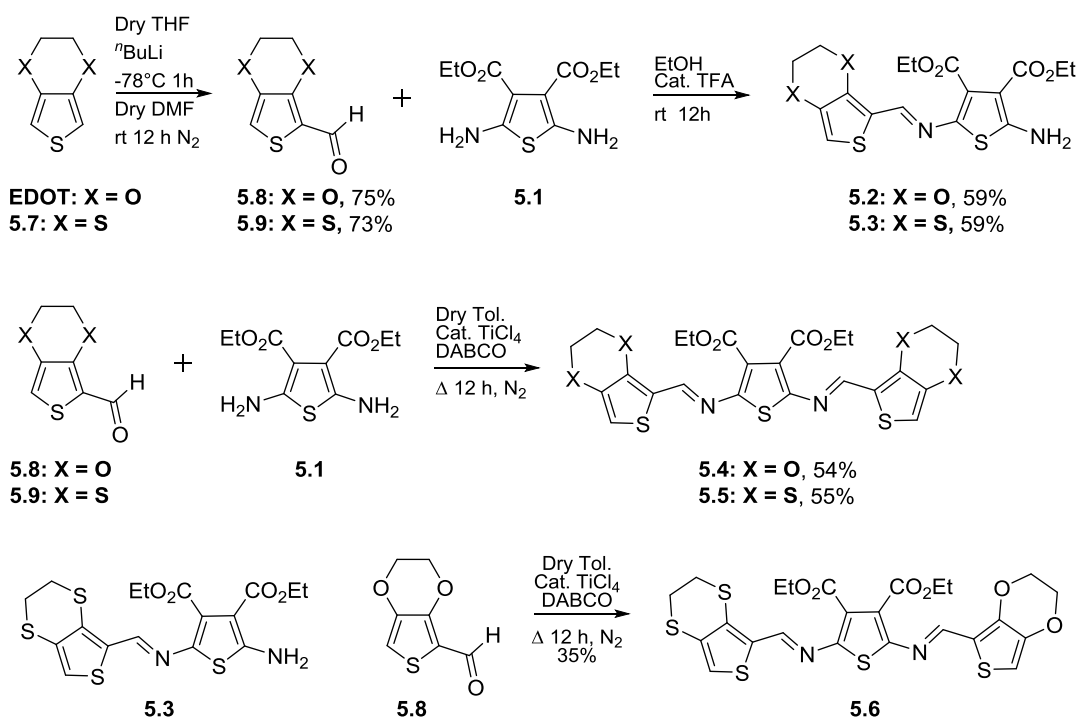
Scheme 5.1: Synthetic procedure adopted for the synthesis of heterocylic conjugated azomethine monomers **5.2**-**5.6**.

In preparation for the synthesis of the conjugated azomethines **5.2**-**5.6**, both EDOT and EDTT were functionalised by standard formylation using *n*-butyllithium (*ⁿ*BuLi) in *N,N*-dimethylformamide (DMF) to form the corresponding aldehyde precursors **5.8** and **5.9** in 75% and 73% yields, respectively.[297] Mono-condensed azomethine monomers can be obtained in good yields by refluxing given aldehyde with stoichiometric amounts of diaminothiophene in anhydrous solvents and catalytic quantity of TFA. The resulting products required only little to no purification, which was achieved either *via* precipitation or recrystallisation.[263] This methodology was adopted for the synthesis of **5.2** and **5.3** from the aldehydes **5.8** and **5.9**, respectively, and diaminothiophene **5.1**. The obtained crude products were subjected to further

purification *via* column chromatography and recrystallisation to give both monocondensed monoazomethines **5.2** and **5.3** in 59% yield. Regardless of which aldehyde or aldehyde/diaminothiophene ratio was used, the described reaction conditions exclusively gave the mono-condensed adduct, indicating that these conditions are a constructive method for preparing new conjugated thiophenes.[222]

In contrast, the double condensation of **5.1** to afford triads **5.4** and **5.5** is not as straightforward. The preparation of these azomethines requires extreme dehydration conditions such as refluxing with stoichiometric amounts of fresh $TiCl_4$ and anhydrous DABCO. This is a result of the electron-withdrawing effect of the newly formed azomethine linkage (imine bond) upon mono-condensation, which significantly reduces the reactivity of the second peripheral amine of **5.1**.[219, 225] Heterocyclic azomethines **5.4** and **5.5** were therefore prepared by refluxing stoichiometric amounts of the required aldehyde (**5.8** or **5.9**), diaminothiophene **5.1**, $TiCl_4$ and anhydrous DABCO for 12 h under inert conditions. The resultant double-condensed azomethines were purified by column chromatography to give the pure azomethines **5.4** or **5.5** in 55% and 54% yields, respectively (see Scheme 5.1).

In contrast, the asymmetric azomethine **5.6** was synthesised *via* a two-step method, see Scheme 5.1.[219] The previously synthesised mono-condensed adduct **5.3** was dissolved in anhydrous toluene, refluxed with compound **5.8**, fresh $TiCl_4$, and chemically dried DABCO for 12 h under N_2. The asymmetric azomethine **5.6** was obtained in 35% yield after purification by column chromatography.

This synthetic approach holds the potential for synthesising many asymmetric derivatives by experimentally overcoming the reduced activity of the remaining amine of the monoazomethine, which is especially attractive, as azomethine bonds are hydrolytically, oxidatively, and reductively robust.[219, 225]

The substituted diaminothiophene **5.1** was successfully synthesised according to a procedure reported by Skene *et al.* (see Scheme 5.2) and was obtained with a yield of 16%.[226] This methodology uses an optimised procedure based on that previously reported by Gewald for the synthesis of diaminothiophenes by eliminating numerous purification steps and thus improving the yield. [226, 265]
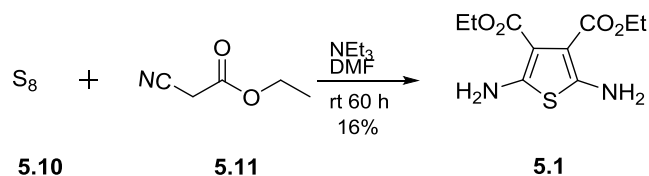
Scheme 5.2: Synthesis of 2,5-diamino-thiophene-3,4-dicarboxylic acid diethyl ester **5.1**.

Following the published procedure,[226] ethylcyano acetate **5.11** was treated with triethylamine, followed by the addition of elemental sulfur **5.10** to form a reactive intermediate.   Instantly, this nucleophilic species is involved in the nucleophilic addition to another ethyl cyanoacetate. After rearrangement, the resulting intermediate undergoes ring closure to give the desired diaminothiophene **5.1**. The product was easily isolated in 16% yield by precipitation in a large excess of water followed by filtration and further recrystallisation from ethyl acetate/hexane.
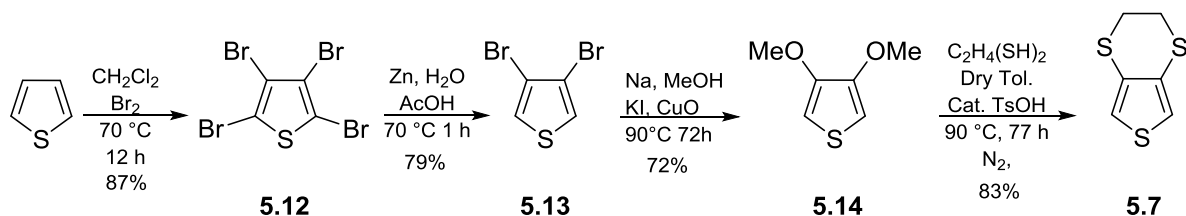
Scheme 5.3: Synthetic scheme for the synthesis of 3,4-ethylenedithiathiophene (EDTT) **5.7**.

The first synthesis of EDTT starting from thieno[3,4-*d*]-1,3-dithiole-2-thione was described by Kanitzidis *et al.*[350]. Meijer *et al.*[302] developed an alternative synthesis of EDTT *via* the transetherification of dimethoxythiophene with 1,2-ethanedithiol (Scheme 5.3), which was applied here for the synthesis of EDTT **5.7**. In the first step, thiophene was brominated to afford tetrabromothiophene **5.12** in good yield (87%). Subsequently, **5.12** was selectively reduced with zinc powder in acetic acid to form 3,4-dibromothiophene **5.13**. Nucleophilic substitution of **5.13** with sodium methoxide yielded dimethoxythiophene **5.14** in 72% yield. Following the optimised procedure by Bendikov[351] *et al.*, dimethoxythiophene was treated with catalytic amounts of *para*-toluenesulfonic acid (TsOH) and heated with ethanedithiol for 77 h to afford 3,4-ethylenedithiathiophene EDTT **5.7** in 83% yield.

5.1.1.2 UV-Vis Spectroscopy

Azomethines **5.2 – 5.6** were studied by UV-Vis spectroscopy and compared to the absorption properties of other azomethine aryl systems that had been reported by Skene *et al.* (see Figure 5.3). These systems were highly conjugated, absorbed within the visible region, exhibiting a bathochromic shift with respect to their benzene analogues, which absorb below 400 nm (see Figure 5.3 and Table 5.1).[222, 223] This indicates more extensive delocalisation than the benzene analogue due to a higher degree of coplanarity and a collective contribution of electronic effects from their π-rich heterocycles.[222, 223] The spectroscopic analysis of azomethine monomers **5.2**-**5.6** was conducted as per the methodology described in Chapter 6.1.12.

BisAzoBenzyl   **MonoAzoTh**   **BisAzoTh**
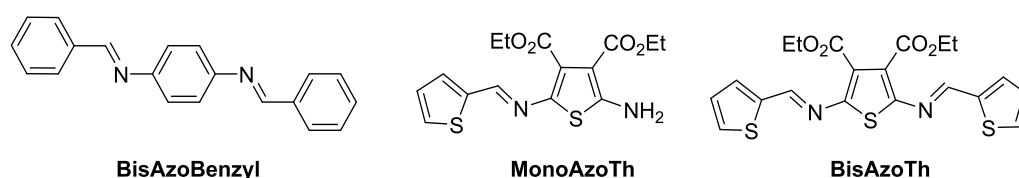
Figure 5.3: Azomethine systems reported by Skene *et al.*[222, 223]

The recorded absorption profiles of the synthesised azomethines **5.2** to **5.6** are depicted in Figure 5.4 and the extracted optical properties are tabulated in Table 5.1. EDTT monoazomethine **5.3** exhibited a strong π-π* absorption with a λ_{max} value of 424 nm, which is 11 nm larger than the λ_{max} value of its EDOT analogue **5.2** (λ_{max} =413 nm). This bathochromic shift is presumably caused by a stronger intramolecular charge transfer (ICT) assisted by intramolecular non-covalent S-N interaction with azomethine unit. On the other hand, the EDOT derivative **5.2** shows a bathochromic shift of 30 nm that with respect to the unsubstituted, literature-reported thiophene analogue **MonoAzoTh**, which only possesses a thiophene ring instead of the EDTT or EDOT moiety (see Figure 5.3). However, the difference in the π-π* absorption between EDOT **5.2** and EDTT **5.3** is rather modest, as they are structural analogues and differ only by their chalocogen atoms. The HOMO-LUMO optical gap is determined from the onset of the longest wavelength absorption edge; the corresponding values for monoazomethines **5.2** and **5.3** were calculated as 2.65 and 2.56 eV, respectively (see Table 5.1). Besides the strong π-π* absorption, monoazomethine EDTT **5.3** absorbs also strongly in the short UV region (~210 nm), possibly due to the n-σ* transition of

the sulfur lone pairs and the influence from the free amine. This highlights that *push-pull* azomethine systems can be tailor-made to further tune optical properties.[222]

Figure 5.4: Top: Absorption profile of monoazomethines **5.2** and **5.3** in CH_2Cl_2. Bottom: Absorption profile of bisazomethines **5.4**-**5.6** in CH_2Cl_2.

Symmetric azomethines **5.4**-**5.5** showed similar spectral profiles like their monoazomethine analogues **5.2** and **5.3**. As mentioned above, the chalcogen difference between the EDTT and EDOT triad systems (**5.4** and **5.5**; see the

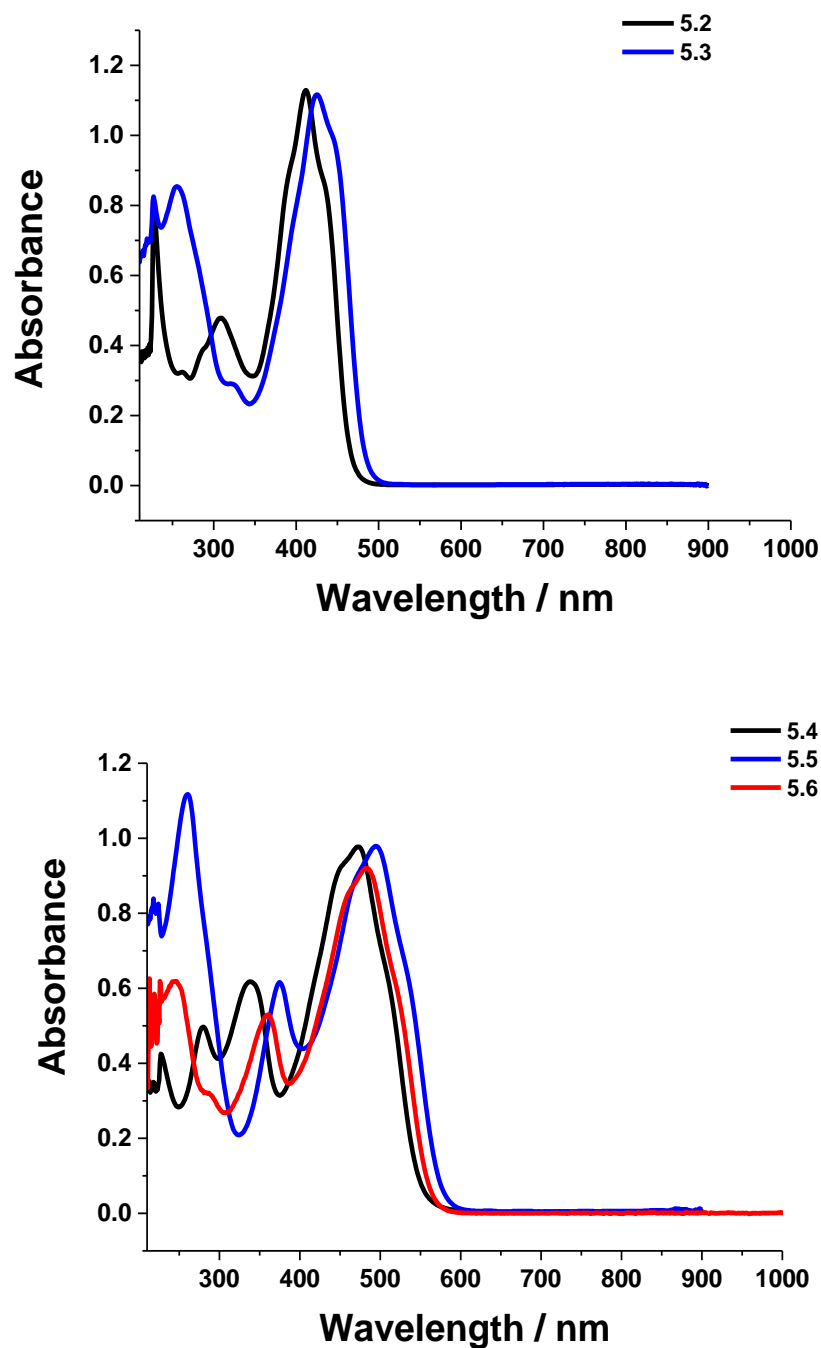bathochromic shift of 21 nm), is indicative of the additional presence of the aforementioned S-N non-covalent interactions between EDTT moieties and azomethine linkages. The π-π* absorption (λ_{max} = 495 nm) of the sulfur analogue **5.5** was bathochromically shifted by 70 nm with respect to the absorption maximum of its mono-condensed analogue **5.3**. In parallel, the EDOT analogue **5.4** also experienced a 61 nm red shift *c.f.* its mono-condensed analogue **5.2** (λ_{max} = 474 nm), see Table 5.1. This bathochromic shift is in agreement with the increase in conjugation length when introducing the additional heterocyclic moiety and formation of a secondary azomethine bond.

The asymmetric EDOT/EDTT triad bisazomethine **5.6** has retained both O-S chalcogen influences and exhibits a π-π* transition at a λ_{max} of 481 nm. The absorption properties of asymmetric azomethine **5.6** lies between those of its symmetric EDOT **5.4** and EDTT **5.5** analogues, respectively. Optical HOMO-LUMO gaps for bisazomethines were determined as 2.37, 2.14, and 2.21 eV for **5.4**, **5.5**, and **5.6**, respectively (see Figure 5.4 and Table 5.1).

Table 5.1: Optical properties of monomer azomethines.

	Monomer	UV-Vis λ_{max} (nm)	ε (mol^{-1} cm^{-1})	Optical Onset (nm)	HOMO-LUMO Optical Gap (eV)
	MonoAzTh[222]	400	-	-	2.60
Dyads	**5.2**	413, 228,307	11340	468	2.65
	5.3	424, 256,325	11184	485	2.56
Triads	BisAzoBenzyl[222, 223]	354	-	-	2.70
	BisAzoTh[222]	440	-	-	2.60
	5.4[219]	472	-	-	2.40
	5.4	474, 278,338	9791	522.9	2.37
	5.5	495, 260,374	9859	579.2	2.14
	5.6	481, 247, 357	9242	561	2.21

All electronic absorption spectra were measured in CH_2Cl_2 at a concentration of 10^{-4} M. Optical HOMO-LUMO values were calculated from the onset of the longest wavelength absorption peak. The electronic properties of literature-reported analogues were obtained from the cited references.

5.1.1.3 Electrochemistry

The electrochemical behaviour of azomethine monomers **5.2**-**5.6** in their solution states was studied by cyclic voltammetry as per the methodology described in Chapter 6.1.11.

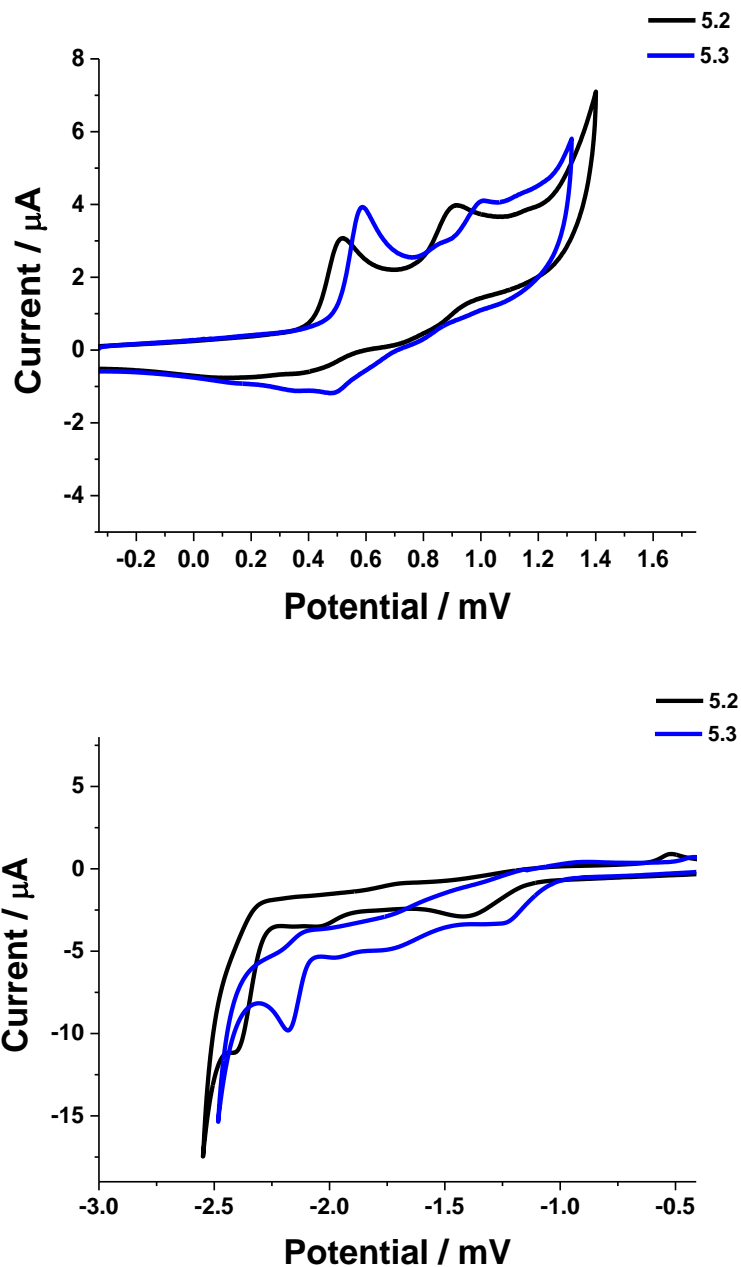Figure 5.5: Cyclic voltammograms: Separate Top: oxidation and Bottom: reduction cycles of monomers **5.2** and **5.3** in CH$_2$Cl$_2$ solution (10^{-4} M).

The separated oxidation and reduction half-cycles of the cyclic voltammograms of the monoazomethine monomers **5.2** and **5.3** are represented in Figure 5.5, and their redox properties are summarised in Table 5.2.   EDOT mono-azomethine **5.2**

demonstrates two quasi-reversible oxidation waves at 0.52 V and 0.91 V, suggesting that two intermediate species, radical cations and dications, are formed. Furthermore, the EDTT analogue **5.3** clearly illustrates one quasi-reversible oxidation at 0.59 V followed by two irreversible oxidations at 0.85 and 1.00 V.

The quasi-reversible nature of the monoazomethines **5.2** and **5.3** is presumably due to the presence of the electron-rich terminal amines.[225] The reduction of both mono-azomethine monomers **5.2** and **5.3** is characterised by several irreversible redox processes, and a weak irreversible anodic wave emerged upon the reverse redox processes at -0.52 and -0.42 V, respectively. This behaviour may be associated to the formation of a radical anion.[225]

The electrochemical HOMO-LUMO gap was determined to be 1.56 and 1.53 eV for **5.2** and **5.3**, respectively. The LUMO level has been determined from the onset of the first reduction wave, which occurs at relatively low potentials due to the influence of the electron-accepting ester groups.

Table 5.2: Electrochemical properties of bisazomethine monomers **5.2** and **5.3**.

Monomer	E_{ox1} (V)	E_{red} (V)	HOMO (eV)	LUMO (eV)	HOMO-LUMO (eV)	Optical Gap (eV)
MonoAzoTh[222]	0.6, 1.1	-	-4.9	-1.2	3.7	2.60
5.2	0.52^a/**0.42**, 0.91^a	-1.41^b/**-1.14**, -2.05^b/**-1.91**, -2.39^b,-0.52^c	-5.22	-3.66	1.56	2.65
5.3	0.59^a/**0.50**, 0.85^b,1.00^b	-1.24^b/**-1.031**, -1.74^b/**-1.49**, -1.97^a, -0.42^c	-5.29	-3.77	1.53	2.56

Peak onset (bold font), ^{a} Quasi-reversible peak, ^{b} irreversible peak, ^{c} irreversible anodic peak. All electronic absorption spectra were recorded in CH_2Cl_2.

The separated anodic and cathodic CV scans of the bis-azomethine monomers **5.4**, **5.5**, and **5.6** are shown in Figure 5.6 and Figure 5.7, and their redox properties are summarised in Table 5.3.

Figure 5.6: Cyclic voltammograms of the oxidation of monomers **5.4**, **5.5**, and **5.6** in CH$_2$Cl$_2$ solution, degassed with Ar.

Bisazomethines **5.4**-**5.6** exhibit several irreversible oxidation waves compared to their monoazomethine analogues with free terminal amines (see Figure 5.6 and Table 5.3). Traditionally, azomethine monomers were considered oxidatively unstable. However, Skene *et al.*[219] reported the successful irreversible oxidation of **5.4** and other asymmetric reactive bisazomethine intermediates, which underwent a successful anodic polymerisation without showing any signs of azomethine bond decomposition.

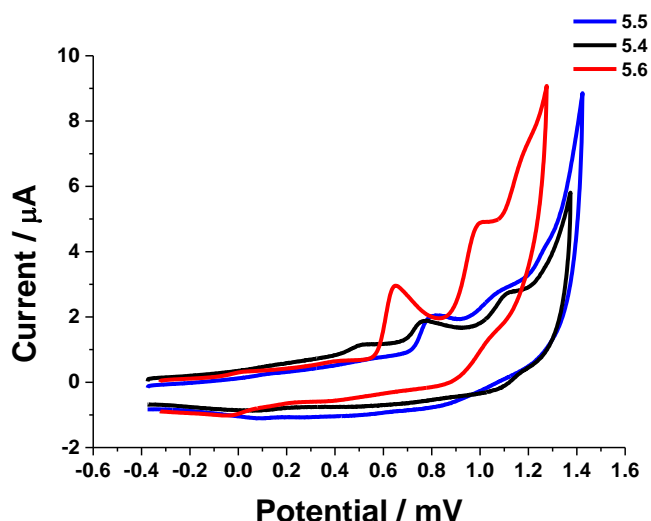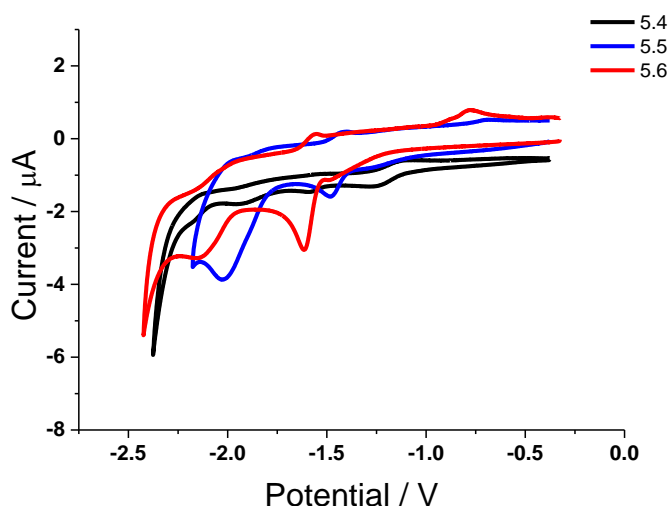Figure 5.7: Cyclic voltammograms of the reduction of monomers **5.4**, **5.5**, and **5.6** in CH$_2$Cl$_2$ solution, degassed with Ar.

Irrespective of the presence of the EDOT or EDTT moiety, all bis-azomethine monomers **5.4**-**5.6** exhibit quasi-reversible first reduction waves, which are followed by

several irreversible waves (see Figure 5.7 and Table 5.3). The initial quasi-reversible reduction wave indicates redox-stable ester groups,[225] and the associated irreversible waves result from the formation of radical anions. HOMO-LUMO gaps were determined as 1.49, 2.11, and 1.81 eV for **5.4**, **5.5**, and **5.6** respectively. However, previous reports calculated an electrochemical HOMO-LUMO gap of about 2.1 eV for **5.4**,[219] calculated from the electrochemical HOMO level and the LUMO level determined from the optical HOMO-LUMO gap.

The electrochemical HOMO-LUMO gap (2.1 eV) of bisazomethine **5.5** is in good agreement with its optical HOMO-LUMO gap (2.14 eV). The mentioned above S-N non-covalent interaction improves conjugation of EDTT and azomethine linker, which lead to the additional stabilisation of the HOMO (see Table 5.3). The most destabilised HOMO is observed for compound **5.4** which is consistent with strong electron-donating character of EDOT unit.

Table 5.3: Electrochemical properties of bisazomethine monomers **5.4**-**5.6**.

Monomer	E_{ox1} (V)	E_{red} (V)	HOMO (eV)	LUMO (eV)	HOMO-LUMO (eV)	Optical Gap (eV)
BisAzoTh[219, 222]	1.3	-	-5.6	-2.5	3.1	2.60
*5.4[219]	1.10	-1.25	-5.4	-3.3	2.1	2.40
5.4	0.50^a/**0.39**, 0.76^a, 1.10^a	-1.24^b/-**1.10**, -1.59^a/-**1.39**, -2.17^a	-5.19	-3.70/ -3.41	1.49/ 1.78	2.37
5.5	0.80^a/**0.72**, 1.06^a,1.27^a	-1.48^b/-**1.39**, -2.02^a, -1.42^c	-5.52	-3.41	2.11	2.14
5.6	0.65^a/**0.57**, 0.99^a, 1.17^a	-1.47^b/ -**1.24**, -1.61^b, -2.12^a, -1.57^c, -0.78^c	-5.37	-3.56	1.81	2.21

Peak onset (bold font), ^{a} irreversible peak, ^{b} quasi-reversible peak, ^{c} irreversible anodic peak. *****5.4**[219] performed with a Pt working electrode, Pt counter wire, and a Ag/AgCl reference electrode using ferrocene as internal reference (E_{pa} = 425mV). All electronic absorption spectra were recorded in CH_2Cl_2.

5.1.2 Polyazomethines 5.4-5.6

5.1.2.1   Electropolymerisation

As discussed in Chapter 1.5.3, aromatic heterocycles such as EDOT, EDTT, and Th readily undergo anodic polymerisations. Skene *et al.* rationalised that the irreversible oxidation of **5.4** does not result from azomethine bond decomposition, but is due to the anodic polymerisation of the unsubstituted 2,2'-thiophene positions. The donor effect of the ethylenedioxy or ethylenedithio groups stabilises the positive charge of the radical cation on the terminal thiophene, causing a high spin-density on the α-position, which facilitates the electropolymerisation.[352]
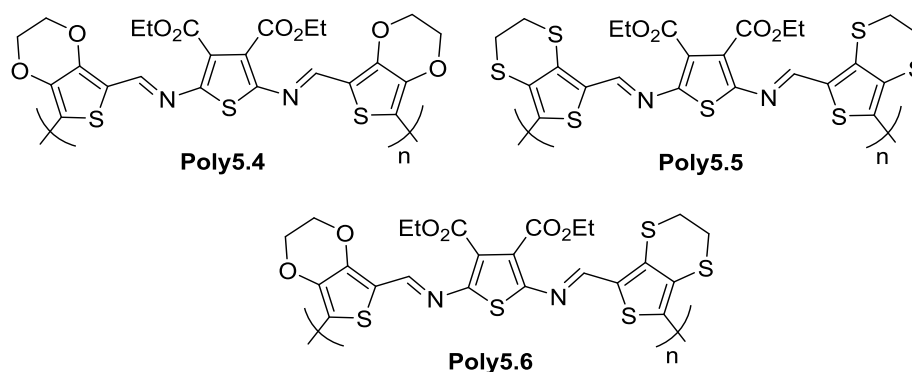
Figure 5.8: Polymeric forms of bisazomethines **5.4**-**5.6**.

Studies have shown the successful anodic polymerisation of **5.4** from a monomer solution in $CHCl_3$ directly onto an ITO substrate.[219] Since **5.5** and **5.6** also exhibited irreversible electrochemical oxidations, their anodic polymerisations were investigated and compared to that of the EDOT analogue **5.4**.

The same experimental setup was used for cyclic voltammetry of monomers **5.2**-**5.6** (10^{-4} M of the respective monomer in 2:1 CH_2Cl_2: hexane solutions and using a CWE). The electropolymersations of monomers **5.5** and **5.6** were achieved by repetitive potential cycling between 0 and 1.2 V, whilst **5.4** was cycled between 0 and 1.3 V in accordance to experimental setup as described in Chapter 6.2. Figures 5.9 – 5.11 depict the successful polymer growth traces of monomers **5.4**-**5.6**, which are not referenced to ferrocene.
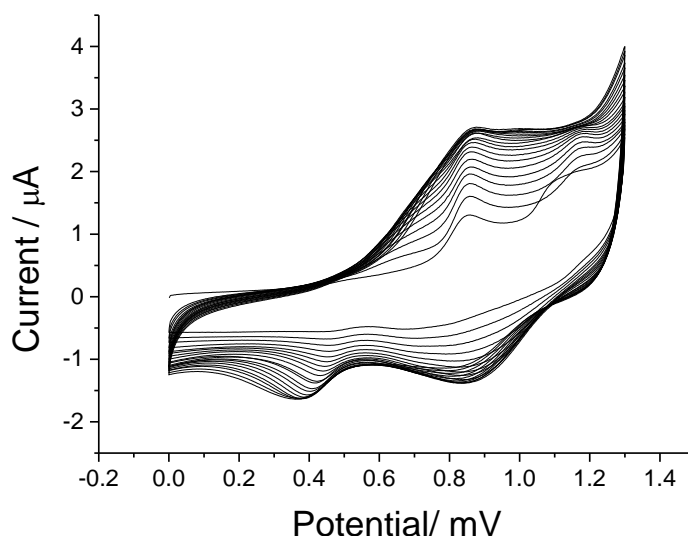
Figure 5.9: Anodic polymerisation growth trace of **Poly5.4**.

Figure 5.9 shows that the polymer growth was only successful for a maximum of 40 oxidative cycles from 0–1.3 V over both oxidation waves of monomer **5.4**. However, excessive oxidative cycling caused a current decrease, indicating the development of a resistive form of the polymer. This resistive behaviour could not be overcome by increasing the monomer concentration.

The initial oxidation peak at 1.1 V decreased upon repetitive oxidative cycling until the predominant development of a new redox wave at lower potentials. Eventually, the quasi-reversible peak at 1.1 V began to increase. The formation of a new, broad peak at lower potentials (0.6 V) indicates the formation of a polymeric species with increased conjugation, which dominates over the polymerisation of **5.4**. Notably, the lower oxidation wave of **Poly5.4** is reversible, and Skene *et al.* have concluded that this anodic wave corresponds to a two-electron process, forming a dicationic species.[219]
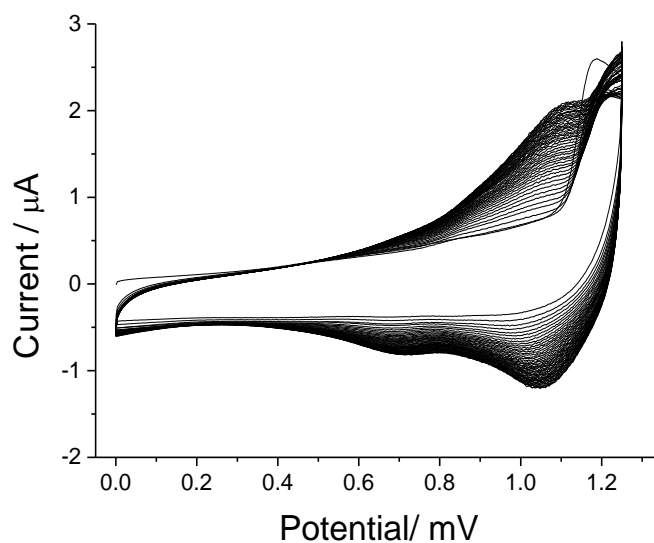
Figure 5.10: Anodic polymerisation growth trace of **Poly5.5**.

The successful anodic polymerisation of the EDTT monomer **5.5** was achieved by oxidative cycling over the first oxidation wave between 0 to 1.2 V for 45 cycles. The polymer growth cycle terminated at 45 cycles – prior to showing any signs of a resistive behaviour and irrespective of an increased monomer concentration. As previously experienced with the EDOT analogue, the current of the monomer oxidation wave at 1.20 V decreased until the successive growth of a new oxidation wave emerged at lower potentials (0.5 V). Subsequently, the wave at 1.20 V began to increase. **Poly5.5** also exhibited a broad, quasi-reversible anodic wave, indicative of the formation of polymeric dications (see Figure 5.10).
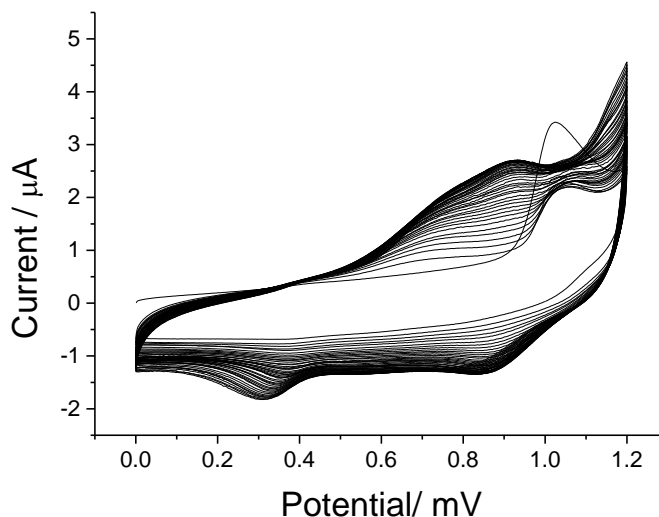
Figure 5.11: Anodic polymerisation growth trace of **Poly5.6**.

Similarly, the asymmetric monomer **5.6** undergoes an anodic polymerisation *via* oxidative cycling over the first monomer oxidation wave between 0-1.2 V for 50 cycles. As before, azomethine polymer growth has been observed here with the formation of a new, reversible oxidation wave emerging at lower potentials (0.5 V) upon successive redox cycling (see Figure 5.11).

5.1.2.2   Electrochemistry

The electropolymerised azomethine polymers **Poly5.4**-**5.6** were dedoped to neutrality (Chapter 6.2.2) and further studied for their redox behaviour as per experimental methodology described in Chapter 6.2.3.
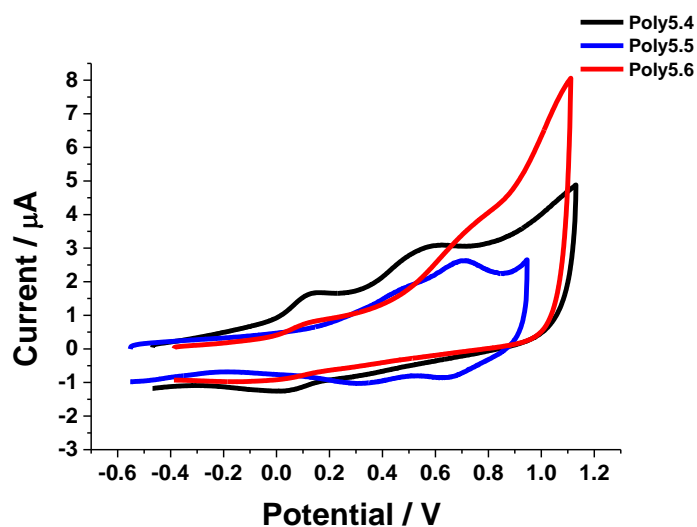
Figure 5.12: Cyclic voltammogram of the oxidations of poly azomethines **Poly5.4**-**5.6** formed on CWE in deoxygenated acetonitrile solution.

145
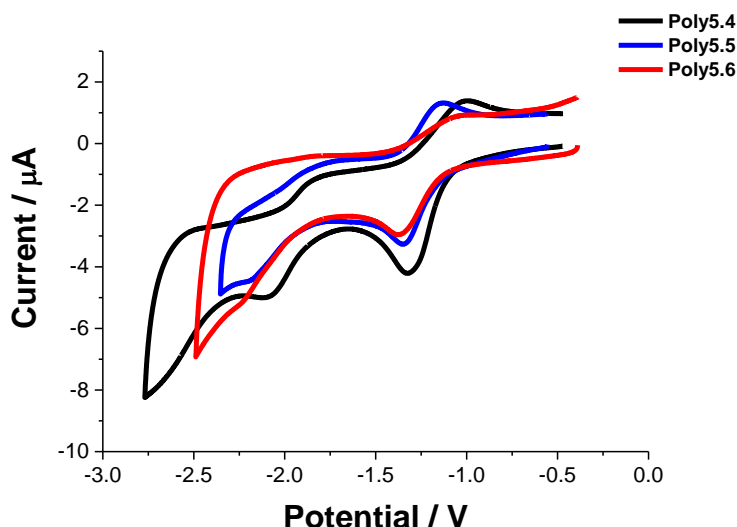
Figure 5.13: Cyclic voltammogram of the reductions of poly azomethines **Poly5.4**-**5.6** formed on CWE in degassed acetonitrile solution.

Figure 5.12 and Figure 5.13 show the oxidations and reductions of **Poly5.4**-**5.6**. Their electrochemical properties are summarised in Table 5.4. The cyclic voltammograms of poly bisazomethine EDOT (**Poly5.4**) and poly bisazomethine EDTT (**Poly5.5**) revealed that both polymers exhibit quasi-reversible oxidation and reduction processes.

Poly5.4 exhibited two quasi-reversible oxidation processes, likely corresponding to the successive generation of a radical cation and a dication at 0.13 V and 0.56 V, respectively. Equally, EDTT poly bisazomethine **Poly5.5** also exhibited two quasi-reversible oxidation waves at 0.44 V and 0.71 V. The first oxidation wave of **Poly5.5** is 0.31 V higher than that of **Poly5.4**, which results from the higher oxidation potential of the bis(EDTT) unit in the polymer structure of **Poly5.5**, compared with the bis(EDOT) unit in **Poly5.4**.[353, 354]

The chalcogen effects are clearly reflected in the electrochemical properties of the asymmetric **Poly5.6**, which exhibited two, broad irreversible oxidations at 0.13 V and 0.69 V, similar to the oxidation processes of its EDOT analogue **Poly5.4**. The oxidation CV of **Poly5.4** suggests that upon anodic polymerisation all possible dimer units (EDOT-EDOT, EDOT-EDTT and EDTT-EDTT) are forming.

Poly5.4 and **Poly5.5** exhibit quasi-reversible reduction waves at -1.32 and -1.36 eV, respectively, whilst the asymmetric **Poly5.6** possesses an irreversible reductive wave at -1.36 V.

The electrochemical HOMO-LUMO band gap of **Poly5.4**, **Poly5.5**, and **Poly5.6** was determined from the onset of their first redox waves to be 1.09 eV, 1.24 eV, and 1.11 eV, respectively (see Table 5.4). Comparing the polymer redox properties with those of their respective monomers shows that the oxidation waves of the polymers occur at lower potentials and the reduction waves at less negative potentials (compare Table 5.3 with Table 5.4). The smaller HOMO-LUMO gap of these polymer systems is indicative of the increased conjugation length.

Table 5.4: Electrochemical and optical properties of poly azomethines, **Poly5.4**-**5.6**.

	E_{ox1} (V)	E_{red} (V)	HOMO (eV)	LUMO (eV)	E_g (eV)	UV-Vis λ_{max} (nm)	Optical E_g (eV)
Poly5.4	0.13^a/**-0.02**, 0.56^b,/-0.04^c	-1.32^a/**-1.11**, -2.09^a, -1.02^c	-4.78,	-3.69	**1.09**	640.4/ **952.4**, 355.4	**1.30**
Poly5.5	0.44^a/**0.14**, 0.71^a,/0.63^c, 0.31^c	-1.36^a/**-1.10**, -2.18^b, -1.13^d	-4.94,	-3.70	**1.24**	629.4/ **855.1**, 424.1	**1.45**
Poly5.6	0.13^a/**-0.02**, 0.69^a	-1.36^b/**-1.13**, -2.23^a, -1.04^c	-4.78,	-3.67	**1.11,**	616.5/ **931.6**	**1.33**

Peak onset (bold font), all electronic absorption solution spectra were recorded in CH_2Cl_2 or as solid state film physisorbed onto an ITO substrate. [a] Quasi-reversible peak, [b] irreversible peak, [c] quasi-reversible cathodic/anodic peak.

5.1.2.3 UV-Vis Spectroscopy

The optical properties of poly azomethines **Poly5.4**-**5.6** were measured by electrochemically preparing the polymer films onto a fresh ITO substrate. Initially, the preparation of the polymer film did not succeed when applying repetitive cyclic voltammetry, not even upon increasing the monomer concentration. This was probably due to the re-dissolution of the doped species in the solvent medium upon reverse cycling during the de-doping process. This would change the solvent medium's composition and the consequent anodic scan would not be positive enough for a

successful deposition of the polymeric material onto the conductive ITO slide. This was supported by the observation that the monomer solution darkened over time from a red solution to a dark brown/black solution, suggesting the formation of an oxidised species in solution, whilst no deposition of polymeric material on the ITO slide was observed.

However, the deposition of the polymer on ITO substrates was succeeded by applying bulk electrolysis. Therein, a constant potential (1.25 V) was retained for a certain period of time (~30 min), which generated an influx of oxidised species to the ITO surface where they underwent anodic polymerisation. The deposited blue/purple material indicated the successful formation of a doped polymer on the ITO surface (ref. Chapter 6.2.1).

The experimental setup for the optimised polymerisation required monomer concentrations of 10^{-3} M, supporting electrolyte (0.1 M) dissolved in 10 mL of 2:1 anhydrous CH_2Cl_2:hexane, and fresh ITO slides as well as an Ag pseudo-reference and a Pt gauze counter electrode. After polymer formation, the ITO slides were dried, rinsed with acetonitrile to remove any monomer residues, and immersed into monomer-free solution. Finally, the polymers were dedoped to neutrality.[167] Figure 5.14 shows the absorption profiles of the polymers **Poly5.4-5.6** in their neutral states, electrochemically prepared on conductive ITO slides.
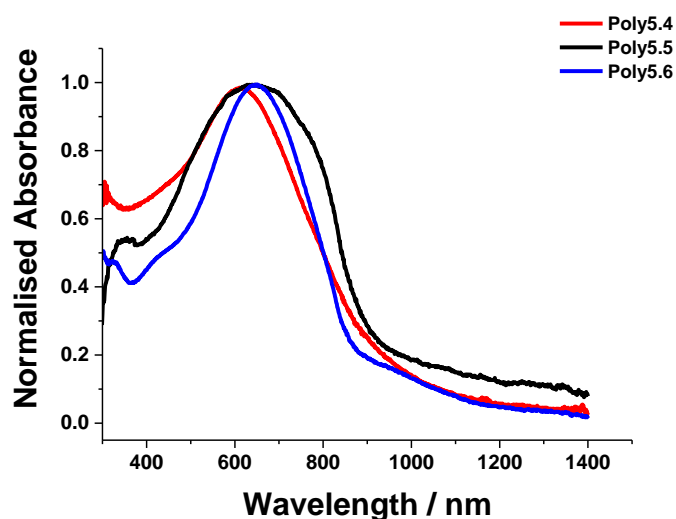

Figure 5.14: Absorption profiles of poly-azomethines **Poly5.4**-**5.6** on ITO substrates.

Comparing the absorption profiles of monomers **5.4**-**5.6** with those of polymers **Poly5.4**-**5.6** shows that the polymerisation induced a bathochromic shift of the absorption maximum in the range of 125-167 nm (see Table 5.3 and Table 5.4). This bathochromic shift can be explained by the increase in the degree of conjugation upon polymerisation.

Poly5.4 is shifted bathochromically by 167 nm compared to its monomer **5.4**, exhibiting a π-π* transition at 640 nm and a small peak at 355 nm. **Poly5.5** shows an absorption band with a λ_{max} of 629 nm (and a shoulder at 424 nm), which is bathochromically shifted by 135 nm with respect to the absorption maximum of its monomer analogue **5.5**. As expected, **Poly5.4** exhibits a bathochromic shift of 11 nm compared to its twisted, sulfur analogue **Poly5.5**, which is caused by the increased degree of conjugation resulting from the presence of alternating bisEDOT units, which support polymer planarity. Furthermore, **Poly5.6** exhibited a bathochromic shift of 125 nm compared to its monomer analogue **5.6** with a λ_{max} of 616 nm (see Table 5.4 and Figure 5.15). The absorption bands of all polymers **Poly5.4**, **Poly5.5**, and **Poly5.6** were rather broad, which indicates that the formed polymers were polydisperse.[219]

The HOMO-LUMO band gaps of polymers **Poly5.4**-**5.6** were determined from the onset of their absorption maxima at higher wavelengths and found to be 1.30, 1.45, and 1.33 eV, respectively (see Table 5.4). The electrochemical band gaps of these polymeric systems differ by about 0.21-0.22 eV from their optical band gaps, which results from the present electroactive acceptor moieties.

The electrochemical manipulation of the above polymer systems, generating quasi-reversible radicals and dications, gives added support that these systems can endorse different optical transitions, which renders them promising electrochromic materials.

5.1.2.4 *Spectroelectrochemistry*

Spectroelectrochemical studies were performed to study optical transition changes under an electrochemical stimulus. This assesses the colour transition and the switching capacity of the polymer under similar experimental conditions to those of a working electrochromic device. **Poly5.4**-**5.6** films were prepared on ITO substrates for spectroelectrochemical analysis as detailed in Chapter 6.3.1. The absorptions of the

polymer films were recorded over a wavelength range of 300-1400 nm while the applied potential was increased from 0 to +2.0 V in 100 mV increments.

Figure 5.15: 2D (top) and 3D (bottom) spectroelectrochemical plots of **Poly5.4**.

Figure 5.15 shows the spectroelectrochemical profile of the oxidation of **Poly5.4**. The 2D plot clearly exhibits that the $\pi - \pi*$ transition at 562 nm begins to diminish upon increasing the potential. This is accompanied by a gradual increase in the absorption at higher wavelengths (680 nm), which indicates the formation of radical cations and, upon successive oxidation, the formation of dications.

Poly5.4 demonstrates optical resistance and stability at low oxidation potentials (<0.5 V) where no spectral changes are observed. Interestingly, **Poly5.4** exhibits electrochromic behaviour in the narrow potential window of 0.5-1.0 V. The development of new absorbance bands at lower wavelengths (the band at 320 nm

occurs at potentials beyond +1.0 V) is indicative of either film decomposition or the formation of new species or by-products.

Visual observation of the ITO slide showed that the blue/purple film turned yellow at potentials larger than 2 V, which is indicative of over-oxidation. Therefore, it is deduced that **Poly5.4** retains good stability with reversible redox behaviour until a potential of 0.9 V. The greatest optical change occurs between 900-1000 nm at 0.9 V.
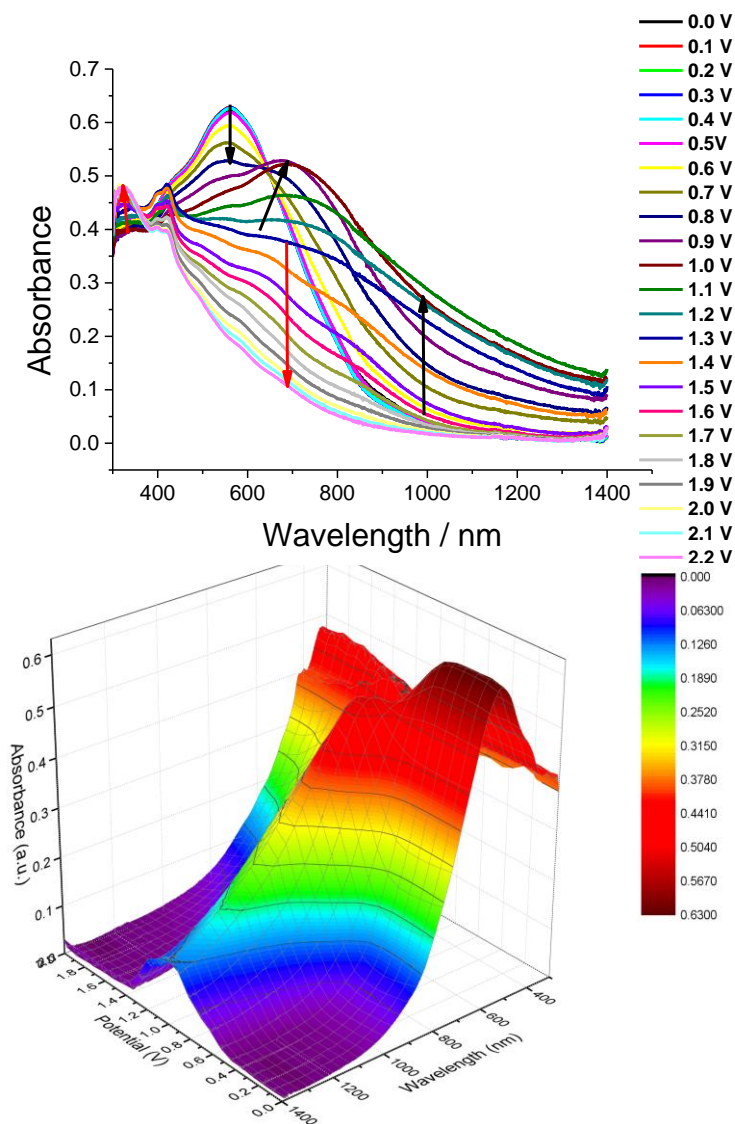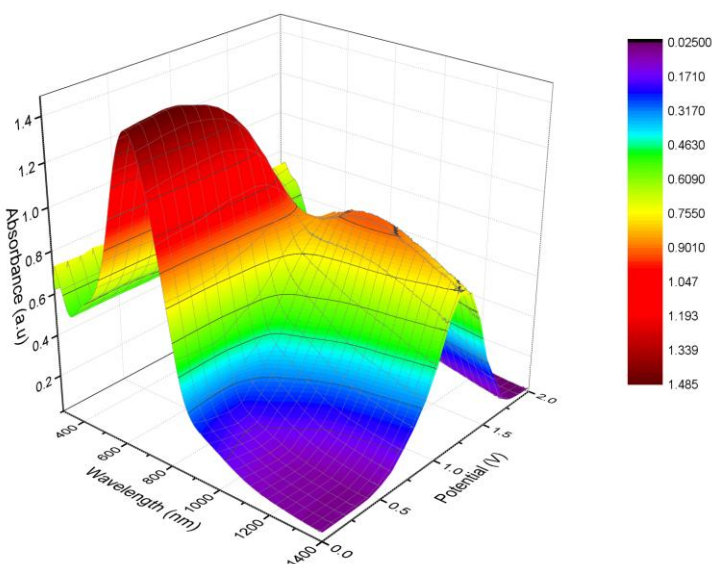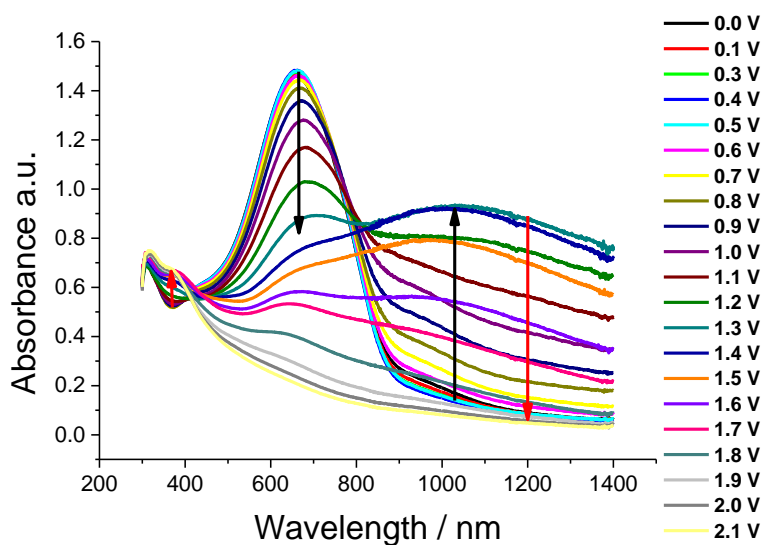

Figure 5.16: 2D (top) and 3D (bottom) spectroelectrochemical plots of **Poly5.5**.

The spectroelectrochemical plots of **Poly5.5** are represented in Figure 5.16. Similar to **Poly5.4**, successive oxidation caused a decrease of the π-π* transition, followed by an increase in the absorbance at higher wavelengths and polymer

degradation at high potentials. The doped polymer film exhibited an optical transformation between 0.5 V and 1.3 V where the π-π* transition at 665 nm diminished and the polarons and bipolarons formed, as indicated by the increased intensity at higher wavelengths of >880 nm. In comparison with **Poly5.4**, which exhibited an oxidative decay beyond 1.0 V, **Poly5.5** is more stable and only decomposed at potentials larger than 1.3 V. Figure 5.16 furthermore exhibits a new absorption peak at lower wavelengths (370 nm) that emerged when potentials larger than 1.2 V were applied. Therefore, the optimal electrochromic parameters for **Poly5.5** would consist of electrochemical stimulation between 0-1.1 V, which avoids polymer decomposition by ensuring reversible redox behaviour and provides the greatest optical change at 1030 nm.
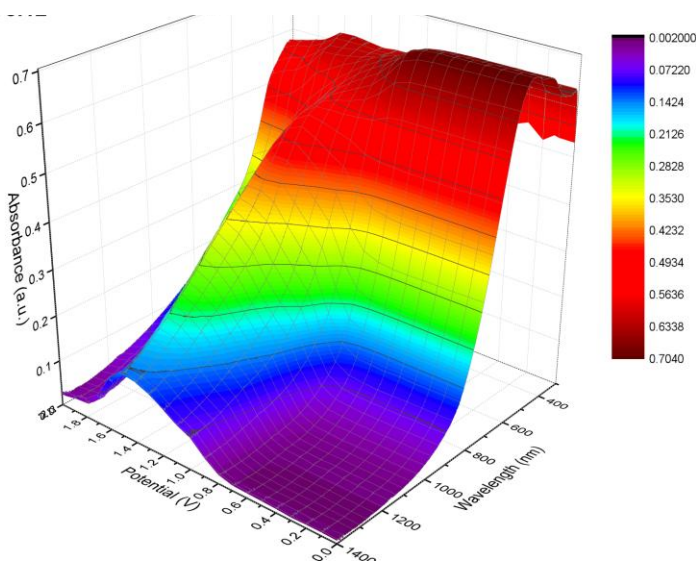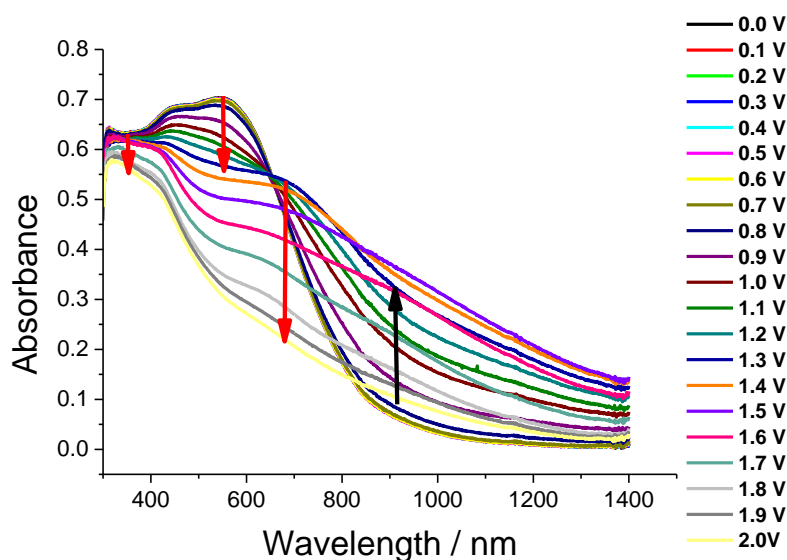
Figure 5.17: 2D (top)and 3D (bottom) spectroelectrochemical plots of **Poly5.6**.

The absorption profile of **Poly5.6** shows similar characteristics to that of **Poly5.4** with a diminishing π-π* transition at 552 nm between 0.6-1.1 V, an emerging peak at 682nm between 1.2-1.3 V, and, finally, polymer degradation at potentials larger than 1.4 V, as indicated by a decrease of all major absorbance peaks (see Figure 5.17).   All three polymers **Poly5.4**-**5.6** revealed to be oxidatively robust at low potentials of <0.5V (see Figure 5.15-Figure 5.17).

The exhibited optical transitions confirm the electrochromic behaviour of the above polyazomethines and render them promising electrochromic materials.   The efficiency of these optical transitions will be further investigated in the following switching studies.

5.1.2.5 Electrochromic Switching Studies

To date, no switching studies have been reported for the heterocyclic azomethine systems **Poly5.4**-**5.6**. Fresh polyazomethine films were prepared on ITO slides, as previously described (Chapter 6.2.1 & 6.2.2), using the same experimental setup used for the spectroelectrochemical experiments.   Thereafter, the relevant experimental parameters were extracted from the polymers' spectroelectrochemical profiles.   The spectroelectrochemical plot of the polyazomethines exhibits the optimum wavelength at which the largest absorbance change occurs upon increasing the oxidation potential.   This applies to two different areas within the spectra – the wavelength where the neutral π-π* absorbance diminished as well as at higher wavelengths where polarons or bipolarons emerged.   The transmission change of the latter wavelength was measured whilst being stimulated between two potentials at various speeds (pulses of 10, 5, 2.5, 1.25, 0.5, and 0.25 s) under ambient conditions.
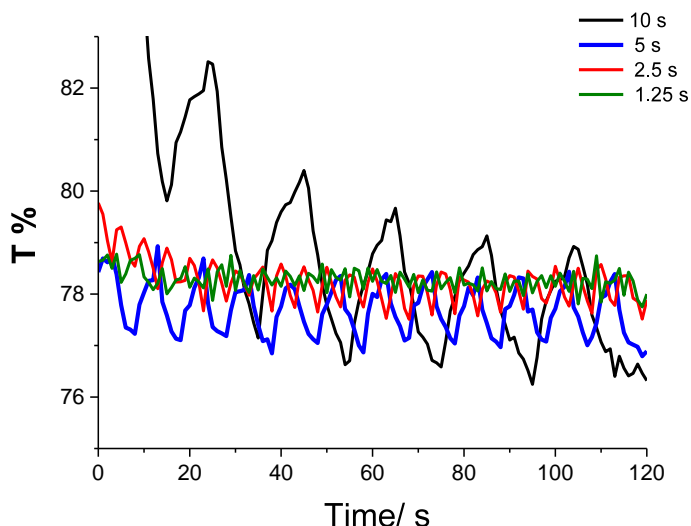
Figure 5.18: Switching studies of **Poly5.4** (λ = 900 nm, pulsed between 0 to 0.85 V).

Poly5.4 exhibited the largest absorption change at 900 nm (see Figure 5.18). The highest non-destructive oxidation potential deduced from the spectroelectrochemistry profile was 0.9 V. However, in order to avoid oxidative decomposition, a lower potential of 0.85 V was applied as the maximum potential in the switching studies.

Poly5.4 showed an initial transmittance drop when subjected to 10 s pulses before the transmittance eventually stabilised. The polymer could be switched for several cycles at various speeds without exhibiting a significant variation in transmittance. The optical switch was not accompanied by a large transmittance change, suggesting slow redox kinetics of counter-ion egression and ingression. The results of the oxidative switching studies of **Poly5.4** are shown in Table 5.5, which exhibits that the optical transmittance of **Poly5.4** is relatively poor with a maximum change of only 4.1% upon the application of oxidising 10 s pulses.

The *push-pull* bisEDOT-azomethine systems were expected to improve the reported switching properties of PEDOT films (ΔT = 44% at 2.2 s).[169] However, the switching performance of **Poly5.4** is slower than that of the reported PEDOT films and only achieved 10% of the reported transmittance change. Generally, the switching performance of a polymer can be limited by the polymer morphology with tight polymer networks result in a slower electrochromic response due to sluggish egression and ingression of electrolyte. Possibly, this is the reason for a limited switching

performance of **Poly5.4,** with a restrictive polymer network being due to the planar bisEDOT units. These results do not encourage the use of **Poly5.4** as a fast-switching electrochromic material. To optimise **Poly5.4**, further work is required to develop a detailed understanding of its limited switching performance.

Figure 5.19: Switching studies of **Poly5.5** (λ = 930 nm, potential pulsed between 0 and 0.95 V).

The transmittance change of **Poly5.5** was measured at 930 nm, whilst the potential was stepped from 0 to 0.95 V at various speeds (see Figure 5.19 and Table 5.5). The improvement in transmittance change is more than eight times greater in **Poly5.5** compared with **Poly5.4**. However, the EDTT system is still not efficient for switching at faster speeds with pulses below 1.25 s.

The improved switching performance of **Poly5.5** with respect to **Poly5.4** can be explained by the morphological orientation of the bisEDTT units, as they are orthogonal to each other throughout the polymer chain due to the disruptive S-S contacts; these allow sufficient egression and ingression of counter ions to the polymer film. However, the number of bisEDTT units in **Poly5.5** is counter-balanced with the number of azomethine linkages, which are known to assist planarity. In Chapter 1.7.4, the influence of polymer morphology on its electrochemical switching performance was discussed.[305]

Skene *et al.*[231] recently reported the first example of an organic azomethine polymer, synthesised from 2,5-diaminothiophene **5.1** and 4,4'-triphenylamine dialdehyde, which was capable of performing epetitive cycling without colour fatigue

or decomposition. The prepared polyazomethine showed optical transitions of 34% upon oxidation with 5 s pulses. The efficient switching ability is attributed to the open morphology induced by large twist angles occurring between the triarylamine monomer and the azomethine linkage.[231]
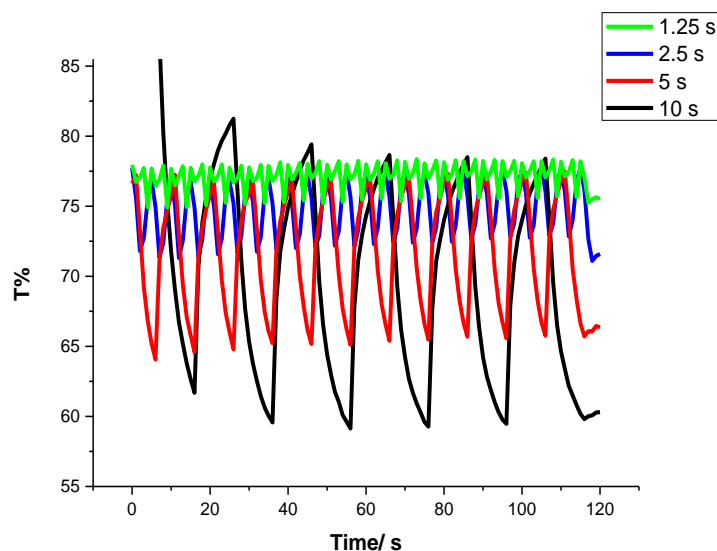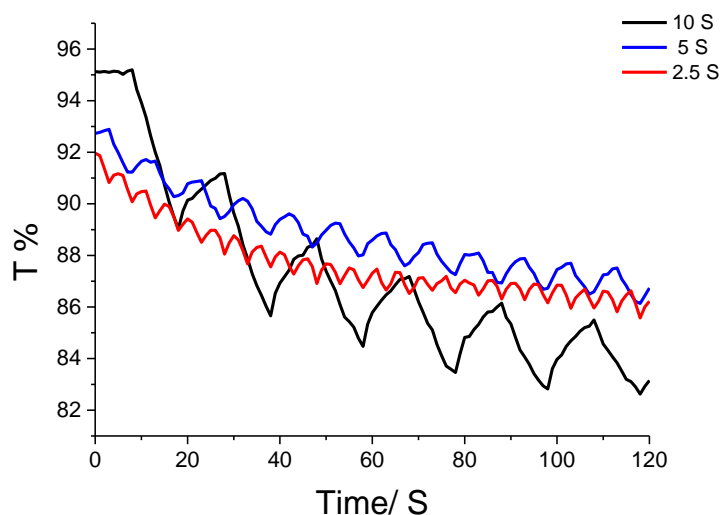

Figure 5.20: Switching studies of **Poly5.6** (λ = 1000 nm, potential pulsed between 0 to 1.0 V).

Finally, the transmittance change of **Poly5.6** was measured at 1000 nm whilst being pulsed between 0 and 1.0 V at various speeds (see Figure 5.20 and Table 5.5). The decrease in transmittance difference with increasing switching speed is a result of a slow diffusion of the bulky electrolyte through the polymer.

Figure 5.20 exhibits that **Poly5.6** has a similar switching performance like its EDOT analogue **Poly5.4** (ΔT = 4.7% *c.f.* ΔT = 4.1% at 10 s), supporting that the EDOT-azomethine-EDTT repeat unit enables O-S chalcogen interactions that enforce a degree of rigidification and planarity within the polymer chain. Both **Poly5.4** and **Poly5.6** systems are not suitable for faster switching speeds of pulses below 1.25 or 2.5 s and have proven to be poor candidates for fast switching, visual, electrochromic materials.

Table 5.5: Oxidative switching performances of **Poly5.4**-**5.6** at various speeds.

	Time (s)			
	10	5	2.5	1.25
ΔT% **Poly5.4**	4.1	1.9	1.1	1.0
ΔT% **Poly5.5**	33	18	7.5	3.9-1.42
ΔT% **Poly5.6**	4.7	1.5	1.0	-

5.1.2.6 Colouration Efficiency

With respect to the switching performances of the polymer azomethines, the following studies will be continued only with **Poly5.5** due to its higher and more consistent optical transitions. The kinetic switching rates are more efficient in this bisEDTT system compared to its EDOT **Poly5.4** and unsymmetrical **Poly5.6** analogues (see Table 5.5).

In chronocoulometry (CC), the charge *vs.* time response to an applied potential step waveform is recorded. CC studies were performed in a monomer-free acetonitrile solution on **Poly5.5**, which had been electrochemically deposited onto an ITO slide and dedoped prior to measurements. Both Figure 5.21 and Figure 5.22 show the simultaneous measuring of the percentage change in film transmittance and the charge flow during a complete switch. The electrochromic film was monitored at λ_{max} = 930 nm as the voltage was pulsed for a 10-s step between its neutral (-0.1 V) and oxidised state (+0.95 V).

In Figure 5.21, charge and optical transmittance are overlayed to determine the efficiency of the dedoping of **Poly5.5** from oxidised to neutral states. Table 5.6 summarises the colouration efficiencies at various percentages of the optical transition.

Figure 5.21: Chronocoulometry doping-dedoping experiment of a **Poly5.5** film on ITO, showing various percentages of the full transmittance change across doping to dedoping step for a 10 s pulse with T% at λ_{max} = 930 nm.

Table 5.6: Colouration efficiencies determined for **Poly5.5** at various percentages of optical changes of a complete colour-dedoping switch. Data has been baseline corrected.

$\Delta T^{a,b}$ (%)	% change	T_1^a(%)	T_2^a(%)	τ (s)	Q (C)	Δ_{OD}^c	Q_d^d	η^e (cm^{2}C^{-1})
10.78	100	71.79	82.57	10.38	5.13E-04	6.08E-02	1.73E-04	3.52E+02
10.24	95	71.79	82.03	7.54	4.67E-04	5.79E-02	1.57E-04	3.68E+02
9.71	90	71.79	81.50	6.15	4.40E-04	5.51E-02	1.48E-04	3.72E+02
9.17	85	71.79	80.96	4.76	4.09E-04	5.22E-02	1.38E-04	3.78E+02
8.63	80	71.79	80.42	3.99	3.89E-04	4.93E-02	1.31E-04	3.76E+02

[a] transmittance measured at λ_{max} = 930 nm, [b] $\Delta T\% = T_2\% - T_1\%$, [c] Δ_{OD}=log [%T_b / %T_c]; [2] [d] Q_d = Q/A, where A (electrode area) = 2.97 cm^2; [e] η = ΔOD(λ)/ Q_d.

In Figure 5.22, charge and optical transmittance are overlayed to determine the efficiency of the doping of **Poly5.5** from neutral to oxidised states.   Table 5.7 summarises the colouration efficiencies at various percentages of the optical transitions.

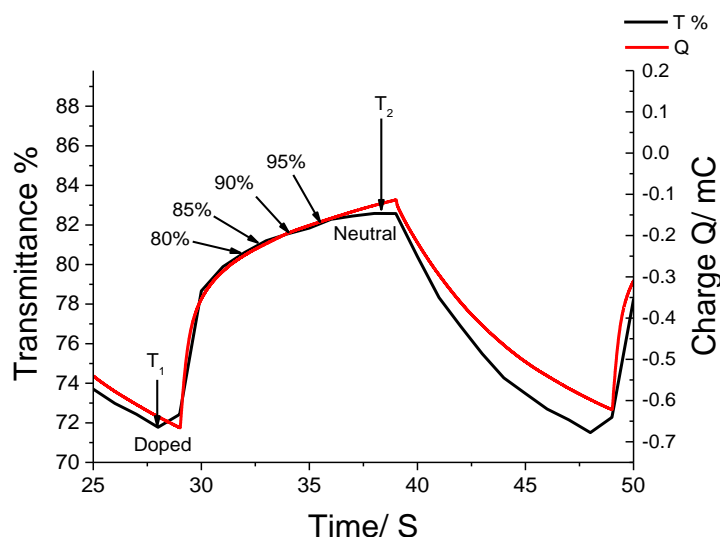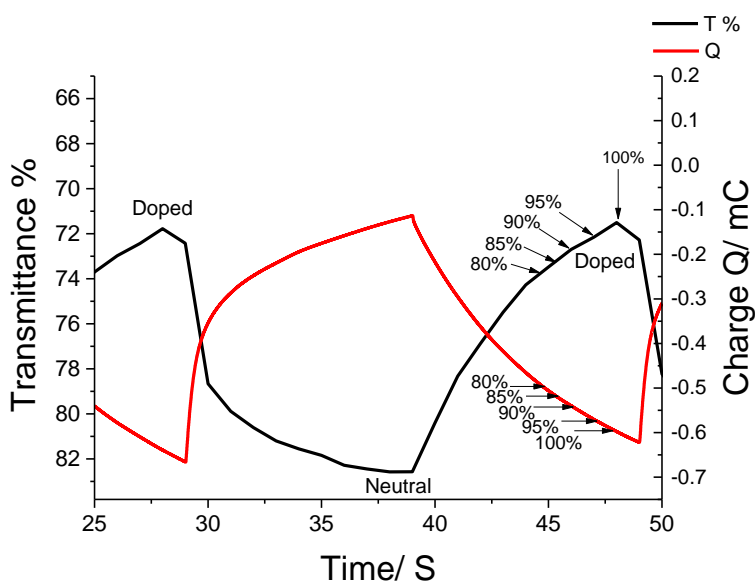Figure 5.22: Chronocoulometry-based doping experiment of a **Poly5.5** film on ITO, showing the transition from doped to neutral (and back to doped state) – a 3-step switch was performed by applying 10-s pulses while T% was measured at λ_{max}= 930 nm.

Table 5.7: Colouration efficiencies determined for **Poly5.5** at various percentages of optical changes of a complete colour-doping switch. Data has been baseline corrected.

ΔT ^{a,b} (%)	% change	$T_1{}^a$(%)	$T_2{}^a$(%)	τ (s)	Q (C)	$\Delta_{OD}{}^c$	$Q_d{}^d$	η ^{e} (cm^{2}C^{-1})
11.05	100	82.56	71.51	8.96	-4.83E-04	-6.24E-02	-1.63E-04	3.84E+02
10.49	95	82.56	72.07	8.10	-4.61E-04	-5.91E-02	-1.55E-04	3.80E+02
9.94	90	82.56	72.62	7.09	-4.29E-04	-5.58E-02	-1.45E-04	3.86E+02
9.39	85	82.56	73.17	6.31	-4.04E-04	-5.25E-02	-1.36E-04	3.85E+02
8.84	80	82.56	73.72	5.66	-3.78E-04	-4.92E-02	-1.27E-04	3.85E+02

^{a} transmittance measured at λ_{max} = 930 nm, ^{b} ΔT% = T_2% - T_1%, ^{c} Δ_{OD} = log [%T_2/ %T_1], ^{d} Q_d = Q/A, where A (electrode area) = 2.97 cm^2, ^{e} η = ΔOD(λ)/ Q_d.

The colouration efficiencies of the optical switch at 930 nm upon doping and dedoping of **Poly5.5** were investigated. It was found that the doping process had a colouration efficiency of 380 cm^{2}C^{-1} for the forward process, with a value of 368 cm^{2}C^{-1} for the reverse switch, at 95% of the full optical transmittance change. The large CE values observed are rationalised by the fact that the **Poly5.5** polymer system requires a minimal amount of charge in order to evoke such an optical transition.
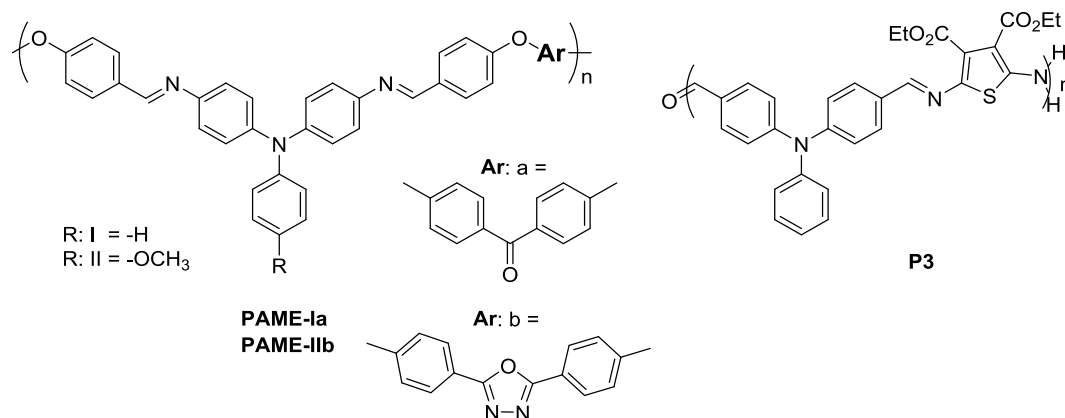
Figure 5.23: Polyazomethine ethers (PAMEs) containing triphenylamine (TPA) units and poly-azomethine. **P3** containing alternating thienyl and TPA units. [355,231]

In comparison, Yen *et al.*[355] have reported other red and blue electrochromic, aromatic poly(azomethine ether)s (PAMEs), containing electroactive triphenylamine (TPA) moieties in the backbone. These PAMEs were prepared from novel azomethine–triphenylamine-based biphenol monomers in high-temperature polycondensations with difluoro compounds. The presence of large, twisted triphenylamine units within the polymer induced fast switching with a high optical transmittance change (ΔT%) and

reported CEs of 162 and 195 cm^{2}C^{-1} (PAME-Ia: ΔT% = 84% in 5 s at λ = 717 nm, and PAME-IIa: ΔT% = 85% in 2 s at λ = 725 nm, respectively).[355] Additionally, Skene *et al.* reported a polymer azomethine device from 2,5-diaminothiophene **5.1** polymerised with 4,4'-triphenylamine dialdehyde. This poly-azomethine device showed repetitive optical transmittance changes from oxidised (dark blue) and neutral (cyan/light green) states without significant colour fatigue or polymer degradation under the applied bias of +3.2 to -1.5 V under ambient conditions. The colouration efficiency of the oxidised state at 690 nm was 102 cm^{2}C^{-1}.[231] These polymers possess a loose, amorphous morphology due to the incorporation of large, twisting triphenylamine units, which improve the electrochemical switching speeds.

These colouration efficiency studies highlight how subtle structural modifications in organic polymers can influence the electrochromic performance. Although the reported polymers possess a higher change in optical transmittance, faster switching speeds, and multiple redox states compared with **Poly5.5**, this novel polymer displayed a superior CE in the near IR range due to its low charge consumption. The electrochromic performance of the bisEDTT heterocyclic azomethine polymer **Poly5.5** has been extensively studied and found to be more efficient than its EDOT analogue **Poly5.4**[219] as well as recently published TPA-bearing PAMs.[231, 355]

5.1.2.7 Chromaticity Analysis

CIE chromaticity coordinates were determined for **Poly5.4**-**5.6**, which had been electrochemically deposited on ITO substrates and measured in monomer-free acetonitrile solution with the same electrolyte concentration as previously stated (Ref. Chapter 6.2.1 & 6.3.3). Each polymer film was subjected to a constant potential of -0.4 V before the respective oxidation potential (0.85, 0.95, and 1.0 V for **Poly5.4**, **Poly5.5**, and **Poly5.6**, respectively) was applied for 120 s to convert the polymers to their neutral or doped states, whilst the colour coordinates were measured to determine the colour transformation (see Table 5.8).

All polyazomethines **Poly5.4**-**Poly5.6** show reversible colour transitions from a range of blue/grey colours to slightly paler blue/grey hues (see inset in Table 5.8), which were visible to the naked eye (*ΔE*= 4.89, 2.36 and 6.82 respectively for **Poly5.4**-**Poly5.6)**. Furthermore, the luminance of the reported systems increased upon doping.

The polymers **Poly5.4-5.6** form doped species that exhibit their optical transition changes in the near infrared (NIR). This renders them suitable as near IR sensors as well as for signalling applications, as opposed to optical displays.

Table 5.8: CIE Coordinates of polyazomethines **Poly5.4**-**5.6** in their neutral and doped states.

	P5.4 N	P5.4 D	Δ	P5.5 N	P5.5 D	Δ	P5.6 N	P5.6 D	Δ
X	44.09	50.00	+5.91	27.79	28.78	+0.99	35.98	44.57	+8.59
Y	44.01	50.28	+6.27	28.54	30.13	+1.59	36.63	44.97	+8.34
Z	52.21	56.66	+4.45	36.51	38.64	+2.13	43.21	50.28	+7.07
x	0.3142	0.3186	+0.044	0.2993	0.2950	-0.0043	0.3107	0.3188	+0.008
y	0.3137	0.3204	+0.007	0.3074	0.3088	+0.0014	0.3163	0.3216	+0.005
z	0.3721	0.3610	-0.0111	0.3933	0.3961	+0.0028	0.3731	0.3596	-0.014
L*	72.23	76.24	+4.01	60.73	61.76	+1.03	67.00	72.87	+5.87
			Lighter			Lighter			Lighter
a*	3.72	2.91	-0.81	0.07	-2.04	-2.11	1.15	2.37	+2.22
			Greener			Greener			Redder
b*	-1.08	1.59	+2.67	-4.31	-4.51	-0.20	-0.75	1.93	+2.68
			Yellower			Bluer			Yellower
Colour									
ΔE			4.89			2.36			6.82

CIE *XYZ* 1931 and *L*a*b** 1964 colour spaces for polymers **Poly5.4-5.6**, **N**-neutral, **D**-doped, 10° standard observer and Source C illuminant. Colour generated from *Lab* coordinates. *Δ* change in colour coordinates and *ΔE* total change in colour coordinates.

5.2   **Conclusion**

The synthesis of bis-EDTT azomethine-containing **Poly5.5** and asymmetrical EDOT/EDTT azomethine-containing **Poly5.6** has been reported, and their electrochromic behaviours investigated and compared to the previously published bisEDOT azomethine-containing **Poly5.4**.[219]

The asymmetric polymer **Poly5.6** behaved in a similar way in terms of its electrochemical and optical properties as the EDOT analogue **Poly5.4**, due to the alternating EDOT-EDTT units that enable S-O chalcogen interactions, mimicking the intramolecular interactions known in PEDOT.[169] However, both **Poly5.4** and **Poly5.6** illustrated in switching studies a less impressive electrochromic performance than the bis-EDTT azomethine-containing **Poly5.5**.

Poly5.5 showed upon oxidation a modest change in optical transmittance of 33% at 10 s pulses but high colouration efficiencies of up to 380 cm^2C^{-1} measured at 930 nm. The high colouration efficiency is due to the low charge consumption required to evoke a redox change. All three polymers showed a visual optical change from blue to pale blue in the doped form and a broad absorption at higher wavelengths.

Typically, electrochromic materials were devised for optical displays and required polychromic transitions within the UV-Vis region of the electromagnetic spectrum. However, greater attention is now devoted to near-infrared (NIR)-absorbing electrochromic materials for optical signalling,[356] biomedicine,[357] military camouflage,[358] electro-optic switching in devices, temperature regulation, and thermal emission for spacecrafts.[359] Interestingly, these reported polyazomethines **Poly5.4**-**5.6** shown the greatest optical transmittance changes to occur within the NIR range from 900-1000 nm upon oxidation. Given **Poly5.5** demonstrated superior EC performance compared to its EDOT analogues, systems obtained from further optimisation of **Poly5.5** could prove to be interesting candidates for NIR-EC materials.

6 Experimental

6.1   General Procedures

6.1.1   Solvents and reagents

All reagents were purchased from Sigma-Aldrich, Alfa Aesar, or Lancaster and used without further purification, unless stated otherwise. Commercially available 1,4-diazabicyclo(2,2,2)octane (DABCO) was dissolved in acetone, dried over Na_2SO_4, and filtered and the solvent was removed under reduced pressure. DABCO was dried under high vacuum for at least 1 h prior to being used in the respective reactions where indicated. Anhydrous solvents were obtained from a PureSolv (SPS 400, Innovation technologies) solvent purification system, using alumina as the drying agent, other anhydrous solvents (DMF, CH_3CN) were commercially available from Aldrich. Solvents were removed under reduced pressure using a rotary evaporator (vacuum supplied by a low vacuum pump) and, where necessary, a high vacuum pump was used to remove residual solvent. All distillations were performed with a Kügelrohr Z24 using either a high or low vacuum pump, assisted by a hot air electrical heating chamber.   For all reactions that required anhydrous conditions, glassware was dried in an oven at 120 °C. Microwave assisted reactions were performed in a Biotage Initiator microwave oven.

2-(Trimethylstannyl)-3-hexylthiophene **2.16** was kindly provided by Dr. F. Vilela and Dr. N. J. Findlay assisted with the successful synthesis of the polymer poly(3,4-vinylidenedithiinafuran) **PBDF**.

6.1.2   NMR Spectroscopy

^{1}H and **^{13}C NMR** spectra were recorded on a Bruker Avance AV3 400 or DRX 500 instrument at either 400.13 and 100.61 MHz or 500.13 and 125.76 MHz in either $CDCl_3$, $(CD_3)CO$, or $(CD_3)_2SO$. Chemical shifts are given in ppm and coupling constants *J* are given in Hz.

6.1.3   Mass Spectrometry

Low resolution mass spectrometry (**MS**-ES) was performed on a Thermo Finnigan LCQDuo system using direct infusion or run as **MALDI-TOF** on a Shimadzu AXIMA-CFR spectrometer (mass range 1-150000 Da) and recorded on a Kratos spectrometer. Elemental analyses (**EA**) were obtained on a Perkin Elmer 2400 analyser. Accurate high resolution mass spectra (**HRMS**) were either recorded on a JEOL JMS-700 High Resolution mass spectrometer at the University of Glasgow, a Micromass Autospec Premier Instrument with Electron Ionisation at Imperial College London, UK, or *via* the EPRSC National Mass Spectrometry Service Centre at Swansea University, UK, using Orbitrap APCI with ASAP as the probe.

6.1.4   IR Spectroscopy

Infrared spectra (IR) were recorded on a Perkin Elmer spectrum ONE FT-IR, ATR Microlab PAL spectrometer (**ATR-IR** thin film deposited onto a diamond plate). Only selected absorptions (υ_{max}) are reported.

6.1.5   Thermogravimetric Analysis

Thermogravimetric analysis (**TGA**) was performed using a Perkin Elmer Thermogravimetric Analyzer TGA7 using heating rate of either 5 or 10 °C/min under a constant flow of helium.

6.1.6   Differential Scanning Calorimetry

Differential Scanning Calorimetry (DSC) was recorded using a TA instruments DSC Q10 V9.8 Build 296. All readings are uncorrected. DSC was performed on vacuum-dried samples of the respective polymers.

Melting points (**Mpt**) were measured using a Stuart Scientific SMP1 Melting Point apparatus and are uncorrected.

6.1.7   Chromatography

Gel permeation chromatography was conducted at Imperial College London, UK using an Agilent Technologies 1200 series **GPC**, which was equipped with two PL mixed B columns running in series with chlorobenzene at 80 °C and calibrated against narrow polydispersity polystyrene standards. All gel permeation chromatography (GPC) in this work was performed by L. Biniek and C. Combe at Imperial College London, UK.

Column chromatography was performed with commercially available solvents using either VWR (40-63 μm) or Zeoprep 60 Hyd (40-63μm mesh) silica gel. Thin layer chromatography (TLC) was performed using aluminium plates pre-coated with Merck silica gel 60 (F_{254}) and visualised by UV radiation and/or iodine vapour. Celite powder was used as a filter aid when indicated.

6.1.8   Powder X-ray diffraction

Powder X-ray diffraction data were collected using a PANalytical X'pert Pro diffractometer with Cu K_α radiation. Measurements over the range $1.6 \leq 2\Theta \leq \Theta\ 30°$ with a step size of 0.017° were performed on a powdered sample scattered onto an aluminium sample holder, revolving at 1 Hz. All powder X-ray diffraction was performed and analysed by F. C. Coomer at the University of Strathclyde, UK.

6.1.9 X-ray crystallography

X-ray crystallographic studies were performed and solved by C. Wilson at National Crystallography Service, Diamond Light Source Ltd, Oxfordshire, UK (see Appendix 1).

6.1.10 Molecular Modelling

Computational modelling calculations were performed by P. J. Skabara at the University of Strathclyde, Glasgow, UK. DFT calculations were performed at the B3LYP/6-31G* level (SPARTAN 10).

6.1.11 Electrochemistry

CV measurements were performed on a CH Instruments 660A Electrochemical Workstation with *i*R compensation using a glassy carbon working electrode (WE), platinum wire counter electrode (CE), and a silver wire reference electrode (RE). Indium tin oxide (ITO) was used as WE and Pt gauze as (CE) for the spectro-electrochemical experiments. Solutions of the monomer substrates (ca. 10^{-4} M unless stated otherwise), containing tetrabutylammonium hexafluorophosphate (*n*-TBAPF$_6$; 0.1 M) as the supporting electrolyte, were degassed (Ar) before being subjected to the electrochemical measurements. The indicated potentials of all measurements are referenced against the half-wave potential $E_{1/2}$ of the ferrocene/ferrocenium (Fc/Fc$^+$) redox couple using a fresh ferrocene solution containing the appropriate solvent and electrolyte. A scan rate of 100 mV/s was applied unless indicated otherwise.

HOMO and LUMO values are given in eV and were calculated from the onset of the first peak of the corresponding redox wave and referenced to the HOMO level of ferrocene, which has a known value of -4.8 eV.[96]

The oxidation and reduction graphs for each experiment were ran independently, as the presence of irreversible peaks or modified species *in situ* can give inaccurate redox behaviours.

6.1.12 UV-Vis Spectroscopy

Electron absorption spectra for materials in Chapters 3 & 4 were measured on a UNICAM UV 300 (190-1100 nm) spectrophotometer. Materials studied in Chapter 5 were measured on a Shimadzu UV-2600 spectrophotometer (190-1400 nm) that uses an integrated sphere and barium sulphate as reference. Solutions of the respective monomers (*ca.* 10^{-4} M) were filled into 1 cm path length quartz cuvette, and the absorption spectra were recorded. The instrument was calibrated by subtracting an absorption spectrum of the pure solvent medium.

Solid-state polymers prepared onto ITO slides in accordance to 6.2.1 and 6.2.2 have their electron absorption spectra recorded and referenced against blank ITO slide.

6.2 **Polymer Chemistry**

6.2.1 Polymer Preparation on Working Electrodes

Polymer preparation with accordance to 6.1.11.

- Chapter 3: Solid-state polymer was electrochemically prepared onto both CWE and ITO by oxidative cycling from its respective monomer solution (10^{-4} M in anhydrous CH_2Cl_2).
- Chapter 4: A thin film of chemically prepared polymer **PBDF** was drop casted onto either the active site of the glassy CWE or ITO slide then dried.
- Chapter 5: Solid-state azomethine polymer films were electrochemically prepared onto CWE from their respective monomer solutions ($>10^{-3}$ M in 2:1 anhydrous CH_2Cl_2:hexane).

Chapter 5: The preparation of solid state azomethine polymer on ITO was achieved *via* bulk electrolysis using a BAS CV-50W Voltammetric Analyser, Bioanalytical system inc. with *i*R compensation using a Pt gauze (CE), and a Ag wire (RE).

6.2.2 Dedoping of Polymers

Electrochemically or synthetically prepared polymers were electrochemically dedoped to their neutral states in monomer-free acetonitrile solution containing *n*-TBAPF$_6$ (0.1 M) as the electrolyte. Prepared films were subjected to potential cycling within a potential region without any electroactivity (-0.1 to 0.1 V for 100 cycles, unless stated otherwise). The polymer films were then dried and rinsed with acetonitrile solution to remove any residual monomer before being spectroelectrochemically studied.

6.2.3 Electrochemistry of Polymers

CV measurements of solid-state polymer films on CWE were recorded in monomer-free, anhydrous acetonitrile solution containing *n*-TBAPF$_6$ (0.1 M) as the supporting electrolyte. The acetonitrile solution was degassed with Ar prior to reduction measurements. All data are referenced against the half-wave potential $E_{1/2}$ of the ferrocene/ferrocenium Fc/Fc$^+$ redox couple.

6.3 **Electrochromism Studies**

6.3.1 *Spectroelectrochemistry*

Spectroelectrochemical experiments were conducted using a CH Instruments 660A potentiostat simultaneously with UV-Vis spectrometer as detailed in Chapter 6.1.12. Measurements are taken of polymer deposited on ITO films (prepared according to Chapter 6.2.1 & 6.2.2) and immersed in monomer-free, anhydrous acetonitrile containing *n*-TBAPF$_6$ (0.1 M) as the supporting electrolyte; Ag wire (RE), and a Pt guaze (CE) were recorded within a quartz cuvette cell (path length 1 cm). Both large Pt guaze (CE) and pseudo- RE Ag wire should not disturb the spectrometer light path. The absorptions of the polymer films were recorded over a wavelength range of 300-1400 nm (according Spectrometer specification described in Chapter 6.1.12) while the applied potential was increased from 0 to +2.0 V in 100 mV increments.

Chapter 4: Solution spectroelectrochemistry of monomer solution involve more specialised cell which can incorporate metallated working and counter electrodes; uses Ag wire (RE), and a Pt wire (CE) and performed on blank ITO slide (WE) in 1 cm quartz cuvette. In addition stirring under flow of Ar is also required for solution spectroelectrochemical studies.

6.3.2 *Switching Studies*

Spectroelectrochemical switching studies of solid state polymers (prepared on CWE, *ref:* 6.2.1 & 6.2.2) monitor the polymer's absorbance maximum (at where the greatest optical transformations occur) whilst switching the potential between two ranges where the polymer switches from neutral to doped state (vs. Ag wire (RE), Pt wire (CE)). Thereby, the polymer is switched between its neutral and p-doped states. The potential is switched by square wave voltammetry applying a potential step wave function with various potential switching rates (10, 5, 2.5, 1.25, 0.5, and 0.25 s). This facilitates the analysis of the polymer's switching rate by recording the time dependence of the percentage transmittance of the polymer film, which can be calculated from the initially monitored absorbance in accordance to Chapters 6.1.11 & 6.1.12 .

6.3.3 *Chromaticity Analysis*

The colour coordinates of investigated polymer films (prepared in accordance to 6.2.1 & 6.2.2) are determined by *in situ* chromaticity analysis recorded on a UNICAM UV 300 instrument and CV strategies according to 6.1.11. The respective polymer was electrochemically prepared on an ITO glass substrate and measured in monomer-free acetonitrile solution containing *n*-TBAPF$_6$ (0.1 M) as electrolyte. The setup used is a 1 cm quartz cuvette with Pt wire (CE) and Ag wire (RE). Two defined potentials are applied to the polymer film (each potential held constant for 90 s) the potentials selected are to convert and equilibrate the polymer into its neutral or doped state,

respectively. The potential-induces colour transformations of the investigated polymer in the UV-Vis range where the formation of polarons and bipolarons occurrence are recorded by colorimetry using a 10° standard observer and source C illuminant (overcast daylight, CIE 1964, 6770 K).[282] The colour transformations are quantified by determining the colour CIE coordinates.

6.4   Synthesis

2-Acetyl-3,4-ethylenedioxythiophene (2.2)[297]

2.2
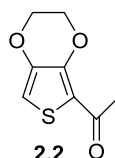
To a solution of **EDOT** (3.13 g, 0.022 mol) in anhydrous CH_2Cl_2 (2 mL), solutions of acetic anhydride in anhydrous CH_2Cl_2 (0.25 M, 114.5 mL, 0.029 mol) and tin tetrachloride in anhydrous MeCN (0.25 M, 114.5 mL, 0.029 mol) was added. The resulting mixture was stirred at room temperature (rt) under anhydrous conditions for 24 h. The red-coloured solution was then poured onto crushed ice containing glacial acetic acid (50 mL). The phases were separated and the aqueous phase extracted with CH_2Cl_2 (3 × 50 mL). The combined organic phases were washed with 10% sodium hydroxide solution until reaching pH 7. Purification was achieved by column chromatography on silica gel using CH_2Cl_2 as solvent, followed by recrystallisation from $CHCl_3$/hexane (1:1) to give off-white crystals (2.64 g, 65%) of compound **2.2**.

^{1}H NMR (500 MHz, $CDCl_3$): δ_H 2.51 (3H, s, CH_3), 4.24 (2H, m, OCH_2), 4.38 (2H, m, OCH_2), 6.68 (1H, s, ArH) ppm; **^{13}C NMR** (100 MHz): δ_C 29.0, 64.0, 65.3, 108.4, 120.2, 141.7, 144.8, 189.72 ppm; **MS**: *m/z* GC/IE: (M+H)$^+$ 184.01 Da and (M+C$_2$H$_5$)$^+$ 212.9 Da; **Mpt**: 100-101.5 °C (Lit.[297] 101-102.5 °C).

0.245 g (0.633 mmol) of compound **2.12** was suspended in 20 mL of acetic acid to which excess zinc powder (1.186 g, 0.018 mol) was added and refluxed for 1 h. Once the reaction mixture was cooled to room temperature, the precipitate suspension was slowly neutralised by treatment of supersaturated sodium bicarbonate solution. The resultant mixture was then sonicated with 3 x 50 mL of Et_2O for 15 minutes and extracted. The organic layers were combined, dried over $MgSO_4$, and filtered, and the solvent was removed under reduce pressure to yield an off-white solid of the monoacetyl EDOT compound **2.2** in 85% (0.099 g).

^{1}H NMR (400 MHz, $CDCl_3$): δ_H 2.51 (3H, s, CH_3), 4.24 (2H, m, OCH_2), 4.38 (2H, m, OCH_2), 6.68 (1H, s, ArH) ppm. **Mpt:** 101-102 °C.

5-Bromo-(2-acetyl)-3,4-ethylenedioxythiophene (2.11)

2.11
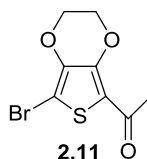
Compound **2.2** (12.75 g, 0.069 mol) was dissolved in CH_2Cl_2 (100 mL), and NBS (18.49 g, 0.104 mol) was slowly added over 2-3 h whilst being stirred at rt. The reaction flask was concealed from any light with tinfoil and continuously stirred at rt for 24 h. Then, the reaction mixture was quenched with ice/water (300 mL), and the organic phase was separated and sequentially washed with 10% sodium thiosulfate (150 mL), water (4 × 100 mL), and finally brine (100 mL). The organic phase was dried over $MgSO_4$ and filtered through a plug of Celite. The solvent was removed under reduced pressure and the crude solid was recrystallised from (1:1) $CHCl_3$/hexane to afford compound **2.11** as off-white crystals (17.50 g, 89%).

^{1}H NMR (500 MHz, $CDCl_3$): δ_H 2.49 (3H, s, CH_3), 4.33 (2H, m, OCH_2), 4.39 (2H, m, OCH_2) ppm; **^{13}C NMR** (125 MHz): δ_C 29.1, 64.4, 65.3, 99.2, 120.3, 140.1, 143.9, 188.7 ppm; **MS**: *m/z* MALDI-TOF: $(M+H)^+$ 246 Da with THAP and cyano Matrices; **EA$_{Calc}$**: C (36.52), H (2.68), S (12.19); **EA$_{Found}$**: C (36.44), H (2.48), S (12.08); **v_{max} ATR-IR**/cm^{-1}: 2950, 2900, 1642, 1487, 1446, 1427, 1375, 1354, 1287, 1084, 1013, 995, 905, 847 and 776; **Mpt**: 122-124 °C.

5-Bromo-2-(2-bromo acetyl)-3,4-ethylenedioxythiophene (2.12)

2.12
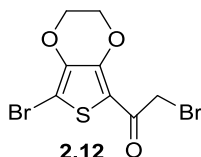
Compound **2.11** (17.00 g, 0.065 mol) was dissolved in anhydrous CH_2Cl_2 (100 mL), and DMA_2HBr_3 (26.61 g, 0.065 mol) was added slowly over 2 h. This mixture was stirred overnight at rt, provoking that the pale yellow solution transformed to an orange/green mixture. This mixture was poured into ice/water (300 mL), and the organic layer was washed with 10% sodium thiosulfate (100 mL), water (4 × 100 mL), and finally brine (100 mL). The reaction mixture was dried over $MgSO_4$ and filtered, and the solvent was removed under reduced pressure to yield a green powder. The product was further purified by column chromatography, using CH_2Cl_2 as eluent, to afford compound **2.12** as an off-white crystalline solid (14.75 g, 67%). Furthermore, unreacted starting material **2.11** (2.35 g, 14%) was recovered.

^{1}H NMR (400 MHz, $CDCl_3$): δ_H 4.35 (2H, s, CH_2), 4.36 (2H, m, OCH_2), 4.44 (2H, m, OCH_2) ppm; **^{13}C NMR** (125 MHz) δ_C 33.2, 64.4, 65.6, 101.4, 117.2, 101.4, 144.5, 182.1 ppm; EA$_{Calc}$: C (28.09), H (1.77), S (9.38); **EA$_{Found}$**: C (28.12), H (1.72), S (9.25); **MS**: *m/z* GC/EI: $(M)^+$ 341.87 Da; **v_{max} ATR-IR**/cm^{-1}: 2960, 1656, 1485, 1422, 1388, 1354, 1300, 1207, 1093, 1078, 993, 901 and 869; **Mpt**: 135-137 °C.

5-Bromo-2-(N,N-dimethylamino)-acetyl-3,4-ethylenedioxythiophene (2.13)

2.13
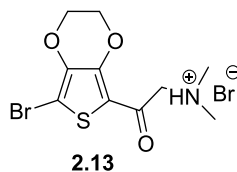
Compound **2.12** (7.00 g, 0.020 mol) was dissolved in diethyl ether (150 mL) and treated with 40% dimethylamine in water (31.05 mL, 0.169 mol). The mixture was stirred at room temperature for 10 min then refluxed for a further 30 min. The mixture was cooled to room temperature and quenched with water (100 mL). The organic phase was separated and the aqueous phase extracted with Et_2O (3 × 50 mL). The organic phases were combined and dried over $MgSO_4$, filtered and the solvent removed under reduced pressure. The resultant oily residue was dissolved in a minimum amount of methanol (MeOH~5 mL) and treated with 48% HBr solution in water (4.22 mL, 1.5 mol). The resultant product recrystallised when placed in the freezer overnight, forming yellow needles of compound **2.13** (6.38 g, 81%).

^{1}H NMR (500 MHz, d_6-DMSO): δ_H 2.87(6H, s, 2 × N(CH$_3$)$_2$), 4.39 (2H, m, OCH$_2$), 4.51 (2H, m, OCH$_2$), 4.59 (2H, s, AcCH$_2$); **^{13}C NMR** (100 MHz) δ_C 43.6, 48.5, 62.9, 64.4, 66.1, 100.5, 115.2, 140.6, 146.6, 181.6 ppm; **EA$_{Calc}$**: C (31.03), H (3.39), N (3.62), S (8.28); **EA$_{Found}$**: C (30.91), H (3.23), N (3.89), S (8.55); **MS**: *m/z* ES: (M+H)$^+$ 306.29 Da and (M+Na)$^+$ 330.04 Da; ν_{max} **ATR-IR**/cm^{-1}: 2900, 2730, 1645, 1491, 1431, 1373, 1353, 1269, 1237, 1134, 1080, 1058, 1028, 987, 924. **Mpt**: 212-213 ˚C.

Bis-N,N-5-bromo-3,4-ethylenedioxythiophene-(2-oxoethyl-1)-N,N dimethyl ammonium bromide (2.14)

2.14
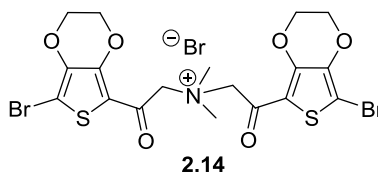
Compound **2.13** (6.00 g, 0.016 mol) was added to Et_2O (100 mL) then slowly treated with of 10% NaOH (50 mL). This mixture was stirred at rt for 20 min, forming the free base form of compound **2.13** and allowing dissolution into Et_2O layer. The two phases were separated and the aqueous layer was extracted with Et_2O (3 × 50 mL). The organic layers were combined, dried over $MgSO_4$, filtered and the solvent was removed under reduced pressure leaving a yellow oily residue. The free base was re-dissolved in Et_2O (100 mL), to which compound **2.12** (5.31 g, 0.016 mol) was added. This mixture was refluxed for 1 h then cooled to rt and refrigerated overnight. The precipitated material was filtered, washed with CHCl$_3$ and dried in a desiccator for 24 h. Compound **2.14** was afforded as a yellow coloured powder (8.75 g, 84%).

^{1}H NMR (400 MHz, d_6-DMSO): δ_H 3.46 (6H, s, N(CH$_3$)$_2$) 4.40 (4H, m, OCH$_2$), 4.53 (4H, m, OCH$_2$), 5.11 (4H, s, CH$_2$N). **^{13}C NMR** (125 MHz) δ_C 35.0, 44.2, 54.0, 63.5, 64.8, 64.9, 66.0, 66.1, 66.3, 66.6, 66.8, 67.1, 101.5, 116.4, 141.2, 146.9, 181.7 ppm; **EA$_{Calc}$**: C (33.35), H (2.80), N (2.16), Br (36.98), S (9.89); **EA$_{Found}$**: C (33.04), H (2.86), N (2.14), Br (37.18), S (9.52); **MS**: *m/z* MALDI-TOF, no matrix: (M)$^+$ 567.9, (M+H)$^+$ 569.9, (M-2H)$^+$

565.9 Da; ν_{max} **ATR-IR**/cm^{-1}: 2943, 1656, 1638, 1492, 1423, 1379, 1353, 1265, 1222, 1133, 1084, 1032, 993, 909, 857, 844. **Mpt**: 205-207 ˚C.

(E)-1,4-Bis(7-bromo-2,3-dihydrothieno[3,4-b][1,4]dioxin-5-yl)but-2-ene-1,4-dione (2.15)
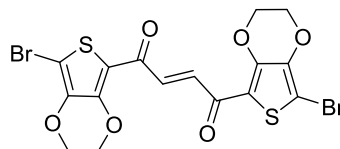
2.15

Successful synthetic procedure 1:

The recovered quaternary amino salt **2.14** (1.01 g, 1.56 mmol) from the 'failed synthetic procedure 2' for **2.15** (*vide infra)* was dissolved in a solution of NaOH prepared in ethanol (150 mL, 1.75 g, 0.044 mol). This mixture was refluxed for 1 h then cooled to room temperature. The reaction mixture changed colour from a pale yellow to a deep, pasty red colour; this was further cooled to -15 °C by immersing into an ice/acetone/salt bath. Once cooled, the reaction mixture was neutralised by slow addition of concentrated hydrochloric acid, HCl (37%, 4.28 g, 0.044 mol). This reaction mixture was further refluxed for 1.5 h, then cooled to rt and refrigerated overnight. The precipitated product was filtered and washed with MeOH and CH_2Cl_2, then dried in a dessicator for 24 h. Compound **2.15** was afforded as a deep yellow-coloured, insoluble powder (0.58 g, 71%).

^{1}H NMR (500 MHz, d$_6$-DMSO): δ_H 4.39 (4H, bm, 2 × OCH$_2$), 4.53 (4H, bm, 2 × OCH$_2$), 7.84 (2H, s, CH); **EA**$_{Calc}$: C (36.80), H (1.93), Br (30.60), S (12.28); **EA**$_{Found}$: C (36.51), H (1.60), Br (30.33), S (12.30); **MS**: *m/z* MALDI-TOF: (M)$^+$ 522.75 Da with THAP and Dithranol matrices; **Mpt**: 320 °C (dec.).

Failed synthetic procedure 2:

A suspension of quaternary amino salt **2.14** (1 g, 1.76 mmol) in 15 mL of ethanol was treated with 40% v/w of dimethylamine (DMA) in water (0.6 mL, 0.048 mol) and stirred for 20 min at room temperature. Thereafter, an addition of 2.1 mL (0.020 mol) of 98% diethylamine (DEA) stock solution was added and resultant mixture was stirred for a further 20 min. The white milky turbid solution gave no indication of compound **2.14** dissolving therefore an additional 4 mL of DMA in 5 mL of ethanol was added and stirred for a further 20 min. The turbid solution was then cooled to -15 °C before slowly acidified with conc. hydrochloric acid (10.5 mL, 12 M) which turned the mixture from milky white to pale yellow colour, turbid solution. This mixture was further refluxed for 1.5 h in attempt to dissolve the suspension. The turbid mixture was cooled to room temperature and left overnight before being filtered through a Buchner funnel and washed with copious amounts of cold ethanol. The resultant pale yellow solid afforded to be recovered starting material **2.14** in 71% (724 mg).

^{1}H NMR (500 MHz, d$_6$-DMSO): δ_H 3.46 (6H, s, 2 x NCH$_3$), 4.39 (4H, m, 2 x OCH$_2$), 4.53 (4H, m, OCH$_{2)}$, 5.12 (4H, s, CH$_2$). **Mpt**: 204-206 °C.

Failed synthetic procedure 3:

Amino ketone salt **2.14** (8.0 g, 0.014 mol) was dissolved in hot dimethyl sulfoxide DMSO (80 mL at 80 °C) giving a transparent yellow solution. The slow addition of 40% w/v DMA in water (48.8 mL, 0.386 mol) transformed the reaction mixture to a transparent red colour solution which was stirred for 20 min at 80 °C. Thereafter, DEA (16.50 mL, 0.156 mol) was treated to this reaction mixture and stirred for further 40 min at 80 °C. The reaction mixture was kept cool at -15 °C whilst acidifying the reaction mixture with the slow addition of 37% HCl (52.9 g, 0.544 mol) which resulted the formation of a dark brown coloured precipitate. This turbid mixture was further refluxed for 1 h, then cooled to rt and stirring overnight. The formed precipitate material was filtered and washed sequentially with copious amounts of water, 3 x 150 mL methanol and 3 x 150 mL diethyl ether then vacuum dried in desiccator for 48 hr. The unidentifiable brown material was obtained in 5.31 g quantity and showed to be insoluble in most common solvents which perturb any further purification.

MS: MALDI: 797.83, 751.87, 579.92, 234.94.

(E)-1,4-Bis(7-(4-hexylthiophen-2-yl)-2,3-dihydrothieno[3,4-b][1,4]dioxin-5-yl)but-2-ene-1,4-dione (2.17)

2.17
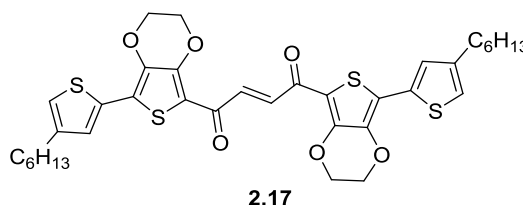
To a solution of compound **2.15** (0.1 g, 19.2 mmol) prepared in dry dimethylformamide (DMF, 5 mL), 3-hexyl(trimethyltin thien-5-yl) **2.16** (0.13 g, 40.4 mmol) and tetrakis(triphenylphosphine)palladium (0) catalyst (11 mg, 5.6 mmol) were added. The Stille cross-coupling microwave mediated reaction was performed within a 2-5 mL microwave vial and radiated at 160 °C for 2 h with constant stirring. The reaction mixture was quenched with water (50 mL) and both phases were separated. The aqueous phase was extracted with CHCl$_3$ (3 × 15 mL), and then the organic layers were combined and dried over MgSO$_4$. The excess solvent was removed under reduced pressure to yield a crude brown-coloured oil. Residual DMF solvent was removed *via* Kügelrohr distillation, (2 mmHg at 45 °C). Further purification was performed by column chromatography on silica gel using CHCl$_3$ as eluent, which separated the desired orange coloured solid compound **2.17** (0.05g, 37%).

^{1}H NMR (500 MHz, CDCl$_3$,): δ_H 0.91 (6H, t, *J* = 6.7 Hz, CH$_3$), 1.32 (12H, m, (CH$_2$)$_3$), 1.66 (4H, m, CH$_2$), 2.62 (4H, t, *J* = 7.2 Hz, CH$_2$-R), 4.41 (4H, m, OCH$_2$), 4.49 (4H, m, OCH$_2$), 6.98 (2H, s, 2 × αH-Th) 7.31 (2H, s, 2 × βH-Th), 8.08 (2H, s, CH); **^{13}C NMR** (100 MHz): δ_C 14.1, 22.6, 28.9, 29.7, 30.3, 30.4, 31.6, 53.4, 64.3, 65.5, 122.0, 127.3, 133.2, 135.4, 136.9, 144.0, 145.8, 180.1 ppm; **MS**: *m/z* MALDI-TOF, no matrix: (M+H)$^+$ 696.97, (M)$^+$ 696.17 Da; **Mpt**: 104-106 °C (dec.).

3,2-Dibromo-2,5-dimethoxytetrahydrofuran (3.17)[309]

3.17
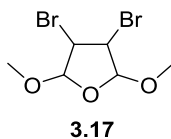
A solution of 2,5 dimethoxy-2,5-dihydrofuran **3.16** (47.28 g, 0.384 mol) in dry CH$_2$Cl$_2$ (150 mL) was cooled to -10 ˚C whilst kept under a positive flow of N$_2$. The solution was maintained at low temperature (below 15 ˚C) and over 2 h, bromine (61.4 g, 19.47 mL, 0.384) was added drop-wise. After addition, the reaction mixture was stirred at 10 ˚C to remove excess bromine (disappearance of colour). The solution was concentrated by the removal of solvent under reduced pressure and product was obtained as a light coloured oil/semi solid residue **3.17** (107.1 g, 95%) and was used without purification.

^{1}H NMR (400 MHz, CDCl$_3$): δ_H 3.48 (3H, s, CH$_3$), 3.51 (3H, s, CH$_3$), 4.18 (1H, dd, J =8.0, 4.0 Hz, BrCH), 4.25 (1H, dd, J = 8.0, 4.0 Hz, BrCH), 4.94 (1H, d, J = 8.0 Hz, OCH), 5.22 (1H, d, J = 8.0 Hz, OCH).[309]

2,3 Dibromo-1,1,4,4-tetramethoxybutene (3.18)[309]

3.18
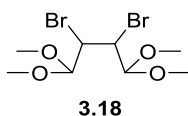
A solution of 3,4-dibromo-2,5-dimethoxytetrahydrofuran **3.17** (107 g, 0.365 mol) dissolved in MeOH (2 L) was prepared in a 3 L, three necked round bottom flask equipped with boiling stones. The reaction mixture was refluxed and treated with the slow addition of 96% sulfuric acid (37.7 g, 0.384 mol) over 30 min. The reaction mixture was further refluxed for 72 h then cooled down to rt before the addition of triethylamine (49 mL, 0.352 mol). Thereafter, the reaction solvent was removed under reduced pressure and the crude material was re-dissolved in heptane (250 mL), stirred and refluxed for 20 min. The lightly coloured heptanes phase was separated from the crude residue and the heptanes extraction was repeated a further 4 times. The combined heptane phases were concentrated under reduced pressure to give the titled compound as a yellow oil **3.18** (91.1 g, 74%, including impurities, and used in the next step without further purification).

^{1}H NMR (400 MHz, CDCl$_3$): δ_H 3.45 (12H, s, OCH$_3$), 4.33 (2H, d, J = 8.0 Hz, BrCH), 4.58 (2H, d, J = 8.0 Hz, OCH).[309]

1,1,4,4-tetramethoxybut-2-yne (3.19)[309]

3.19
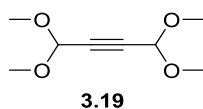
A 1L flask was charged with dry THF (300 mL), tris[2-(2-methoxyethoxy)-ethyl]amine (TMEEA, 10.1 g, 31.2mmol) and crude **3.18** (91.1g, 0.271 mol). To this homogenous solution, 85% potassium hydroxide pellets (70 g, 1.06 mol) were

introduced and mixture was refluxed under N_2 for 24 h. Solvent was removed under reduced pressure then the crude residue was treated with water (250 mL) and back extracted with Et_2O (3 × 250 mL). The combined Et_2O phases were washed with water (100 mL), dried over $MgSO_4$, filtered and concentrated under low vacuum to yield a yellow oil **3.19** (37.31 g, 79%).

**¹H NMR** (400 MHz, $CDCl_3$): δ_H 3.40 (12H, s, OCH_3), 5.23 (2H, s, CH).[309]

4,4-Dimethoxy-2-butynal (3.8)[309]

3.8
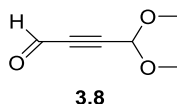
A solution of crude **3.19** (61.2 g, 0.351 mol) was dissolved in CH_2Cl_2 (150 mL) and cooled to 0 ˚C. A second solution of formic acid (280 g, 235 mL, 6 mol) dissolved in CH_2Cl_2 (150 mL) and water (1.5 mL) was also chilled to 0 ˚C. The chilled formic acid solution was rapidly charged to the diacetal solution, while the reaction vessel was tightly sealed with rubber septum, equipped with a stainless steel syringe needle as source for gas exhaust. The reaction vessel was concealed from light and allowed to stir for 60 hr at 16-19 ˚C. The resultant brown crude solution was extracted with water (3 × 250 mL) and the combined aqueous phases then extracted with CH_2Cl_2 (3 × 250 mL). The combined organic phase was dried over a mixture of $Na_2SO_4/NaHCO_3$ (10:1), filtered and the solvent removed under reduced pressure to give a brown oil. The crude brown oil was further purified by vacuum distillation using high vacuum (0.15 mmHg at 72 ˚C) to give a light yellow coloured oil **3.8** (18.75 g, 42%).

¹H NMR (400 MHz, $CDCl_3$): δ_H 3.48 (6H, s, OCH_3), 5.31 (1H, s, CH), 9.29 (1H, s, OCH).[309]

Bis(tetraethylammonium) bis (1,3-dithiole-2-hione-4,5-dithiolate)-zincate (3.22) [308]

3.22
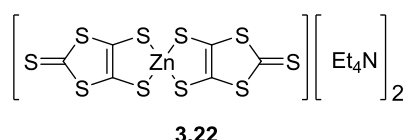
Nitrogen gas was purged through a solution of DMF (240 mL) for 30 min at -5 °C and, whilst maintaining an inert atmosphere at low temperature, carbon disulfide was added (120 mL, 2.0 mol). The solution mixture was kept under N_2 and was vigorously stirred at low temperature (-5 to 0 °C). Finely cut sodium metal pieces (7.2 g, 0.31 mol) were carefully added. This mixture was maintained at low temperature for 6 h and thereafter left to stir overnight at rt whilst under a positive flow of N_2. Residual sodium was destroyed by cooling reaction mixture in an ice bath and carefully adding MeOH (50 mL). The red solution mixture formed was then simultaneously treated with two solutions; $ZnCl_2$ (10.65 g, 0.078 mol) in water (50 mL) and ammonium hydroxide (175 mL) and tetraethylammonium bromide (33 g, 0.157 mol) in water (250 mL) to produce the zincate salt. The resulting mixture/precipitate was further stirred at 0 °C for 16 h before being filtered and washed with a copious volume of propan-2-ol until washings

were clear. The crude product was subsequently washed with Et$_2$O (150 mL) and vacuum dried to give bright red coloured zincate salt **3.22** (40.37 g, 85%).[308]

1,3-Dithiole-2-thione-4,5-dithiolate (DMIT) 3.9[308]
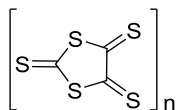
3.9

Zincate salt **3.22** (36.0 g, 50 mmol) was dissolved in acetone (250 mL) and cooled to -15 °C for 30 min. A solution of iodine (26.0 g, 102 mmol) dissolved in ethanol (350 mL) was added drop-wise to the cooled zincate solution with continuous stirring over 2 h. The reaction mixture was allowed to warm to rt and resulted in an orange coloured solid precipitating. The crude material was filtered and subsequently washed with acetone, water and ethanol (200 mL of each), then dried in vacuum desiccator to give an orange microcrystalline solid **3.9** (19.0 g, 97%).[308] The product was used without any further purification.
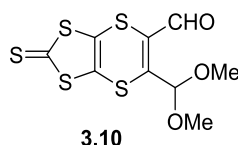
6-(Dimethoxymethyl)-2-thioxo-[1,3]dithiolo[4,5-b][1,4] dithiine-5-carbaldehyde (3.10)[305]

3.10

To a solution of 4,4-dimethoxybut-2-ynal **3.8** (4.30 g, 0.034 mol, 3.50 mL) in dry toluene (500 mL), oligo trithioxo-1,3-dithiole (DMIT) **3.9** (6.50 g, 0.50 mol) was added and the mixture was refluxed for 2 h. The solvent was removed under reduced pressure and the crude product was purified by column chromatography using toluene as eluent to give a red-orange solid **3.10** (7.64 g, 70%).

^{1}H NMR (400 MHz, CDCl$_3$): δ_H 3.46 (6H, s, 2 × CH$_3$), 5.58 (1H, s, CH), 10.02 (1H, s, CHO); **^{13}C NMR** (100 MHz): δ_C 53.8, 99.8, 128.5, 134.1, 154.7, 181.7 ppm; **MS**: *m/z* GC/CI: (M+H)$^+$ 324.01 Da; **EA$_{Calc}$**: C, (33.31); H, (2.49); S, (49.41); **EA$_{Found}$**: C, (33.19); H (2.31); S (49.30). **ν_{max} ATR-IR**/cm^{-1}: 2958, 2833, 1669, 1552, 1496 and 1069; **Mpt**:128–130 °C.[305]

5-(Dimethoxymethyl)-6-(hydroxymethyl)-[1,3]dithiolo[4,5-b][1,4] dithiine-2-thione (3.11)[305]
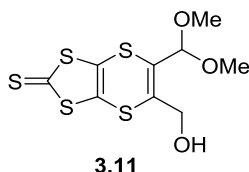
3.11

Sodium borohydride (2.94 g, 0.074 mol) was added to a stirred solution of aldehyde **3.10** (3.00 g, 9.25 mmol dissolved in 100 mL of THF) at rt. After 2 min, the reaction mixture was poured into saturated NaHCO$_3$ (100 mL), potassium bromide (19.5

g) was added and the product was extracted with ethyl acetate (3 × 100 mL). The extract was dried over $MgSO_4$ and evaporated in vacuo to dryness affording the product **3.11** as a brown/yellow oil (2.94 g, 97%), which was used in the next step without further purification.

^{1}H NMR (400 MHz, $CDCl_3$): δ_H 2.11 (1H, s, OH), 3.39 (6H, s, 2 × CH_3), 4.48 (2H, s, CH_2), 5.24 (1H, s, CH); **MS**: MALDI-TOF, matrix used THAP: $(M+Na)^+$ 345 Da.[305]

[1,3]-Dithiolo[4',5':5,6][1,4]dithiino[2,3-c]furan-2-thione (3.12)[307]

3.12

Alcohol **3.11** (5.24 g, 0.02 mol) was dissolved in a solvent mixture of CH_2Cl_2 (100 mL), acetic acid (100 mL) and 98% formic acid (75 mL). This mixture was stirred at room temperature for 1 h and then the solvent was removed under reduced pressure to afford a yellow-orange product (4.09 g, 97%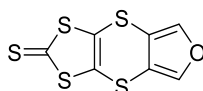). Further purification was achieved by column chromatography on silica gel, using toluene as solvent yielding an orange product **3.12** (3.67 g, 87%).

^{1}H NMR (400 MHz, $CDCl_3$): δ_H 7.41 (2H, s, Ar-H); **^{13}C NMR** (125 MHz): δ_C 29.7, 118.2, 138.3, 189.4 ppm; **MS**: m/z GC/CI: $(M+H)^+$ 262.9 Da; **Mpt**: 168-170 ℃ (Lit[307] 172-173 ℃).

[1,3]Dithiolo[4',5':5,6][1,4]dithiino[2,3-c]furan-2-one (3.13)[307]
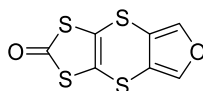
3.13

To a solution of thione dervative **3.12** (0.525 g, 2.00 mmol) in CH_2Cl_2/acetic acid (3:1 v/v 100 mL) was added mercuric acetate (1.275 g, 4.00 mmol). The mixture was stirred at room temperature for 4 h before being filtered. Water (100 mL) was added and the mixture extracted with dichloromethane (3 × 100 mL). The combined organic layers were washed with saturated sodium bicarbonate solution (250 mL) and water (250 mL) before drying with $MgSO_4$. The solvent was removed under reduced pressure and the residue purified by column chromatography on silica gel, using toluene, to afford an off-white product **3.13** (0.493 g, 84%).

^{1}H NMR (400 MHz, $CDCl_3$): δ_H 7.41 (2H, s, Ar-H); **^{13}C NMR** (100 MHz): δ_C 29.7, 117.6, 138.3, 209.7 ppm; **MS**: m/z GC/CI: $(M+H)^+$ 246.8 Da; **Mpt**: 128-130 ℃ (Lit[307] 129-131 ℃).

2,3-Bis(methylthio)-[1,4]dithiino[2,3-c]furan (3.1)
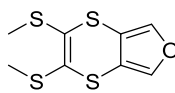
3.1

To a cold (-15°C) mixture of carbonyl derivative **3.13** (0.333 g, 1.36 mmol) in THF (20 mL) was added sodium methoxide (25%, 4.37 M, 0.22 mL) dropwise. The mixture was stirred for 30 min whilst under N_2. Then iodomethane (0.70 mL, 10.8 mmol) was added dropwise and the mixture allowed to reach rt and left to stir overnight. The solvent was removed under reduced pressure, and the residue was dissolved in CH_2Cl_2, filtered and, after removal of the solvent, the crude product was subjected to column chromatography on silica gel using 20% dichloromethane in hexane as eluent. The product was isolated as a yellow crystalline solid **3.1** (0.245 g, 46%).

^{1}H NMR (400 MHz, CDCl$_3$): δ_H 2.46 (6H, s, S(CH$_3$)$_2$), 7.26 (2H, s, (Ar-H)); **^{13}C NMR** (125 MHz): δ_C 18.4, 119.2, 128.8, 137.2 ppm; **MS**: *m/z* GC/CI: (M)$^+$ 248.9 Da; **EA$_{Calc}$**: C, (38.68); H, (3.25); S, (51.63); **EA$_{Found}$**: C, (39.06); H (3.23); S (51.15); ν_{max} **ATR-IR**/cm^{-1}: 3120, 2922, 1537, 1410, 1032, 873 and 842; **Mpt**: 67–69 °C.

2,3-Bis(hexylthio)-[1,4]dithiino[2,3-c]furan (3.2)
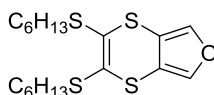
3.2

To a cold (-15°C) mixture of carbonyl derivative **3.13** (0.140 g, 53.4 mmol) in dry THF (30 mL) was added sodium methoxide (25%, 4.37 M, 0.52 mL) dropwise. The mixture was stirred for 30 min whilst under constant flow of N_2. 1-Bromohexane (0.62 mL, 3.2 mmol) was added drop wise and the mixture was allowed to reach room temperature and stirred overnight. The solvent was removed under reduced pressure, and the residue was treated with CH_2Cl_2, filtered and after removal of solvent, the crude product was subjected to column chromatography on silica gel using (1:1) CH_2Cl_2:hexane as eluent. The product was isolated as a colourless oil **3.2** (0.167 g, 81%).

^{1}H NMR (400 MHz, CDCl$_3$): δ_H 0.87 (6H, t, *J* = 6.6 Hz, 2 × CH$_3$), 1.26 (8H, m, 4 × CH$_2$), 1.38 (4H, quintet, *J* = 7.4 Hz 2 × (CH$_2$)), 1.56 (4H, quintet, *J* = 7.4 Hz, 2 × (CH$_2$)), 2.92 (4H, t, *J* = 7.3 Hz, 2 × (SCH$_2$)), 7.25 (2H, s, Ar-H); **^{13}C NMR** (100 MHz): δ_C 13.5, 21.9, 27.8, 29.2, 30.8, 34.5, 119.3, 128.7, 136.6 ppm; **MS**: *m/z* **HRMS**/EI: (C$_{18}$H$_{28}$OS$_4$) theoretical mass: 388.1023, found mass: 388.1021 Da; ν_{max} **ATR-IR**/cm^{-1}: 3114, 2954, 2924, 2853, 1500, 1226, 1125, 1032 and 955.

5,7-Dibromo-2,3-bis(methylthio)-[1,4]dithiino[2,3-c]furan (3.14)

3.14
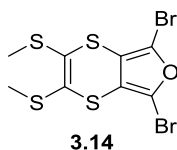
Compound **3.1** (0.100 g, 4.00 mmol) was dissolved in dichloromethane (20 mL) and treated with NBS (0.150 g, 0.841 mmol). This mixture was stirred for 4 h at room temperature then quenched with water (50 mL) and the organic phase was separated. The organic layer was further washed with saturated sodium sulfite solution (50 mL) and water (50 mL), before drying with MgSO$_4$. The solvent was removed under reduced pressure and the crude product was purified by passing through a plug of silica gel with 10% CH$_2$Cl$_2$/hexane eluent to afford a pale brown semi solid **3.14** (0.146 g, 91%). This was used immediately without further purification.

^{1}H NMR (400 MHz, CDCl$_3$): δ_H 2.46 (6H, s, 2 × (CH$_3$)); **^{13}C NMR** (125 MHz): δ_C 18.6, 29.7 (traces of hexane), 117.1, 120.8, 127.5 ppm; **MS**: *m/z* GC/EI, monoisotopic peak: (M-H)$^+$ 404.01 Da.

2,3-Bis(methylthio)-5,7-di(thiophen-2-yl)-[1,4]dithiino[2,3-c] furan (3.3)

3.3
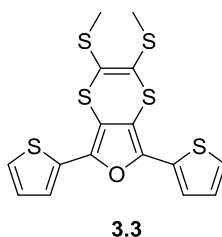
Tetrakis(triphenylphosphine) palladium(0), (46 mg, 0.4 mmol, 10% mol) was added to a mixture of compound **3.14** (150 mg, 4.0 mmol) and 2-(tributylstannyl)thiophene **3.15** (0.3 mL, 8.9 mmol), dissolved in N,N-dimethylformamide (20 mL). The reaction mixture was refluxed under N$_2$ for 24 h. The mixture was then cooled, quenched with water (200 mL) and extracted with dichloromethane (3 × 100 mL). The organic phases were combined and dried over MgSO$_4$ and the solvent removed under reduced pressure. The residue was purified by column chromatography on silica gel, using 20% CH$_2$Cl$_2$ in hexane as eluent, to give a yellow crystalline solid **3.3** (37 mg, 22%).

^{1}H NMR (500 MHz, CDCl$_3$): δ_H 2.51 (6H, s, 2 × CH$_3$), 7.12 (1H, d, ^3J = 3.5 Hz, Ar-H), 7.13 (1H, d, ^3J = 3.5 Hz, Ar-H), 7.36 (2H, dd, ^3J = 5.3 Hz, ^4J = 1.0 Hz, Ar-H), 7.42 (2H, dd, ^3J = 3.8 Hz, ^4J = 1.0 Hz, Ar-H); **^{13}C NMR** (100 MHz): δ_C 18.2, 114.8, 123.9, 124.0, 125.2, 128.1, 130.7, 141.3 ppm; **MS**: *m/z* MALDI-TOF, no matrix: (M)$^+$ 412.0 Da; **HRMS**/EI: (C$_{16}$H$_{12}$OS$_6$) theoretical mass: 411.9212, found mass: 411.9213; **ν_{max} ATR-IR**/cm^{-1}: 3101, 2915, 1466, 1418, 1257, 1080, 1045, 1030 and 989; **Mpt**: 97–98 °C.[305]

2,5-Dibromo-3,4-vinylenedithiinafuran (4.1)

4.1
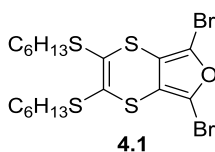
Compound **3.2** (1.14 g, 2.93 mmol) was dissolved in CH_2Cl_2 (45 mL) and *N*-bromosuccinimide NBS (1.1 g, 6.16 mmol) added in one portion. The reaction flask was covered in foil and stirred in the dark at room temperature, while being continually monitored by TLC (100% hexane). After 2 h, the reaction mixture was quenched by addition of water (50 mL) and the organic layer separated. The aqueous layer was further extracted with dichloromethane (25 mL) and the organic layers combined, before being washed with sodium sulfite (1M, 70 mL) and water (70 mL). The organic layer was dried over $MgSO_4$, filtered and concentrated to a light brown oil. Silica gel column chromatography, eluting with hexane, afforded the product as a clear, slightly pale green oil that was immediately used in the next step to avoid decomposition **4.1** (1.40 g, 87%).

^{1}H NMR (500 MHz, CDCl$_3$): δ_H 0.89 (6H, t, *J* = 6.8 Hz, CH$_3$), 1.29 (8H, m, CH$_2$), 1.39 (4H, q, *J* = 7.5 Hz, CH$_2$), 1.56 (4H, q, *J* = 7.7 Hz, CH$_2$), 2.93 (4H, t, *J* = 7.3 Hz, SCH$_2$); **^{13}C NMR** (125 MHz): δ_C 13.1, 18.7, 22.7, 29.4, 29.7, 31.9, 117.1, 120.8, 127.4 ppm; **MS**: *m/z* LC:(M-H)$^+$ 546.04 Da, (M+H)$^+$ 548.00 Da; **HRMS**/EI: (C$_{18}$H$_{26}$Br$_2$OS$_4$) theoretical mass: 545.9233; found mass: 545.9207; *ν*$_{max}$ **ATR-IR**/cm^{-1}: 2954, 2924, 2870, 2853, 1550, 1498, 1459, 1302, 1110, 972.

Poly(3,4-vinylidenedithiinafuran) PBDF

PBDF
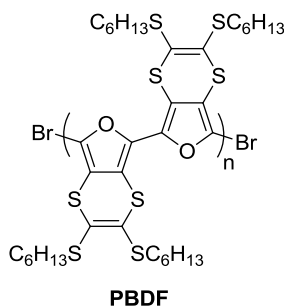
Bis(1,5-cyclooctadienyl) nickel(0) (350 mg, 1.27 mmol) was weighed out in a glovebox and sealed in a reaction flask equipped with a condenser. Toluene (5 mL) and *N,N*-dimethylformamide (DMF, 5 mL) were added and the solution stirred under Ar. A solution of monomer **4.1** (496 mg, 0.91 mmol), 1,5-cyclooctadiene (0.11 mL, 0.91 mmol) and 2,2'bipyridal (199 mg, 1.27 mmol) in toluene (5 mL) and DMF (5 mL) was added, causing an immediate formation of a dark brown solution. The reaction mixture was heated to 80 °C and stirred under Ar for 48 h. After this time, the reaction mixture was cooled to room temperature and concentrated to a dark brown residue. Cold MeOH (150 mL) was added causing a precipitate to form. The precipitate was filtered and dried, then subjected to Soxhlet extraction with MeOH (18 h), acetone (24 h) and

CH_2Cl_2 (24 h). The CH_2Cl_2 layer was concentrated to afford the *title compound* as a dark brown, shiny solid **PBDF** (214 mg, 43%).

^{1}H NMR (500 MHz, $CDCl_3$): δ_H 0.70-0.97 (6H, bm), 1.10-1.65 (16H, bm), 2.90-2.96 (4H, bm); ν_{max} **ATR-IR**/cm^{-1}: 2954, 2924, 2853, 1444, 1412, 1282, 1256; **GPC**: M_w = 6200, M_n = 3800, PDI = 1.63.

2,3,4-5 Tetrabromothiophene (5.13)[302]
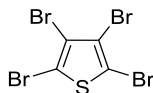
5.13

To a solution of thiophene **5.12** (30 g, 0.357 mol) in CH_2Cl_2 (100 mL) was added bromine (80 mL, 1.6 mol) drop-wise at -10 °C with continuous stirring. After addition, the ice bath was removed and the solution was heated to 70 °C and left overnight. The solution was transferred to a beaker and an ice bath was used to cool the contents for 1 h with occasional stirring. During cooling a white solid compound precipitated out. The solid was recovered, washed with copious amounts of water, until the washings became clear, then subsequently washed with MeOH and vacuum dried. The crude product was recrystallised from hot ethanol to form large white crystals **5.13** (125 g, 87%).

MS: *m/z* GC/CI: (M$^+$H)$^+$ 400.6 Da, (M-Br)$^+$ 319.6 Da; **Mpt:** 112-114 °C, (Lit.[302] 112-116 °C).

3,4-Dibromothiophene (5.14)[360]
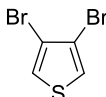
5.14

2,3,4,5-Tetrabromothiophene **5.13** (112 g, 0.28 mol), zinc powder (112 g, 1.71 mol) and water (315 mL) were charged to a round bottom flask fitted with a mechanical stirrer. Acetic acid (112 mL, 1.96 mol) was slowly added to the flask whilst stirring at a temperature of 70 °C. Once all the materials had dissolved, the reaction was heated at 70 °C for a further 1 h, and then continuously stirred at rt for 12 h. The reaction mixture was filtered through Celite and extracted with copious amounts of Et_2O. The combined organic phase was washed several times with $NaHCO_3$ solution until neutralised, then water (250 mL). The organic phase was dried over $MgSO_4$, filtered and solvent removed under reduced pressure. The crude product was further purified by vacuum distillation at low vacuum (4.5 mmHg at 65 °C) to yield a colourless oil **5.14** (53.5 g, 79%).

^{1}H NMR (400 MHz, $CDCl_3$): δ_H 7.32 (2H, s, CH); **MS:** *m/z* (EI): (M$^+$) 242 Da.[360]

3,4-Dimethoxythiophene (5.15)[360]
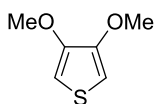
5.15

Sodium metal (35.2 g, 1.53 mol) was cut into small pieces and placed into a 500 mL three neck round bottom flask with MeOH (310 mL) under N_2. The solution was kept at 0°C during the addition of 3,4-dibromothiophene **5.14** (61.74 g, 0.255 mol), potassium iodide (423.5 mg, 2.6 mmol) and copper oxide (20.3 g, 0.255 mol). The reaction was stirred at 90 °C for 72 h, before cooling the solution to 50 °C and adding a further portion of potassium iodide (423.5 mg, 2.6 mmol). The reaction was reheated to 90 °C and left to stir overnight. The mixture was filtered through Celite and the filtrate extracted with diethyl ether (3 × 250 mL). The combined organic phases were washed with water (2 × 150 mL) and then dried over anhydrous $MgSO_4$. Removal of the solvent under reduced pressure yielded a crude oil. Distillation under high vacuum (0.04 mmHg at 70 °C) yielded a colourless oil **5.15** (26.5 g, 72%).

1H NMR (400 MHz, $CDCl_3$): δ_H 3.89 (6H, s, CH_3); 6.19 (2H, S, CH); **MS**: *m/z* LC: (M) 144 Da.[360]

3,4-Ethylenedithiathiophene (5.7) EDTT[171]
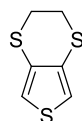
5.7

To a 500 mL round bottom flask was added 3,4-dimethoxythiophene **5.15** (6 g, 0.042 mol), 1,2-ethylenedithiol (15.67 g, 0.167 mol), a catalytic amount of *p*ara-toluenesulfonic acid (357 mg, 1.87 mmol) and dry toluene (300 mL). The reaction mixture was kept under a positive flow of N_2 and stirred at 90 °C for 72 h. Thereafter, a second catalytic amount of *p*ara-toluenesulfonic acid (142.86 mg, 0.75 mmol) was added and stirred for an additional 5 h at 90 °C before cooling down to rt. The reaction mixture was diluted with Et_2O (500 mL) and repetitively washed with a large volume of 20% NaOH solution, until the organic phase became odourless. The combined aqueous phases were washed twice with Et_2O then discarded. The organic phases were subsequently combined and washed with sat. $NaHCO_3$ (250 mL), brine (250 mL) and then dried over $MgSO_4$, filtered and the solvent evaporated. The crude compound was purified by high vacuum distillation (0.02 mmHg at 110 °C) to afford a colourless oil **5.7** (6.09 g, 83%).

1H NMR (400 MHz, $CDCl_3$): δ_H 3.25 (4H, s, CH_2), 6.99 (2H, s, CH); **MS**: *m/z* GC/CI: (M+H)$^+$ 174.8 Da, (M+C$_3$H$_5$)$^+$ 202.8 Da.[171]

2,3-Dihydrothieno[3,4-b][1,4]dioxine-5-carbaldehyde (5.8)[297]
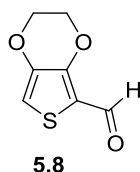
5.8

3,4-Ethylene dioxythiophene **5.7** (2.0 g, 0.014 mol) was weighed into a 2 neck round bottom flask, evacuated and purged several times with N_2 before being dissolved in dry THF (40 mL). The solution was cooled to -78 °C then treated with ^{n}BuLi (8.5 mL, 0.021 mol) and left to stir for 1 h under a positive flow of N_2. The reaction temperature was raised to 0 °C for 5 min before re-cooling back to -78 °C, followed by addition of dry DMF (9 mL, 0.11 mol) drop wise. The reaction mixture was left to stir overnight at rt, under a positive flow of N_2. Thereafter, the reaction mixture was poured over crushed ice (200 mL) and conc. HCl (5 mL). The aqueous phase was extracted with CH_2Cl_2 (3 × 250 mL). All organic phases were combined and subsequently washed with saturated $NaHCO_3$ solution (150 mL), saturated NH_4Cl solution (150 mL), de-ionised water (150 mL) and brine (150 mL). The organic phase was dried over $MgSO_4$, filtered and the solvent removed under reduced pressure. The crude material was further purified by precipitation from hot CH_2Cl_2/hexane solution to afford an off white yellow powder **5.8** (1.81 g, 75%).

^{1}H NMR (400 MHz, CDCl$_3$): δ_H 4.30 (2H, m, CH$_2$), 4.39 (2H, m, CH$_2$), 6.18 (1H, s, CH), 9.94 (1H, s, CHO); **MS**: m/z GC: (M) 170 Da; **Mpt:** 137-139°C, (Lit.[297] 142 °C).

2,3-Dihydrothieno[3,4-b][1,4]dithiine-5-carbaldehyde (5.9)
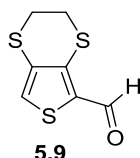
5.9

EDTT **5.7** (1.0 g, 5.74 mmol) was weighed into a 2 neck round bottom flask, evacuated and purged several times with N_2, then dissolved in dry THF (70 mL). The solution was cooled to -78 °C and ^{n}BuLi (2.7 mL, 6.31 mmol) added dropwise, then stirred for 1 h at -78 °C under N_2. The reaction temperature was raised to -50 °C for 5 min then treated with dry DMF (3.6 mL, 0.046 mol). The reaction mixture was stirred overnight at rt under N_2. Thereafter, the reaction mixture was poured over crushed ice (200 mL) and conc. HCl (5 mL). The aqueous phase was extracted with CH_2Cl_2 (3 × 250 mL). All organic phases were combined and subsequently washed with saturated $NaHCO_3$ solution (150 mL), saturated NH_4Cl solution (150 mL), de-ionised water (150 mL) and brine (150 mL). The organic phase was dried over $MgSO_4$, filtered and the solvent removed under reduced pressure. The crude material was further purified by column chromatography using (1:1) CH_2Cl_2:hexane as eluent, yielding a yellow powder solid **5.9** (0.846 g, 73%).

^{1}H NMR (500 MHz, CDCl$_3$): δ_H 3.26 (2H, m, CH$_2$), 3.33 (2H, m, CH$_2$), 7.33 (1H, s, CH), 9.89 (1H, s, CHO); **^{13}C NMR** (100 MHz): δ_C 26.1, 26.8, 126.7, 127.3, 132.8, 135.8,

179.8; EA$_{Calc}$: C (41.56), H (2.99), S (47.55); **EA$_{Found}$**: C (41.52), H (2.80), S (46.94); **MS**: *m/z* GC/CI: (M+H)$^{+}$ 202.8 Da; ν_{max} **ATR-IR**/cm^{-1}: 3087, 2909, 1638, 1412, 1230, 1046, 952; **Mpt:** 82-84 °C.

2,5-Diamino-thiophene-3,4-dicarboxylic acid diethyl ester (5.1)[226]
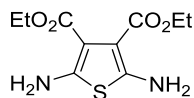
5.1

To a 50 mL round bottom flask, elemental sulfur **5.10** (2.0 g, 0.063 mol), DMF (10 mL), ethyl cyanoacetate **5.11** (14.24 g, 0.13 mol) and triethylamine (2 mL, 14.2 mmol) were added and the mixture stirred at rt for 60 h. The slurry was filtered and resulting filtrate was poured into ice cold water (250 mL) causing yellow powder precipitate. The precipitate was filtered, dried and recrystallised from a mixture of ethyl acetate/hexane to yield yellow needles **5.1** (2.57 g, 16%).

^{1}H NMR (400 MHz, (CD$_3$)CO): δ_H 1.26 (6H, t, ^3J = 6 Hz, CH$_3$), 4.19 (4H, q, ^3J = 9 Hz CH$_2$), 6.14 (4H, s, NH$_2$); **MS**: *m/z* EI: (M)$^{+}$ 258.05 Da, (M-C$_2$H$_5$O)$^{+}$ 212.01 Da; **Mpt:** 151-154 °C, (Lit.[226] 155-156 °C).

2-Amino-5-[(2,3-dihydro-thieno{3,4-b][1,4]dioxin-5-ylmethylene)-amino]-thiophene-3,4-dicarboxylic acid diethyl ester (5.2)[219]
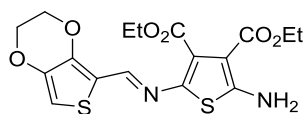
5.2

To a round bottom flask, compound **5.8** (0.172 g, 1.01 mmol) and **5.1** (0.142 g, 5.64 mmol), ethanol (20 mL) and a catalytic amount of trifluoroacetic acid, (TFA, 0.1 mL) were added. The mixture was stirred at rt overnight and the resultant precipitate formed was filtered, washed with copious amounts of ethanol to leave a red/orange coloured solid. The crude material was purified by column chromatography using (1:1) CH$_2$Cl$_2$:hexane, spiked with 10% NEt$_3$, as eluent and further recrystallised from hot MeCN to give orange crystals **5.2** (244 mg, 59%).

^{1}H NMR (500 MHz, DMSO): δ_H 1.18 (3H, t, ^3J = 7.5 Hz, CH$_3$), 1.28 (3H, t, ^3J = 7.5 Hz, CH$_3$), 4.11 (2H, q, ^3J = 7.2 Hz, CH$_2$), 4.23 (2H, q, ^3J = 7.8 Hz, CH$_2$), 4.24 (2H, m, CH$_2$), 4.33 (2H, m, CH$_2$), 6.83 (1H, s, CH), 7.81 (2H, s, NH$_2$), 7.95 (1H, s, NCH); **MS**: *m/z* LC: (M+H)$^{+}$ 411.0 Da; **Mpt:** 218-220 °C, (Lit.[219] 219-221 °C).

2-Amino-5-[(2,3-dihydro-thieno{3,4-b][1,4]dithiin-5-ylmethylene)-amino]-thiophene-3,4-dicarboxylic acid diethyl ester (5.3)

5.3
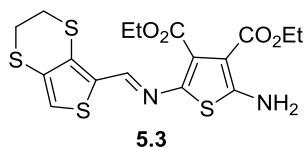
Both **5.9** (300 mg, 1.48 mmol) and **5.1** (421 mg, 1.63 mmol) were dissolved in 40 mL of ethanol before adding a catalytic amount of TFA (0.5 mL, 0.75 mmol). The reaction mixture was stirred at rt for 12 h and the resultant precipitate was filtered and washed with excess ethanol. The crude material was subjected to column chromatography using (1:1) CH_2Cl_2:hexane, spiked with 10% NEt_3 as eluent, to afford a bright yellow solid. Further recrystallisation from hot MeCN yielded orange crystal clusters **5.3** (386 mg, 59%).

^{1}H NMR (500 MHz, DMSO): δ_H 1.18 (3H, t, ^3J = 7 Hz, CH_3), 1.28 (3H, t, ^3J = 7 Hz, CH_3), 3.25 (2H, m, CH_2), 3.26 (2H, m, CH_2), 4.12 (2H, q, ^3J = 7 Hz, CH_2), 4.22 (2H, q, ^3J = 7 Hz, CH_2), 7.47 (1H, s, CH), 7.89 (2H, s, NH_2), 7.98 (1H, s, NCH); **^{13}C NMR** (125 MHz): δ_C 14.5, 14.6, 27.6, 27.0, 59.9, 61.2, 100.6, 123.2, 127.0, 130.0, 130.2, 131.9, 132.6, 142.5, 161.31, 163.7, 165.1; **EA$_{Calc}$**: C (46.13), H (4.10), N, (6.33), S (28.98); **EA$_{Found}$**: C (46.02), H (3.91), N (6.68), S (29.15); **MS**: *m/z* LC: (M+H)$^+$ 443.0 Da; ν_{max} **ATR-IR**/cm^{-1}: 3420, 3315, 3263, 3173, 2975, 2928, 1710, 1673, 1598, 1538, 1501, 1426, 1337, 1240, 1098, 1023, 777, 695; **Mpt:** 229-231 °C.

Diethyl-2,5-bis((E)-(2,3-dihydrothieno[3,4-b][1,4]dioxin-5-yl)-methyleneamino) thiophene-3,4-dicarboxylate (5.4)[219]

5.4
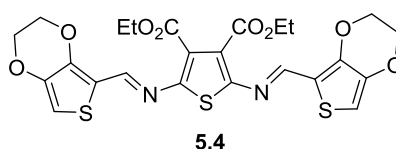
Both **5.8** (165 mg, 0.968 mmol) and **5.1** (100 mg, 0.389 mmol) were weighed into a 2 neck round bottom flask, evacuated and purged with N_2 and dissolved in dry toluene (20 mL). The solution mixture was heated to ensure complete dissolution occurred and then dried DABCO (348 mg, 3.09 mmol) was immediately added. The reaction mixture was treated with fresh titanium tetrachloride (TiCl$_4$) in toluene 1 M (1.0 mL, 0.34 mM) and further refluxed for 12 h under N_2. The reaction mixture was concentrated, re-dissolved in acetone, filtered and the solvent removed under reduced pressure before being subjected to column chromatography, using (30%) CH_2Cl_2 in hexane spiked with 10% NEt_3 as eluent. The separated product was precipitated from CH_2Cl_2 with hexane, yielding a red powder solid (118 mg, 54%). For analytical analysis, crystals were achieved by slow evaporation of acetone to give black red crystals.

^{1}H NMR (400 MHz, (CD$_3$)CO): δ_H 1.36 (6H, t, ^3J = 7.2 Hz, CH_3), 4.32 (4H, q, ^3J = 7.2 Hz, CH_2), 4.35 (4H, m, CH_2), 4.45 (4H, m, CH_2), 6.88 (2H, s, CH), 8.55 (2H, s, NCH); **MS**: *m/z* MALDI-TOF: (M+H)$^+$ 562.99 Da; **Mpt:** 183-185 °C, (Lit.[219] 179-181 °C).

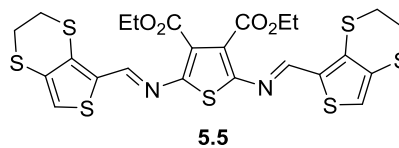### *Diethyl-2,5-bis((E)-(2,3-dihydrothieno[3,4-b][1,4]dithiin-5-yl)-methyleneamino) thiophene-3,4-dicarboxylate (5.5)*

5.5

Both **5.9** (127 mg, 0.626 mmol) and **5.1** (77 mg, 0.298 mmol) were weighed into a 2 neck round bottom flask, evacuated and purged with N_2 and dissolved in dry toluene (20 mL). The reaction mixture was heated to ensure complete dissolution occurred and then dried DABCO (268 mg, 2.37 mmol) was immediately added. The reaction mixture was treated with fresh $TiCl_4$ in toluene 1 M (0.6 mL, 0.204 mM) and further refluxed for 12 h under N_2. The reaction mixture was concentrated, re-dissolved in acetone, filtered and the solvent removed under reduced pressure before being subjected to column chromatography using (30%) CH_2Cl_2 in hexane, spiked with 10% NEt_3 as eluent. The separated product was precipitated from CH_2Cl_2 with hexane, yielding a dark purple powder solid **5.5** (103 mg, 55%). Analytical samples were obtained by recrystallisation from hot MeCN to give fine dark purple needles.

^{1}H NMR (400 MHz, $(CD_3)CO$): δ_H 1.36 (6H, t, ^3J = 7 Hz, CH_3), 3.37 (4H, m, CH_2), 3.42 (4H, m, CH_2), 4.32 (4H, q, ^3J = 6.8 Hz, CH_2), 7.52 (2H, s, CH), 8.61 (2H, s, NCH); **MS**: *m/z* MALDI-TOF: $(M+Na)^+$ 648.7 Da, $(M)^+$ 625.7 Da; **HRMS**/EI: $(C_{24}H_{22}N_2O_4S_7)$ theoretical mass: $(M+H)^+$ 626.9697, found mass: 626.9693; ν_{max} **ATR-IR**/cm^{-1}: 3076, 2979, 2927, 1718, 1568, 1441, 1404, 1389, 1322, 1240, 1210, 1158, 1031, 859, 792, 678; **Mpt:** 196-199 °C.

Diethyl 2-((E)-((2,3-dihydrothieno[3,4-b][1,4]dioxin-5-yl)methylene) amino)-5-((E)-2-(2,3-dihydrothieno[3,4-b][1,4]dithiin-5-yl)vinyl) thiophene-3,4-dicarboxylate (5.6)

5.6
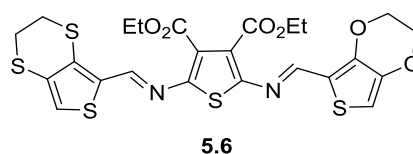
Both **5.8** (150 mg, 0.34 mmol) and **5.3** (192 mg, 1.31 mmol) were weighed into a round bottom flask, evacuated and purged with N_2 several times and then dissolved in a mixture of dry THF (20 mL) and dry toluene (50 mL). The solution mixture was heated to ensure complete dissolution occurred, before dried DABCO (305 mg, 2.71 mM) was added. The reaction mixture was treated with fresh $TiCl_4$ in toluene 1 M (0.2 mL, 0.68 mM) and further refluxed for 12 h under N_2. The reaction mixture was concentrated, re-dissolved in acetone, filtered and the solvent removed under reduced pressure before being subjected to column chromatography using (30%) CH_2Cl_2 in hexane, spiked with 10% NEt_3 as eluent. The separated product was precipitation from CH_2Cl_2 with hexane, yielding a black powder solid **5.6** (71 mg, 35%). Analytical samples were

obtained by recrystallisation from hot MeCN to give fine dark red/black coloured needles.

^{1}**H NMR** (400 MHz, (CD$_3$)CO): δ$_H$ 1.36 (6H, t, ^3J = 7 Hz, CH$_3$), 3.37 (2H, m, CH$_2$), 3.41 (2H, m, CH$_2$), 4.29 (4H, q, ^3J = 7 Hz, CH$_2$), 4.33 (2H, m, CH$_2$), 4.44 (2H, m, CH$_2$), 6.88 (1H, s, CH), 7.48 (1H, s, CH), 8.56 (2H, s, NCH); **MS**: *m/z* MALDI-TOF: (M-H)$^+$ 593.92 Da ; **HRMS**/EI: (C$_{24}$H$_{22}$N$_2$O$_6$S$_5$) theoretical mass: (M$^+$H)$^+$ 595.0154, found mass: 595.0143; ν_{max} **ATR-IR**/cm^{-1}: 3016, 2979, 2927, 1718, 1583, 1546, 1471, 1426, 1359, 1210, 1173, 1061, 1016, 978, 777, 717; **Mpt:** 216-217 °C.

7　Appendix

7.1 X-ray Crystallography of Monomer 3.3
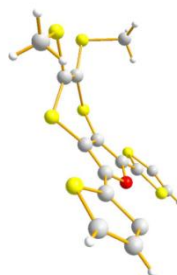
Figure 7.1: X-ray crystal diagram of monomer **3.3** viewed along the a-axis.

Data for monomer **3.3** was collected on an Enraf Nonius Kappa CCD using Mo-Kα radiation, as Φ scans and ω scans to fill the Ewald sphere. Data collection, cell refinement and data reduction were carried out using COLLECT[361] and DENZO.[362] The structure solution was obtained by direct methods (SHELXS-97)[363] and a full-matrix least squares refinement on F^2 was performed on all reflections by SHEXL-97[363] in the OLEX2 environment.[364]

Crystal structure determination of monomer 3.3

Crystal data. $C_{16}H_{12}OS_6$, M = 412.61, monoclinic, a = 22.338(3), b = 4.7901(7)°, U = 1744.7(4)Å^3, T = 120 K, space group Pc (no. 7), Z = 4, 11 738 reflections measured, 5748 unique (R_{int} = 0.142) which were used in all calculations. The final $wR(F^2)$ was 0.265, R_1 = 0.12 for 3919 observed data. The CCDC deposition number is: 879413.

1. P. Atkins and J. de Paula, *Physical Chemistry*, 8th edn., Oxford University Press, Oxford, 2006.
2. C. H. Hamann, A. Hamnett and W. Vielstich, *Electrochemistry* 2nd edn., Wiley-VCH, Weinheim, 2007.
3. M. R. Bryce, *Chem. Soc. Rev.*, 1991, **20**, 355-390.
4. A. J. B. a. L. R. Faulkner, ed. J. W. a. S. inc, John Wiley and Sons inc, 2001.
5. J. C. Bernede, *J. Chil. Chem. Soc*, 2008, **53**, 1549-1564.
6. B. L. R. F. Brovelli, J. C. Bernede, M. A. del Valle, F. R. Diaz, Y. Berredjem, *Polymer Bulletin*, 2006, **58**, 521-527.
7. S. T. N. Kirsten. J. Steenberg Harrell, *Handbook of Advanced Electronic and Photonic Materials Devices*, Science, 2001.
8. M. Mas-Torrent and C. Rovira, *Chem. Soc. Rev.*, 2007, 827-838.
9. A. D. a. M. G. René Dost, *J. Phys. D: Appl. Phys.*, 2007, **40**, 3563-3566.
10. R. G. Arns, *Engineering Science and Education*, 1998, **7**, 233-240.
11. C. K. Chiang, C. R. Fincher, Y. W. Park, A. J. Heeger, H. Shirakawa, E. J. Louis, S. C. Gau and A. G. MacDiarmid, *Phys. Rev. Lett.*, 1977, **39**, 1098-1101.
12. C. Pratt, in *Conducting polymers*, Kingston University, London, 1996.
13. F. Garnier, G. Tourillon, M. Gazard and J. Dubois, *J. Electroanal. Chem.*, 1983, **148**, 299-303.
14. S. K. Deb, *Sol. Energy Mater.*, 1995, **39**, 191-201.
15. Z. Y. Wang, J. Zhang, X. Wu, M. Birau, G. Yu, H. Yu, Y. Qi, P. Desjardins, X. Meng, J. P. Gao, E. Todd, N. Song, Y. Bai, A. M. R. Beaudin and G. LeClair, in *Pure Appl. Chem.*, 2004, vol. 76, p. 1435.
16. G. Inzelt, *Conducting Polymers: A new era in electrochemistry*, Springer, Berlin/ Hiedelberg, 2008.
17. A. A. Argun, P.-H. Aubert, B. C. Thompson, I. Schwendeman, C. L. Gaupp, J. Hwang, N. J. Pinto, D. B. Tanner, A. G. MacDiarmid and J. R. Reynolds, *Chem. Mater.*, 2004, **16**, 4401-4412.
18. H. Dong, C. Wang and W. Hu, *Chem. Commun.*, 2010, **46**, 5211-5222.
19. S. Allard, M. Forster, B. Souharce, H. Thiem and U. Scherf, *Angew. Chem., Int. Ed.*, 2008, **47**, 4070-4098.
20. H. Klauk, *Chem. Soc. Rev.*, 2010, **39**, 2643-2666.
21. C. M. Lampert, *Mater. Today*, 2004, **7**, 28-35.
22. J. L. Delgado, P.-A. Bouit, S. Filippone, M. A. Herranz and N. Martin, *Chem. Commun.*, 2010, **46**, 4853-4865.
23. B. C. Thompson and J. M. J. Frechet, *Angew. Chem.-Int. Edit.*, 2008, **47**, 58-77.
24. C. Li, M. Liu, N. G. Pschirer, M. Baumgarten and K. Müllen, *Chem. Rev.*, 2010, **110**, 6817-6855.
25. E. Bundgaard and F. C. Krebs, *Sol. Energy Mater.*, 2007, **91**, 954-985.
26. Y.-J. Cheng, S.-H. Yang and C.-S. Hsu, *Chem. Rev.*, 2009, **109**, 5868-5923.
27. G. Sonmez, *Chem. Commun.*, 2005, 5251-5259.
28. P. M. Beaujuge, C. M. Amb and J. R. Reynolds, *Acc. Chem. Res.*, 2010, **43**, 1396-1407.
29. P. M. Beaujuge and J. R. Reynolds, *Chem. Rev.*, 2010, **110**, 268-320.
30. J. Roncali, *Chem. Rev.*, 1992, **92**, 711-738.
31. R. J. Mortimer, A. L. Dyer and J. R. Reynolds, *Displays.*, 2006, **27**, 2-18.
32. C. Freudenrich, HowStuffWorks.com, 2005.
33. L. Groenendaal, G. Zotti, P. H. Aubert, S. M. Waybright and J. R. Reynolds, *Adv. Mater.*, 2003, **15**, 855-879.
34. J. Jensen, M. Hösel, A. L. Dyer and F. C. Krebs, *Adv. Funct. Mater.*, 2015, **25**, 2073-2090.
35. H. Antonladis, in *Overview of OLED display Technology*, 2006.

36.   B. W. D'Andrade and S. R. Forrest, *Adv. Mater.*, 2004, **16**, 1585-1595.

37.   S. K. Deb, *Appl. Opt.*, 1969, **8**, 192-195.

38.   A. C. Y. Coskun, L. Toppare, *Material Science*, 2007, **42**, 368-372.

39.   C. Pratt, 1996.

40.   A. L. Kanibolotsky, L. Kanibolotskaya, S. Gordeyev, P. J. Skabara, I. McCulloch, R. Berridge, J. E. Lohr, F. Marchioni and F. Wudl, *Organic Letters*, 2007, **9**, 1601-1604.

41.   E. J. L. H. Shirakawa, A.G. MacDiarmid, C.K. Chiang and A.J. Heeger, *Journal of the Chemical Society, Chemical Communications*, 1977, 578.

42.   D. J. Crouch, P. J. Skabara, J. E. Lohr, J. J. W. McDouall, M. Heeney, I. McCulloch, D. Sparrowe, M. Shkunov, S. J. Coles, P. N. Horton and M. B. Hursthouse, *Chem. Mater.*, 2005, **17**, 6567-6578.

43.   R. Berridge, S. P. Wright, P. J. Skabara, A. Dyer, T. Steckler, A. A. Argun, J. R. Reynolds, W. H. Ross and W. Clegg, *J. Mater. Chem.*, 2007, **17**, 225-231.

44.   C. M. Lambert, *Mater. Today*, 2004, **7**, 28-35.

45.   R. J. Mortimer, *Electrochim. Acta*, 1999, **44**, 2971-2981.

46.   J. Roncali, *Chem. Rev.*, 1997, **97**, 173-205.

47.   D. F. Perepichka and M. R. Bryce, *Angew. Chem.-Int. Edit.*, 2005, **44**, 5370-5373.

48.   H. Naarmann, in *Polymers, Electrically Conducting*, Wiley, 2005.

49.   R. R. C. J. E. Frommer, *Encyclopedia of Polymer Science and Engineering*, Wiley, New York, 1986.

50.   H. S. T. Ito, J.S. Ikeda, *Polymer Science Chemistry Edition*, 1974, **12**, 11.

51.   J. Roncali, *Chem. Rev.*, 1992, **92**, 711.

52.   W. Shockley, in *Electrons and Holes in Semiconductors*, ed. D. V. N. C. Inc, New York, 1950, vol. Ch. 12.

53.   H. Shirakawa, *Reviews of Modern Physics*, 2001, **73**, 713.

54.   R. J. Waltman and J. Bargon, *Can. J. Chem.*, 1986, **64**, 76-95.

55.   A. L. Dyer and J. R. Reynolds, *Handbook of Conducting Polymers*, 2007.

56.   F. J. L. 'Bert' Groenendaal, Dieter Freitag, Harald Pielartzik, and John R. Reynolds, *Adv. Mater.*, 1999.

57.   H. J. Spencer, P. J. Skabara, M. Giles, I. McCulloch, S. J. Coles and M. B. Hursthouse, *J. Mater. Chem.*, 2005, **15**, 4783-4792.

58.   R. Berridge, I. M. Serebryakov, P. J. Skabara, E. Orti, R. Viruela, R. Pou-Amerigo, S. J. Coles and M. B. Hursthouse, *J. Mater. Chem.*, 2004, **14**, 2822-2830.

59.   M. R. Andersson, D. Selse, M. Berggren, H. Jaervinen, T. Hjertberg, O. Inganaes, O. Wennerstroem and J. E. Oesterholm, *Macromolecules.*, 1994, **27**, 6503-6506.

60.   G. Barbarella, M. Zambianchi, L. Antolini, U. Folli, F. Goldoni, D. Iarossi, L. Schenetti and A. Bongini, *J. Chem. Soc., Perkin Trans. 2*, 1995, 1869-1873.

61.   V. M. Niemi, P. Knuuttila, J. E. Österholm and J. Korvola, *Polymer*, 1992, **33**, 1559-1562.

62.   Y. Katsumi, H. Shigenori and S. Ryu-ichi, *Japanese J. Appl. Phys*, 1984, **23**, L899.

63.   R. Sugimoto, S. Taketa, H. B. Gu and K. Yoshino, *Chem. Express*, 1986, **11**, 635-638.

64.   M. S. A. Abdou, X. Lu, Z. W. Xie, F. Orfino, M. J. Deen and S. Holdcroft, *Chem. Mater.*, 1995, **7**, 631-641.

65.   T. Cai, Y. Zhou, E. Wang, S. Hellström, F. Zhang, S. Xu, O. Inganäs and M. R. Andersson, *Sol. Energy Mater.*, 2010, **94**, 1275-1281.

66.   G. Koßmehl and G. Chatzitheodorou, *Die Makromolekulare Chemie, Rapid Commun.*, 1983, **4**, 639-643.

67.   G. Kossmehl and J. Hocker, Google Patents, 1986, p. US4611032.

68.   M. B. Zaman and D. F. Perepichka, *Chem. Commun.*, 2005, 4187-4189.
69.   R. D. McCullough, *Adv. Mater.*, 1998, **10**, 93-116.
70.   T. Yamamoto, T. Maruyama, Z.-H. Zhou, T. Ito, T. Fukuda, Y. Yoneda, F. Begum, T. Ikeda and S. Sasaki, *J. Am. Chem. Soc.*, 1994, **116**, 4832-4845.
71.   T. Yamamoto, T. Maruyama, Z. H. Zhou, Y. Miyazaki, T. Kanbara and K. Sanechika, *Synth. Met.*, 1991, **41**, 345-348.
72.   T. Yamamoto, A. Morita, Y. Miyazaki, T. Maruyama, H. Wakayama, Z. H. Zhou, Y. Nakamura, T. Kanbara, S. Sasaki and K. Kubota, *Macromolecules.*, 1992, **25**, 1214-1223.
73.   S. Cosnier and A. Karyakin, *Electropolymerization: concepts, materials and applications*, John Wiley & Sons, 2011.
74.   J. Roncali, *Chemical Reviews*, 1992, **92**, 711-738.
75.   R. Waltman and J. Bargon, *Canadian Journal of Chemistry*, 1986, **64**, 76-95.
76.   S. Patel, T. Mlsna, B. Fruhberger, E. Klaassen, S. Cemalovic and D. Baselt, *Sensors and Actuators B: Chemical*, 2003, **96**, 541-553.
77.   *Handbook of Thiophene-Based Materials*, John Wiley & Sons Ltd., 2009.
78.   J. Roncali, *Chemical Reviews*, 1992, **92**, 711-738.
79.   J. Heinze, B. A. Frontana-Uribe and S. Ludwigs, *Chemical Reviews*, 2010, **110**, 4724-4771.
80.   A. F. Diaz, J. I. Castillo, J. Logan and W.-Y. Lee, *Journal of Electroanalytical Chemistry and Interfacial Electrochemistry*, 1981, **129**, 115-132.
81.   E. Genies, G. Bidan and A. Diaz, *Journal of Electroanalytical Chemistry and Interfacial Electrochemistry*, 1983, **149**, 101-113.
82.   J. Roncali, *Chem. Rev.*, 1997, **97**, 173-206.
83.   E. Poverenov, M. Li, A. Bitler and M. Bendikov, *Chemistry of Materials*, 2010, **22**, 4019-4025.
84.   R. J. Mortimer, A. L. Dyer and J. R. Reynolds, *Displays*, 2006, **27**, 2-18.
85.   S. Roquet, P. Leriche, I. Perepichka, B. Jousselme, E. Levillain, P. Frère and J. Roncali, *Journal of Materials Chemistry*, 2004, **14**, 1396-1400.
86.   W. Domagala, D. Palutkiewicz, D. Cortizo-Lacalle, A. L. Kanibolotsky and P. J. Skabara, *Opt. Mater.*, 2011, **33**, 1405-1409.
87.   A. I. F. Vogel, B.S. Hannaford, A.J. Smith, P.W.G. Tatchell, A.R., *Vogel's Textbook of Practical Organic Chemistry 5th Edition*, Longman Scientific & Technical, Essex, 1989.
88.   D. H. Williams and I. Fleming, *Spectroscopic Methods in Organic Chemistry*, 5 edn., McGraw-Hill, Maidenhead, 1995.
89.   A. Jaboski, *Nature*, 1933, **131**, 839-840.
90.   A. J. Bard and L. R. Faulkner, in *Russian J. Electrochem.*, 2001, vol. 38, pp. 1364-1365.
91.   J. Wang, in *Analytical Electrochemistry*, Wiley-VCH, Weinheim, 2nd edn., 2001, pp. p1-32.
92.   P. Monk, R. Mortimer and D. Rosseinsky, *Electrochromism and electrochromic devices*, Cambridge University Press, 2007.
93.   A. Balan, D. Baran, G. Gunbas, A. Durmus, F. Ozyurt and L. Toppare, *Chemical Communications*, 2009, 6768-6770.
94.   A. H. C. H. Hamann, and W. Vielstich, *"Electrochemistry", WILEYVCH*, 2007.
95.   T. Anjos, A. Charlton, S. J. Coles, A. K. Croft, M. B. Hursthouse, M. Kalaji, P. J. Murphy and S. J. Roberts-Bleming, *Macromolecules*, 2009, **42**, 2505-2515.
96.   M. Kumada and K. Tamao, in *Adv. Organomet. Chem.*, eds. F. G. A. Stone and W. Robert, Academic Press, 1968, vol. Volume 6, pp. 19-117.
97.   J. J. Lagowski, *The Chemistry of Nonaqueous Solvents VA: Principles and Applications*, Elsevier Science, 2012.

98. T. A. Skotheim and J. Reynolds, *Handbook of Conducting Polymers, 2 Volume Set*, CRC press, 2007.

99. J. Pommerehne, H. Vestweber, W. Guss, R. F. Mahrt, H. Bässler, M. Porsch and J. Daub, *Adv. Mater.*, 1995, **7**, 551-554.

100. B. W. D'Andrade, S. Datta, S. R. Forrest, P. Djurovich, E. Polikarpov and M. E. Thompson, *Organic Electronics*, 2005, **6**, 11-20.

101. E. Brillas, G. Antón, T. F. Otero and J. Carrasco, *J. Electroanal. Chem.*, 1998, **445**, 125-133.

102. B. C. Thompson, P. Schottland, K. Zong and J. R. Reynolds, *Chem. Mater.*, 2000, **12**, 1563-1571.

103. R. J. Mortimer, *Chem. Soc. Rev.*, 1997, **26**, 147-156.

104. K. Bange and T. Gambke, *Adv. Mater.*, 1990, **2**, 10-16.

105. S.-F. Hong, S.-C. Hwang and L.-C. Chen, *Electrochim. Acta*, 2008, **53**, 6215-6227.

106. R. Vergaz, D. Barrios, J. M. Sánchez-Pena, C. Pozo-Gonzalo, M. Salsamendi and J. A. Pomposo, *Displays*, 2008, **29**, 401-407.

107. N. Leventis and Y. C. Chung, *Chem. Mater.*, 1992, **4**, 1415-1422.

108. J. Nagai, *Solid State Ionics*, 1990, **40**, 383-387.

109. H. J. Byker, *Electrochim. Acta*, 2001, **46**, 2015-2022.

110. I. Schwendeman, R. Hickman, G. Sönmez, P. Schottland, K. Zong, D. M. Welsh and J. R. Reynolds, *Chem. Mater.*, 2002, **14**, 3118-3122.

111. S. P. Mishra, K. Krishnamoorthy, R. Sahoo and A. Kumar, *Journal of Polymer Science Part A: Polymer Chemistry*, 2005, **43**, 419-428.

112. G. W. Jang, C. Chen, R. W. Gumbs, Y. Wei and J. M. Yeh, *J. Electrochem. Soc.*, 1996, **143**, 2591-2596.

113. P. R. Somani and S. Radhakrishnan, *Mater. Chem. Phys.*, 2003, **77**, 117-133.

114. P. M. Monk, R. J. Mortimer and D. R. Rosseinsky, *Electrochromism: fundamentals and applications*, John Wiley & Sons, 2008.

115. I. Chang, B. Gilbert and T. Sun, *J. Electrochem. Soc.*, 1975, **122**, 955-962.

116. C. Bird and A. Kuhn, *Chem. Soc. Rev.*, 1981, **10**, 49-82.

117. P. Y. Chen, C. S. Chen and T. H. Yeh, *J. Appl. Polym. Sci.*, 2014, **131**, 40485.

118. P. Bäuerle and K. U. Gaudl, *Adv. Mater.*, 1990, **2**, 185-188.

119. H. C. Ko, M. Kang, B. Moon and H. Lee, *Adv. Mater.*, 2004, **16**, 1712-1716.

120. G. Bidan, A. Deronzier and J.-C. Moutet, *J. Chem. Soc., Chem. Commun.*, 1984, 1185-1186.

121. E. A. Duek, M. A. De Paoli and M. Mastragostino, *Adv. Mater.*, 1992, **4**, 287-291.

122. A. Cirpan, A. A. Argun, C. R. Grenier, B. D. Reeves and J. R. Reynolds, *J. Mater. Chem.*, 2003, **13**, 2422-2428.

123. A. Ribeiro, D. Machado, P. F. dos Santos Filho and M.-A. De Paoli, *J. Electroanal. Chem.*, 2004, **567**, 243-248.

124. S. Alkan, C. A. Cutler and J. R. Reynolds, *Adv. Funct. Mater.*, 2003, **13**, 331-336.

125. A. Watanabe, K. Mori, Y. Iwasaki, Y. Nakamura and S. Niizuma, *Macromolecules*, 1987, **20**, 1793-1796.

126. R. M. Walczak and J. R. Reynolds, *ADVANCED MATERIALS-DEERFIELD BEACH THEN WEINHEIM-*, 2006, **18**, 1121.

127. J. L. Bredas and G. B. Street, *Acc. Chem. Res.*, 1985, **18**, 309-315.

128. D. M. Welsh, A. Kumar, E. Meijer and J. Reynolds, *Adv. Mater.*, 1999, **11**, 1379-1382.

129. P. M. Beaujuge and J. R. Reynolds, *Chemical Reviews*, 2010, **110**, 268-320.

130. E. J. L. H. Shirakawa, A.G. MacDiarmid, C.K. Chiang and A.J. Heeger, *J. Chem. Soc., Chem. Commun.*, 1977, 578-580.

131. A. A. Syed and M. K. Dinesan, *Talanta*, 1991, **38**, 815-837.

132. B. C. Sherman, W. B. Euler and R. R. Force, *J. Chem. Educ.*, 1994, **71**, A94.

133. G. D'Aprano, M. Leclerc and G. Zotti, *J. Electroanal. Chem.*, 1993, **351**, 145-158.

134. J. Jang, J. Ha and J. Cho, *Adv. Mater.*, 2007, **19**, 1772-1775.

135. S. J. Yoo, J. Cho, J. W. Lim, S. H. Park, J. Jang and Y.-E. Sung, *Electrochemistry Communications*, 2010, **12**, 164-167.

136. B. P. Jelle and G. Hagen, *Sol. Energy Mater.*, 1999, **58**, 277-286.

137. M. M. Verghese, M. Ram, H. Vardhan, B. Malhotra and S. Ashraf, *Polymer*, 1997, **38**, 1625-1629.

138. A. Siove, D. Ades, E. N'gbilo and C. Chevrot, *Synth. Met.*, 1990, **38**, 331-340.

139. C. Chevrot, E. Ngbilo, K. Kham and S. Sadki, *Synth. Met.*, 1996, **81**, 201-204.

140. B. Bezgin, A. Cihaner and A. M. Önal, *Thin Solid Films*, 2008, **516**, 7329-7334.

141. T. Yamamoto, K. Sanechika and A. Yamamoto, *Journal of Polymer Science: Polymer Letters Edition*, 1980, **18**, 9-12.

142. B. Krische and M. Zagorska, *Synth. Met.*, 1989, **28**, 263-268.

143. C. G. Granqvist, P. C. Lansåker, N. R. Mlyuka, G. A. Niklasson and E. Avendaño, *Sol. Energy Mater.*, 2009, **93**, 2032-2039.

144. J. r. Heinze, B. A. Frontana-Uribe and S. Ludwigs, *Chem. Rev.*, 2010, **110**, 4724-4771.

145. M. Mastragostino, C. Arbizzani, A. Bongini, G. Barbarella and M. Zambianchi, *Electrochimica Acta*, 1993, **38**, 135-140.

146. C. Arbizzani, M. Mastragostino, L. Meneghello, M. Morselli and A. Zanelli, *J. Appl. Electrochem.*, 1996, **26**, 121-123.

147. R. Elsenbaumer, K. Jen, G. Miller and L. Shacklette, *Synth. Met.*, 1987, **18**, 277-282.

148. J. C. Forgie, A. L. Kanibolotsky, P. J. Skabara, S. J. Coles, M. B. Hursthouse, R. W. Harrington and W. Clegg, *Macromolecules*, 2009, **42**, 2570-2580.

149. C. Arbizzani, A. Bongini, M. Mastragostino, A. Zanelli, G. Barbarella and M. Zambianchi, *Adv. Mater.*, 1995, **7**, 571-574.

150. R. J. M. a. D. R. R. P.M.S Monk, *Electrochromism and Electrochromic Devices*, Cambridge University Press, United Kingdom, Cambridge, 2007.

151. A. P. Yair H. Wijsboom, Sanjio S. Zade, Yana Sheynin, Mao Li, Linda J. W. Shimon and Micheal Bendikov*, *Angew. Chem. Int Ed*, 2009, **48**, 5443.

152. P.-H. A. Avni A. Argun, Barry C. Thompson, Nicholas J. Pinto, Irina Schwendeman, Carelton L. Gaupp, Jungseek Hwang, Nicholas J. Pinto, David B. Tanner, Alan G. MacDiarmid and John R. Reynolds, *Chem. Mater*, 2004, **16**, 4401-4412.

153. A. L. D. a. J. R. Reyonlds, *Conjugated Polymers: Theory, Synthesis, Properties and Characterisation*, 3 edn., 2007.

154. A. H. A. K. Mohanakrishnan, Micheal A. Lyon, M.V. Lakshmikantham and Micheal P. Cava, *Tetrahedron Lett.*, 1999, **55**, 11745.

155. A. L. K. John C. Forgie, Peter J. Skarbara, Simon J. Coles, Micheal B. Hursthouse, Ross W. Harrington, and William Clegg, *Macromolecules*, 2009, **42**, 2570-2580.

156. W. C. Chen, C. L. Liu, C. T. Yen, F. C. Tsai, C. J. Tonzola, N. Olson and S. A. Jenekhe, *Macromolecules.*, 2004, **37**, 5959-5964.

157. L. Groenendaal, F. Jonas, D. Freitag, H. Pielartzik and J. R. Reynolds, *Adv. Mater.*, 2000, **12**, 481-494.

158. F. Jonas and L. Schrader, *Synth. Met.*, 1991, **41**, 831-836.

159. I. Winter, C. Reese, J. Hormes, G. Heywang and F. Jonas, *Chem. Phys.*, 1995, **194**, 207-213.

160. Y. Wang, *J Phys: Conference Series*, 2009, **152**, 012023.

161. E. Havinga, C. Mutsaers and L. Jenneskens, *Chem. Mater.*, 1996, **8**, 769-776.

162. S. A. Sapp, G. A. Sotzing and J. R. Reynolds, *Chem. Mater.*, 1998, **10**, 2101-2108.

163. A. Kumar and J. R. Reynolds, *Macromolecules*, 1996, **29**, 7629-7630.

164. B. Sankaran and J. R. Reynolds, *Macromolecules*, 1997, **30**, 2582-2588.

165. D. M. Welsh, A. Kumar, M. C. Morvant and J. R. Reynolds, *Synth. Met.*, 1999, **102**, 967-968.

166. A. A. Argun, P.-H. Aubert, B. C. Thompson, N. J. Pinto, I. Schwendeman, C. L. Gaupp, J. Hwang, N. J. Pinto, D. B. Tanner, A. G. MacDiarmid and J. R. Reynolds, *Chem. Mater*, 2004, **16**, 4401.

167. Y. Wang, MRS International Materials Research Conference, 2009.

168. Y. H. Wijsboom, A. Patra, S. S. Zade, Y. Sheynin, M. Li, L. J. W. Shimon and M. Bendikov*, *Angew. Chem. Int Ed*, 2009, **48**, 5443.

169. H. J. Spencer, P. J. Skabara, M. Giles, I. McCulloch, S. J. Coles and M. B. Hursthouse, *J. Mater. Chem.*, 2005, **15**, 4783-4792.

170. R. Blanco, C. Seoane and J. L. Segura, *Tetrahedron. Lett*, 2008, **49**, 2056-2059.

171. Y. H. Wijsboom, A. Patra, S. S. Zade, Y. Sheynin, M. Li, L. J. W. Shimon and M. Bendikov, *Angew. Chem. Int. Ed.*, 2009, **48**, 5443-5447.

172. H. J. Spencer, P. J. Skabara, M. Giles, I. McCulloch, S. J. Coles and M. B. Hursthouse, *Mater. Chem. Phys.*, 2005, **15**, 4783.

173. H. J. Spencer, P. J. Skabara, M. Giles, I. McCulloch, S. J. Coles and M. B. Hursthouse, *J. Mater. Chem.*, 2005, **15**, 4783.

174. C. Pozo-Gonzalo, T. Khan, J. J. W. McDouall, P. J. Skabara, D. M. Roberts, M. E. Light, S. J. Coles, M. B. Hursthouse, H. Neugebauer, A. Cravino and N. S. Sariciftci, *Mater. Chem. Phys.*, 2002, **12**, 500-512.

175. Y. Coskun, A. Cirpan and L. Toppare, *J. Mater. Sci*, 2007, **42**, 368-372.

176. E. Yildiz, P. Camurlu, C. Tanyeli, I. Akhmedov and L. Toppare, *J. Electroanal. Chem*, 2008, **612**, 247-256.

177. C. G. Granqvist, P. C. Lansåker, N. R. Mlyuka, G. A. Niklasson and E. Avendaño, *Sol. Energy. Mater.*, 2009, **In Press, Corrected Proof**.

178. J. C. Forgie, A. L. Kanibolotsky, P. J. Skarbara, S. J. Coles, M. B. Hursthouse, R. W. Harrington and W. Clegg, *Macromolecules*, 2009, **42**, 2570-2580.

179. P. M. S. Monk, R. J. Mortimer and D. R. Rosseinsky, *Electrochromism and Electrochromic Devices*, 2007, ch. 4.5, pp. 62.

180. A. Patra, Y. H. Wijsboom, S. S. Zade, M. Li, Y. Sheynin, G. Leitus and M. Bendikov, *J. Am. Chem. Soc.*, 2008, **130**, 6734-6736.

181. M. Li, Y. Sheynin, A. Patra and M. Bendikov, *Chem. Mater.*, 2009, **21**, 2482-2488.

182. M. Li, A. Patra, Y. Sheynin and M. Bendikov, *Adv. Mater.*, 2009, **21**, 1707-1711.

183. F. Garnier, G. Tourillon, M. Gazard and J. Dubois, *Journal of Electroanalytical Chemistry and Interfacial Electrochemistry*, 1983, **148**, 299-303.

184. M. Druy and R. Seymour, *Le Journal de Physique Colloques*, 1983, **44**, C3-595-C593-598.

185. F. Jonas, G. Heywang, W. Schmidtberg, J. Heinze and M. Dietrich, Google Patents, 1990.

186. A. Kumar, D. M. Welsh, M. C. Morvant, F. Piroux, K. A. Abboud and J. R. Reynolds, *Chem. Mater.*, 1998, **10**, 896-902.

187. B. D. Reeves, C. R. Grenier, A. A. Argun, A. Cirpan, T. D. McCarley and J. R. Reynolds, *Macromolecules*, 2004, **37**, 7559-7569.

188. P. J. Skabara, R. Berridge, K. Prescott, L. M. Goldenberg, E. Orti, R. Viruela, R. Pou-Amerigo, A. S. Batsanov, J. A. K. Howard, S. J. Coles and M. B. Hursthouse, *J. Mater. Chem.*, 2000, **10**, 2448-2457.

189. L. M. Goldenberg, P. J. Skabara, D. M. Roberts, R. Berridge, E. Orti, P. M. Viruela and R. Pou-Amerigo, *J. Mater. Chem.*, 2000, **10**, 2458-2465.

190. R. Berridge, S. P. Wright, P. J. Skabara, A. Dyer, T. Steckler, A. A. Argun, J. R. Reynolds, R. W. Harrington and W. Clegg, *J. Mater. Chem.*, 2007, **17**, 225-231.

191. P. J. Skabara, R. Berridge, I. M. Serebryakov, A. L. Kanibolotsky, L. Kanibolotskaya, S. Gordeyev, I. F. Perepichka, N. S. Sariciftci and C. Winder, *J. Mater. Chem.*, 2007, **17**, 1055-1062.

192. O. Gidron, A. Dadvand, E. Wei-Hsin Sun, I. Chung, L. J. W. Shimon, M. Bendikov and D. F. Perepichka, *J.Mater.C.C*, 2013, **1**, 4358-4367.

193. I. G. Cuesta, J. Aragó, E. Ortí and P. Lazzeretti, *J. Chem. Theory. Comput.*, 2009, **5**, 1767-1775.

194. C. H. Woo, P. M. Beaujuge, T. W. Holcombe, O. P. Lee and J. M. J. Fréchet, *J. Am. Chem. Soc.*, 2010, **132**, 15547-15549.

195. Y.-S. Lin, C.-Y. Lin, D.-Y. Huang and T. Y. R. Tsai, *J. Chin. Chem. Soc.*, 2005, **52**, 849-852.

196. T. Minari, Y. Miyata, M. Terayama, T. Nemoto, T. Nishinaga, K. Komatsu and S. Isoda, *Appl. Phys. Lett.*, 2006, **88**, 083514.

197. U. H. F. Bunz, *Angew. Chem. Int. Ed.*, 2010, **49**, 5037-5040.

198. M. J. González-Tejera, E. S. de la Blanca and I. Carrillo, *Synth. Met.*, 2008, **158**, 165-189.

199. M. Talu, M. Kabasakaloḡlu, F. Yıldırım and B. Sarı, *Appl. Surf. Sci.*, 2001, **181**, 51-60.

200. F. Benvenuti, A. M. Raspolli Galletti, C. Carlini, G. Sbrana, A. Nannini and P. Bruschi, *Polym.*, 1997, **38**, 4973-4982.

201. O. Gidron, A. Dadvand, Y. Sheynin, M. Bendikov and D. F. Perepichka, *Chem. Commun.*, 2011, **47**, 1976-1978.

202. O. Gidron, Y. Diskin-Posner and M. Bendikov, *J. Am. Chem. Soc.*, 2010, **132**, 2148-2150.

203. O. Gidron, L. J. W. Shimon, G. Leitus and M. Bendikov, *Org. Lett.*, 2012, **14**, 502-505.

204. S. Glenis, M. Benz, E. LeGoff, J. L. Schindler, C. R. Kannewurf and M. G. Kanatzidis, *J. Am. Chem. Soc.*, 1993, **115**, 12519-12525.

205. A. Benahmed-Gasmi, P. Frère and J. Roncali, *J. Electroanal. Chem.*, 1996, **406**, 231-234.

206. G. Distefano, D. Jones, M. Guerra, L. Favaretto, A. Modelli and G. Mengoli, *J. Phys. Chem.*, 1991, **95**, 9746-9753.

207. B. Demirboğa and A. M. Önal, *Synth. Met.*, 1999, **99**, 237-242.

208. S. Tirkeş and A. M. Önal, *J. Appl. Polym. Sci.*, 2007, **103**, 871-876.

209. L. Li, X.-b. Wan and G. Xue, *Chinese J. Polym.*, 2002, **20**, 419-423.

210. X. Wan, F. Yan, S. Jin, X. Liu and G. Xue, *Chem. Mater.*, 1999, **11**, 2400-2407.

211. J. P. Ferraris and T. R. Hanlon, *Polymer*, 1989, **30**, 1319-1327.

212. X. Wang, S. Chen, Y. Sun, M. Zhang, Y. Li, X. Li and H. Wang, *Polym. Chem.*, 2011, **2**, 2872-2877.

213. T. A. Skotheim and J. R. Reynolds, *Handbook of conducting polymers-conjugated polymers; synthesis, properties and characterization*, CRC Press, Boca Raton, FL, 2007.

214. H. Z. Akpinar, Y. A. Udum and L. Toppare, *J Polym. Sci. Part A: Polym. Chem.*, 2013, **51**, 3901-3906.

215. A. Hucke and M. P. Cava, *J. Org. Chem.*, 1998, **63**, 7413-7417.

216. C. J. Yang and S. A. Jenekhe, *Chem. Mater.*, 1991, **3**, 878-887.

217. M. Bourgeaux, S. A. P. Guarin and W. G. Skene, *J. Mater. Chem.*, 2007, **17**, 972-979.

218. J. E. G. Kuder, W. Harry and n. Wychick, *Darlene J. Org. Chem.*, 1975, **40**, 875.

219. A. Bolduc, S. Dufresne and W. G. Skene, *J. Mater. Chem.*, 2012, **22**, 5053-5064.

220. J. Cai, P. Zhao, H. Niu, Y. Lian, C. Wang, X. Bai and W. Wang, *Polym. Chem.*, 2013, **4**, 1183-1192.
221. S. Dufresne, A. Bolduc and W. G. Skene, *J. Mater. Chem.*, 2010, **20**, 4861-4866.
222. S. Dufresne, M. Bourgeaux and W. G. Skene, *J. Mater. Chem.*, 2007, **17**, 1166-1177.
223. S. Dufresne and W. G. Skene, *J. Phys. Org. Chem.*, 2012, **25**, 211-221.
224. C. Mallet, M. Le Borgne, M. Starck and W. G. Skene, *Polym. Chem.*, 2013, **4**, 250-254.
225. A. Bolduc, S. Dufresne and W. G. Skene, *J. Mater. Chem.*, 2010, **20**, 4820-4826.
226. M. Bourgeaux, S. Vomscheid and W. G. Skene, *Synth. Commun.*, 2007, **37**, 3551-3558.
227. M. Bourgeaux, S. Vomscheid and W. G. Skene, *Synth. Commun.*, 2007, **37**, 3551.
228. K. A. Hansford, S. A. P. Guarin, W. G. Skene and W. D. Lubell, *J. Org. Chem.*, 2005, **70**, 7996.
229. S. A. Pérez Guarìn, M. Bourgeaux, S. Dufresne and W. G. Skene, *J. Org. Chem.*, 2007, **72**, 2631.
230. S. A. Pérez Guarìn, S. Dufresne, D. Tsang, A. Sylla and W. G. Skene, *J. Mater. Chem.*, 2007, **17**, 2801.
231. L. Sicard, D. Navarathne, T. Skalski and W. G. Skene, *Adv. Funct. Mater.*, 2013, **23**, 3549-3359.
232. W. G. Skene and S. Dufresne, *Org. Lett.*, 2004, **6**, 2949.
233. W. G. Skene and S. A. Pérez Guarìn, *J. Fluores.*, 2007, **17**, 540.
234. O. Thomas, O. Inganäs and M. R. Andersson, *Macromolecules.*, 1998, **31**, 2676-2678.
235. Z. Kucybala, I. Pyszka, B. Marciniak, G. L. Hug and J. Paczkowski, *J. Chem. Soc., Perkin Trans 2*, 1999, 2147.
236. J. Skopalová, K. Lemr, M. Kotouèek, L. Èáp and P. Barták, *Fresenius' J. Anal. Chem.*, 2001, **370**, 963.
237. R. Adams, J. E. Bullock and W. C. Wilson, *J. Am. Chem. Soc.*, 1923, **45**, 521.
238. G. F. D'Alelio and R. K. Schoenig, *Macromol. Sci. Rev.: Macromol. Chem.*, 1969, **C3**, 105.
239. P. W. Morgan, S. L. Kwolek and T. C. Pletcher, *Macromolecules.*, 1987, **20**, 729-739.
240. C. Noel and J. Billard, *Mol. Cryst. Liq. Cryst. Lett.*, 1978, **41**, 260.
241. C. J. Yang and S. A. Jenekhe, *Macromolecules.*, 1995, **28**, 1180-1196.
242. S. A. Jenekhe, C. J. Yang, H. Vanherzeele and J. S. Meth, *Chem. Mater.*, 1991, **3**, 987.
243. K. S. Lee, J. C. Won and J. C. Jung, *Macromol. Chem.*, 1989, **190**, 1547.
244. S. B. Park, H. Kim, W. C. Zin and J. C. Jung, *Macromolecules.*, 1993, **26**, 1627-1632.
245. S. A. Jenekhe and C. J. Yang, *Chem. Mater.*, 1991, **3**, 878.
246. C. J. Yang and S. A. Jenekhe, *Chem. Mater.*, 1994, **6**, 196-203.
247. J.-C. Chen, Y.-C. Liu, J.-J. Ju, C.-J. Chiang and Y.-T. Chern, *Polym.*, 2011, **52**, 954-964.
248. T. Moriuchi and T. Hirao, *Acc. Chem. Res.*, 2011, **45**, 347-360.
249. A. Iwan, M. Palewicz, A. Chuchmała, L. Gorecki, A. Sikora, B. Mazurek and G. Pasciak, *Synth. Met.*, 2012, **162**, 143-153.
250. F. C. Krebs and M. Jørgensen, *Synth. Met.*, 2004, **142**, 181-185.
251. S. Mittler-Neher, *Macromol. Chem. Phys.*, 1998, **199**, 513-523.
252. S. A. Jenekhe, C. J. Yang, H. Vanherzeele and J. S. Meth, *Chem. Mater.*, 1991, **3**, 985-987.

253.   C. Wang, S. Shieh, E. LeGoff and M. G. Kanatzidis, *Macromolecules*, 1996, **29**, 3147.
254.   K. Suematsu, K. Nakamura and J. Takeda, *Colloid. Polym. Sci.*, 1983, **261**, 493.
255.   F. C. Tsai, C. C. Chang, C. L. Liu, W. C. Chen and S. A. Jenekhe, *Macromolecules*, 2005, **38**, 1958-1966.
256.   S. Destri, I. A. Khotina and W. Porzio, *Macromolecules.*, 1998, **31**, 1079-1086.
257.   S. Destri, I. A. Khotina, W. Porzio and C. Botta, *Opt. Mater.*, 1998, **9**, 411.
258.   S. Destri, W. Porzio and Y. Dubitsky, *Synth. Met.*, 1995, **75**, 25.
259.   S. Destri, W. Porzio and Y. Dubitsky, *Synth. Met.*, 1995, **69**, 287.
260.   M. Bourgeaux, S. Vomsheid and W. G. Skene, *Acta Crystallogr., Sect. E: Struct. Rep. Online*, 2006, **E62**, o5529.
261.   S. Dufresne, M. Bourgeaux and W. G. Skene, *Acta Crystallogr., Sect. E: Struct. Rep. Online*, 2006, **E62**, o5602.
262.   W. G. Skene, *Polym. Prepr.*. 2004, **45**, 254.
263.   H. Lütjens, A. Zickgraf, H. Figler, J. Linden, R. A. Olsson and P. J. Scammells, *J. Med. Chem.*, 2003, **46**, 1870-1877.
264.   H.-P. Buchstaller, C. D. Siebert, R. H. Lyssy, I. Frank, A. Duran, R. Gottschlich and C. R. Noe, *Monatsh. Chem.*, 2001, **132**, 279-293.
265.   K. Gewald, *Chem. Heterocycl. Compd.*, 1976, **12**, 1077-1090.
266.   V. I. Shvedov and A. N. Grinev, *Chem. Heterocycl. Compd.*, 1967, **2**, 385-387.
267.   M. Bourgeaux and W. G. Skene, *J. Org. Chem.*, 2007, **72**, 8882-8892.
268.   M. Bourgeaux and W. G. Skene, *Macromolecules.*, 2007, **40**, 1792-1795.
269.   H. Pang, P. J. Skabara, D. J. Crouch, W. Duffy, M. Heeney, I. McCulloch, S. J. Coles, P. N. Horton and M. B. Hursthouse, *Macromolecules.*, 2007, **40**, 6585-6593.
270.   J. Roncali, P. Blanchard and P. Frere, *J. Mater. Chem.*, 2005, **15**, 1589-1610.
271.   G. A. Sotzing, J. R. Reynolds and P. J. Steel, *Chem. Mater.*, 1996, **8**, 882-889.
272.   Y.-M. Zhang, X. Wang, W. Zhang, W. Li, X. Fang, B. Yang, M. Li and S. X.-A. Zhang, *Light: Science & Applications*, 2015, **4**, e249.
273.   P. C. Ersin Yildiz, Cihangir Tanyeli, Idris Akhmedov, Levent Toppare, *J. Electroanal. Chem.*, 2008, **612**, 247-256.
274.   R. Rauh, F. Wang, J. Reynolds and D. Meeker, *Electrochimica Acta*, 2001, **46**, 2023-2029.
275.   P. S. Monk, R. J. Mortimer and D. R. Rosseinsky, *J. Am. Chem. Soc.*, 1996, **118**, 10678-10678.
276.   A. A. Argun, A. Cirpan and J. R. Reynolds, *Adv. Mater.*, 2003, **15**, 1338-1341.
277.   D. Mecerreyes, R. Marcilla, E. Ochoteco, H. Grande, J. A. Pomposo, R. Vergaz and J. M. S. Pena, *Electrochim. Acta*, 2004, **49**, 3555-3559.
278.   C. Ma, M. Taya and C. Xu, *Electrochim. Acta*, 2008, **54**, 598-605.
279.   L. Kullman, A. Azens, G. Vaivars and C. Granqvist, *Solar energy*, 2000, **68**, 517-522.
280.   W. van Gool and P. Hagenmuller, *Solid Electrolytes: General Principles, Characterization, Materials, Applications*, Academic Press, 1978.
281.   R. J. Gale, *Spectroelectrochemistry: theory and practice*, Springer Science & Business Media, 2012.
282.   *CIE Colorimetry (Official Recommendation of the international Commision on Illumination)*, CIE Publication No. 15: Paris 1971.
283.   R. J. Mortimer and J. R. Reynolds, *J. Mater. Chem.*, 2005, **15**, 2226-2233.
284.   H. S. Fairman, M. H. Brill and H. Hemmendinger, *Color Research & Application*, 1997, **22**, 11-23.
285.   B. D. Reeves, C. R. G. Grenier, A. A. Argun, A. Cirpan, T. D. McCarley and J. R. Reynolds, *Macromolecules.*, 2004, **37**, 7559-7569.

286. W. Wagner, F. Rauch, C. Ottermann and K. Bange, *Nuclear Instruments and Methods in Physics Research Section B: Beam Interactions with Materials and Atoms*, 1990, **50**, 27-30.
287. V. K. Thakur, G. Ding, J. Ma, P. S. Lee and X. Lu, *Adv. Mater.*, 2012, **24**, 4071-4096.
288. C. O. Avellaneda, M. A. Berton and L. O. Bulhoes, *Sol. Energy Mater.*, 2008, **92**, 240-244.
289. J. Padilla and T. Otero, *Electrochemistry Communications*, 2008, **10**, 1-6.
290. G. A. Sotzing and K. Lee, *Macromolecules*, 2002, **35**, 7281-7286.
291. M. A. Invernale, V. Seshadri, D. M. D. Mamangun, Y. Ding, J. Filloramo and G. A. Sotzing, *Chem. Mater.*, 2009, **21**, 3332-3336.
292. B. Zaifoglu, M. Sendur, N. A. Unlu and L. Toppare, *Electrochim. Acta*, 2012, **85**, 78-83.
293. U. H. F. Bunz, *Angew. Chem. Int. Ed.*, **49**, 5037.
294. F. Benvenuti, A. M. Raspolli Galletti, C. Carlini, G. Sbrana, A. Nannini and P. Bruschi, *Polymer*, 1997, **38**, 4973.
295. C.-Y. L. Yu-Sheng Lin, Deng-Yi Huang and Thomas Y. R. Tsai, *J. Chinese Chem. Soc.*, 2005, **52**, 849-852.
296. C. H. Woo, P. M. Beaujuge, T. W. Holcombe, O. P. Lee and J. M. J. Freı̀•chet, *J. Am. Chem. Soc.*, **132**, 15547.
297. A. K. Mohanakrishnan, A. Hucke, M. A. Lyon, M. V. Lakshmikantham and M. P. Cava, *Tetrahedron*, 1999, **55**, 11745-11754.
298. W. Heffe and F. Kröhnke, *Chem. Ber.*, 1956, **89**, 822-836.
299. A. L. Kanibolotsky, L. Kanibolotskaya, S. Gordeyev, P. J. Skabara, I. McCulloch, R. Berridge, J. E. Lohr, F. Marchioni and F. Wudl, *Org. Lett.*, 2007, **9**, 1601-1604.
300. W. D. Ollis, M. Rey, I. O. Sutherland and G. L. Closs, *J. Chem. Soc., Chem. Commun.*, 1975, 543-545.
301. O. Mert, E. Sahin, E. Ertas, T. Ozturk, E. A. Aydin and L. Toppare, *J. Electroanal. Chem.*, 2006, **591**, 53-58.
302. F. Goldoni, B. M. W. Langeveld-Voss and E. W. Meijer, *Synth. Commun.*, 1998, **28**, 2237-2244.
303. C. Lin, T. Endo, M. Takase, M. Iyoda and T. Nishinaga, *J. Am. Chem. Soc.*, 2011, **133**, 11339-11350.
304. N. Z. a. M. B. Sanjio S. Zade, *Chem. Eur. J.*, 2009, **15**, 8613-8624.
305. S. Kaur, N. J. Findlay, A. L. Kanibolotsky, S. E. T. Elmasly, P. J. Skabara, R. Berridge, C. Wilson and S. J. Coles, *Polym. Chem.*, 2012, **3**, 2277-2286.
306. P. J. Skabara, I. M. Serebryakov, D. M. Roberts, I. F. Perepichka, S. J. Coles and M. B. Hursthouse, *J. Org. Chem.*, 1999, **64**, 6418-6424.
307. R. Berridge, I. M. Serebryakov, P. J. Skabara, E. Orti, R. Viruela, R. Pou-Amerigo, S. J. Coles and M. B. Hursthouse, *J. Mater. Chem.*, 2004, **14**, 2822-2830.
308. N. Svenstrup and J. Becher, *Synthesis*, 1995, **1995**, 215-235.
309. R. Akué-Gédu and B. Rigo, *Org. Synth.*, 2005, **82**, 179-187.
310. A. Gorgues, A. Simon, A. Le Coq, A. Hercouet and F. Corre, *Tetrahedron*, 1986, **42**, 351-370.
311. S. K. Ritter and R. E. Noftle, *Chem. Mater.*, 1992, **4**, 872-879.
312. M. İçli, A. Cihaner and A. M. Önal, *Electrochim. Acta*, 2007, **52**, 8039-8043.
313. J. L. Brédas, G. B. Street, B. Thémans and J. M. André, *J. Chem. Phys.*, 1985, **83**, 1323.
314. A. J. Heeger, S. Kivelson, J. R. Schrieffer and W. P. Su, *Rev. Mod. Phys.*, 1988, **60**, 781-850.
315. H. Münstedt, *Polymer.*, 1986, **27**, 899-904.

316. B. Sun, J. J. Jones, R. P. Burford and M. Skyllas-Kazacos, *J. Mater. Sci.*, 1989, **24**, 4024-4029.

317. Z. T. de Oliveira Jr and M. C. dos Santos, *Solid State Commun.*, 2000, **114**, 49-53.

318. *Michael A. Invernale, Muge Acik and Gregory A. Sotzing, Handbook of Thiophene-Based Materials*, 2009, ch. 20, 757.

319. A. W. Bott, *Current Separations*, 2001, **19**, 71.

320. A. W. Bott and W. R. Heineman, *Current Separations*, 2004, **20**, 121.

321. C. L. Gaupp, D. M. Welsh, R. D. Rauh and J. R. Reynolds, *Chem. Mater.*, 2002, **14**, 3964-3970.

322. K.-H. Ong, S.-L. Lim, H.-S. Tan, H.-K. Wong, J. Li, Z. Ma, L. C. H. Moh, S.-H. Lim, J. C. de Mello and Z.-K. Chen, *Adv. Mater.*, 2011, **23**, 1409-1413.

323. S. Kaur, N. J. Findlay, F. C. Coomer, R. Berridge and P. J. Skabara, *Macromolecular Rapid Commun.*, 2013, **34**, 1330-1334.

324. G. J. McEntee, P. J. Skabara, F. Vilela, S. Tierney, I. D. W. Samuel, S. Gambino, S. J. Coles, M. B. Hursthouse, R. W. Harrington and W. Clegg, *Chem. Mater.*, 2010, **22**, 3000-3008.

325. H. Pang, P. J. Skabara, S. Gordeyev, J. J. W. McDouall, S. J. Coles and M. B. Hursthouse, *Chem. Mater.*, 2007, **19**, 301-307.

326. D. J. Crouch, P. J. Skabara, M. Heeney, I. McCulloch, S. J. Coles and M. B. Hursthouse, *Chem. Commun.*, 2005, 1465-1467.

327. T. Khan, P. J. Skabara, P. Frère, M. Allain, S. J. Coles and M. B. Hursthouse, *Tetrahedron Lett.*, 2004, **45**, 2535-2539.

328. P. Frere and P. J. Skabara, *Chem. Soc. Rev.*, 2005, **34**, 69-98.

329. P. Leriche, M. Turbiez, V. Monroche, P. Frère, P. Blanchard, P. J. Skabara and J. Roncali, *Tetrahedron Lett.*, 2003, **44**, 649-652.

330. I. Carrillo, F. Fernández-Martín, C. Barba, E. Sánchez de la Blanca, M. J. González-Tejera and I. Hernández-Fuentes, *Polym. Bull.*, 1999, **43**, 269-276.

331. A. F. Diaz, J. I. Castillo, J. Logan and W.-Y. Lee, *J. Electroanal. Chem.*, 1981, **129**, 115-132.

332. J. Poater, J. Casanovas, M. Solà and C. Alemán, *J. Phys. Chem. A.*, 2009, **114**, 1023-1028.

333. C. Alemán, E. Armelin, J. I. Iribarren, F. Liesa, M. Laso and J. Casanovas, *Synth. Met.*, 2005, **149**, 151-156.

334. J. Casanovas and C. Alemán, *Phys. Chem. C.*, 2007, **111**, 4823-4830.

335. H. Koezuka, A. Tsumura and T. Ando, *Synth. Met.*, 1987, **18**, 699-704.

336. L. E. Alexander, *X-ray diffraction methods in polymer science*, Wiley-Interscience, 1969.

337. S. M. Mulla, P. S. Phale and M. R. Sharaf, *AdMet*, 2012, **OM 006**.

338. J. V. Gilfrich, I. C. Noyan, R. Jenkins, T. C. Huang, D. K. Smith, R. L. Snyder, P. K. Predecki and M. A. Zaitz, *Advances in X-ray analysis. 39. [Proceedings of the Forty-fourth Annual Conference on Applications of X-Ray Analysis]*, Springer US, 1998, 505.

339. Z. A. King, C. M. Shaw, S. A. Spanninga and D. C. Martin, *Polymer*, 2011, **52**, 1302-1308.

340. A. Moliton and R. C. Hiorns, *Polym. Int.*, 2012, **61**, 337-341.

341. H. A. M. van Mullekom, J. A. J. M. Vekemans, E. E. Havinga and E. W. Meijer, *Materials Science & Engineering, R*, 2001, **32**, 1-40.

342. J.-i. Yamada, H. Akutsu, H. Nishikawa and K. Kikuchi, *Chem. Rev.*, 2004, **104**, 5057-5084.

343. D. Gupta, in *Directions*, 2007, pp. 111-117.

344. A. Facchetti, *Chem. Mater.*, 2011, **23**, 733-758.

345. T. Tshibaka, I. Ulliel Roche, S. Dufresne, W. D. Lubell and W. G. Skene, *J. Org. Chem.*, 2009, **74**, 9497-9500.

346. A. K. Agrawal and S. A. Jenekhe, *Macromolecules.*, 1993, **26**, 895-905.

347. C. J. Yang, S. A. Jenekhe, J. S. Meth and H. Vanherzeele, *Ind. Eng. Chem. Res.*, 1999, **38**, 1759-1774.

348. W. G. Skene, S. Dufresne, T. Trefz and M. Simard, *Acta Crystallogr., Sect. E: Struct. Rep. Online*, 2006, **E62**, o2382.

349. W. G. Skene and S. Dufresne, *Acta Crystallogr., Sect. E: Struct. Rep. Online*, 2006, **E62**, o1116.

350. C. Wang, J. L. Schindler, C. R. Kannewurf and M. G. Kanatzidis, *Chem. Mater.*, 1995, **7**, 58-68.

351. Y. H. Wijsboom, A. Patra, S. S. Zade, Y. Sheynin, M. Li, L. J. W. Shimon and M. Bendikov, *Angew. Chem Int. Ed.*, 2009, **48**, 5443.

352. A. Smie, A. Synowczyk, J. Heinze, R. Alle, P. Tschuncky, G. Götz and P. Bäuerle, *J. Electroanal. Chem.*, 1998, **452**, 87-95.

353. M. Turbiez, P. Frère, M. Allain, N. Gallego-Planas and J. Roncali, *Macromolecules*, 2005, **38**, 6806-6812.

354. M. Turbiez, P. Frère, P. Blanchard and J. Roncali, *Tetrahedron Lett.*, 2000, **41**, 5521-5525.

355. H.-J. Yen and G.-S. Liou, *Org. Electron.*, 2010, **11**, 299-310.

356. A. M. McDonagh, S. R. Bayly, D. J. Riley, M. D. Ward, J. A. McCleverty, M. A. Cowin, C. N. Morgan, R. Varrazza, R. V. Penty and I. H. White, *Chem. Mater.*, 2000, **12**, 2523-2524.

357. S. Xun, G. LeClair, J. Zhang, X. Chen, J. P. Gao and Z. Y. Wang, *Org. Lett.*, 2006, **8**, 1697-1700.

358. G. Sonmez, P. Schottland, K. Zong and J. R. Reynolds, *J. Mater. Chem.*, 2001, **11**, 289-294.

359. Y. Zheng, J. Cui, J. Zheng and X. Wan, *J. Mater. Chem.*, 2010, **20**, 5915-5922.

360. F. Goldoni, B. M. W. Langeveld-Voss and E. W. Meijer, *Synth. Commun.*, 1998, **28**, 2237.

361. R. W. W. Hooft, *COLLECT*, Nonius BV, Delft, The Netherlands, 1998.

362. Z. Otwinowski and W. Minor, Macromolecular Crystallography Part A, in *Methods Enzymol.*, eds. W. Carter Jr and R. M. Sweet, Academic Press, 1997, vol. 276, pp. 307-326C.

363. G. Sheldrick, *Acta Crystallographica Section A*, 1990, **46**, 467-473.

364. O. V. Dolomanov, L. J. Bourhis, R. J. Gildea, J. A. K. Howard and H. Puschmann, *J. Appl. Crystallogr.*, 2009, **42**, 339-341.